FUNDAMENTAL STUDY OF PHASE TRANSFORMATIONS IN Si-Al TRIP STEELS

by

Chad Michael Parish

BS in Material Science and Engineering, North Carolina State University, 2000

Submitted to the Graduate Faculty of

the School of Engineering in partial fulfillment

of the requirements for the degree of

Master of Science in Material Science and Engineering

University of Pittsburgh

2003

UNIVERSITY OF PITTSBURGH

SCHOOL OF ENGINEERING

This thesis was presented

by

Chad Michael Parish

it was defended on

April 22, 2003

and approved by

Dr. C. I. Garcia, Research Professor, Material Science and Engineering

Dr. I. Nettleship, Associate Professor, Material Science and Engineering

Thesis Advisor: Dr. A. J. DeArdo, William Kepler Whiteford Professor, Material Science and Engineering

ABSTRACT

FUNDAMENTAL STUDY OF PHASE

TRANSFORMATIONS IN Si-Al TRIP STEELS

Chad Michael Parish, M.Sc.

University of Pittsburgh, 2003

TRIP steels are under development for automotive applications that require high strength and simultaneous high formability. This study was undertaken to examine the phase transformations occurring during the processing of a cold-rolled TRIP steel. The TRIP microstructure is comprised of ferrite, bainite and retained austenite. This microstructure is obtained by controlled cooling from the intercritical annealing temperature to the isothermal bainitic holding temperature. The effects of cooling rate from intercritical annealing temperature to isothermal transformation temperature, as well as isothermal transformation time, were studied via optical microscopy, SEM, TEM, XRD, magnetometry, dilatometry and mechanical testing. A CCT curve for one intercritically annealed TRIP steel was produced. Conclusions are drawn regarding the effects of processing parameters on phase balance (ferrite, bainite, austenite, martensite and pearlite) and mechanical properties. Suggestions for future work are also made.

ACKNOWLEDGEMENTS

Thanks, firstly and foremost, to Dr. Ken Goldman for advice, guidance and continual good humor. Dr. Goldman is BAMPRI's greatest asset. Thanks to my thesis advisors Dr. DeArdo, Dr. Garcia, and Peter Wray, for all the help and supervision over these years. The US Steel Corporation provided funding for this research, as well as my summer 2002 research internship at the USS Research and Technology center. Also thanks to the US Steel Corporation for providing experimental equipment, advice and expertise; especially, Dr. Matt Merwin for help with the Gleeble 3500 unit, Brandon Hance for more advice on more different occasions than I can name, and the metallography group for scores and scores of samples mounted and polished. I'm especially grateful to Dr. Dennis Haezebrouck at US Steel. Without his help and advice, especially while performing my Gleeble experiments, this work would only be a shadow of its current self. Dennis, more than anyone else, provided me with the encouragement and support necessary to pursue these experiments. The Pitt-MSE graduate students all provided invaluable help over the years, especially Predrag Kisa for help with XRD. Dr. Hua also provided much help on various problems, primarily TEM and APFIM, over the years. Also, Al Stewart and Cole van Ormer provided help with SEM/XRD and TEM, respectively. Prof. Soffa and Dr. Saha provided the magnetometry experiments and access to their VSM. Finally, thanks to Dr. Nettleship for sitting on my committee.

TABLE OF CONTENTS

LIST OF TABLES

LIST OF FIGURES

1.0 INTRODUCTION

1.1 Automotive Materials

1.1.1 Strength vs Formability

The most basic paradigm of material science is that an increase in strength leads to a loss of ductility, and an increase in ductility can only be achieved through sacrifices in strength.

Sheet material for auto bodies requires both high strength and formability. High strength allows for thinner gauge material, which reduces weight and increases fuel efficiency. High strength also improves the dent resistance of a material, which is important esthetically, and improves the crash resistance of the material, important for passenger safety. Formability is necessary to create the parts. For example, a door panel must be press-formed from thin gauge sheet.

As a result, many materials have been examined by the auto industry in an attempt to strike a balance between strength and formability. These materials are microalloyed steel, interstitial-free (IF)/ultra-low carbon (ULC) steel, bake hardening (BH) steel,

aluminum, composites, dual-phase (DP) steels, and -- our subject of emphasis -- transformation-induced plasticity (TRIP) steel.

A brief review of each material, as pertains to automotive body applications, is presented in the following sections.

1.1.2 Microalloyed Steel

Microalloyed steels are low-carbon steels (<0.1 wt%) alloyed with small amounts (~0.1 wt%) of carbide-forming elements, especially niobium, titanium, and vanadium, occasionally encompassing chromium, tungsten and molybdenum[1]. This alloying, combined with controlled rolling and coiling practices, produces alloys with fine grains and subgrains, fine strain-induced precipitates of the microalloy additions with carbon or nitrogen, especially on grain/subgrain boundaries, and precipitation hardening and solid solution hardening of the ferrite[1,2,3]. These contributions, especially the extreme grain/subgrain refinement, produce improved strength and ductility.

1.1.3 Interstitial Free Steel

IF/ULC steel is similar to microalloyed steel in that it contains small additions of strong carbide forming metals, such as niobium, titanium, and vanadium. However, vacuum degassing reduces the carbon and nitrogen levels to ~30 ppm. Phosphorus is sometimes added to increase the hardness, and boron is sometimes added to counteract the detrimental effects of phosphorus[4].

IF/ULC steels, processed similarly to microalloyed steels, exhibit low-moderate strength and excellent formability[2,5].

1.1.4 Bake-Hardening Steel

BH steels are often ULC grades that are resistant to aging at room temperature, but not at slightly elevated temperature, especially after deformation[5]. Thus, the interstitials diffuse to dislocations when the paint is baked onto the formed parts at ~180°C, hardening the metal *after* the part is press-formed, providing an elegant means to avoid the strength/formability paradigm.

1.1.5 Aluminum

Aluminum is much lighter and often more ductile than steel, but softer and more expensive. As aluminum is softer, is requires a thicker gauge for a piece of given strength. Steel has a density of ~8 g/cc and yield strengths ~500-1000MPa, whereas aluminum has a density ~3g/cc but strengths of only ~20-600MPa[6]. Because aluminum is more expensive, it is typically reserved for applications where weight is of primary importance, such as aerospace. The high-strength grades of aluminum, especially, require both expensive alloying and processing. Further, because of aluminum's low strength, it will not have the crashworthiness of steel in automotive structural members.

1.1.6 Composites

Fiber-reinforced polymer composites are not press-formed, but rather "laid-up" and "cured;" that is, manufactured into shape from its constituent components, typically fibers of polymer, graphite, ceramic or boron, and a matrix of polymer resins[7]. Typical fiber-reinforced laminate composites are very strong and tremendously light, but are also fantastically expensive. Further, composites typically have no ductility. As such, they are currently restricted to applications where weight is the overriding design consideration, such as military aerospace or high-performance, exotic automobiles[8]. Many engineering composites have strengths comparable to steel, but densities of ~1-2 g/cc[(6)], about one-quarter the density of steel.

1.1.7 Dual-Phase Steels

DP steels are low carbon (~0.05-0.2%) HSLA grades that usually contain manganese, silicon and microalloying additions. DP steels are produced by intercritical annealing (producing an $\alpha+\gamma$ microstructure) and then severe cooling/quenching, resulting in a soft ferrite matrix containing hard martensite particles, and often small amounts of retained austenite or other phases[5,9]. The intercritical anneal can follow either finish rolling for hot strip product or cold rolling for CRA (cold-rolled-and-annealed) or HDG (hot-dip-galvanized) product. DP steels have both high tensile strengths and moderate total elongations, excellent for auto applications, such as cold-pressed wheel rims.

1.1.8 TRIP Steels

Zackay et al.[10] coined the term 'TRIP' when working with high-alloy steels that could be made fully austenitic at room temperature. By processing a steel, they argued, such that its M_S temperature was below room temperature and the M_d temperature above room temperature, high strength and ductility could both be obtained through the austenite-to-martensite deformation-induced transformation[10,11].

More recent TRIP steels, formally referred to as "TRIP-assisted multiphase steels," are materials that contain small volume fractions of retained austenite in a ferrite-bainite matrix, and this retained austenite improves ductility by transforming ("tripping") to martensite. Retained-austenite TRIP steels were first demonstrated by Matsumura et al.[12] in 1987. Although 1970's era dual phase steels often contained appreciable quantities of retained austenite and showed some TRIP-like effects, the term TRIP is probably best reserved to steels with deliberately introduced retained austenite, rather than the accidental retained austenite in DP steels.

1.2 Advantages of TRIP Steel

TRIP Steels are, thus, of interest to the automotive industry because of their potential for a combination of high strength and high formability at reasonable cost. The high strength will lead to excellent crash resistance, dent resistance and weight reduction.

TRIP steels have been shown to have excellent stretch-formability, and the potential for applications in other severe-forming applications, such as deep-drawing.

2.0 BACKGROUND

2.1 Basics of TRIP Steel

2.1.1 Mechanical Premise

A classical quenched and tempered steel increases its yield and tensile strengths at the price of uniform elongation[10].

Figure 1 shows the variation of yield and tensile strengths and total and uniform elongations with heat treatment in 4340 steel. As the strength increases, the elongation is reduced. Uniform elongation is of special importance in forming applications, such as auto component press-forming, but uniform elongation is sacrificed for strength improvements in quenched and tempered steel.

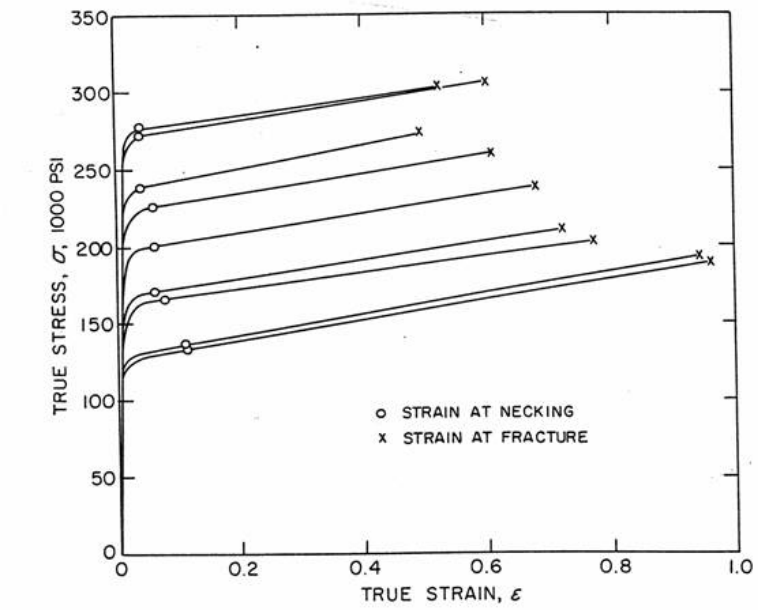

Figure 1 Variation of strength/ductility balance in quenched and tempered 4340 steel[10].
(Specific heat treatment not reported.)

Zackay et al. state, "the rate of strain hardening produced by dislocation interactions is inadequate to compensate for the increase in stress in the region of the neck[10]." This results in a lower strain to necking (uniform elongation) and a higher strain-hardening value, n.

How can this be overcome? Obstacles, harder than dislocation tangles, must be used to delay the onset of necking. Further, these obstacles must be introduced during plastic straining; if they were present in the starting material, they would simply result in an increase in the yield strength. Martensite plates, Zackay et al. decided, fulfill the first requirement, and they can be formed from austenite during plastic deformation, fulfilling the second.

When the stress in a particular region of the sample reaches a sufficiently high value, such as near the onset of necking, austenite (in a metastable-austenitic steel) or retained austenite (in a multiphase steel) will trip to martensite, increasing the local strain hardening rate and delaying necking. This process leads to a greatly improved total elongation, and the commensurate increases in ductility and formability, without sacrificing strength.

2.1.2 Processing of TRIP Steel

Modern TRIP steels come in two varieties: as-hot-rolled or cold-rolled and annealed.

As-hot-rolled-strip TRIP steels are produced by a TMP path similar to that shown in Figure 2[5,13,14,15].

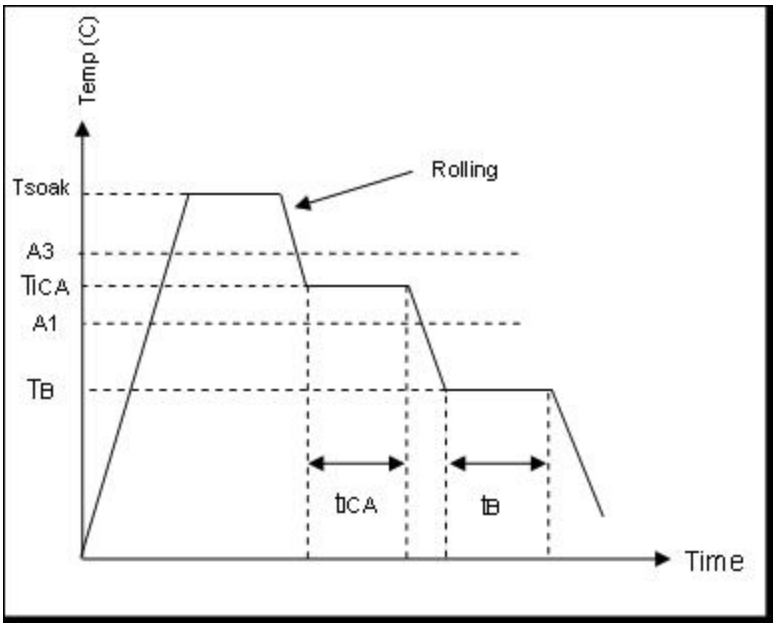

Figure 2 Hot-band TRIP steel processing path

First, slabs are reheated and soaked at some temperature T_{SOAK}, well into the austenite regime, followed by roughing and finishing deformation at decreasing temperature. Then, the material is intercritically annealed at T_{ICA} ($A_1 < T_{ICA} < A_3$) for some time t_{ICA}, and then rapidly cooled to a temperature T_{IBT} ~300-500°C ($M_S < T_{IBT} << A_1$) for the isothermal bainitic transformation, IBT. During the rapid cool from T_{ICA} to T_{IBT}, it is hoped that little of the austenite transforms to ferrite or pearlite[5,13,14,15]. The material is coiled at or near this IBT temperature, resulting in isothermal or near-isothermal holding for some time, t_{IBT}.

Figure 3 shows this processing path superimposed on a TTT curve for these steels[5]. At T_{IBT}, much of this retained austenite transforms to bainitic ferrite (preferably) or bainite (undesirably). The coil is then cooled to room temperature, and some of the austenite is still retained, leading to a complex microstructure consisting of intercritical ferrite, epitaxial ferrite, bainite/bainitic ferrite, retained austenite, and perhaps small amounts of pearlite or martensite[5,15,16,17,18].

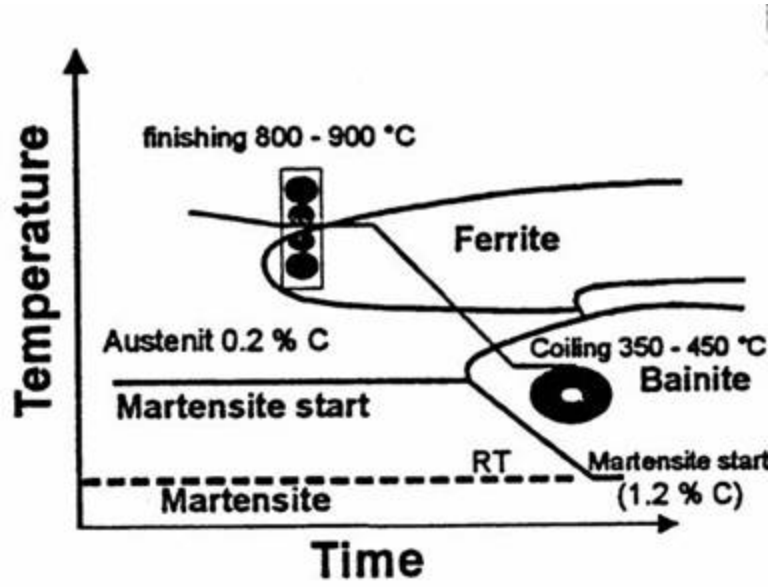

Figure 3 Hot-band TRIP processing path superimposed on a TRIP steel TTT curve[5]

TRIP steel strips are less common than sheets. For the more common sheet material, processing is by continuous annealing line (CAL) or continuous hot-dip galvanizing/ galvannealing line (CGL). The processing path is similar to Figure 4: the material is hot-rolled in the austenite range, then cooled to room temperature (resulting in a ferrite + pearlite structure). The material is cold-rolled at this point. Then, the steel is reheated in the CAL/CGL to T_{ICA}. During this intercritical anneal, the pearlite formed after hot rolling will dissolve, forming austenite, assuming t_{ICA} is sufficiently long (>~30-60 seconds). This results in an $\alpha+\gamma$ intercritical structure, which is then cooled rapidly (to avoid pearlite or excessive epitaxial ferrite formation) and subjected to the isothermal bainite hold at T_{IBT}. This processing path can be realized through the use of continuous annealing lines or hot-dip galvanizing lines that contain a proper section for performing the isothermal bainite transformation[19,20]. Recent work[21,22] has indicated the possibility -- it is not yet generally accepted nor proven -- that properly designed TRIP steels may

not need an isothermal bainitic hold, and may be processed in conventional hot-dipping lines. This possibility was studied in this work, see Section 5.3.1.

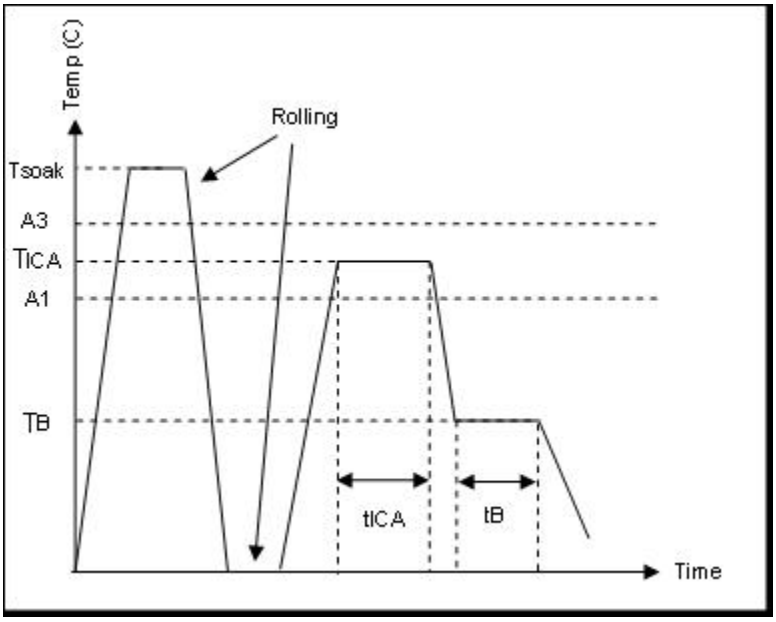

Figure 4 TRIP steel sheet processing path

2.2 Fundamental Behavior

2.2.1 Intercritical Anneal

During the intercritical anneal, austenite will form and carbide will dissolve, producing an $\alpha+\gamma$ structure. As such, the ferrite will have a low carbon content C_α; typically <0.02wt%. The austenite will be correspondingly enriched in carbon. In hot-rolled material, this enrichment is due to solute rejection from the newly formed ferrite. In cold rolled and intercritically annealed material, the austenite will nucleate at ferrite/cementite boundaries and dissolve the cementite, resulting in carbon enrichment.

Carbon is the most powerful austenite-stabilizing element; consider Figure 5 and Figure 6[23]. Figure 5 shows the depression of M_S temperature with carbon content; Figure 6 shows how the amount of retained austenite can increase with carbon content.

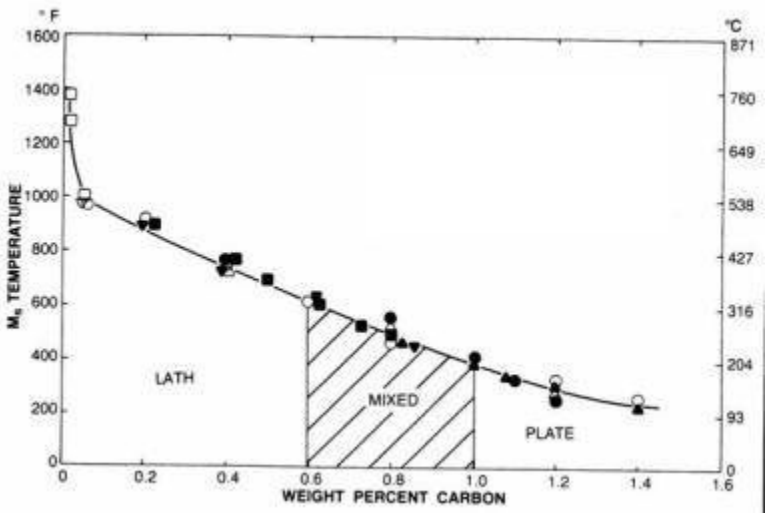

Figure 5 Variation of martensite start temperature and martensite morphology with carbon content[23]

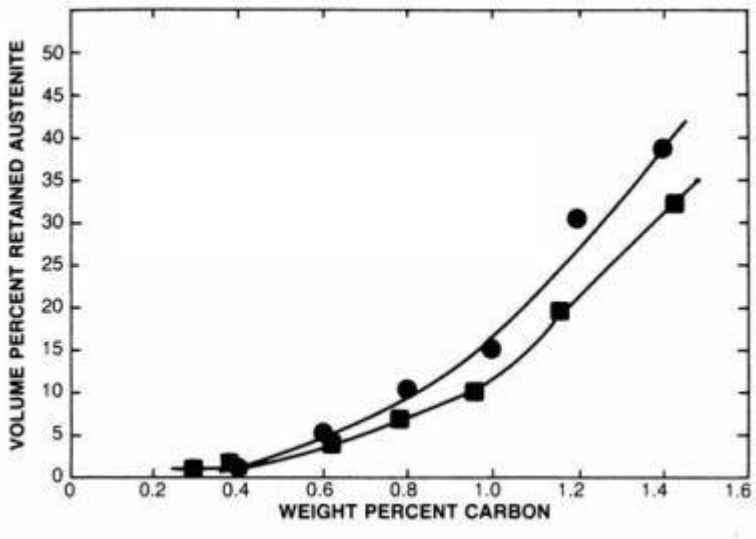

Figure 6 Variation of retained austenite with carbon content[23]

For example, the equation of Sverdlin and Ness[24] for M_S is:

$$M_s\left(^oC\right) = 520 - 320\,C - 50\,Mn - 30\,Cr - 20\left(Ni + Mo\right) - 5\left(Cu + Si\right) \qquad (2\text{-}1)$$

where the symbols C, Mn, etc. represent the weight percent of the particular element. Carbon, with a coefficient of -320°C/wt%, most strongly depresses the martensite start temperature. As such, the carbon concentration of austenite during the intercritical anneal is of paramount importance in increasing the stability of the austenite in dual-phase steels that contain retained austenite[25]. In TRIP-type steels, the segregation of carbon during the isothermal bainitic transformation is the dominant factor.

Thus, the temperature of the intercritical anneal will determine -- at least in part -- the volume fraction of austenite before the cooling cycle, as well as its carbon content, size, texture, etc., and thus, stability.

2.2.2 Behavior during Cooling/Holding

During the bainitic transformation, unstable intercritical austenite transforms into various products, such as ferrite ("epitaxial ferrite," as opposed to "intercritical ferrite"), bainite/bainitic ferrite and retained austenite[16]. Chen et al.[16], using TEM, observed structures such as seen in Figure 7, where different phases are observed: TF, epitaxial ferrite ("transformed ferrite" in their terminology); B, bainite/bainitic ferrite; and γ_R, retained austenite.

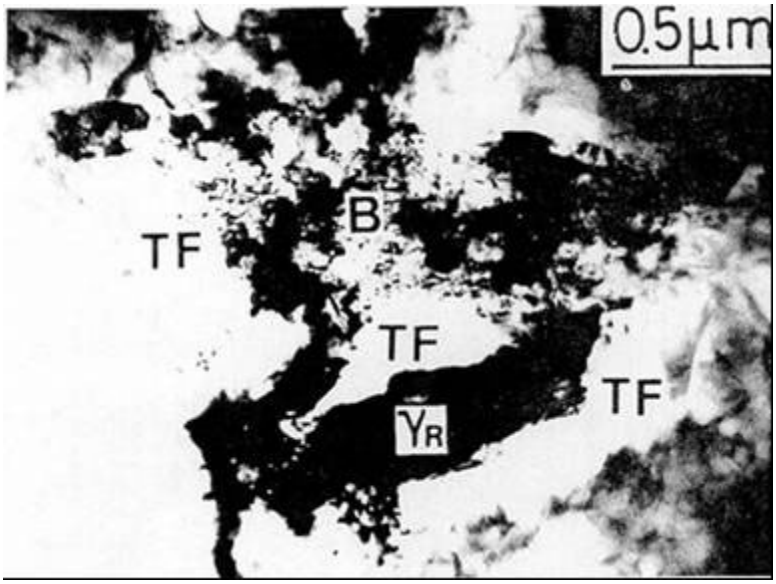

Figure 7 BF-TEM micrograph of phases present in a typical TRIP steel[16]

In Figure 8[(16)], this process is schematically illustrated. In Figure 8a, ferrite and austenite grains are present ($\alpha+\gamma$) during the intercritical anneal. In Figure 8b, parts of the austenite have transformed to epitaxial ferrite, TF, during the bainitic isothermal hold. The carbon content of the austenite is uneven, as shown by the darker color of the γ field in Figure 8b, due to carbon rejected into the austenite from the transformed ferrite. In Figure 8c, some of the austenite has transformed to bainite B, and areas of retained austenite γ_R are now stable, due to further enrichment as carbon is rejected from the bainite during transformation.

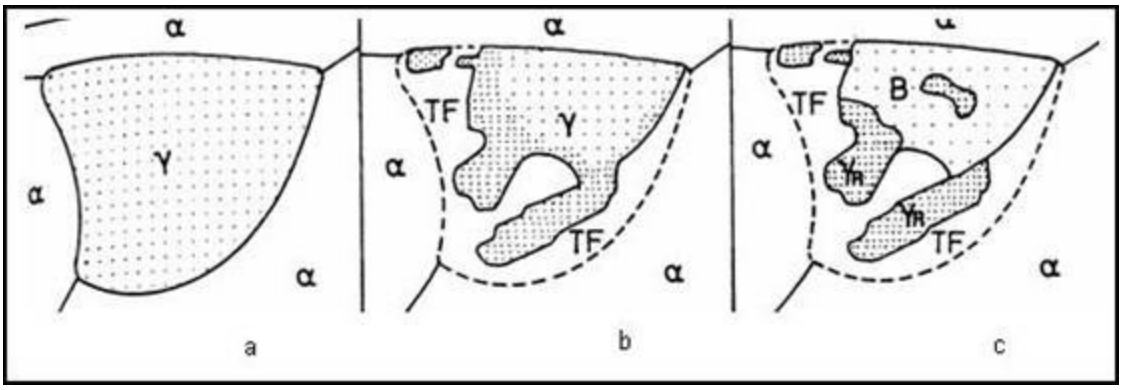

Figure 8 Schematic illustration of transformations during the IBT[16]

Jacques et al.[17], using a 0.18C-0.39Si-1.33Mn steel, estimated that at an intercritical anneal temperature of 780°C, their material would be 75% austenite, the austenite containing 0.24wt% C, and an M_S of 400°C. At T_{ICA}=730°C, they estimated 25% austenite at 0.72wt% C and M_S=200°C. These estimates, especially ΔM_S, demonstrate the importance of controlling carbon segregation.

2.3 Alloying Effects

2.3.1 Alloying Elements Introduction

Figure 9, from Bleck[28], summarizes the processing effects of major alloying elements.

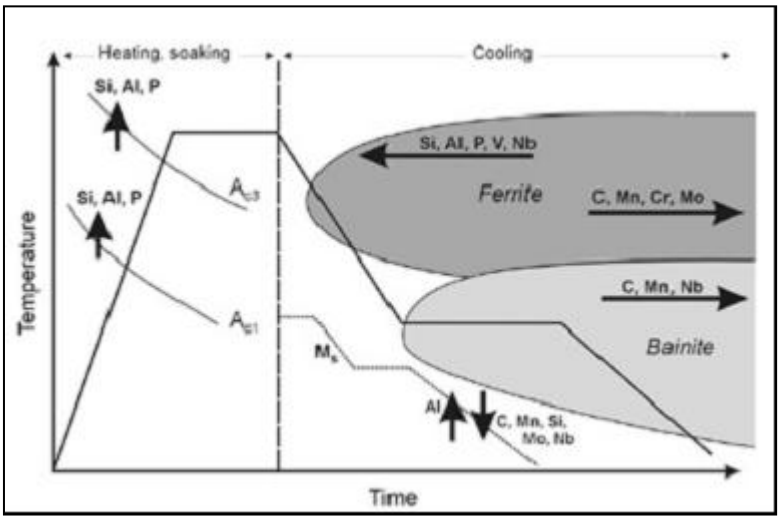

Figure 9 Effects of alloying elements[28]

Major alloying elements (Al, Si, P, Mn) have been well studied; some secondary elements (Cu, Cr, Mo, V, Nb) have also been studied. The author has found no literature relating to Co, Ti or W.

2.3.2 Manganese

Manganese is, first and foremost, an austenite stabilizing element. In equation 2-1, manganese has an M_S depressing coefficient of –50°C/wt%, the highest of the

substitutional elements. Hadfield's Steel, for example, contains 12wt% manganese and can be made austenitic at room temperature[26]. Large additions of manganese are used in most TRIP steels, ~1.5-2.5wt%[17]. Because of manganese's propensity for stabilizing austenite, it contributes to the volume fraction of retained austenite (f_γ).

Manganese is attractive economically, as it is relatively cheap, and can depress the two-phase field, and thus the intercritical temperatures, into the range of conventional annealing equipment[27].

Manganese increases carbon solubility in austenite, allowing for further enrichment, and slows the pearlite reaction, which allows for a wider range of cooling rates; however, excessive levels of manganese can promote carbide precipitation in the austenite[28]. Manganese, especially in conjunction with silicon, can affect the steel's surface chemistry and make hot-dip coating impossible[21,22]

2.3.3 Silicon

Silicon is not an austenite-stabilizing element; in fact, it raises the ferrite-austenite eutectoid temperature and significantly reduces the activity of carbon in ferrite[29]. However, it is usually added to TRIP steels, typically ~1.5-2.5wt%[17], and increases in silicon content lead to an increase in f_γ[15,16]. For example, Figure 10 shows f_γ curves for materials containing two different levels of silicon.

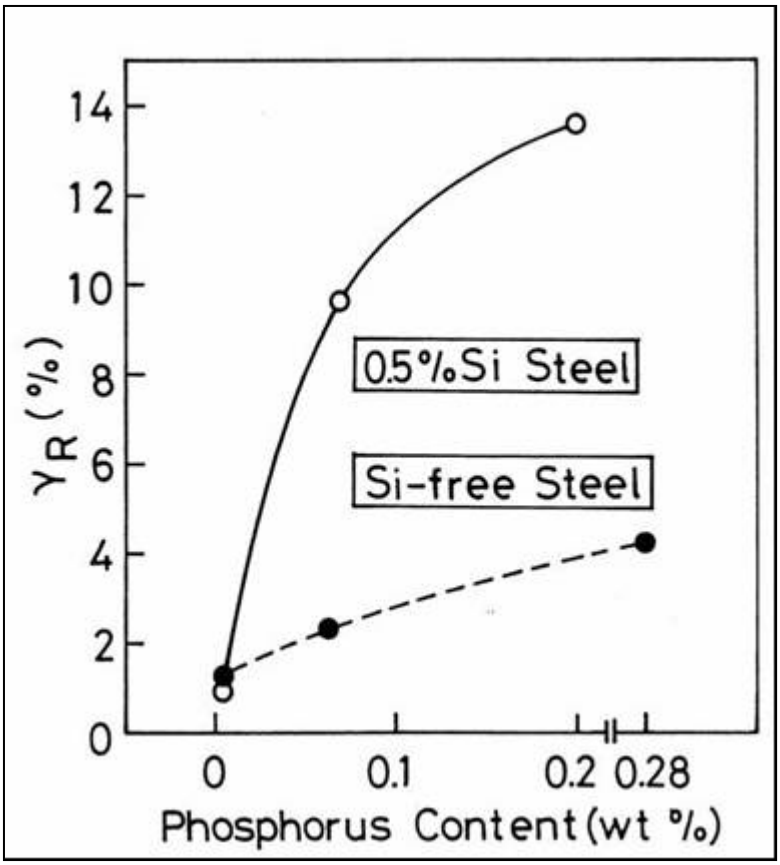

Figure 10 Effects of silicon and phosphorus on retained austenite content[16]

So, why is an element that does not stabilize austenite used to increase f_γ? Silicon slows the precipitation of carbides, especially cementite[30,31,32]. Silicon has a very low solubility in cementite; thus, high-silicon steel would be an inhospitable environment to cementite[30,33]. This leaves more carbon available for enrichment (and consequential stabilization) of the austenite. A study performed on a 2Si-0.60C steel showed no carbide precipitation, even after several hours at the isothermal transformation temperature[33].

One study[17] showed that lower silicon contents (0.39wt%) can produce reasonable f_γ values (just below 10%) if the bainite transformation is tightly controlled; this will be discussed in more detail later (Section 2.5.5).

Silicon, however, has a number of detrimental effects that will be discussed in section 2.5.6.

2.3.4 Phosphorus

Chen et al.[16] performed their study to determine the effects of phosphorus on TRIP steel. They found increases in phosphorus increased the f_γ, especially in the presence of silicon (Figure 10). They attribute this to several different, simultaneous processes.

First, phosphorus, like silicon, inhibits the formation of carbides, leaving more carbon in solution for segregation to austenite. Fewer carbides were observed in the phosphorus-steel than the non-phosphorus-steel in their study.

They estimated that the austenite did not have sufficient chemical partitioning to be stabilized to room temperature, and suggested that "matrix constraints" prevented the transformation to martensite. Because phosphorus is a strong solid-solution hardening element, they suggested that it increased these constraints, and thus increased the austenite retention. (These mechanical effects on stabilization will be discussed later, section 2.4.4.)

Although phosphorus causes cold work embrittlement in low and ultra-low carbon steels, this is not expected to be an issue in TRIP-type steels, as the carbon content is usually in excess of 0.1 wt%[20,34].

Bleck[28] contends that phosphorus will only be useful as a carbide inhibitor in conjunction with silicon or aluminum.

2.3.5 Aluminum

Aluminum behaves in a manner similar to silicon; that is, it slows the precipitation of carbides[28,30,33]. Recent studies have shown that although aluminum or aluminum + phosphorus may be substituted for all or part of the silicon in a TRIP steel[18,34], other studies disagree. This will be discussed in section 2.5.6. GDOES data indicates that aluminum does not segregate to the surface as silicon does, and as a result, Al-bearing TRIP steels were found to be galvanizable, where Si-based TRIP steels were not[21,22].

2.3.6 Niobium

Hanzaki et al.[13,14,35] studied a TRIP steel microalloyed with niobium, specifically 0.22C-1.55Si-1.55Mn-0.035Nb-0.028Al, and compared it to the same steel, minus the niobium addition. Although the thrust of these three studies pertained to TMP, and will be discussed later, several niobium-related effects can be listed.

First, the austenite in the microalloyed silicon-manganese TRIP steel has a higher tendency to be stabilized, compared to the niobium-free material[13].

Second, under TMP conditions that maximize the Nb(C,N) precipitate content, f_γ is at its lowest. This is attributed to the loss of [Nb] in solution[14,35]. (The author estimated this f_γ loss is <u>not</u> due to the loss of [C] to the precipitates: at 0.035wt% niobium bulk, the loss of carbon if *all* niobium is in the form of NbC would be only ≈0.005% overall, a negligible amount, compared to the 0.22% bulk.)

Niobium is observed to increase the f_γ; niobium is a powerful solid solution hardener, and may result in mechanical stabilization of the small austenite particles[13,14,35].

Niobium also slows ferrite and pearlite formation, leaving more austenite available for retention, and depresses the bainite transformation temperature. Further, [Nb] is preferred to Nb(C,N) as the precipitates will act as nucleation sites that will increase transformation kinetics, especially that of pearlite, reducing the carbon available for retention[14].

2.3.7 Molybdenum

Bleck[28] notes that molybdenum thermodynamically favors the formation of carbides, but that kinetically, it is found to slow carbide precipitation. Jiao et al.[36] added molybdenum to slow the formation of Nb(C,N) in their steel. Mintz[20] notes that molybdenum allows

the use of slower cooling rates, as molybdenum decreases the critical cooling rate for the bainite transformation and it suppresses the formation of pearlite.

2.3.8 Copper

The effects of copper on general processing and properties of steel are summarized in their own section, 2.8, but a few points specific to TRIP steels can be summarized here.

A number of studies examined the effects of copper additions to TRIP steel, often in combination with chromium and nickel, as these three elements are common tramp elements in any recycled steel and nearly unavoidable if a heat contains any re-melt.

Primarily, copper slows the precipitation of carbides in a manner like silicon or aluminum[37,38]. It is also a potent solid-solution hardener and precipitation hardener, and promotes corrosion resistance. Also, as an austenite stabilizer, it will behave in a manner qualitatively similar (though quantitatively less in magnitude) to manganese. The presence of copper precipitates should make the nucleation of austenite easier.

2.3.9 Nickel

Nickel has been studied in TRIP steels only in addition to copper, as nickel reduces the detrimental effects of copper on surface quality. Nickel is an austenite stabilizer and behaves in a manner similar to manganese, but with effects of lesser magnitude.

2.3.10 Chromium

Kim et al.[39], in a study of tramp elements on steel properties, prepared 0.15C-1.5Mn-1.5Si-0.5Cu steels with additions of either 0.4Cr, 0.4Ni, or 0.4Cr-0.4Ni. They found that the Cr-added steels had significantly higher tensile strengths (1000-1100MPa) with only slightly reduced elongation (15-25%) in comparison to the non-Cr steels. Likely, chromium's effect is to increase the hardenability of the intercritical austenite and prevent its conversion to ferrite during cooling, leading to a larger bainite fraction, and to slow the bainite reaction, leading to some martensite in the final structure. As the Cr-steels showed no yield-point elongation, which the non-Cr-steels did show, it seems that the material is similar to DP steel (which shows no YPE). However, the Cr-steels had superior elongations to DP steels of similar strengths, indicating a TRIP effect is also at play.

Mishra and Jha[40] and Jha and Jha[41] studied V- and Cr-added trip steels. They found that chromium promoted an acicular ferrite, but lead to massive (rather than inter-lath-film) type retained austenite, with inferior stability in comparison to the V-steel

2.3.11 Vanadium

Mishra and Jha[40] and Jha and Jha[41] showed that the V-added steel had superior austenite stability to the Cr-added steel. Using TEM, they attributed this to the inter-lath-film character of the retained austenite in the V-steel. However, the V steel contained twice as much carbon as the Cr-steel, which they neglected to account for.

2.4 Austenite Stability

2.4.1 Fundamental Considerations

The most straightforward manner to quantify austenite stability is through the M_S temperature -- a lower M_S denotes more stable austenite. This, and stability in general, will be affected by austenite size, composition, morphology, texture and surrounding phases.

A compressive hydrostatic pressure results in a reduction of the A_3 and M_S temperatures in iron alloys[42]; this is because the $\gamma \rightarrow \alpha$ and $\gamma \rightarrow \alpha'$ transformations involve a volume expansion. Similarly, a tensile stress increases the transformation temperature: applying a tensile stress to a sample at a temperature just above M_S will result in transformation; also, a shear stress can cause transformation in the temperature regime just above M_S[42]. This temperature, the temperature below which

stress-induced martensite can form, is called M_d ($M_S < M_d$). Recent computer modeling of TRIP steels found that hydrostatic pressure cannot cause retained austenite to trip, compression causes only weak tripping, shear moderately destabilizes the austenite, tension severely destabilizes the austenite, and biaxial tension causes the most destabilization[43,44].

Tamura and Wayman[45] observe that martensite morphology and the difference between M_S and M_d appear related to austenite stacking-fault energy.

2.4.2 Effect of deformation Temperature

Consider Figure 11[(42)] and Figure 12[(45)], in which TRIP steels were tested at different temperatures; importantly, the maximum elongations occur at temperatures between M_S and M_d. Nishiyama[42] lists three contributions to this behavior.

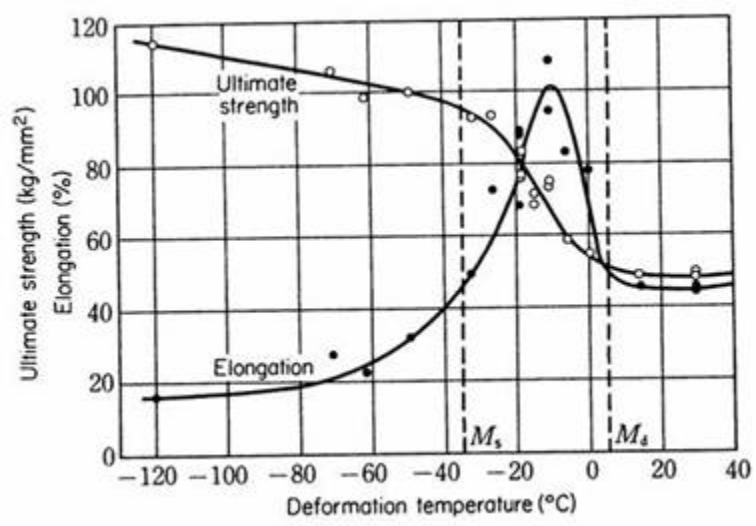

Figure 11 Effect of deformation temperature on strength and ductility[42]

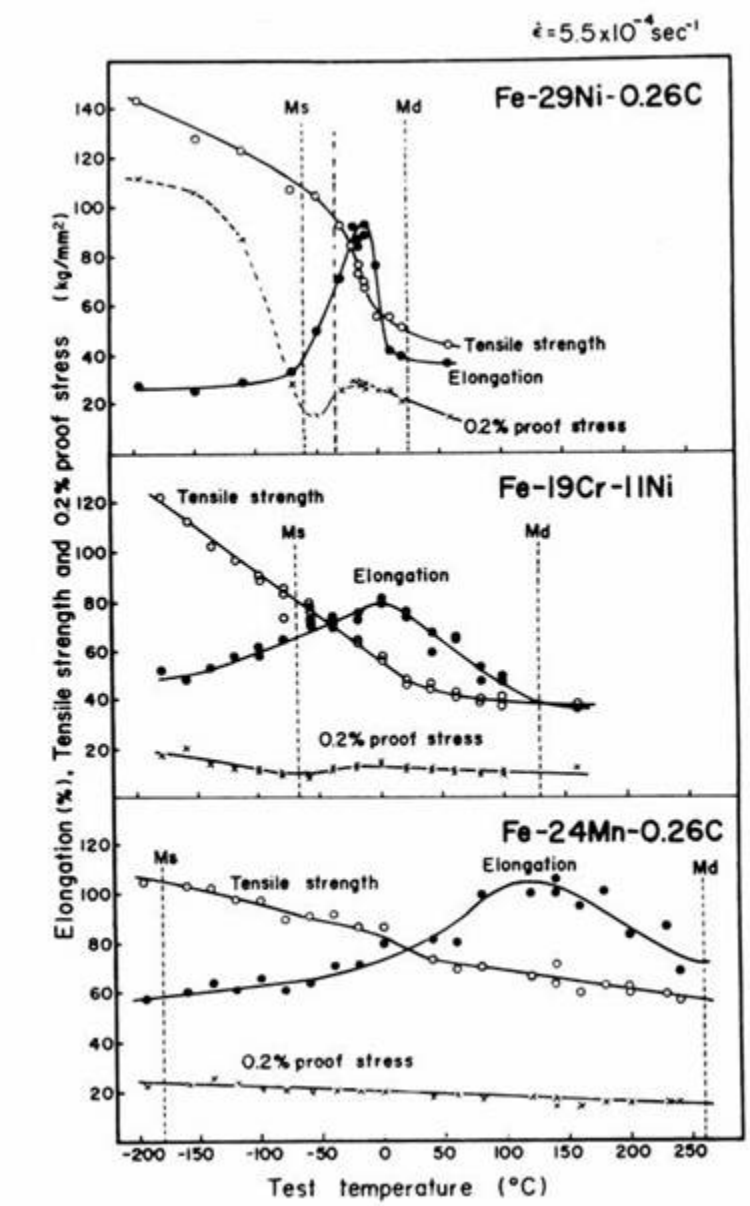

Figure 12 Effect of deformation temperature on strength and ductility[45]

First: near or below M_S, the chemical driving force is very high and randomized variants of martensite easily form, which do not greatly benefit elongation. However, nearer M_d (under lower driving force conditions) variants in the direction of stress will form preferentially, which *does* improve ductility.

Second: the suppression of necking discussed in section 2.1.1, inherent to TRIP steels in the range M_S to M_d.

Third: microcrack initiation and propagation will be suppressed by stress relaxation by the formation of the strain-induced martensites.

At deformation above M_d, the TRIP effect will not be manifested; below M_S, the presence of martensite before straining will deleteriously affect ductility.

2.4.3 Effect of Strain Rate

The metallurgical community has not yet determined the effects strain rate alone has on the TRIP effect, although empirical crashworthiness studies -- which necessarily include strain rate -- will be discussed in section 2.6.5. Unfortunately, in these studies, adiabatic heating dominates any pure effect of strain rate.

2.4.4 Effect of Austenite Morphology

The size and arrangement of the retained austenite particles in steel can move the M_S temperature by several hundred degrees. Rigsbee and VanderArend[46] and Rigsbee[47], using dual-phase steels, produced structures containing some retained austenite, in addition to martensite. The austenite particles were on the order of 1 micron in size. They found that after cryogenic treatment of the samples to –269°C, the austenite did not convert to martensite. However, assuming complete partitioning of the carbon to

the austenite and "significant" partitioning of the manganese, the calculated M_S was still above 0°C. Of course, total partitioning of carbon is not possible (due to carbide formation and the solubility of carbon in the other phases); further, significant partitioning of the manganese is unlikely due to the slow diffusion of this substitutional element. So, by chemical effects alone, M_S should be higher than 0°C.

The question remains: why should a small austenite particle be more stable than a large particle? Rigsbee and VanderArend[46] list several possible reasons. First, a sufficiently small particle might not contain an effective martensite nucleation site. Cech and Turnbull[48] examined an Fe-23Ni-3.7Mn high-alloy steel, and found that a powder of 30-100μm particles underwent a –176°C depression of M_S as compared to the bulk material. Figure 13[(48)] shows the variation of percent martensite-vs-quench temperature for particles of different sizes. For a given percent martensite, the smaller particles require a quench to lower temperature.

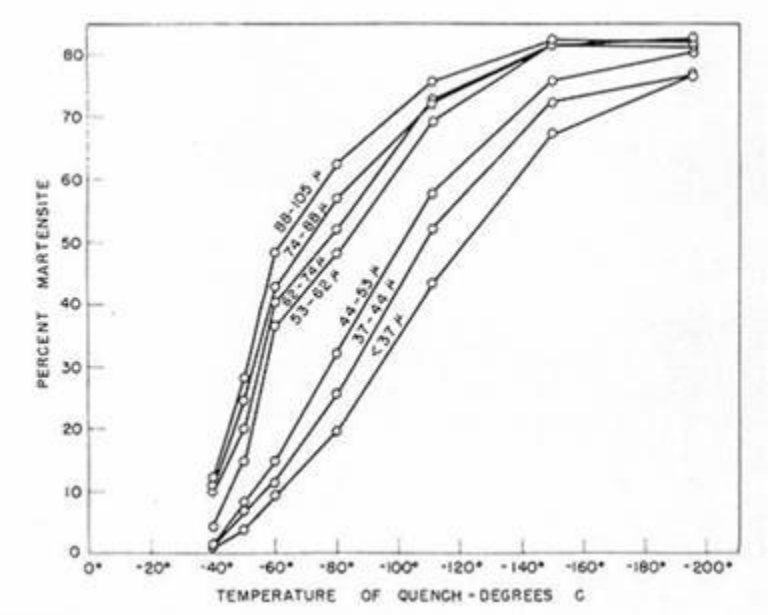

Figure 13 Martensite fraction-vs-quench temperature for various particle sizes[48]

Cech and Turnbull also found that the relative number of particles that underwent transformation was proportional to the diameter raised to the power of 2 or 3, depending on temperature. Figure 14[(48)] shows this dependence. Further, when transformation was finally initiated in a particle, it transforms to a volume fraction of martensite characteristic to all transformed particles at that temperature.

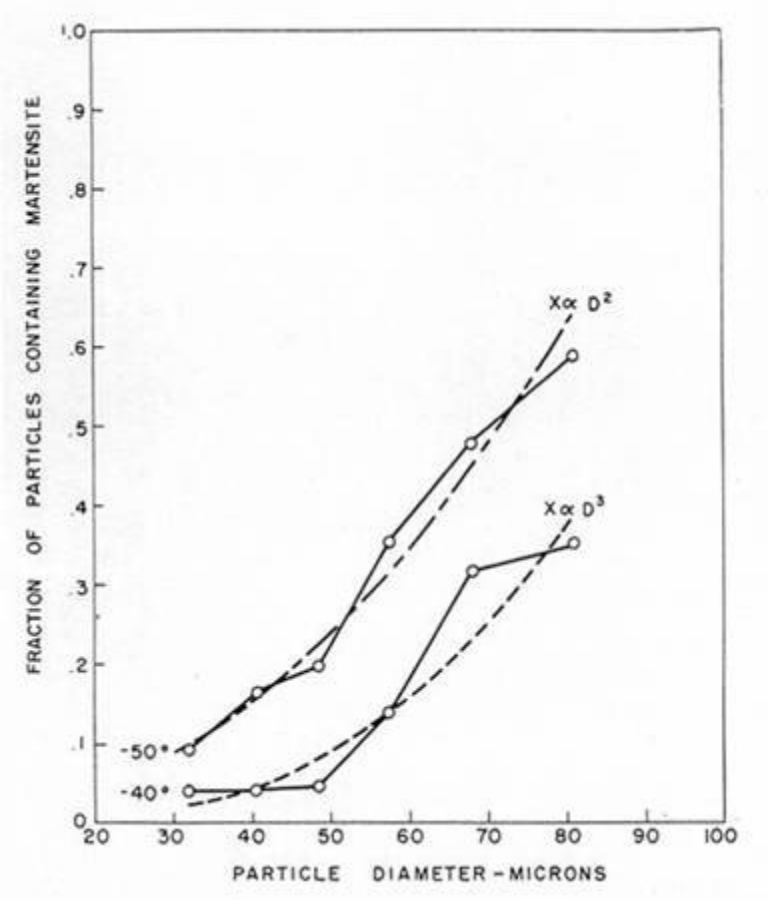

Figure 14 Transformation-vs-particle diameter[48]

As Magee[49] summarized the results of Cech and Turnbull[48]:

> "This is one of the clearest experimental demonstrations of the heterogeneous nature of martensite nucleation: as a given volume of austenite is divided into disconnected regions, one can isolate regions which do not contain an effective nucleation site."

(Finer powder would increase the surface area to volume ratio of the particles; yet, this does not seem to affect the transformation as the smaller volume does.)

Second, Rigsbee and VanderArend[46] said, when an austenite particle does contain possible heterogeneous nucleation sites, the transformation may be arrested by "matrix constraints." Figure 15[(46)], from Rigsbee and VanderArend, is a TEM micrograph (Figure 15a: bright field; Figure 15b: dark field) of an austenite particle that contains stacking faults, which are potent martensite nucleation sites. They suggest that the austenite is stabilized by the constraints imposed upon it by the partially coherent α/γ interface.

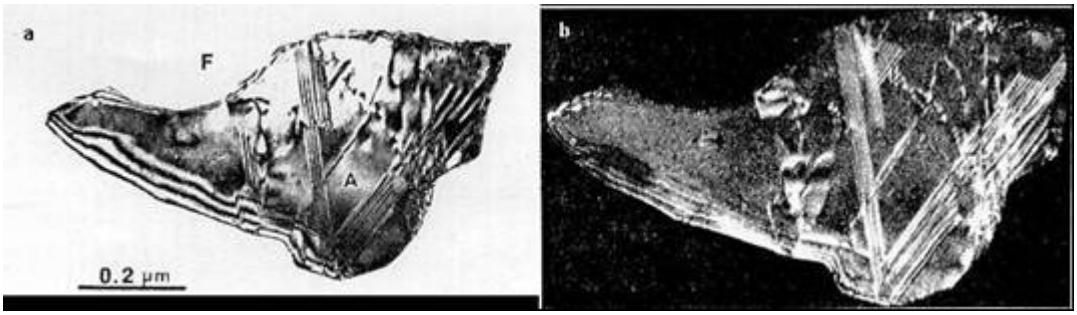

Figure 15 (a) BF-TEM and (b) DF-TEM of untransformed retained austenite. Note stacking faults[46]

These restraints seem to have two primary, interrelated, causes: hydrostatic pressure and resistance to deformation. As discussed in 3.2.1, a hydrostatic stress will depress the M_S temperature of a particle, resulting in stabilization to a lower temperature.

An example: Sugimoto et al.[50] processed a 0.17C-1.41Si-2.00Mn steel to produce three different retained austenite morphologies. "Type I" produced austenite islands in ferrite matrix, "type II" produced narrow austenite films along bainite lath boundaries and "type III" produced acicular austenite islands in a ferritic matrix.

The type II steel exhibited poor mechanical properties, especially elongations, as compared to the other two types. They attribute this to a high hydrostatic pressure being exerted on the retained austenite films in the type II steels.

The transformation of austenite to martensite results in a volume expansion. This volume expansion is[51,52] (for $T=M_S$):

$$\left(\frac{\Delta V_{\gamma\to\alpha'}}{V_\gamma}\right) = 0.017 + 0.013[C]_\gamma \qquad (2\text{-}2)$$

The martensite will form into different variants, and lattice invariant deformation[53] will result in an approximately isotropic expansion of the austenite upon transformation. As this expansion will be reasonably isotropic, the transformation strain ε^* is assumed to be one-third of $(\Delta V_{\gamma\to\alpha'})/(V_\gamma)$, therefore $\varepsilon^*=0.0058+0.0045[C]_\gamma$.

Using a transformation strain ε^* for the martensite reaction, they calculated the hydrostatic pressure as[50,51]:

$$\sigma_P = \frac{2}{3}\left(Y_0 + 2H_0\varepsilon^*\right) + \frac{2}{3}Y_0 \ln\left(\frac{E\varepsilon^*}{(1-\upsilon)Y_0}\right) \qquad (2\text{-}3)$$

where σ_P is the hydrostatic pressure, Y_O, H_O are the yield stress and strain hardening rate of the phase surrounding the austenite; E, υ are the modulus and Poisson's ratio. They calculated σ_P~900 MPa for their type I and III steels, but σ_P~1560 MPa for the type II steel, because of the film-like character of the austenite and the stiffness of the

surrounding bainite. Radcliffe and Schatz[50,54] estimated each 100 MPa increment of σ_P results in a 6°C reduction of M_S. In this case, ΔM_S ~ -40°C for type II, merely due to applied stress. Thus, the stiffness of the surrounding matrix resists this volume expansion and inhibits transformation by depressing M_S. Un-transformable films of retained austenite have been observed[55].

When also accounting for compositional differences, Sugimoto et al. estimated the type II M_S at 70-110°C lower than the other materials. (Naturally, as M_S is depressed, so will M_d.) As a result, the retained austenite in the type II steel will be overly stable, resulting in the poor observed elongations. The steel is not a TRIP-steel, despite its large fraction of retained austenite.

Why should hydrostatic pressure, resulting from the surrounding phases, affect the austenite so profoundly? First, the hydrostatic pressure will compress the atoms, and thus their atomic orbitals, modifying their transformation behavior and lowering M_S[42].

More importantly, the martensitic transformation is a shear transformation, and this back-stress makes the shearing of the particle inherent in the transformation more difficult. As a result, the transformation is suppressed to lower M_S. That is, a higher driving force (proportional to undercooling) is required to overcome the imposed stress by shearing. Similarly, a harder matrix will suppress the transformation (Y_0 functional dependence of equation 2-3), as the harder matrix is more difficult for the transforming particle to deform.

Rigsbee[47] also notes more possible reasons for this inhibition. TEM examination showed the ferrite/retained austenite interfaces to be faceted, which implies semi-coherency. Computer modeling[56] and TEM[57] studies by Rigsbee and Aaronson showed that a semi-coherent FCC/BCC interface would mechanically constrain the particle, as the interface would be incapable of the inhomogeneous shear-type lattice invariant deformation necessary for a martensitic transformation; the only remaining option would be LID by motion of glissile dislocations, and the misfit-accommodating dislocations in the interface would not be mobile in a direction normal to the interface (**b** is in the interface plane, not normal to the interface), which pins the interface.

2.4.5 Response to Strain

Sugimoto et al.[58] strained a TRIP steel to various degrees at different temperatures and examined the resulting microstructures via TEM and SEM. At low deformation temperatures (27°C), the coarse retained austenite islands often contained twinned α' martensite. By using SAD, they determined that these martensite-austenite particles obeyed the Kurdjumov-Sachs relationship. The untransformed retained austenite contained many dislocations. Similar behavior was noted in this study, see Section 5.1.3.

At higher temperatures (150°C), they found that the strain-induced martensite content was much lower, whereas the retained austenite contained deformation twins, which were not observed at 27°C.

After 350°C deformation, the samples contained what Sugimoto et al. described as "strain-induced bainite" in prior-austenite islands. The remaining austenite contained many twins. Sugimoto e al. did not describe any "B_s" or "B_D" phenomena, which presumably exist.

2.5 Effects of Processing

2.5.1 Introduction

Many empirical studies of the effects of processing parameters on the final properties of TRIP steels have been performed, and will be reviewed here.

It is important to keep in mind the different processing involved in either hot-band or cold-rolled and annealed TRIP-steels.

2.5.2 Effect of Hot Deformation/TMP

Hanzaki et al.[13,14,35] studied the effects of different TMP paths on the final properties of two TRIP steels, one containing niobium, one without (2.3.6). First, steels were processed by soaking in the austenite regime and then deforming to various degrees, intercritical annealing, isothermal bainitic transformation, and cooling to room

temperature. The hot deformation consisted of strain ε=0, ε=0.3 or a double hit of two ε=0.3 passes.

This resulted in materials of varying austenite grain sizes, where the materials that received more deformation had a finer austenite grain structure. In the niobium steel, the largest austenite grain size gave the highest volume fraction of retained austenite and the highest total elongation. In the base steel, volume fraction of retained austenite decreased with increasing austenite grain size, and total elongation peaked at the middle grain size. (For summary, see Table I).

Table I Effects of hot deformation[13,14,35]

	Nb Steel			Base Steel		
ε (HOT)	Grain size (μm)	VRA Vol%	TEL %	Grain size (μm)	VRA Vol%	TEL %
0	230	12.1	40	350	5.1	48
0.3	70	9.9	---	80	6.5	51
0.3+0.3	40	9.5	37	45	7.1	43

For the base steel, they attributed this to a number of properties of bainite that depend on grain size. First, finer austenite grains result in finer bainite packets; second, a coarser austenite results in slower bainite nucleation. However, as discussed below, many recent studies show that deformation below the austenite recrystallization-stop temperature favors ferrite growth at the expense of bainite. Fine bainite packets result in finer retained austenite, which results in more stable austenite. Slower bainite

kinetics more slowly enriches the austenite in carbon, leaving it to transform to lower bainite or martensite on cooling to room temperature.

The niobium-steel follows the opposite trend due to the presence of niobium. The niobium in solution increases the f_γ due to solid solution hardening and other factors discussed in section 2.3.6. The unstrained austenite (largest grain size) also had the highest $[Nb]_\gamma$, as prestraining results in strain-induced acceleration of Nb(C,N) precipitation, reducing the niobium available for solid solution hardening and the other austenite-retaining effects discussed above.

Hanzaki et al.[14] also varied the deformation finishing temperature T_{FINISH}. Both steels were strained at temperatures of 1050°C and 1000°C; the base steel showed the same f_γ at both temperatures, and a slightly longer TEL to 1050°C. The niobium-steel demonstrated a much higher f_γ at 1050 than 1000°C, and slightly higher TEL (Table II). The variation of f_γ is attributed to the presence of pearlite in samples strained at 1000°C and the increased Nb(C,N) precipitation at the lower temperature.

Hanzaki et al.[35] varied the strain rates of their deformation to obtain both statically and dynamically recrystallized samples. Samples were strained at two temperatures, 1000°C and 1050°C, and the second hit of the double hit tests were performed at $d\varepsilon/dt$ =0.1/sec (static recrystallization) or at $d\varepsilon/dt$=0.001/sec (dynamic recrystallization). In the niobium steel, the lower deformation temperature for both strain rates produced a lower f_γ. At 1050°C, both strain rates gave the same f_γ=9.5%, and the dynamic process

gave slightly higher f_γ at 1000°C. They suggest that the dynamically recrystallized dislocation substructure will be more prone to the retention of austenite, but not why. This is likely due to a lower magnitude of precipitation.

Studies on dual-phase steels -- reviewed in section 2.7 -- have unequivocally proven that a refined structure leads to better work hardening. Both similar and dissimilar trends have been observed for TRIP steels.

Godet et al.[59] have shown that larger hot deformations in the intercritical region of a hot-band TRIP steel resulted in fantastically better mechanical properties. Samples given a deformation pass of ε=0.7 in the intercritical regime reached a strain hardening parameter, n, of 0.28 during subsequent tensile tests, whereas samples undeformed below the austenite no-recrystallization temperature only reached n=0.20. Additionally, the heavily deformed material had a higher tensile strength in addition to its better strain hardening and a longer total elongation. Interestingly, both steels exhibited nearly the same value of $f\gamma$. (Values of 9.3-vs-9.8% $f\gamma$ were measured, and the 0.5% difference is less than the typically quoted value of $\pm$1-2% for the accuracy of X-ray diffraction measurements; see Section 5.1.1.) This improvement in properties seems entirely due to microstructural refinement. Godet et al. noted the same behavior for a medium-carbon TRIP steel deformed in the fully austenitic, non-recrystallization, regime.

Tsukatani et al.[15] studied a number of TRIP steels of varying silicon and manganese content, but without microalloying, and found that a lower finishing temperature resulted

in a higher f_γ. This finishing deformation was performed at lower temperatures than those used by Hanzaki et al., ~750-860°C.

Basuki and Aernoudt[60] found intercritical deformation reduced the volume fraction of bainite while increasing the volume fractions of ferrite and retained austenite, refining the retained austenite, and increasing the carbon content of retained austenite -- a spectacular result for ductility. However, a decrease in bainite fraction will probably result in steel with a lower strength level. This is attributed to increased defect density in the austenite favoring rapid nucleation and growth of ferrite.

Using deformation dilatometry, Papaefthymiou et al.[61] showed that partial ferrite transformation cannot be suppressed during cooling to the bainite isothermal transformation, and that increased intercritical deformation strongly suppresses the bainite transformation. They noted improved mechanical properties, but did not report retained austenite measurements. Similarly, Kim and Thomas[62] noted, in a direct-quenched ferrite-bainite material, that reduction of the finishing temperature lead to ferrite grain refinement and a loss of bainite volume fraction as well as a refinement of bainite packet size. DeArdo et al.[2] note that finer austenite grains (resulting from thermomechanical treatment of the steel) suppress upper bainite reactions upon transformation as the proeutectiod ferrite and pearlite reactions can completely consume the austenite. In an intercritically treated steel, the easy growth of epitaxial ferrite (as opposed to proeutectiod ferrite) should greatly enhance this phenomenon, as has been shown.

The reader is reminded that the above discussion refers to hot-band TRIP steel strips, and not the more common CRA sheet material.

2.5.3 Effects of Intercritical Annealing

Intercritical annealing parameters have been more thoroughly studied in cold-rolled and annealed TRIP steels than in hot-band TRIP steels. Unless noted, the below review applies to CRA materials.

Chen et al.[16] varied the temperature of the intercritical anneal for their steels, and found the dependence shown in Figure 16[(16)]. This figure demonstrates a maximum in f_γ at intermediate T_{ICA}. The same general dependence has been found elsewhere[25,40,63].

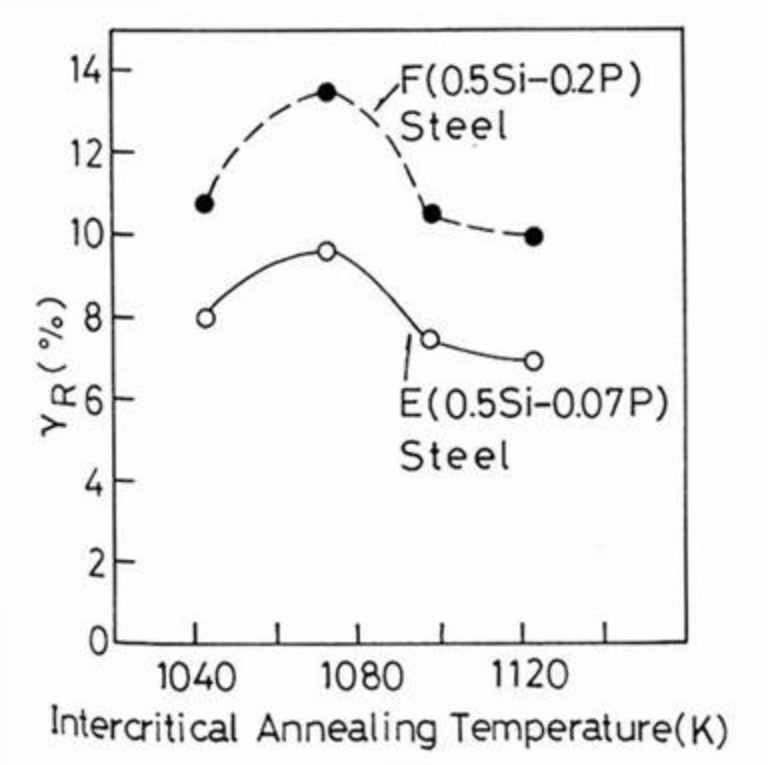

Figure 16 Fraction retained austenite-vs-annealing temperature[16]

This can be explained in terms of the Fe-C phase diagram. At T_{ICA}, the material is in the $\alpha+\gamma$ two-phase region. At high T_{ICA}, the material is mostly in the γ form, and the γ will be only slightly enriched in carbon. As such, when this material is cooled or quenched, it consists of a large amount of highly unstable (high M_S) austenite; this austenite is very difficult to retain without a profound bainitic reaction, and the f_γ is low.

Conversely, at low T_{ICA}, only a small fraction of the sample will be in the γ form, but it will be highly enriched in carbon (due to rejection from the high fraction of α); this is the austenite that would transform predominantly to pearlite upon slow cooling, rather than

ferrite. Thus, when quickly cooled and further enriched during the bainite reaction, most or all of the austenite will be retained, but the small starting fraction will result in a low f_γ.

Thus, a compromise of T_{ICA} -- and thus, of f_V^γ and C_γ -- will produce a maximum f_γ in the finished product. See Figure 17.

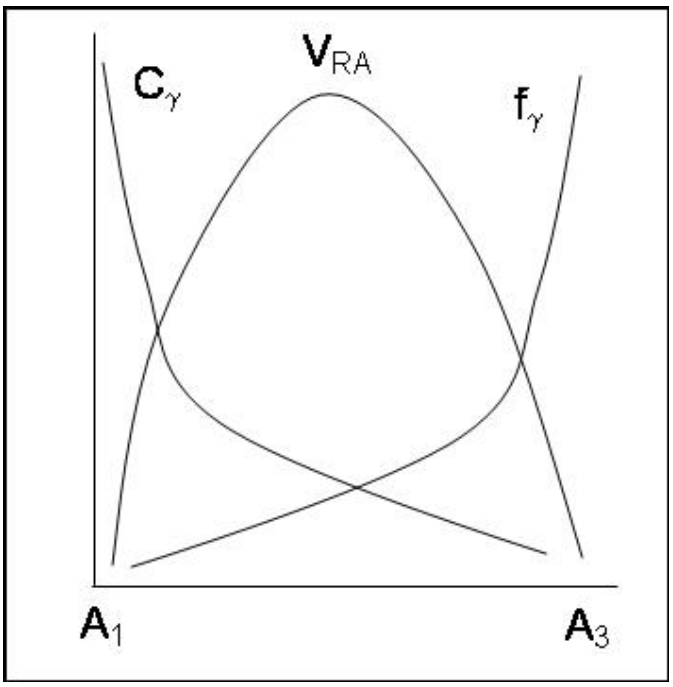

Figure 17 Schematic of intercritical annealing temperature effects

Matsuda et al.[64] reported variations of yield stress, ultimate tensile stress and uniform elongation with intercritical annealing temperature at constant t_{ICA}, cooling rates and bainitic isothermal hold conditions. They noted a loss of UEL at higher T_{ICA}; this is likely because the time of the bainitic reaction t_{IBT} was too short to compensate for high T_{ICA}, only 180 seconds. The less enriched austenite present at high intercritical temperatures

should require a longer bainitic reaction (under constant T_{IBT}) to achieve the same level of enrichment and concomitant stabilization.

Sakuma et al.[65] noted almost constant retained austenite volume fractions at differing T_{ICA}, but the balance of ferrite and bainite was necessarily different; higher temperatures lead to more volume fraction intercritical austenite (which transforms to bainite) and lower volume fractions of intercritical ferrite. Although the higher hardness of bainite would lead one to expect higher strengths at higher T_{ICA} when all other conditions are equal, they did not report data of strength-vs-T_{ICA}. Figure 18 shows Sakuma et al.'s data[65].

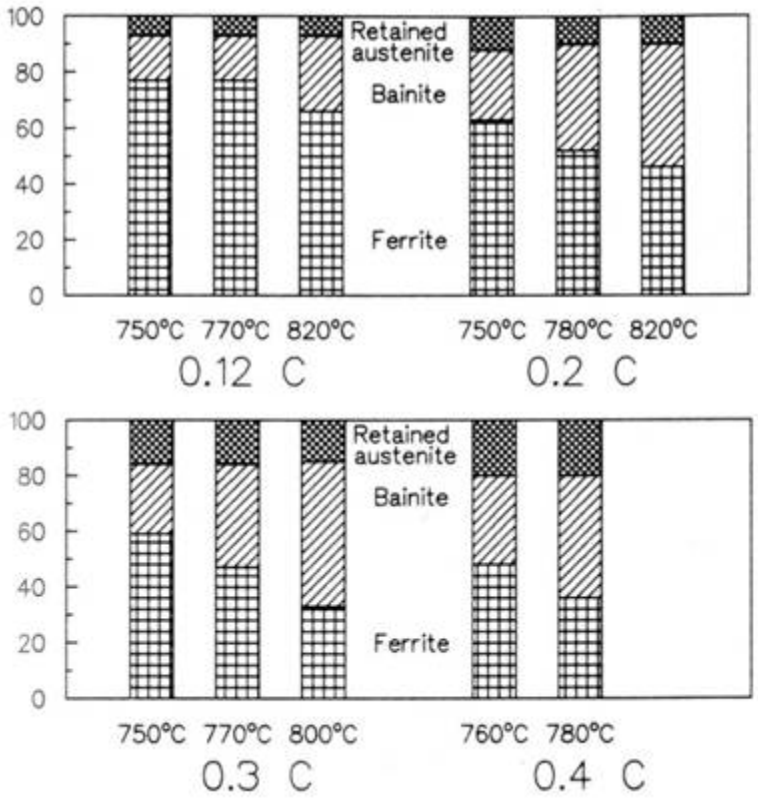

Figure 18 Variation of phase fractions with T_{ICA} in Si-Mn TRIP steel[65] at constant cooling rate (after salt pot treatments)

Industrially, intercritical annealing temperature seems not to have a large influence on the material's final properties, despite the results reported by Sakuma et al. Perhaps this discrepancy can be explained as follows: Sakuma et al.'s material was heat treated by transferring 0.8mm thick sheets from a salt pot at T_{ICA} to a second salt pot at T_{IBT}. This should result in very rapid cooling rates, effectively a salt-quench, being much more rapid than the gas-jet cooling applied to sheet in a commercial continuous annealing line or hot-dip coating line (or a laboratory simulator of CAL or HDG lines). Due to the favorable formation of epitaxial ferrite under the slower industrial cooling conditions, the volume fraction of ferrite (original + epitxial) and austenite (austenite being potential ferrite) upon reaching T_{IBT} will likely be insensitive to T_{ICA} under industrial cooling rates, whereas Sakuma et al.'s cooling rates may have inhibited or arrested epitaxial ferrite growth, resulting in more bainite. More discussion of epitaxial ferrite is found in section 2.5.4, below. This indicates a need for a better understanding of the CCT behavior of intercritically annealed steels, which will be a function of austenite size, distribution and composition, all of which will be strong functions of bulk composition, as-cold-rolled structure, and annealing time, temperature, and heating rate.

Pichler et al.[66] found properties to be relatively insensitive to T_{ICA} or line speed (which is related to t_{ICA}), and also note that the slow cooling rates in CAL or hot-dip galvanizing lines allow for ferrite growth to compensate for the loss of intercritical ferrite at high annealing temperatures.

Chen et al.[16] studied the effect of t_{ICA} on f_γ in cold-rolled and annealed steels. They found, as shown in Figure 19[(16)], that f_γ will peak after about 2.5 minutes and then decrease for the steels tested. The peak in f_γ probably corresponds to complete dissolution of cementite. The subsequent decrease is harder to explain, but may be due to a coarsening effect or diffusion of silicon or phosphorus to ferrite. Given the short times and low temperatures involved, however, neither of these explanations is satisfying. The author speculates that is may be due to an "evening out" of carbon gradients; if the boundary-areas or prior-carbide-areas, for example, were enriched in carbon, this would lead to an increased propensity for retention in those areas. Because boundary areas will likely be enriched in substitutional elements, such as Mn or P, the thermodynamically dictated carbon contents near the boundaries should be different from the carbon contents in the bulk of the austenite pools, leading to carbon gradients. A longer hold might destroy this gradient in carbon content and lead to a lower overall retention propensity.

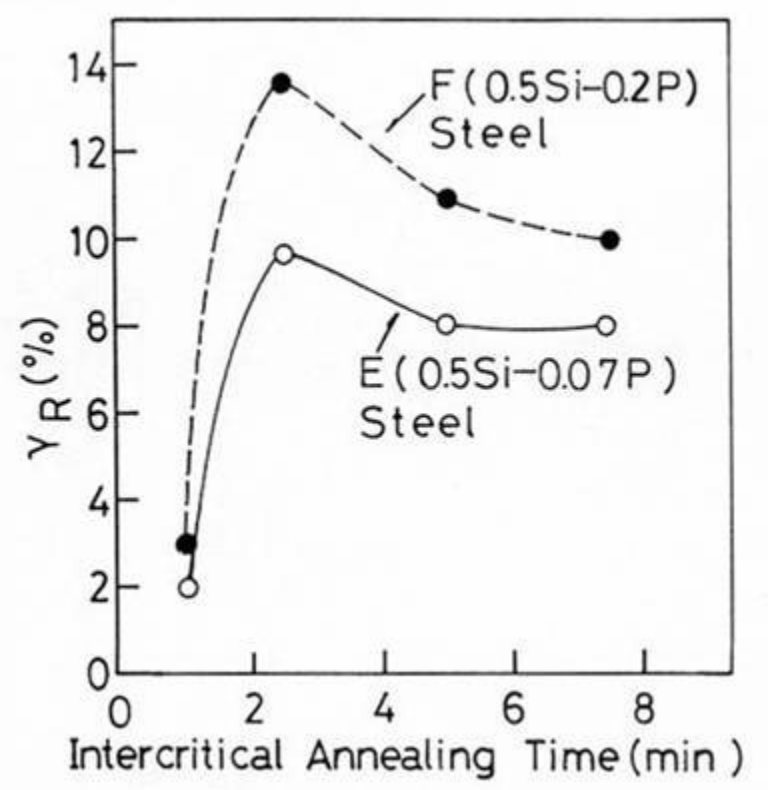

Figure 19 Effect of intercritical time on austenite fraction[16]

Recent studies have concluded that intercritical annealing parameters have only minimal effect on final properties, as the isothermal bainite transformation dominates the final properties. Matsuda et al.[64] noted that mechanical properties were unaffected by t_{ICA} at T_A=825°C. It seems likely that, so long as all carbides are dissolved, the intercritical hold time should have little effect, as it will be less than a few minutes on modern industrial continuous annealing or hot-dip equipment, and in such a short time, no appreciable coarsening or substitutional diffusion could result.

Indeed, Pichler and Staiszny[67] found that, so long as the time was long enough to dissolve all cementite (~60sec), the mechanical properties were unchanged. Traint et al.[68] also showed that the volume fraction of austenite stabilizes after about 60 seconds.

It has been noted[20,69] that at temperatures very near A_1, cementite dissolution is very slow, but even a slight increase in temperature accelerates the dissolution by several orders.

An unorthodox -- but potentially important -- alternative mechanism has been proposed for the formation of austenite upon reheating into the intercritical regime[20,70]. Navara et al.[70] contend that austenite nucleates on ferrite-ferrite grain boundaries that have suffered diffusion-induced grain-boundary migration, rather than at ferrite/cementite boundaries. This they attribute to the rapid diffusion of manganese along the grain boundaries, and that grain-boundary regions rich in manganese nucleate austenite. They base this assertion on extensive optical and STEM microscopy, as well as STEM-EDS chemical microanalysis. They note massive manganese enrichment in the austenite particles after as short a time at temperature as one hour. They also note that, because of the rapid diffusion of manganese along grain boundaries but its slow diffusion through the austenitic matrix, the manganese was segregated to the edges of the austenite particles, as observed by STEM-EDS.

Although Navaro et al. held their materials for times too long to have industrial significance (>1 hour), Minote et al.[71] found manganese and silicon segregation at their

shortest examined intercritical time of only five minutes, and that the segregation level did not change between annealing times of 5 and 1000 minutes. Minote et al. showed, however, using STEM-EDS of as-cold-rolled material, that this segregation was inherited from the hot strip mill, rather than by the mechanism of Navarro et al. In Minote et al.'s as-cold-rolled material, the pearlite was manganese-enriched and the adjoining ferrite silicon-enriched to nearly the exact degrees measured in the intercritical austenite.

Although Navaro et al.'s mechanism seems doubtful, Minote et al. have shown that the intercritical austenite in CRA TRIP-steels will have some benefit from manganese segregation. Unfortunately, the ferrite will contain much of the silicon (or aluminum, or other ferrite-stabilizing alloying additions) that would otherwise have helped inhibit carbide precipitation in the bainitic ferrite during the isothermal bainite transformation. Carbon is a more powerful austenite stabilizer than manganese; this manganese enrichment is unlikely to compensate for the silicon depletion and its associated loss of carbon enrichment in the final retained austenite population. Perhaps TRIP steel hot bands coming off the finishing stands should be subjected to severe cooling schedules to minimize segregation before cold-rolling. This would, however, result in harder hot-band and higher rolling loads and extra roll wear during the subsequent cold-rolling campaign. Using copper to replace Si/Al might make slow-cooling a feasible approach, as copper is an austenite stabilizer and should segregate to austenite pools, rather than ferrite.

If rapid manganese diffusion along grain boundaries does, indeed, happen, it might be an important mechanism for stabilization of austenite. However, the areas near the ferrite/austenite boundaries will be the most likely (from nucleation and growth arguments) to transform into epitaxial ferrite or bainite during the cooling stage to the IBT. It would be interesting to see STEM-EDS/PEELS or SIMS studies (such as linescan chemical analyses across a prior-intercritical-austenite region) comparing the substitutional alloying content of the different phases in fully processed TRIP steels.

2.5.4 Cooling Rate Effects

The cooling rate from the intercritical anneal to the bainite hold, <dT/dt>, also affects the final properties of the material.

Sakuma et al.[72] found that increasing the cooling rate resulted in higher values for f_γ, UEL and TEL, although increases to the highest rates (<dT/dt> $\geq$100°C/sec) result in steady or somewhat reduced values of f_γ, UEL and TEL.

Slow cooling[71,72] (<dT/dt> low) results in pearlite formation and poor elongation values. Minote et al.[71] observed that a slow cooling rate (3°C/sec) produced a high volume fraction of epitaxial ferrite, as compared to faster cooling rates. This would result in more carbon partitioning to the austenite, which would seem beneficial. However, this excessive carbon led to pearlite formation, which would be detrimental to the

mechanical properties. At 30°C/sec or faster, no pearlite was formed. They did not perform mechanical tests.

This work used cooling rates of 4°C/sec and did not observe pearlite, however. Pearlite was observed at ~0.4°C/sec cooling, as would be expected. Figure 20, from Speer and Matlock[73], demonstrates the effect of cooling rate on the formation of epitaxial ferrite in dual-phase steels.

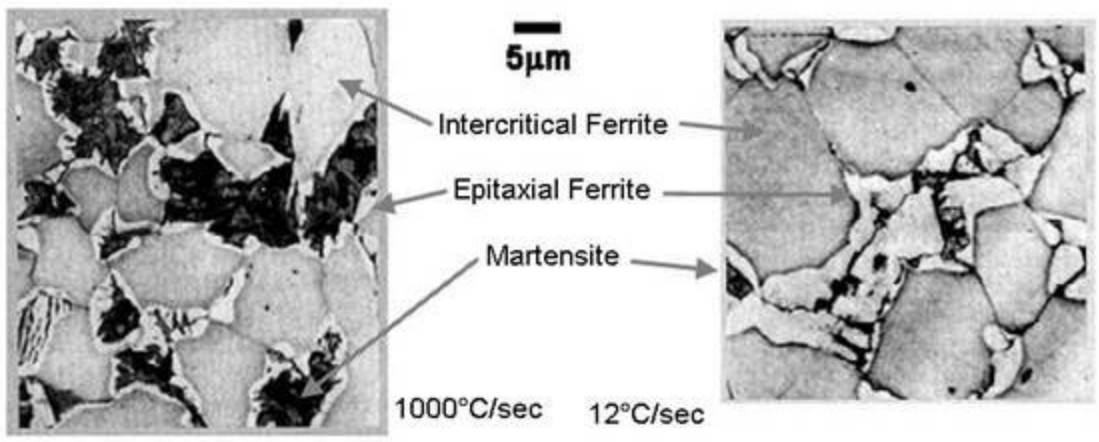

Figure 20 Epitaxial ferrite growth in Dual-Phase steel under different quenching conditions[73]

At ~1000°C/sec quenching, relatively little epitaxial ferrite has time to form. At 12°C/sec, almost all of the intercritically formed austenite is lost to epitaxial ferrite, leading to a tiny volume fraction of martensite. As the nucleation barrier for epitaxial ferrite should be minor or zero, only reducing its growth time or growth rate will suppress it. However, epitaxial ferrite is not necessarily detrimental; it will, after all, reject carbon into the remaining austenite.

Excessively fast cooling[72] results in growth of ferrite supersaturated in C or transformation to martensite (that is, dual phase steel). Thus, a compromise value of <dT/dt> seems to give optimum final properties.

Matsuda et al.[64] noted almost no effect of cooling rate at values of 20-60°C/sec. At 80°C/sec, they found a slight decrease in uniform elongation. They did not discuss the mechanism behind this result, but it seems likely the loss of carbon rejection from epitaxial ferrite may be to blame. Pichler et al.[66] and Traint et al.[38] independently noted constant mechanical properties with cooling rate except at the very slowest values. Pichler and Stiaszny[67] found only negligible effects of cooling rate. However, all of these studies varied cooling rate by less than one order of magnitude, rather than over multiple orders.

In summary, the effects of cooling rate are major, but only when <dT/dt> varies over one or more decades.

2.5.5 Isothermal Bainitic Transformation Effects

The temperature, T_{IBT}, and time, t_{IBT}, of the isothermal bainite/coiling hold have the most profound effects on the final properties of the steel.

As Jacques et al.[17] observed, a t_{IBT} of zero -- that is, direct cooling from T_{ICA} to room temperature -- results in an effectively dual-phase (ferrite + martensite) material, and the longest t_{IBT}'s result in ferrite-bainite-carbide structures. (Although silicon, phosphorus,

copper and aluminum suppress carbide formation, they cannot arrest it entirely; their effects are kinetic, rather than thermodynamic.) Intermediate t_{IBT}'s produced structures containing retained austenite and thus acted as TRIP-assisted multiphase steels. Samples processed at t_{IBT}=0 showed the highest UTS, but the lowest elongations; similarly, the ferrite + bainite structure had the lowest UTS, and elongations lower than the intermediate t_{IBT}, multiphase steels. The moderate t_{IBT} steels exhibited good UTS and the highest elongations, as they contained retained austenite. Jacques summarized this in Figure 21 [(17)]. Also see Figure 22[(74)]; this demonstrates the changes in phase distribution with time t_{IBT} for a given material (0.383C-1.46Si-1.20Mn) at a constant T_{IBT} (400°C). Matsumura et al. reported that the ferrite fraction is constant (≈40%) over all t_{IBT}, and that this f_α is a function of T_{ICA}[74]; Matsumura et al. reported a cooling rate of 100°C/sec from T_{ICA} to T_B.

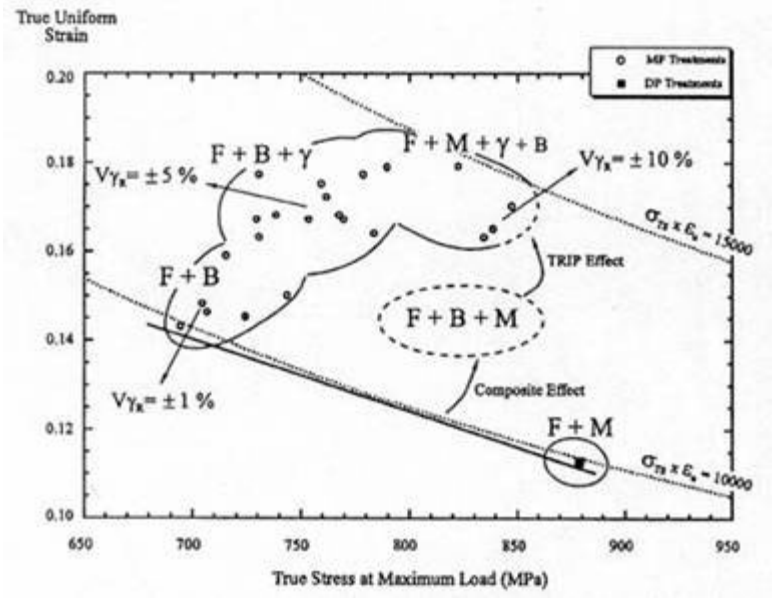

Figure 21 Effects of phase fraction on mechanical properties[17]

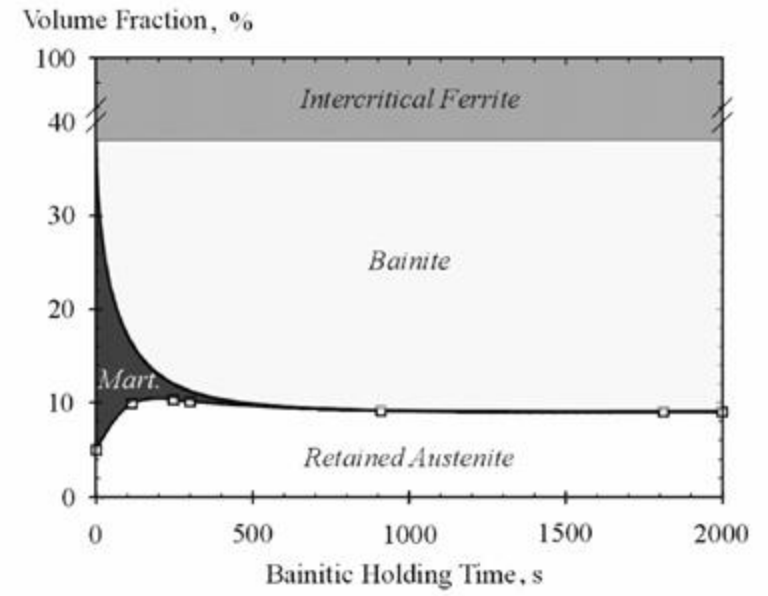

Figure 22 IBT time effects on phase distribution[76]

Retained austenite volume fraction, f_γ, varies strongly with the temperature of the bainite hold T_{IBT}. In general[13,15,16,17,18,34,64,67,68,72,75], f_γ and elongations will peak at a moderate T_{IBT}, typically ~350-450°C (dependant on composition and prior processing), and decrease to either side of this peak. For example, Figure 23[(40)] shows the f_γ behavior of a function of T_{IBT}. The three curves are for three different T_{ICA}'s, and t_{ICA}, t_{IBT} are constant for all samples.

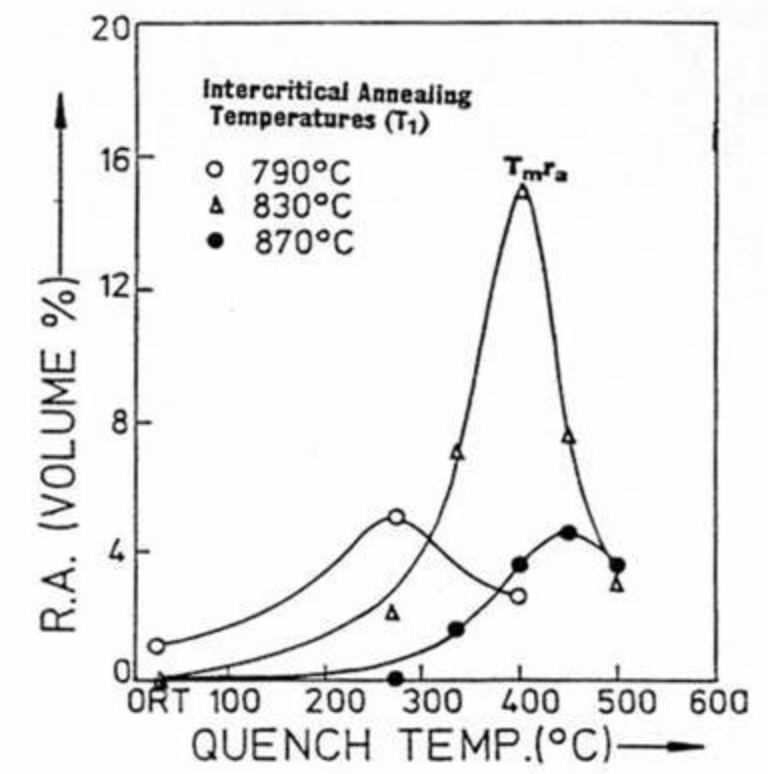

Figure 23 Effect of IBT temperature on retained austenite fraction[40]

Pichler et al.[66] noted an inverse bell-curve for f_γ-vs-T_{IBT}, but offered no explanation. As Pichler et al.'s results are for material processed in a CAL line simulator by imposing commercial thermal schedules on the material, rather than by typical laboratory salt-pot or furnace processing, it may indicate trends that will be observed as more TRIP steel is industrially produced in the future. Pichler et al.'s results of mechanical properties-vs-T_B were consistent with other reports, however. Their results of f_γ-vs-T_{IBT} and mechanical properties vs T_{IBT} in galvanized material followed the normal trends.

Similarly, f_γ as a function of t_{IBT} is typically a curve displaying a maximum, see Figure 24 (adapted from Zarei-Hanzaki et al.[13]) for two steels, as described in section 2.3.6.

Jacques et al.[76] noted this same trend in TRIP steels containing normal quantities of carbide inhibitors (1.4-1.5% Si) but monotonically decreasing retained austenite volume fraction in steels containing either 0.4%Si or zero Si-1.5%Al. Evidently, the two low-silicon steels are insufficiently inhibited to retain the austenite. Figure 22, in contrast, shows a fairly level retained austenite-vs-time curve, indicating that steel is more effectively stabilized.

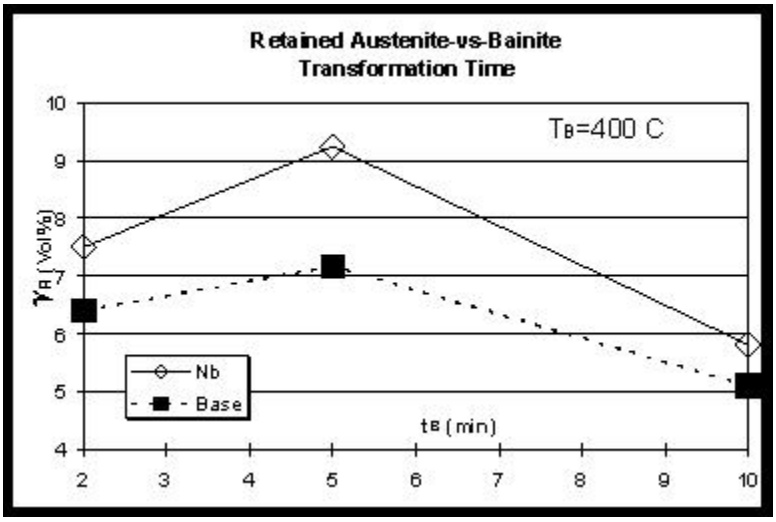

Figure 24 Effect of IBT temperature on austenite fraction; adapted from Zarei-Hanzaki et al.[13]

Why is this behavior manifested? The process of the bainite transformation passes through several regimes with increasing t_{IBT}. Near zero time, the non-enriched austenite will be unstable, and the result upon cooling will be a structure of ferrite + martensite, with small amounts of other phases: a dual-phase steel. At short times, some of the austenite will transform to bainite or bainitic ferrite. As TRIP steels contain large amounts of silicon or other carbide-inhibiting additions, the carbide precipitation is slowed, and carbon is rejected from the newly formed phases into the remaining austenite. If the isothermal hold is terminated at this point, the austenite may be

sufficiently stabilized by the rejected carbon to be retained. As this reaction proceeds, the volume fraction of austenite will be reduced as the bainite consumes austenite, but the remainder of the austenite will be enriched in carbon; this will lead to some optimal $t_{IBT,}$ for a given T_{IBT}, resulting in a compromise between fraction and stability of austenite to maximize f_{γ}. Traint et al.[68] show a TEM micrograph (Figure 25) from a steel annealed at T_B=525°C; at this high temperature, the austenite transformed to ferrite+carbides; this steel contained ~3% retained austenite, as opposed to ~10% in optimally treated material.

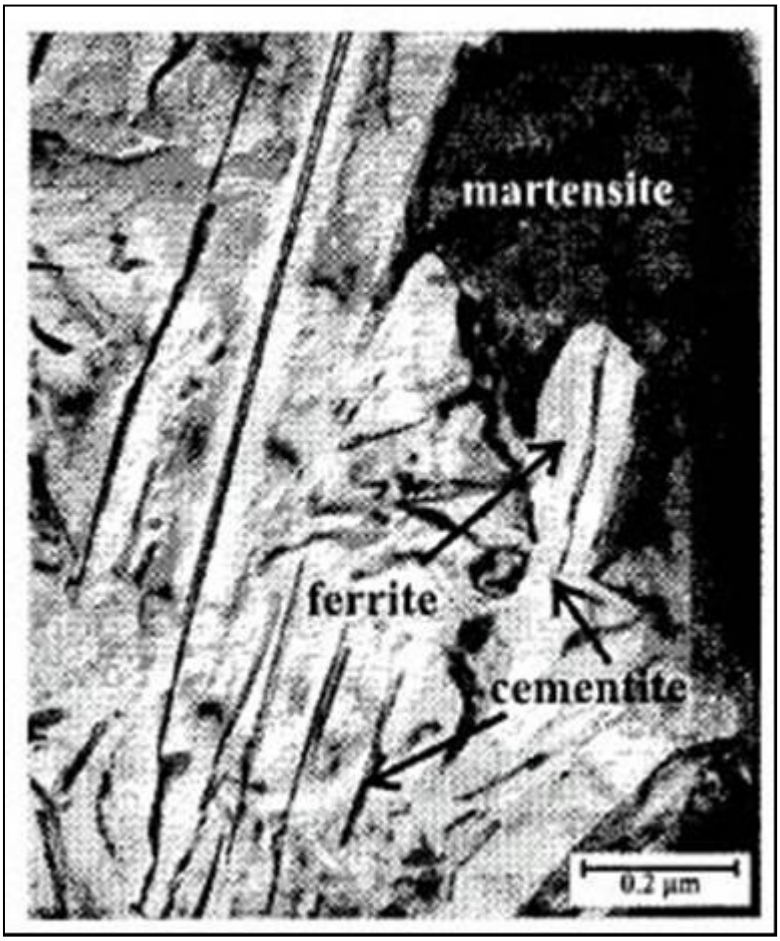

Figure 25 Carbides in TRIP steel aged at too high a temperature (525°C)

Those papers that studied the carbon content of the retained austenite, C_γ, found that the carbon content increased steadily with t_{IBT}[74,77]; this will result in more stable (lower M_S) austenite.

However, at long t_{IBT}, Matsumura et al.[74] found decreasing C_γ. Jacques et al.[76] noted increasing C_γ with time, up to a saturating value, in 1.4Si, 1.5Si and 1.5Al TRIP steels, whereas in the 0.4Si steel, C_γ peaked and then decreased due to the low level of carbide inhibition.

As the reaction proceeds to longer t_{IBT} and the carbon content in austenite increases, another process can come into play. Consider Figure 26[(33)]. Note the <u>extrapolated</u> $\gamma/\gamma+Fe_3C$ phase boundary (extrapolated below the eutectoid temperature). If, during the isothermal hold, C_γ exceeds the value of the extrapolated $\gamma/\gamma+\theta$ phase line at the particular isothermal temperature, cementite precipitation from the austenite becomes possible[17,33]. This further reaction will result in a poorer final f_γ, and a larger fraction of other phases, such as carbides and bainite/bainitic ferrite. For sufficiently long times, the carbon content in the austenite will cross the extrapolated $\gamma/\gamma+Fe_3C$ line on the Fe-C phase diagram, Figure 26. This will result in massive losses of austenite carbon content and thus losses in f_γ upon cooling to room temperature. In this regime, the material is no longer TRIP-steel. TEM micrographs of carbides in a TRIP steel -- such as Figure 25 -- are indicative of an overaged TRIP steel with poor mechanical properties. All TRIP steel research programs should correlate TEM imaging to mechanical properties in this way.

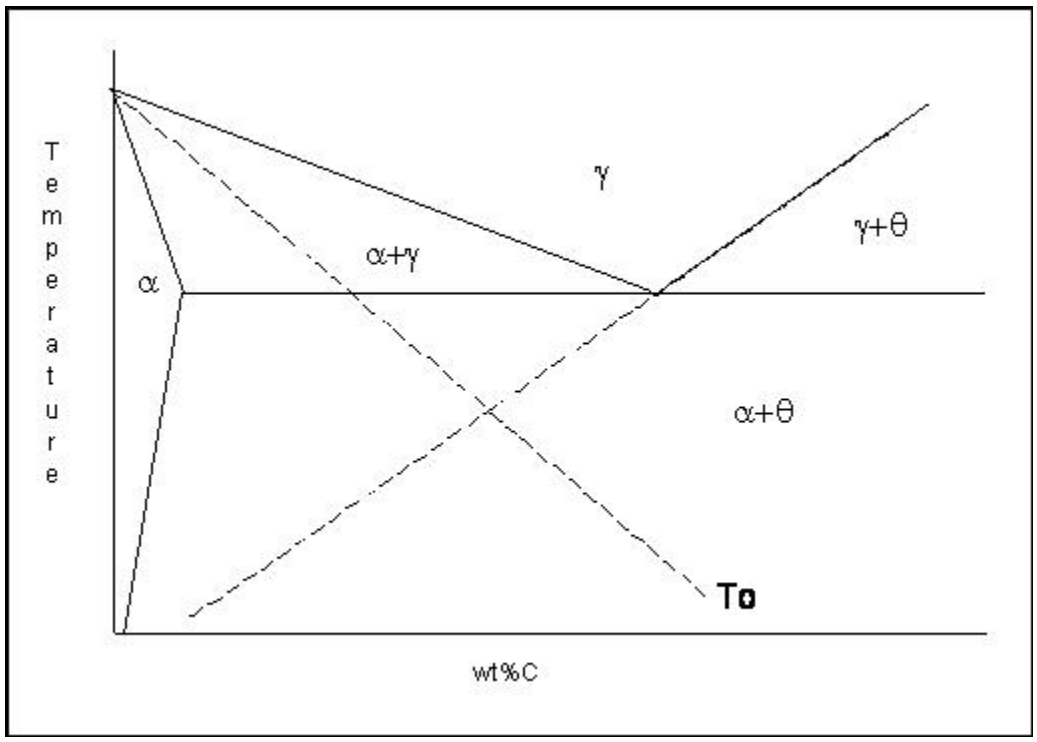

Figure 26 Fe-Fe_3C phase diagram with extrapolated phase boundaries (schematic)

Jacques et al.[76] elegantly demonstrated this: in their steels of high silicon content, they found few carbides, Figure 27a, but in a low-silicon steel, they observed excessive carbide precipitation, Figure 27b.

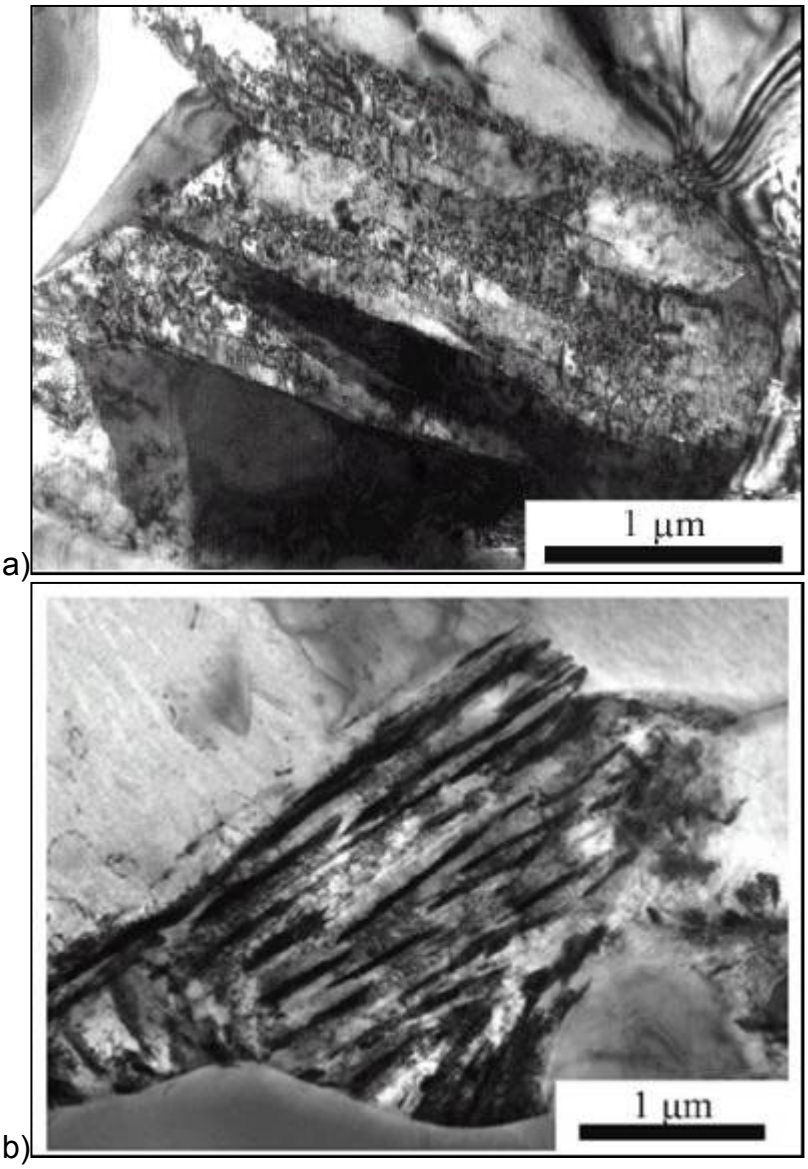

Figure 27 (a) High-Si and (b) low-Si TRIP microstructures; (a) retained austenite vs (b) carbides[76]

Hanzaki et al.[13] (in hot-band) published TEM images of carbides at the bainitic ferrite/austenite interface in samples annealed for excessive times. They also noted lower retained austenite volume fractions at lower values of T_{IBT} (~300°C) and attributed this to the ease of carbide formation in lower bainite. This was confirmed by TEM of carbide-containing bainitc ferrite.

De Meyer et al.[75] note three possible types of isothermal bainitic reactions, Figure 28.

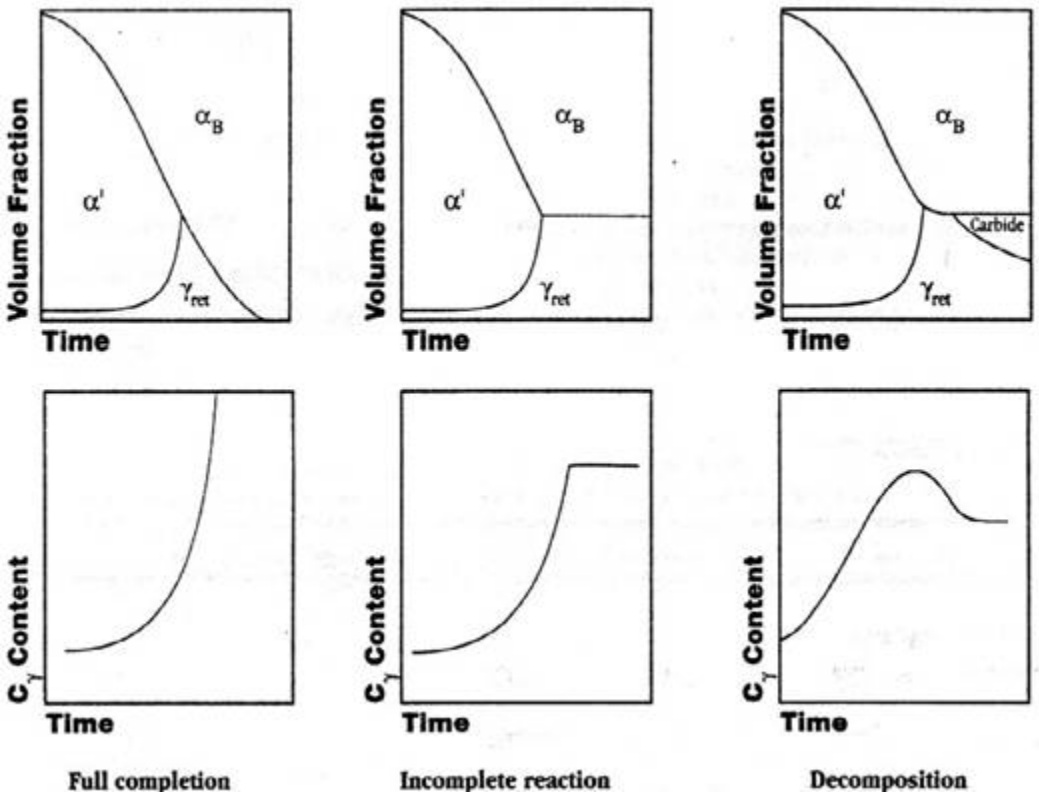

Figure 28 Three potential reactions in TRIP-steel during the IBT[75]

First, the "full completion reaction," in which the carbon content of the austenite increases montonically and the volume fraction of retained austenite reaches a peak at moderate times. Second, the "incomplete reaction," in which carbon content increases to a maximum at which point the volume fraction of retained austenite and its carbon content will become constant. Third, the "decomposition reaction," in which, as t_{IBT} increases, the austenite decomposes to ferrite and carbides, which reduces the austenite volume fraction and carbon content (eventually to zero).

The full completion reaction probably will not be encountered. The incomplete reaction will most likely be observed in well-inhibited steels, (those with large carbide-inhibiting additions), such as high-silicon or silicon-aluminum steels. In steels that are partially inhibited, the carbide reaction can take place under industrial (i.e., short) holding times, especially at high temperature, leading to the decomposition reaction. This will probably only be observed in no-silicon or low-silicon grades.

What effects will T_{IBT} have? First, at higher temperatures, the diffusion and segregation of carbon will be faster. The material will reach its optimum aging regime and its overaging regime sooner due to the faster enrichment and carbide formation.

Second, Sakuma et al.[72] and Bhadeshia[33] note that as the isothermal bainite transformation temperature increases, the strength (hardness) of the bainite decreases. This could decrease the associated "matrix constraints" (section 2.4.4, equation 2-3) resulting from a weaker surrounding phase will reduce the stability of the retained austenite packets, and could thus result in a lower f_γ. It will certainly reduce the UTS of the finished product.

Although the general f_γ-vs-T_{IBT} or f_γ-vs-t_{IBT} behaviors are bell curves exhibiting maximas at intermediate values for either the temperature or the time, exceptions do exist.

Sakuma et al.[72] found that f_γ increased constantly with T_{IBT} in two steels of high silicon and manganese contents (1.22Si-1.55Mn and 1.24Si-1.80Mn). Chen et al.[16] found that f_γ increased continuously with t_{IBT}; however, the t_{IBT}'s measured were limited to 5 min, and the steels contained large additions of phosphorus (0.07 and 0.2P), which retards carbide kinetics (section 2.3.4). Likely, these steels had simply not reached their peak yet. Similarly, Matsumura et al.[74] found only decreasing f_γ with t_{IBT} in some specimens; they attributed this to the omission of measurements at very short t_{IBT}. This result seems surprising, as Matsumura et al.'s steels contained large amounts of silicon, which should push the time for maximum $f\gamma$ to larger values. They performed TEM studies, but did not report the presence or absence of carbides. Matsumura et al. also note that the times for maximum carbon enrichment in retained austenite were much longer than the times for maximum $f\gamma$, and carbides would not be expected until after $f\gamma$ is reached. This indicates that effects than other carbide precipitation may be at play.

Total and uniform elongations also vary with changes in the bainite transformation parameters. Elongation typically varies in proportion to the retained austenite content[13,16,18,72]. As such, processing to increase f_γ will typically lead to improved elongations for the steel. Subtleties exist; see section 2.6.1.

Recent work[21,22] indicates that in C-Mn-Si-Al grades, and perhaps others, optimized for high T_{IBT} and short t_{IBT} processing, hot dipping followed by slow cooling would allow the achievement of good to excellent mechanical properties without the isothermal bainite

transformation; this is important, as many hot-dip coating facilities do not have the capability of performing the isothermal treatment.

(It is noted that the commercially galvannealed steel used in this study, as well as the steels annealed and galvannealed on the laboratory hot-dip process simulator, were processed with an isothermal hold, as some commercial lines do have this capability.)

2.5.6 Alloying Effects in Processing

The reader is reminded that the effects of niobium additions during hot deformation were discussed in the thermomechanical treatment section, 2.5.2, above. Effects of niobium on CRA properties will be discussed below.

Increases in silicon, manganese, phosphorus or aluminum content will increase the final f_γ for a given processing path[13,14,15,16,17,18,34,35,72,74]. Consider Figure 29 [(15)]. Steels of varying manganese and silicon content were processed through the same path, and then either air-cooled (AC) from the bainite hold to room temperature, or furnace-cooled (FC). As Figure 29 shows, in general, increasing manganese or silicon results in a higher f_γ. Similarly, phosphorus will increase f_γ[16,18] (Figure 10).

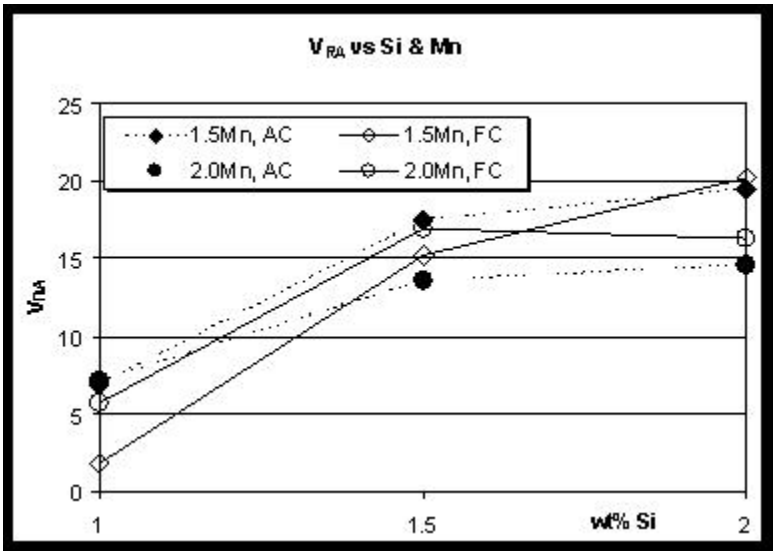

Figure 29 Effects of silicon and manganese on austenite fraction; adapted from Tsukatani et al.[15]

As seen in Figure 29, for 2.0%Mn, the curves seem to level off after ~1.5wt% Si, indicating that under those particular processing conditions, ~1.5%Si leads to full inhibition, and further additions are not particular beneficial. The 1.5%Mn conditions, however, do show a significant improvement between 1.5 and 2.0%Si; likely, the combination of low Mn level, and in the FC sample additional time for reaction due to the slow furnace cool, make merely 1.5%Si insufficient to stabilize the austenite.

However, high silicon contents tend to form very adherent oxides on the surface during rolling or continuous annealing that are very difficult to remove. This oxide can render a work piece uncoatable, and thus unusable[78]. It is important to note that these oxides are invisible to the eye.

Mintz[20] and De Cooman et al.[21,22] note that silicon's effect is due to the segregation of silicon to the surface and the formation of complex manganese-silicon-oxides that resist

wetting by the zinc bath. Excessive manganese levels, in excess of 2%, may also degrade coatability even in the absence of silicon[20]. De Cooman et al., using glancing-angle XRD, observed the presence of iron-aluminum-oxides, but these did not effect the coatability of zero/low-silicon, high-aluminum steels. It has been noted[75], and is evident from examination of glow-discharge optical emission spectroscopy traces[21,22], that silicon segregates to the surface of the steel, whereas the aluminum segregates to just below the surface. In general, it is accepted that a level of silicon in excess of 0.5% will prevent coating. (The 0.5%Si steel used in this study showed borderline coatablility.) Mintz notes that aluminum up to 1.5% and phosphorus to 0.1% will not affect galvanizing, although phosphorus does slow galvannealing[20]. Manganese, chromium and silicon are also all believed to slow galvannealing kinetics[20].

As such, there has been interest in using aluminum[18,34], phosphorus[16], aluminum with phosphorus[18], or copper[37,38,39,79] as substitutes for silicon.

De Meyer et al.[34] studied a silicon bearing (0.19C-1.57Mn-1.46Si) and an aluminum-silicon (0.31C-1.57Mn-0.34Si-1.23Al) TRIP steel. The aluminum-silicon steel had higher formability than the Si-steel, as well as a more stable strain-hardening rate, which would result in better stretch-formability. The silicon steel's n value peaked at low strains, whereas the aluminum-silicon steel's n value was very steady, showing no pronounced peak. This indicates more stable retained austenite.

De Meyer et al.[34] felt that the silicon could not be completely replaced by aluminum, as excessive aluminum additions, as predicted by computational phase diagram software, result in extending the intercritical region to the point that the fully austenitic region disappears entirely. Jacques et al.[76] found that elimination of silicon and replacement by aluminum lead to poor TRIP steel, and also noted that low-silicon (0.4%Si) TRIP steel was worst of all. Traint et al.[18], however, felt that silicon could be substituted fully by aluminum, and that their aluminum-phosphorus steels showed the best mechanical properties. Pichler and Stiaszny[67] found a 0.6Si-0.11P steel to have superior properties to a 1.05Si steel, and a 0.6Si-residual phosphorus steel to have poor properties; in fairness to silicon, however, 1.05 is a fairly low value to use as a baseline material, especially as all materials in the study had a low value of manganese, 1.50Mn. Of course, even the 0.6%Si materials will be uncoatable. Traint et al.[38] found a 1.5Si steel had superior strength and ductility, compared to 0.6Si-1.0Al, 0.6Si-0.1P, 0.6Si-0.84Cu-0.4Ni steels, and that 0.6Si had the poorest mechanical properties. There is, as yet, no general agreement in the literature on minimal or optimum Si contents.

In light of these results, high silicon steel seems to give the best mechanical properties. Aluminum, by itself, simply does not provide the carbide-inhibition of silicon unless large additions of aluminum are used. For carbide inhibition, the author would estimate that 1 unit of silicon provides 1.5-2 units of "aluminum equivalence," and that a steel needs about 1.5 weight percent total "aluminum equivalent." For example, the 1.0Al-0.5Si steel in this work would thus have 1.75-2.0% "aluminum equivalent," and showed excellent properties. This equivalence, however, is only with respect to carbide

inhibition; there is no simple equivalence between Si and Al with respect to hardness increments from solid-solution-hardening. For example, the 1.5wt%Al-zero Si steel showed excellent elongation, but somewhat low -- though still adequate -- tensile strength. This is because aluminum does not provide the same solid-solution hardening of silicon.

Given silicon's effects on surface quality, however, it is inevitable that silicon-only steels will be replaced by alternate alloying schemes. Further research will be necessary to optimize the properties of the low-silicon compositions. Unfortunately, aluminum leads to problems in casting[20,80]. Ultra-low nitrogen levels or additions of titanium will likely be necessary to continuously cast high-aluminum compositions.

Eberle et al.[81] explored a novel scheme for reducing the silicon contents of TRIP steels. Using a 0.16C-1.4Mn-0.014Nb steel with no aluminum or silicon, they were able to achieve properties of 600MPa tensile strength at 26% total elongation without a bainite isothermal transformation. This was achieved by soft-annealing the hot-rolled-strip under batch annealing conditions in the range of 400-700°C before cold-rolling. This results in manganese segregation to the cementite. Upon intercritical annealing, this enriched cementite transforms to austenite with a high propensity for retention. As the intercritical annealing time was only 36 seconds, there will be effectively no additional manganese diffusion, leading to a paraequilibrium condition. As shown by computational models[43], manganese is second only to carbon in stabilization potential of austenite. Although properties of 600MPa and 26% elongation are not impressive in

comparison to the current generation of silicon-based TRIP steels (The 0.2%C-0.5%Si-1.0%Al steels in this study gave values of 650-675MPa at 35-45% total elongation), the improved surface quality/coatabilty of the low-silicon steels may result in the application of this soft-annealing technique at the industrial level. Further optimization research of chemistry and processing can surely improve the properties of the soft-annealed material; higher microalloying content is an obvious first step. Another suggestion would be a prolonged intercritical hold, as Eberle et al. noted the existence of non-transformed cementite in the final structure. Cementite is both inherently brittle and contains carbon that would be better used in solution in austenite. Eberle et al.'s intercritical hold was only 36 seconds, so even a "prolonged" hold would be within the bounds of acceptable industrial practice (<~120 seconds).

However, in light of the results of Minote et al.[71] above, a very slow cooling from the hot strip mill might achieve the same segregation of manganese, allowing non-inhibited steels to be produced without a separate soft-annealing step.

Recent studies[37,38,39,79] on tramp element effects resulted in data concerning chromium, copper and nickel additions. Copper was universally found to improve the properties of the TRIP-steels, as was nickel. Copper slowed the carbide precipitation, allowing longer holding times and increasing the volume fraction of retained austenite. The copper steels tended to show high tensile strengths[37,38], likely due to the solid solution hardening and precipitation hardening associated with it. The copper-nickel steel (0.15C-1.5Mn-1.5Si-0.5Cu-0.4Ni) of Lee et al.[39] had spectacular mechanical properties

(~850MPa UTS at ~25% uniform elongation), but it is interesting to note that the copper-nickel steel (0.15C-0.6Si-1.5Mn-0.85Cu-0.4Ni) of Traint et al.[38] had unimpressive mechanical properties (~800MPa UTS, ~15% uniform elongation). The silicon content of the copper-nickel steel[38] was low (0.6%) whereas the silicon addition in Lee et al.[39] was 1.5%. It seems likely future copper-bearing compositions will require large additions of aluminum or phosphorus in addition to copper to reach full inhibition.

Copper was found to reduce total elongation in CRA steel, likely because it prevented full recrystallization of the cold-rolled ferrite during the soak[37]. In this case, intercritical anneal time (or perhaps heating rate to the soak) will be important. Un-recrystallized steel is obviously unsuited to high-formability applications.

Nickel was found to improve the retention of austenite[79], but it is important to note that in commercial steels, nickel will probably only be added to copper bearing steels, and then only to reduce or eliminate hot-shortness (see section 2.8.2).

Chromium tended to increase strength, but decrease austenite retention and elongations[39,79]. This may be helpful if it is desired to produce high strength steels that require ductility superior to dual-phase material, but the extraordinary elongations found in TRIP steels (at their lower strengths) are not required. Chromium (or Mo, Co, W, V, etc.) poisoning of TRIP-steel to produce a compromise between dual-phase and TRIP properties is an important field for future research. Product application areas, such as cold-pressed automotive wheel rims, could make this an important field of study. Mintz

notes that chromium can have an effect on carbide precipitation similar to that of aluminum, silicon and phosphorus, but that >0.5% chromium can lead to poor galvanizing; molybdenum, however does not have this problem and thus molybdenum additions may be preferable to chromium[20]. Cr can slow the precipitation of copper, so this may lead to

2.5.7 Effect of Deformation Temperature

As described in section 2.4, the retained austenite stability and transformation behavior will be a strong function of the temperature. As a consequence, results of tensile tests of TRIP materials, pulled at varying temperatures, indicate wide variations in the measured mechanical properties.

Consider Figure 30[(63)]; the different TRIP steels (of constant starting structure and processing, but different chemical composition) show little variation in YS over the range $T\varepsilon\approx$-100 to 400°C. UTS, however, displays a local minima and then a local maxima. Total elongation shows a simple bell-like curve with the maximum values between 100-200°C.

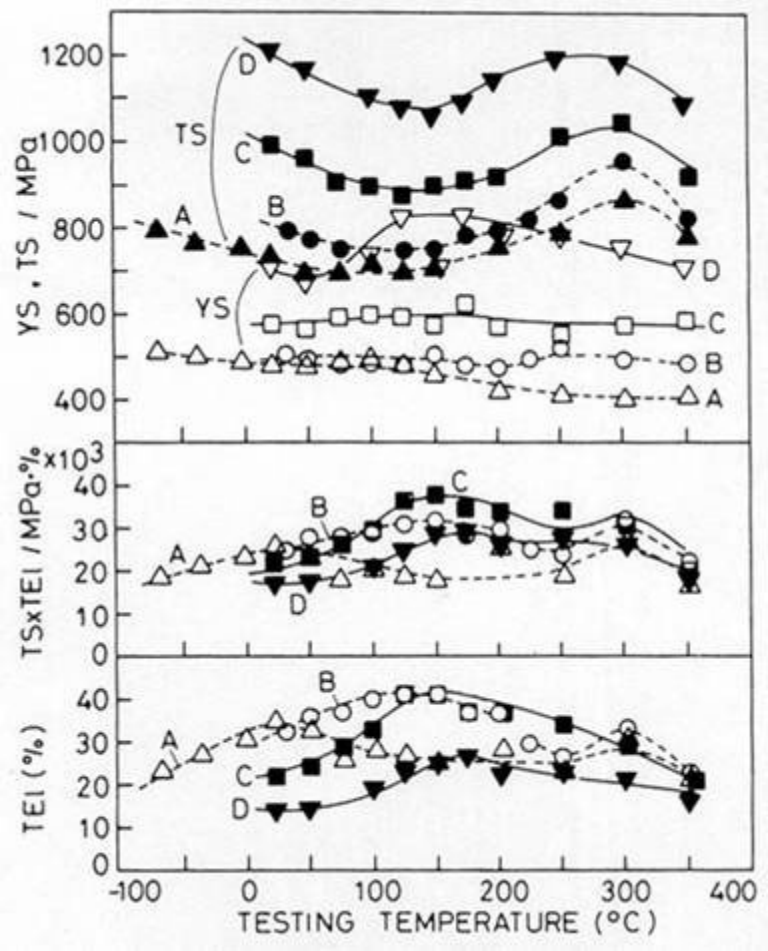

Figure 30 Elongation and strength as a function of testing temperature[63]

Consistent with section 2.4.2, they observed maximum elongations to peak in the temperature regime between M_S and M_d.

Tsukatani et al.[15] found the same general behavior. They explained the UTS increase at the higher temperatures as an effect of, first, "dynamic strain aging" and second, the change in martensite transformation morphology with temperature. (No justification, experimental or bibliographical, is given for this assertion.)

One exception is found in the data from[63] (Figure 30): the YS-vs-Tε curve for steel "D" shows a bell-like curve, and is far higher than curves for the other steels. Steel "D" is 0.21C-0.15Si-2.51Mn, whereas the other steels contain less (1.5-2.0) manganese. D also has somewhat lower TEL and higher UTS values than the other steels. They speculate that the excessive manganese addition, and attendant reduction of the A_3 and T_O temperatures, accelerates the bainite transformation (i.e., section 2.5.5).

Figure 31[(50)], from Sugimoto et al., gives the mechanical properties of three steels as functions of Tε. These three steels, "Types I, II and III" (as discussed in section 2.4.4), vary not in chemistry but only in TMP, and thus phase distribution/morphology. Type II, which consists of retained austenite films between bainite laths, shows the lowest TEL and UTS×TEL values. Also, it shows little of the expected curvature in UTS or YS-vs-Tε.

The Type I steel was produced by heating as-cold-rolled to 900°C, air-cooling, and then performing an intercritical anneal-IBT TRIP treatment. Type II was produced by heating to 900°C, air-cooling, re-heating to 900°C, cooling to 730°C (intercritical) and then performing an IBT. Type III was produced by heating as-cold-rolled to 900°C, oil-quenching, and then performing an intercritical anneal-IBT TRIP treatment.

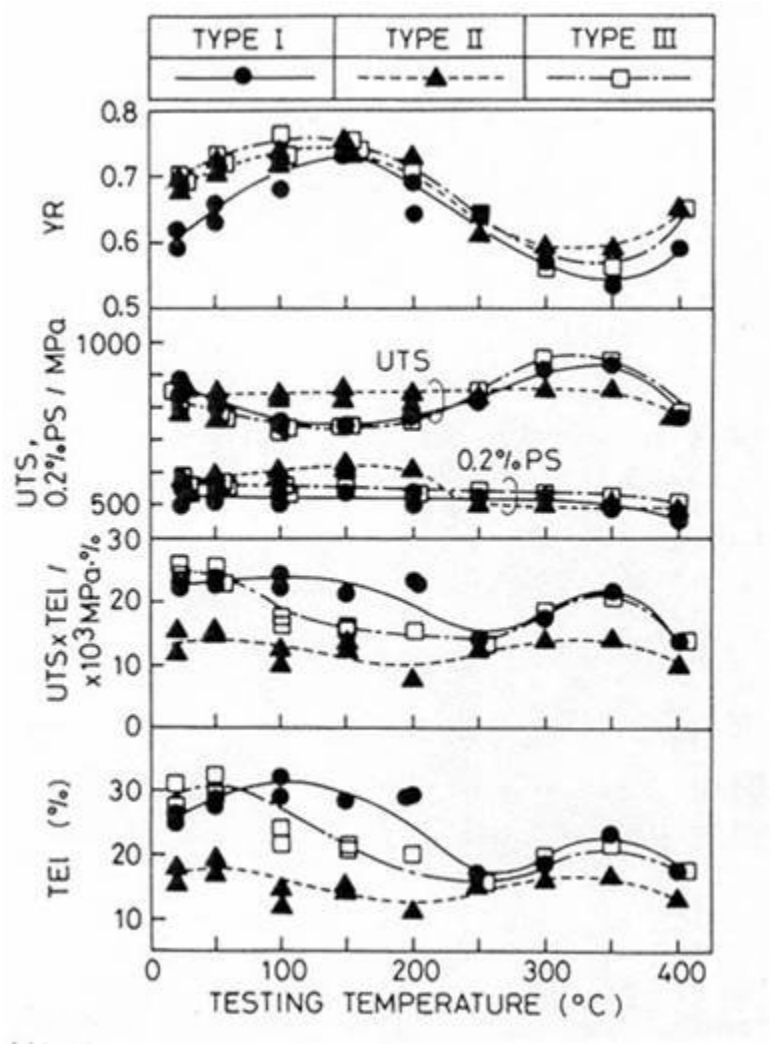

Figure 31 Effect of testing temperature and austenite morphology on mechanical properties[50]

As the austenite in the Type II steel is overly stable (discussed in section 2.4.4), it appears that the M_D temperature is likely below the lowest testing temperature, and the material does not exhibit TRIP-like mechanical properties.

These results imply that increases in austenite stability are not always desirable, and excess stability -- in the form of very low M_D -- results in a material of poor mechanical properties.

An excellent summary of different effects of temperature on mechanical properties is shown in Figure 32[58]. Here, samples of the same material were tested at different temperatures, and the flow curves are given.

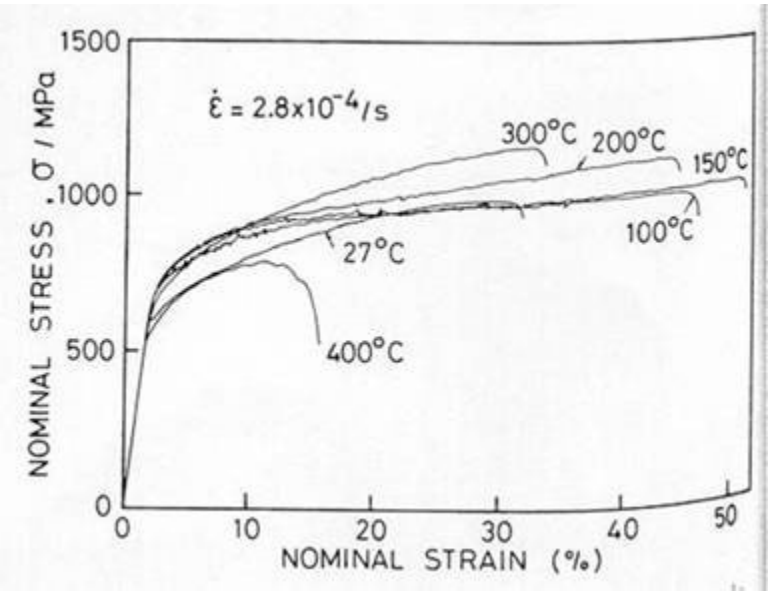

Figure 32 Flow curves at different temperatures[58]

Also from Sugimoto et al.[58] is a result from SEM examination of samples tensile tested to failure: at Tε=27°C, voids were observed where second phases met the ferrite matrix, whereas this was not observed at Tε= 150 or 350°C. They attribute this to the isotropic expansion of the martensite transformation relaxing the interfacial stresses. (The author questions this explanation; lower temperatures would result in a higher driving force and thus more random martensite variant nucleation (section 2.4.2), which would seem more isotropic. The author speculates that at higher temperatures, less martensite formed and more retained austenite survived beyond uniform strain; this effect was

probably fairly level above ~150°C, leading to the slight variation in the range 150-300°C.)

2.5.8 Effect of Strain Rate

Sugimoto et al.[58] studied a 0.4C-1.5Si-1.5Mn TRIP steel by performing tensile tests at different temperatures and different strain rates; $d\varepsilon/dt=2.8\times10^{a}$ /sec, where a=-2, -3, -4 or -5. (These strain rates are well below industrially interesting strain rates, ~10^{0} to 10^{3}/sec; high strain rate effects are discussed in 2.6)

UTS peaked around 300°C and at the lowest strain rate, 2.8×10^{-5} /sec. Total elongation peaked around 150°C at the second lowest strain rate, 2.8×10^{-4} /sec. See Figure 33[(58)].

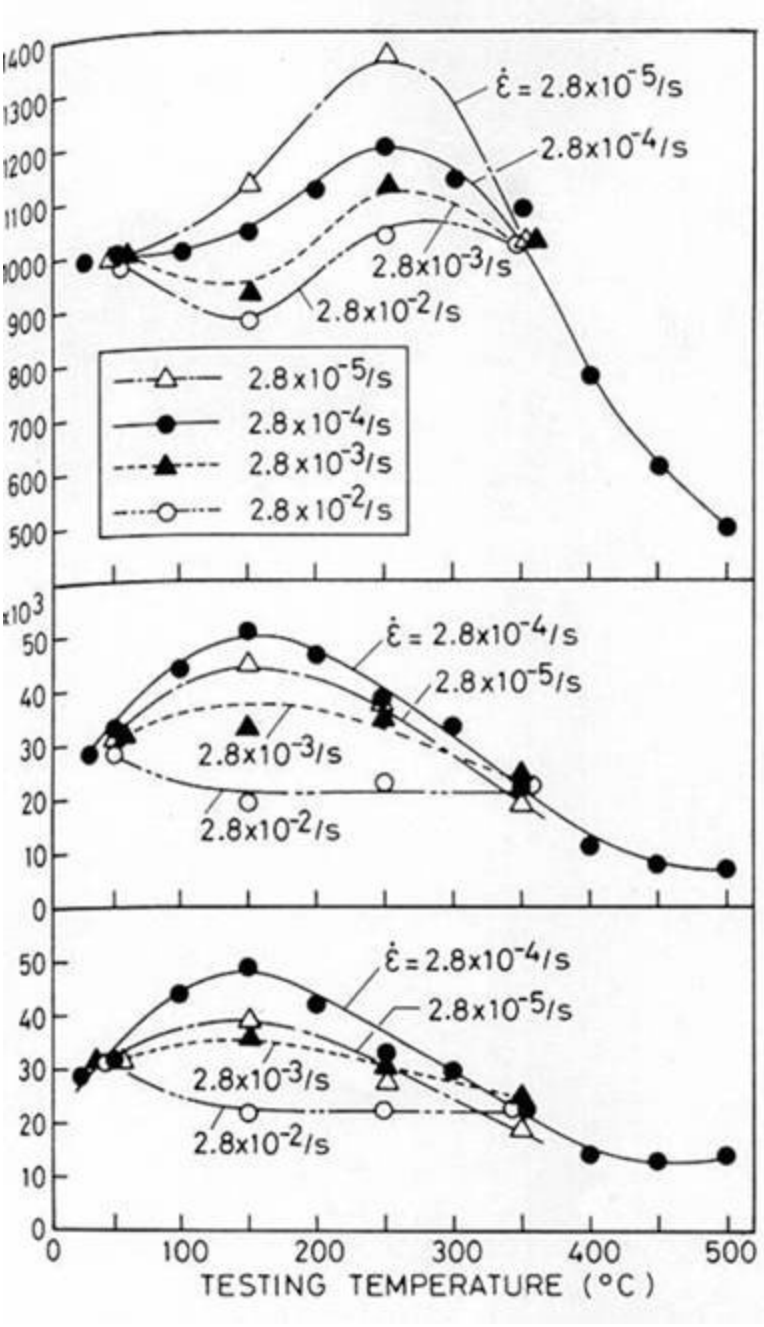

Figure 33 Effect of strain rate on mechanical properties[58]

It is important to note that at temperatures ~0-50°C, which would be more typical of service or fabrication of automotive sheet, there is almost no variation between the different strain rates.

No explanations were proposed for this behavior.

Sugimoto et al.[58] observed via TEM what they call "strain-induced bainite" in the samples deformed at or above 250°C. Although it might seem that this bainite might simply form as the sample is "annealed" at the elevated testing temperature, this does not seem to be the case. They annealed as-processed samples at the same temperatures for 1000 seconds, but without straining, and found the retained austenite fraction stable at temperatures below 400°C; thus, there was no austenite-to-bainite transition in the unstrained samples held at the same temperature as the tensile samples. Obviously, strain-induced defects in the austenite nucleated bainite precipitation. Although this implies existence of a "B_D" (bainite-start under deformation) temperature, no discussion was given.

2.5.9 Effect of Tensile Strain

All papers that measured f_γ as a function of tensile strain found an exponential decrease[15,18,40,72]. For example, Figure 34[(40)] shows the variation of "normalized" retained austenite fraction (f_γ/f_γ^O)-vs-percent deformation for the two steels they studied.

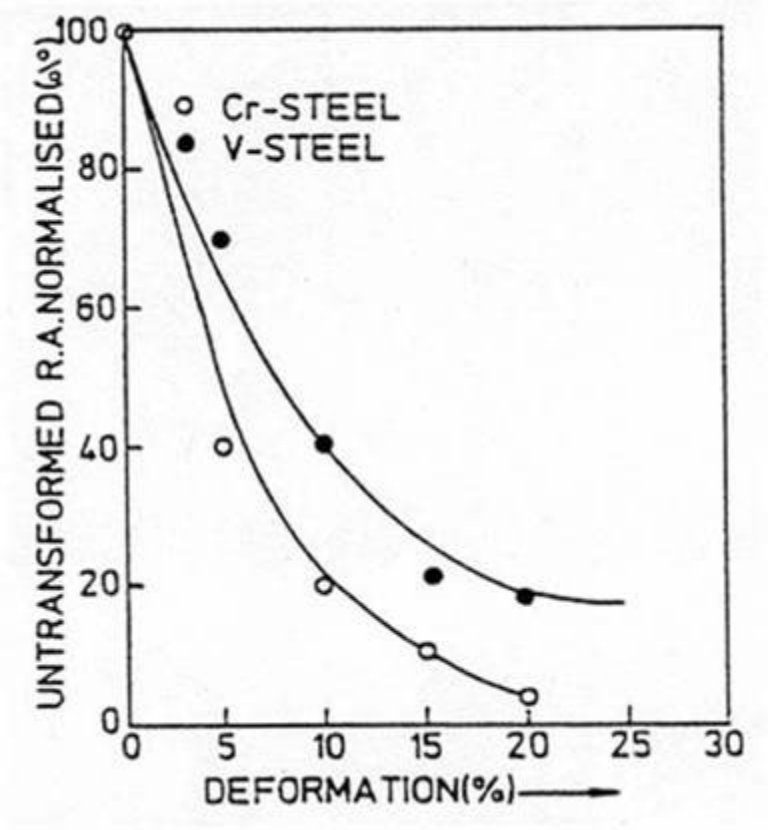

Figure 34 Decomposition of retained austenite with strain[40]

The austenite stability parameter, k, is well known in the TRIP literature:

$$f_\gamma = f_\gamma^O \exp\left[-k\varepsilon\right] \tag{2-4}$$

This k is useful as an "indicator of mechanical instability"[40] and allows quantitative comparison of retained austenite behavior under different conditions of alloying, processing or straining. This 'k' value will obviously be a factor determined by all stability-influencing parameters: austenite size, composition, shape, surrounding phases, etc.

Sugimoto et al.[58] studied f_γ-vs-ε at different testing temperatures, Figure 35[(58)]. At T=150°C, the temperature where total elongation was greatest, f_γ decayed most slowly (k was smallest). At temperatures associated with progressively worse total elongations (T=27°C and T=350°C) the f_γ decayed more quickly with increasing ε (k was large).

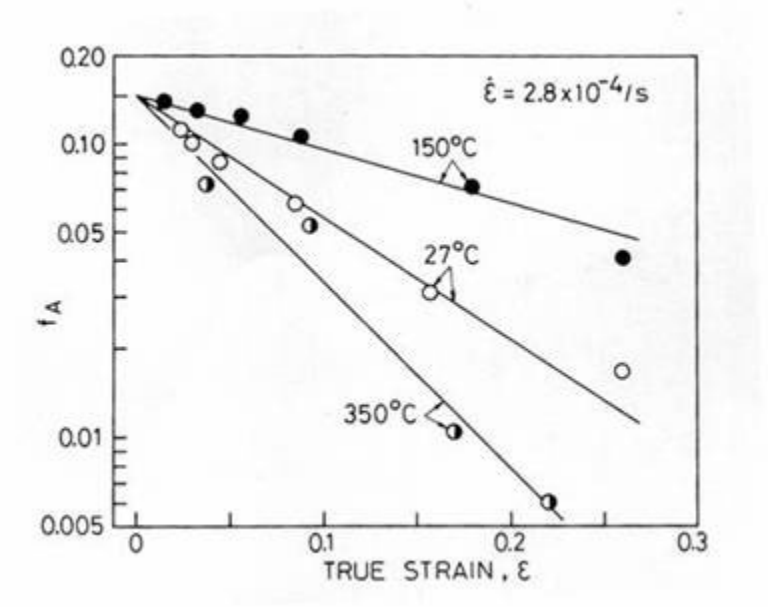

Figure 35 Variation of austenite stability with testing temperature[58]

2.5.10 Summary

The huge quantity of information in section 2.5 is only a review of the available empirical data obtained regarding the processing of TRIP-assisted multiphase steels. The most important point to remember is that the segregation of carbon into the austenite will be a primary factor deciding the stability of the retained austenite. However, as discussed in section 2.4.4, the morphology of the retained austenite is almost as important, or perhaps even more important.

As Yue et al.[82] summarized, "formability increases linearly with $f_\gamma \times [C]_\gamma$, but the sensitivity to the latter is different for each microstructural type… since other compositional and morphological factors also contribute to the stability."

2.6 Formability and Crashworthiness

Formability and crashworthiness are complex functions of many variables, predominately (but not limited to):

1. Forming/crashing conditions
    a. Stress state
    b. Temperature/adiabatic heating
    c. Strain rate
2. Austenite characteristics
    a. Volume fraction
    b. Distribution
    c. Alloying content -- especially $C\gamma$ and $Mn\gamma$
    d. Matrix constraints / surrounding phases
    e. Morphology
3. Other phases
    a. Bainite fraction, hardness, and composition
    b. Is it bainite -- containing carbides -- or carbide-free bainitic ferrite?
    c. Presence or absence of carbides, and their distribution

d. Presence or absence of martensite, and its distribution

These issues will be discussed below.

2.6.1 Formability

Although TRIP-assisted multiphase steels have seen some use in the automotive industry, many potential applications are still beyond the reach of current technology; for example, TRIP steels have excellent stretch-formability and deep-drawabilty, but poor stretch-flangeability[83]. Sugimoto et al.[83], for example, suggest A stretch-flangeable TRIP steel could be used in suspension parts, significantly reducing vehicle weight.

2.6.2 Stretch Forming

Various studies have confirmed and re-confirmed the superior stretch-formability of TRIP-type steels[83,84,85,86,87,88,89,90,91,92,93,94]. Typically, stretch-formability is quantified by a measure of maximum stretching-height, H_{max}, or more often, the product of H_{max} and tensile strength, $H_{max} \times UTS$. Using this definition, stretch-formability has been found to increase as a strong function of initial retained austenite volume fraction[84,86,88,89,90]. It has also been found that a low value of the retained austenite stability parameter, k, is desirable[92]. Steels with a bainitic, rather than ferritic, matrix tend to have superior TS at a constant value of H_{max}[83,85,86,87].

Sugimoto et al. found that even slight changes in forming temperature will result in large changes in formability for a given steel[86,88,89,91]. They found a temperature T_P for each steel at which formability was highest. This temperature increased with increasing M_S of the retained austenite. Forming at T_P, rather than room temperature, could significantly improve the formability of steels with low retained austenite volume fractions or low austenite stabilities.

It was also found that biaxial stretching, rather than simple tension, resulted in faster decomposition of the retained austenite (that is, a higher effective k value)[89,90]. For example, see Figure 36.

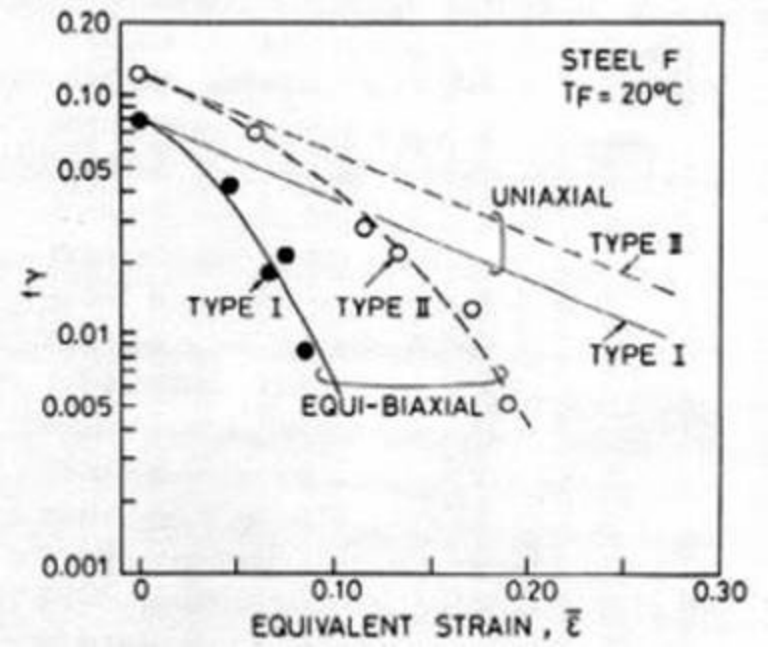

Figure 36 Effect of uniaxial vs biaxial stress on austenite decomposition[90]

In other words, austenite decomposition is strain-path dependent.

This is attributed to a change in micro-mechanical stress state around the retained austenite particles, resulting in an increase of effective M_S. Streicher et al.[95] debated this result. The author, however, feels the preponderance of evidence sides with Sugimoto et al., rather than Streicher et al.

Sugimoto et al.[89,90] also studied the effects of the morphology and distribution of retained austenite. They processed steels to obtain two different microstructures: "Type I," in which the retained austenite consists of a network of circular retained austenite particles, and "Type II," which consists of isolated, fine, acicular retained austenite particles. Although Type I had a larger total elongation and uniform elongation, Type II had superior local (post-uniform) elongation. Further, the optimum forming temperatures, T_P, for Type II structures were found to be on the order of room temperature, whereas for Type I structures it was ~100-200°C. Because of the fine and isolated structure of the Type II austenite, they did not act as stress-concentrators, thus avoiding void initiation, like observed in the Type I austenite. Thus, despite lower elongation, Type II was found to be of superior formability.

Bleck and co-workers[96] have noted that formability of TRIP steels shows improvements with slightly increased temperature. In their specific work[96], ~50°C was found to lead to improvements in various grades of TRIP steel.

2.6.3 Minimum Bending Radius

Matsumura et al. studied the minimum bending radius of TRIP-type steels[92]. They found that low to moderate initial retained austenite volume fractions were ideal, rather than large initial volume fractions, because of the concomitant enrichment of carbon and associated lower k value. Thus, in bending, stability of austenite outweighs the volume fraction of austenite.

2.6.4 Stretch-Flangeability

Stretch-flanging is typically quantified in a hole-expanding-limit test and the maximum hole expansion ratio λ, or as the product $\lambda \times$TS.

TRIP steels have, to date, poor stretch-flanging. This can be somewhat ameliorated by reducing the initial volume fraction of retained austenite[84,92] or increasing the stability (lower k) of the retained austenite[92]. Typically, microcracks present at the edge of the hole prior to the hole-expansion test quickly propagate through the structure[83,84]. This is often caused by differences in hardness between adjacent phases in multiphase steels, which results in void formation[84], and large particles of tripped martensite are a primary culprit in TRIP-type sheets[83]. This surface damage around the hole is often quantified as a critical damage depth ℓ^*.

Sugimoto et al.[83,85,86,87] found that replacing the ferritic-matrix steels with bainite-matrix steels significantly improves stretch-flanging. The steel used in these studies consisted

of bainitic ferrite laths and interlath retained austenite. This resulted in a short diffusion distance of carbon during heat treatment and resulted in high-stability austenite. Further, the fine size of the interlath retained austenite meant that it would not act as void initiation sites upon transformation to martensite. A low value of ℓ^* resulted, and what little damage was present propagated very slowly. Thus, steel consisting of bainite/bainitic ferrite and interlath austenite was concluded to possess the best formability.

This effect is consistent with classical formability concepts. Steels with small volume fractions of inclusions, for instance, have superior λ values to those with more inclusions. Similarly, at a constant volume fraction of inclusions, a steel with shape control will show superior hole-expansion to a steel in which the inclusions are not shape controlled[97]. See Figure 37.

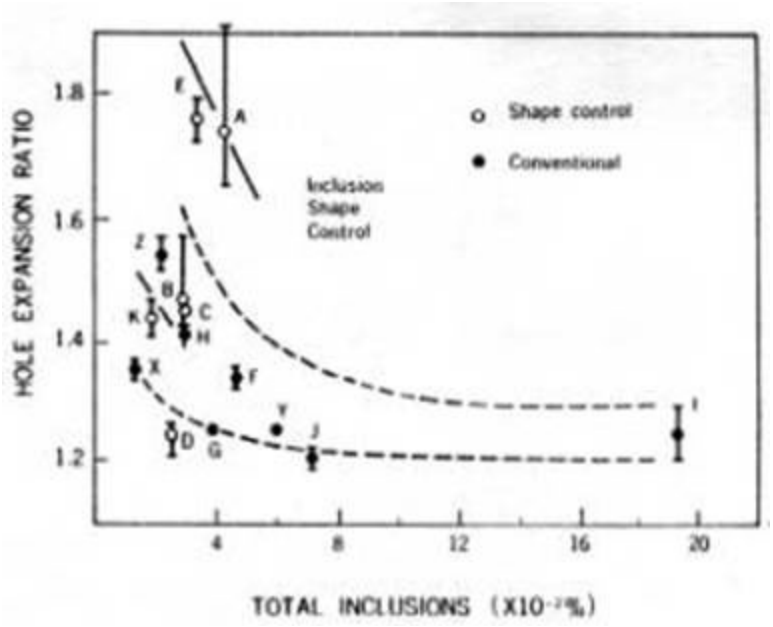

Figure 37 Effect of inclusions with and without shape control on hole-expansion limit[97]

2.6.5 Crashworthiness

TRIP steels are often considered for crashworthiness applications because of their high strength-ductility balance. As shown in Figure 38[98], non-TRIP steels of many different microstructures follow a strength-ductility law below that followed by the TRIP steels.

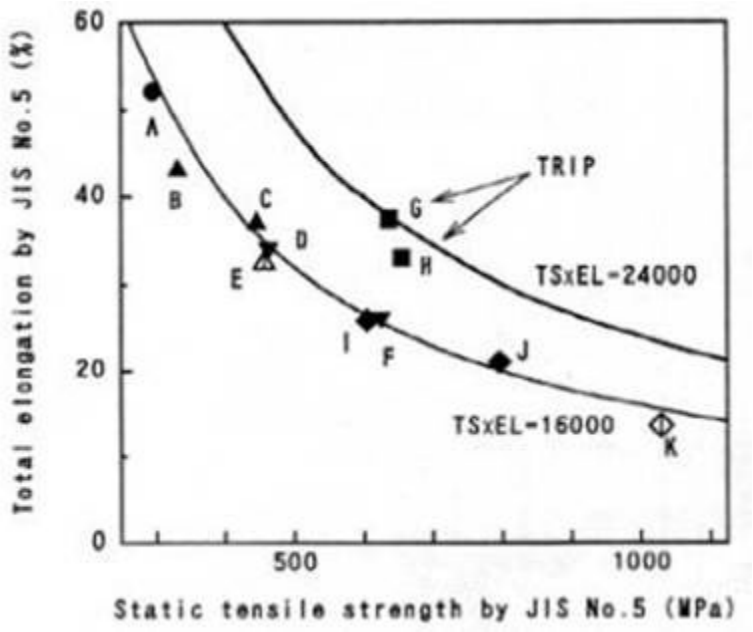

Figure 38 Strength-ductility balance for TRIP and traditional steels[98]

Most published crashworthiness data relates the crashworthiness of a steel to its energy absorption during a dynamic test; typically tensile tests[99,100,101] or compressive-column-buckling tests[98]. These reports often leave the reader with more questions than answers; some papers[98,99,101] take a mechanical engineering point of view, showing interesting results of dynamic tests, often encompassing the powerful and elegant finite-element method (FEM) to simulate results. However, these studies never perform metallographic analyses of the steels tested, except a brief comment on the micro-constituents present, annotated by "hot rolled" or "cold rolled." The paper of Bleck and Schael[100] reported some microstructural data, but took a highly simplistic view of the mechanics of crashworthiness, depending on tensile tests alone.

Before definitive conclusions can be made regarding retained austenite in crashworthiness applications, microstructural characterization of retained austenite both before forming of parts, between forming and dynamic tests, and after crashing, must be made. However, some preliminary conclusions have been drawn in the literature, and the author will make some speculations based upon these conclusions.

Bleck and Schael[100] performed tensile tests at strain rates varying from 0.005/second to 200/second on two ferritic steels, three dual-phase steels, one TRIP-assisted multiphase steel and two austenitic stainless steels. Although the stainless steels were found to possess the best energy absorption properties, this result is meaningless to the automotive industry due to the cost of 18Cr-8Ni and 18Cr-6Ni grade steels.

Of the remaining steels, Bleck and Schael found the TRIP steel to have the most energy absorption when strained to failure, although the high-strength dual-phase grades were best when strained, not to failure, but rather to 10%.

Interestingly, Bleck and Schael found the dual-phase and TRIP steels to have minimum tensile elongations at moderate strain rates. At very high (200/second) and very low (0.005/second) strain rates, their elongations were greater than at 1-3.5/second. Bleck and Schael attributed this to adiabatic heating, estimated at ~120K, during the high strain rate tests. However, no mechanism (i.e., austenite stability vs. temperature) was proposed.

Mizui et al.[98] tested various steels: one Ti-bearing IF, several low carbon mild steels, two Nb-microalloyed mild steels, a bainitic steel, two dual phase steels, and two Al-bearing TRIP grades. Mizui et al. formed 1.2mm sheet or strip into columns and crushed the columns at speeds of either 4m/s or 0.2m/min. Finite element models indicated the highest strain rate achieved within the dynamically crushed column would reach 2000/second, so Mizui et al. also performed tensile tests at 0.004/second and 2000/second.

They correlated energy absorbed in the dynamic buckling tests to static UTS, Figure 39.

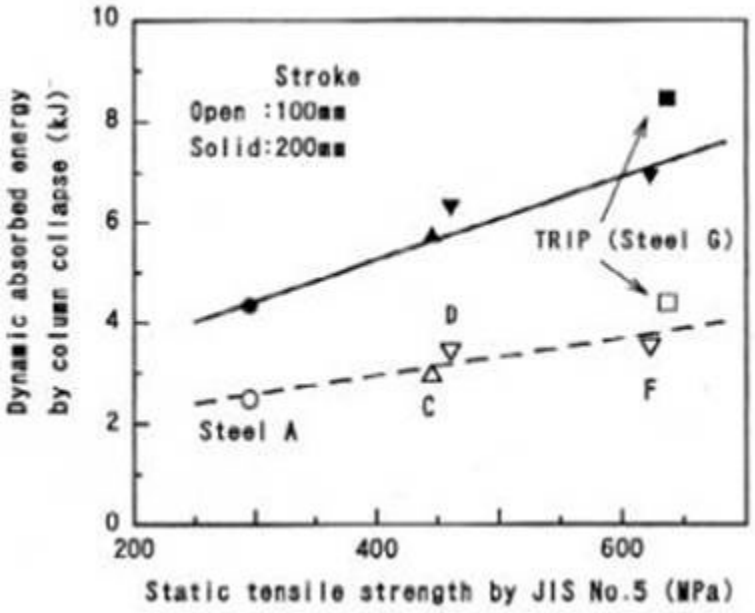

Figure 39 Dynamic energy absorption vs tensile stress[98]

The most important result is that non-TRIP steels fall on a straight line on an absorbed energy-UTS graph, but TRIP steels fall above this extrapolated curve. Takahashi et al.[94] found this identical result, but for both TRIP and dual-phase steels.

Mizui et al. compared the dynamic tensile curves of a TRIP steel to a 0.10%C-0.040%Nb ferrite-pearlite steel, Figure 40.

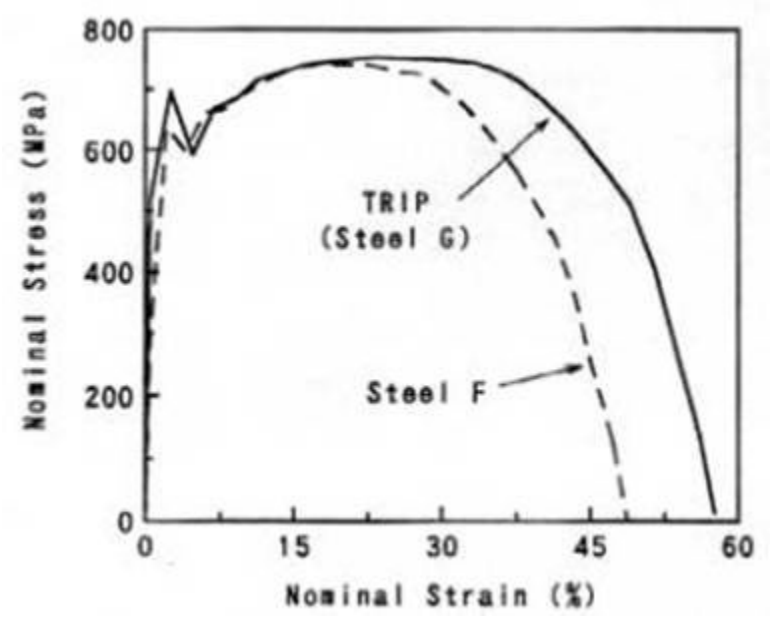

Figure 40 High-strain-rate stress-strain curves for TRIP steel (G) and 0.10%C pearlitic Nb-microalloyed steel (F) [98]

Although both steels have the same dynamic UTS, the greater strain-hardening rate and concomitant higher ductility of the TRIP steel result in a higher absorbed energy. Thus, strain-hardening behavior is as important as strength in determining a steel's crashworthiness.

Another interesting result from Mizui et al. is shown in Figure 41.

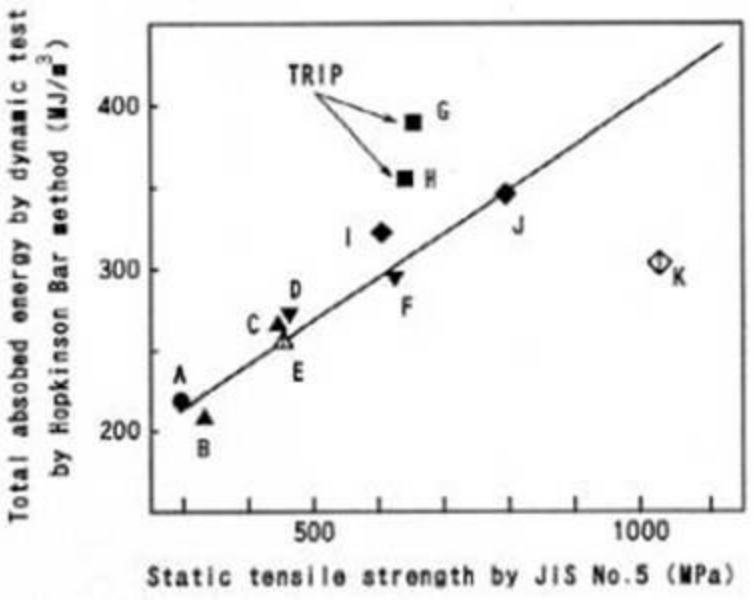

Figure 41 Dynamic energy absorption vs static tensile strength[98]

They graph energy absorbed during a dynamic tensile test vs. static UTS. The mild steels and dual-phase steels fall on a straight line, with the TRIP steels above that line, as expected. However, the bainitic steel falls well below that line, indicating poor crashworthiness. As discussed in section 2.6.4, Sugimoto et al.[83] concluded that bainitic-matrix retained-austenite-bearing steels should have superior formability. The crashworthiness of these steels should be investigated before they are put into practice, however, as their bainitic matrix may leave them with poor crashworthiness, in light of the results of Mizui et al.[98].

Nakanishi et al.[101] performed a very through study of strain-rate-sensitivity effects on the energy absorption of various steels during crashworthiness, even going so far as to crush press-formed front-end members at 15.6m/s

First, Nakanishi et al. assert that increasing static tensile strength of constant strain rate sensitivity provides increasingly diminishing returns with respect to energy absorption; thus, simple linear increases of strength are not an effective means of improving crashworthiness. Rather, strain rate sensitivity is the material parameter of relevance.

Unfortunately, Nakanishi et al. quantified strain rate sensitivity as the ratio of dynamic UTS to static UTS, yielding a value "D/S," ~1.2-1.6, rather than as the well-known metallurgical "m" value, m~0.2 to 0.3 for steels.

Firstly, from FEM computer modeling, Nakanishi et al. confirmed the result that at constant strength (in this case, 590 MPa), increasing strain rate sensitivity improves crashworthiness. They also confirm that at a constant D/S value, an increase of UTS provides only minimal improvement in energy absorption.

Nakanishi et al. then performed dynamic tensile tests on unstrained and pre-strained materials to determine strain rate sensitivity D/S at different levels of pre-strain. The pre-strain was intended to simulate forming operations performed on automotive steels. As dual-phase and TRIP steels had high D/S values initially, and maintained these high values after pre-straining, dual-phase and TRIP steels should show excellent energy absorption properties, especially after pre-straining, due to the work-hardening during pre-straining. Crash-testing actual front-end members confirmed this result. Nakanishi et al. concluded that 15% weight savings are possible by replacing conventional steels with the dual-phase steel they tested; the TRIP steel would likely give similar results,

especially if optimized to provide excellent strain-hardening and strain-rate sensitivity behavior.

Optimization of TRIP steels for crashworthiness applications will not necessarily be easy. De Cooman's research group[102,103] found that an Al-added TRIP steel showed improved total elongation and absorbed energy increased under dynamic conditions, whereas a Si-only steel suffered a loss of elongation.

On the topic of pre-strain, Takahashi et al.[94] found that a 5% tensile pre-strain greatly improved the dynamic energy absorption of a dual-phase steel, while pre-strain had almost no effect (beneficial or detrimental) on a TRIP or a Ti-precipitation hardened mild steel.

Thus, these results[98,100,101] lead to the conclusion that TRIP steels show the potential for excellent crashworthiness, although dual-phase steels may show the same crashworthiness at the same strength level[94,104,105]. Even if the ductility enhancement of TRIP steels should be found to be a second-order benefit, the high strength and strain-rate-sensitivity of TRIP steels will still provide benefits to crashworthiness.

2.6.6 Commentary

Formability -- such as stretching, cupping or flanging -- correlates in a non-linear way with the easiest parameter to measure experimentally, volume fraction of retained austenite. This is because of variations in austenite stability with the composition of

austenite and the shape, size and surroundings of the austenite. As described above, retained austenite volume fraction is only one of many critical factors. In some applications, volume fraction is not even the most critical factor, although published literature often unduly fixates on it.

To truly understand the formability of TRIP steels, it will first be necessary to characterize them properly. Any fundamental formability study or industrial alloy development must be backed by proper microscopy. The proper tool for this would be an analytical electron microscope (AEM).

SIMS (secondary ion mass spectrometry) has, in theory, nanometer resolution; typical SIMS operation gives spatial resolution of about 250nm in practice, and when provided with good standards, can easily quantify solute concentrations well below the parts-per-million level[106]. However, SIMS is an extremely costly experimental technique and will never have the versatility of an electron-beam instrument. Unlike SIMS, an AEM can simultaneously provide micrographs (from under 1000x magnification up to lattice resolution, as required), diffraction patterns, and chemical microanalysis.

The substitutional alloy composition of the austenite should be examined by EDS and PEELS, especially for Mn segregation. Soft-annealing studies, for example[81] have measured manganese segregation using STEM and EDS. Modeling (see section 2.4.1) has found Mn segregation levels in retained austenite to be second only to C in importance in chemically determining stability.

Carbon contents of retained austenite can be estimated by x-ray or neutron diffraction, or by in-STEM convergent beam electron diffraction using HOLZ (higher-order Laue-zone) lines. However, these measurements depend upon comparing experimental lattice parameter measurements to standard measurements. Standard measurements are typically carried out on ultra-high purity Fe-C binary alloys, rather than on steels, and these measurements are carried out at high temperatures. Onink et al.[107] are typically considered to have performed the most accurate measurements of this variety (to date).

These lattice parameter measurements, however, require extrapolation to room temperature and do not account for alloying additions other than carbon. Thus, any measurement of the lattice parameter of retained austenite in a TRIP-steel will allow, at best, only an estimate of its actual carbon content. Further, diffraction studies will average across many austenite grains, when the carbon content of every austenite grain will be different. Indeed, Scott and Drillet[108] found the carbon contents to vary within individual austenite grains.

The only diffraction technique that will allow examination of localized carbon content is in-AEM CBED using HOLZ lines. This, however, is by no means a simple experiment. Scott and Drillet[108] note a number of artifacts. Any defects in the retained austenite, such as dislocations, will result in broadening of the HOLZ lines, which makes them harder to interpret -- or even see. Further, CBED should be performed at liquid nitrogen

temperatures to eliminate thermal diffuse scattering[108,109], but reducing a TRIP specimen's temperature to this degree will transform much of the austenite. Simply performing the technique of Scott and Drillet requires tilting the austenite grain of interest to a **B**=<119 595 243>γ zone axis orientation -- a hideously difficult exercise. Further, only crystals thick enough to enter the dynamical regime of electron diffraction (~50nm) will exhibit HOLZ lines, but a crystal much thicker than ~200nm will have patterns that are of insufficient intensity[108], and also beyond ~200nm, energy losses of the electrons within the specimen will become substantial[109]. As a diffraction technique, HOLZ analysis will be subject to the uncertainties in lattice parameter standards discussed above. Scott and Drillet estimated their error in carbon concentration at $\pm$0.2%. (The author would desire 0.1% or better, if possible, for formability studies.) Further, diffraction can only be applied to austenite. Examination of phases with other crystal structures would require the development of proper experimental procedures. Further, if a BCC/BCT technique were developed, the defect density of martensite would likely render the martensite HOLZ lines invisible. Thus, the examination of prior-retained austenite would be impossible using CBED techniques.

In diffraction's defense, however, it should allow easy and accurate relative measurements of average carbon content from one sample condition to the next, even if the exact or local carbon contents cannot be determined. Sugimoto et al. showed an increase in average carbon content with tensile strain, indicating the preferential decomposition of less-enriched austenite grains[90]. (Scott and Drillet noted that martensite areas that had transformed from retained austenite were of lower carbon

content than the remaining austenite in the M-A island, micro-chemically verifying Sugimoto's macroscopic observation.)

PEELS analysis, of an exquisitely clean specimen after calibration of the microscope with excellent standards, has allowed determination of austenite carbon contents to an accuracy measured in parts-per-million[108]. Further, this measurement can be localized to areas only nanometers across in austenite, as well as martensite, ferrite or carbides. Although PEELS is a technique fraught with artifacts[108,110,111,112], these artifacts can be corrected for by diligent work[113,114]. The author believes that only though analytical electron microscopy, and correlation to standard formability testing, will the mechanics of TRIP steels truly be understood. Scott and Drillet examined highly localized areas within individual retained austenite grains and determined the carbon content of these areas to accuracies better than 0.1%. They note that the current generation of PEELS systems should allow detection of carbon contents to 200 parts per million, and they quoted a value of 400ppm in their older system (Gatan PEELS 666 mated to a Phillips CM200 FEG-STEM). PEELS is, by far, the best technique for determining carbon contents of retained austenite. Although time-consuming, no other technique could approach a $\pm$200ppm carbon determination with the same combination of diffraction, chemical and micrographic data.

In any formability study, SEM and conventional TEM must be performed to look for martensite and carbides. If the bainite isothermal transformation is allowed to proceed for too long a time, or if the alloy does not contain a high enough level of carbide-

inhibiting elements (see sections 2.5.5 and 2.5.6), carbides will form in the retained austenite or bainite. This will result in a loss of C in the austenite and thus a worsening of k value and formability. In Traint et al.[68], carbides were observed (via TEM) in TRIP-steels of poor ductility (Figure 25). Scott and Drillet[108] examined a TRIP steel intercritically annealed for only 36 seconds; this inadequate holding time left un-dissolved carbides, which were observed by TEM. Eberle et al.[81], using SEM, noted envelopes of retained austenite surrounding non-transformed carbides. However, the particles labeled as "austenite" or "carbide" in the micrographs of Eberle et al. appear similar under SEM with the etching techniques used. It would have been beneficial to see selected area or convergent beam electron diffraction patterns from TEM of these particles to confirm their identity. Baring TEM analysis, in-SEM electron backscatter diffraction would have allowed identification of phases or reasonably large (1 micron) particles.

Techniques exist (see Sections 4.2.3, 4.2.4) for differentiating martensite, bainite and austenite via SEM and optical microscopy. TRIP steels should be examined before formability testing to quantify the martensite and bainite distributions. Although the presence of martensite is not necessarily detrimental, steels to be used in applications of the highest formability should be martensite-free. TRIP steels intended for higher-strength applications (where less ductility is needed) might benefit from increased martensite and bainite levels, where even a small fraction of austenite would still give the steel ductility values superior to dual-phase steel, if not quite on par with lower-strength TRIP steels.

Comprehensive microscopy is necessary for understanding the properties of TRIP steels during their original laboratory-scale development, and, should the need arise, for trouble-shooting of industrial production.

Additionally, various mechanical effects have gone unstudied to date in TRIP steels. None of the above cited crashworthiness studies investigated the possible Baushinger effect (BE) softening or compressive work embrittlement (CWE) of steels subjected to complex forming strains. The BE[115,116] and CWE[116,117] both have the potential to ruin the properties -- static or dynamic -- of improperly formed sheets. The BE has been found to be particularly severe in α-γ duplex alloys[115]. As the BE is due to the interaction of positive and negative dislocations from the same sources, the author speculates that the increased BE in two-phase materials may be due to the increased dislocation density predicted by the Ashby dislocation model inherent to any multiphase microstructure (see section 2.7). Nakanishi et al.[101] did not clearly define their pre-strain path, but the author infers it was a purely tensile stretch and did not include the compressive component necessary for the BE or CWE to become important. Takahashi et al.[94] explicitly used only tensile pre-strain and tensile crash-testing strains, ignoring the BE.

Only by crash testing of formed parts made of TRIP and dual-phase steels can the influence -- or lack thereof -- of the BE and CWE be determined. Simple pre-straining

or crushing of columns is not sufficient to determine whether or not these materials have the expected improved crashworthiness.

2.6.7 Summary

Although the formability issues of TRIP steels have been studied intensively, providing many important results, it is the author's feeling that many more, equally important, questions have not yet been answered, simply because the wrong techniques have been applied. Proper micro-chemical analysis is a necessary addition to the standard macro-level tests. Further, subtle mechanical effects such as CWE have been studiously ignored.

2.7 Work Hardening of Mulitphase Steels

2.7.1 Introduction

A number of papers, published in the late 1970's and early 1980's, give profound insight into the work hardening of dual-phase steels[46,118,119,120,121]. Balliger and Gladman[120] and Lanzalotto and Pickering[121] make use of Ashby's elegant work hardening theory[122].

2.7.2 Dual-Phase Steels and Applicability to TRIP Steel

Dual-phase steels, in this context, are defined as steels with low yield strengths, high tensile strengths, high rates of work-hardening, large elongations, and little or no yield-point-elongation. This is achieved by manufacturing steels with a soft ferrite matrix containing 5-50% volume percent "second phase," where the second phase consists of martensite, bainite and retained austenite. These steels may either be as-hot-rolled with proper temperature control in finishing, run-out and coiling, or cold-rolled and intercritically annealed.

Because the martensite, bainite, and retained austenite constituents are classified as "hard phases"[46,120,121], especially when in the context of Ashby's theory, these results and models should be applicable to TRIP-type multiphase steels.

2.7.3 Effects of Microstructural Parameters

The studies all agreed in general terms: an increase in second-phase volume-fraction, f_{M-A}, results in a strong increase in tensile strength of the material and an increase in work hardening rate, often as measured by the work-hardening parameter $n = (\varepsilon/\sigma)(d\sigma/d\varepsilon)$. Figure 42 demonstrates the effect of f_{M-A} on the flow stress of dual-phase steels at various strains, and Figure 43 demonstrates the effect of f_{M-A} on work-hardening rate.

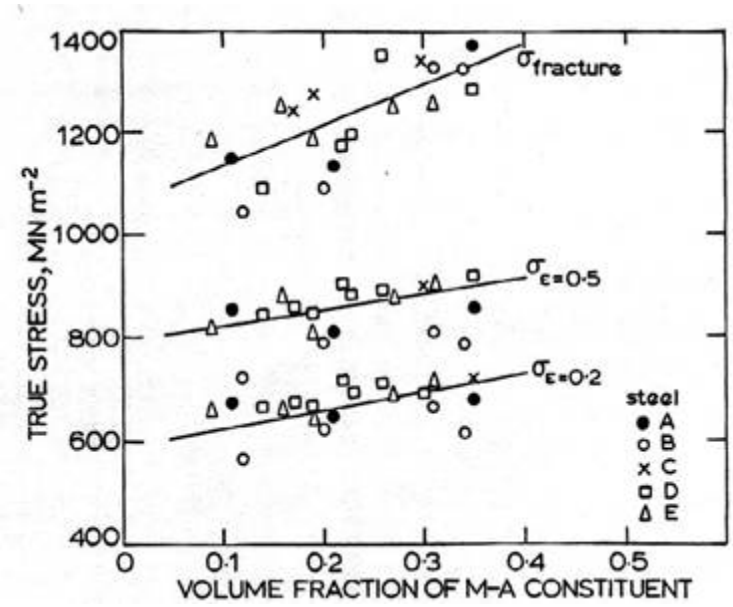

Figure 42 Effect of M-A volume fraction of ultimate tensile stress[121]

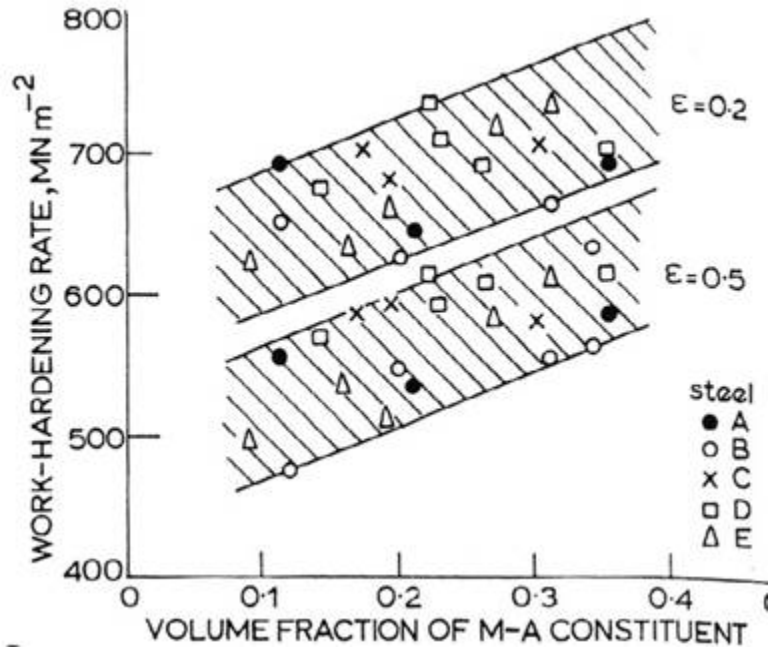

Figure 43 Effect of M-A volume fraction of work hardening rate[121]

Whether an increase in f_{M-A} results in an increase in elongation depended on the specific material studied, as elongation scales as n and as inversely as tensile strength. The effect on elongations was typically very minor, see Figure 44.

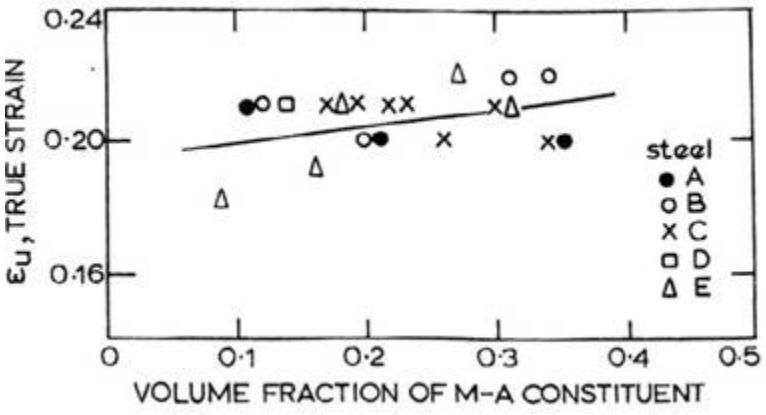

Figure 44 Effect of M-A volume fraction on uniform elongation[121]; effect is minor

All studies found that an increase in f_{M-A} resulted in a decrease in yield stress; Rigsbee and VanderArend[46] found that this trend reversed at large martensite volume fractions. The decrease in yield stress is attributed to the micromechanical deformation in the ferrite matrix around the particles, typically to a depth of ~1 micron into the matrix, which produces a high density of mobile dislocations. Rigsbee et al.[118] found that increasing f_{M-A} drastically reduced both the yield stress to tensile stress ratio and the Lüders strain. This is likely due to the increased dislocation density around the martensite islands. Yield stress is reduced because of the high density of mobile dislocations, and this high density results in less effective pinning by the solute carbon and a concomitant loss of yield point elongation. Rigsbee et al.[118] also found that the formability -- quantified as the product of tensile strength with total elongation -- increases rapidly with increasing f_{M-A} up to about 5 volume%, then becomes steady, Figure 45.

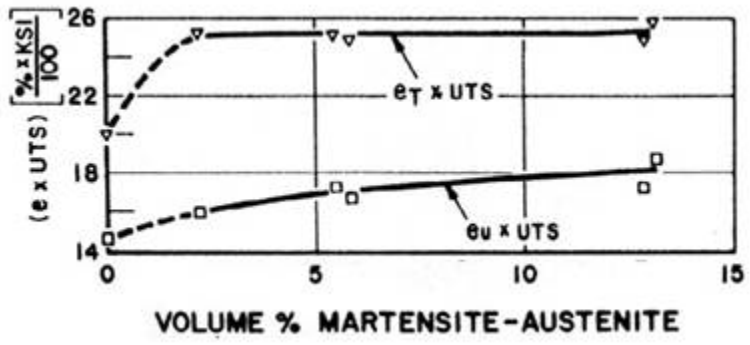

Figure 45 Effect of second phase volume fraction on strength-ductility balance[118]; "dual-phase" behavior sets in at approximately 5 vol%

Obviously, as $f_{M\text{-}A}$ increases beyond 0.05, strength will increase and total elongation will decrease, leading to a steady balance. This initial 5% appears to be a transition from classical to dual-phase behavior.

All studies also found that at constant $f_{M\text{-}A,}$ a decrease in particle size, $d_{M\text{-}A}$, (called $\lambda_{M\text{-}A}$ by Lanzillotto and Pickering) had minimal effects on strength, but greatly increased ductility. Note that through stereological relations, decreasing $d_{M\text{-}A}$ at constant $f_{M\text{-}A}$ will result in a decrease in interparticle spacing, $L_{M\text{-}A}$. Figure 46 shows the effect of particle size on work hardening rate and Figure 47 shows the effect of island size $d_{M\text{-}A}$ on work hardening rate, uniform elongation, and tensile stress.

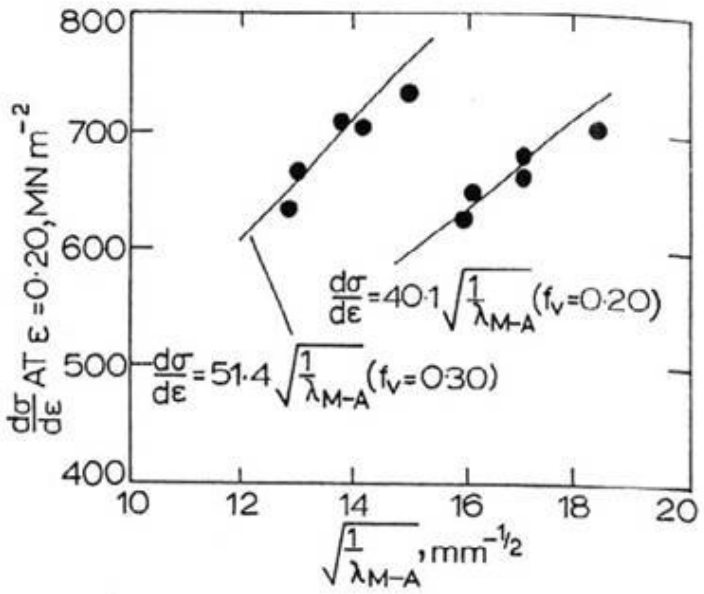

Figure 46 Effect of inter-island spacing on work-hardening rate[121]

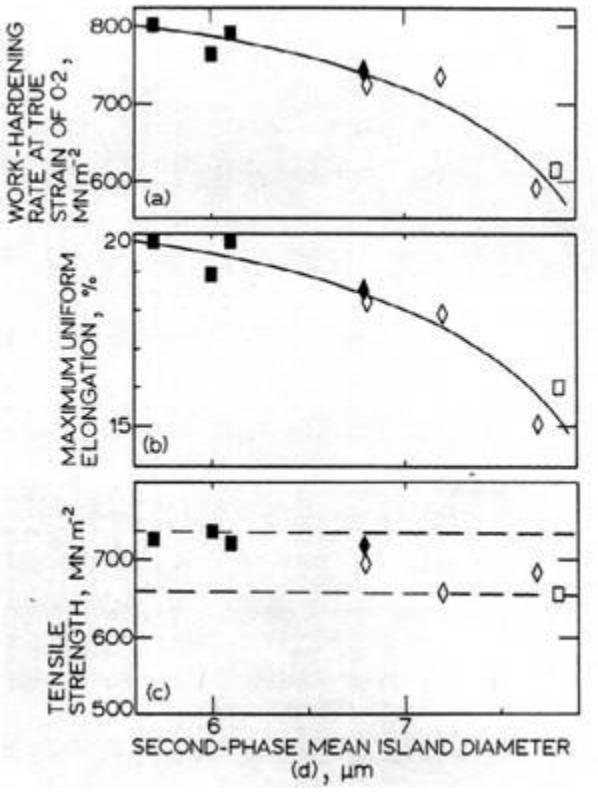

Figure 47 Effect of second phase size on (a) work hardening rate; (b) uniform elongation; (c) tensile strength[120]. All at constant f_{M-A}=21±2vol%.

Rigsbee and VanderArend[46], Cribb and Rigsbee[119], and Rigsbee et al.[118] also found that the volume fraction of retained austenite, and its distribution, had a more beneficial effect than the martensite itself -- despite the classical definition of dual-phase steel being that of a ferrite/martensite composite. First, they noted that work hardening, n, was degraded at large volume fractions of "second phase," Figure 48. However, work hardening parameter, n, increased monotonically with retained austenite volume fraction, Figure 49. Secondly, work hardening improved monotonically with decreasing retained austenite interparticle spacing, Figure 50. Lastly -- and most interestingly in the context of this work -- uniform elongation increased monotonically with retained austenite volume fraction, Figure 51.

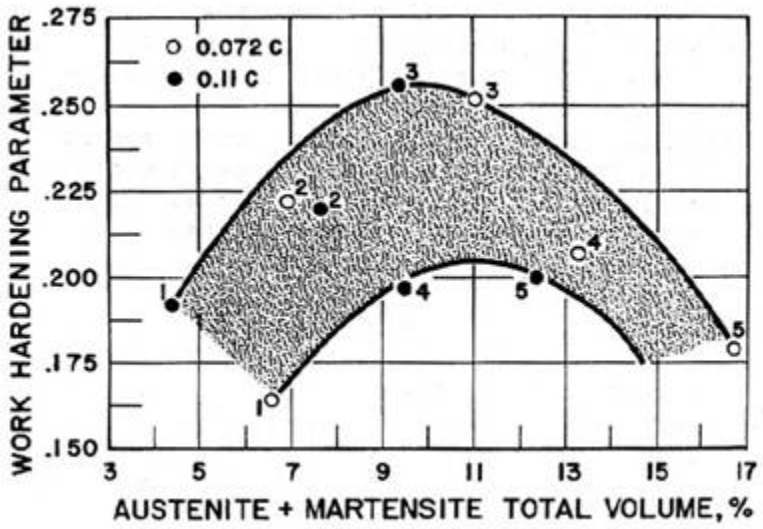

Figure 48 Effect of M-A fraction on work hardening[46]

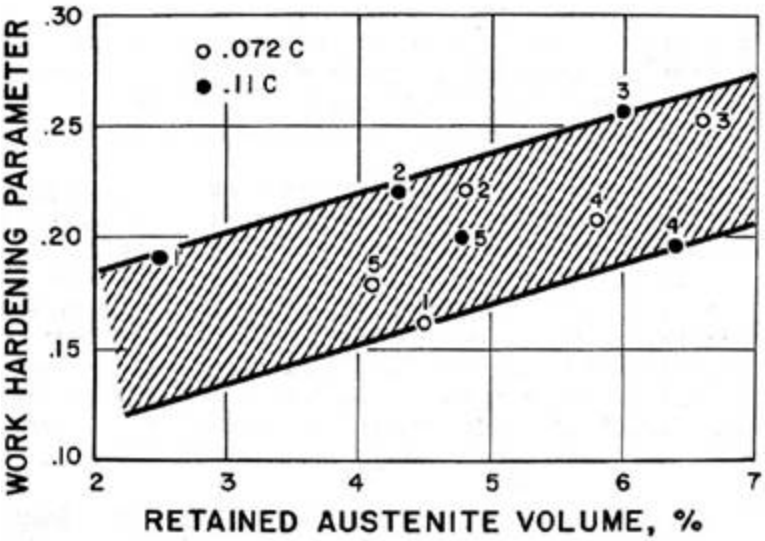

Figure 49 Effect of volume fraction of austenite constituent alone on the work hardening parameter[46]

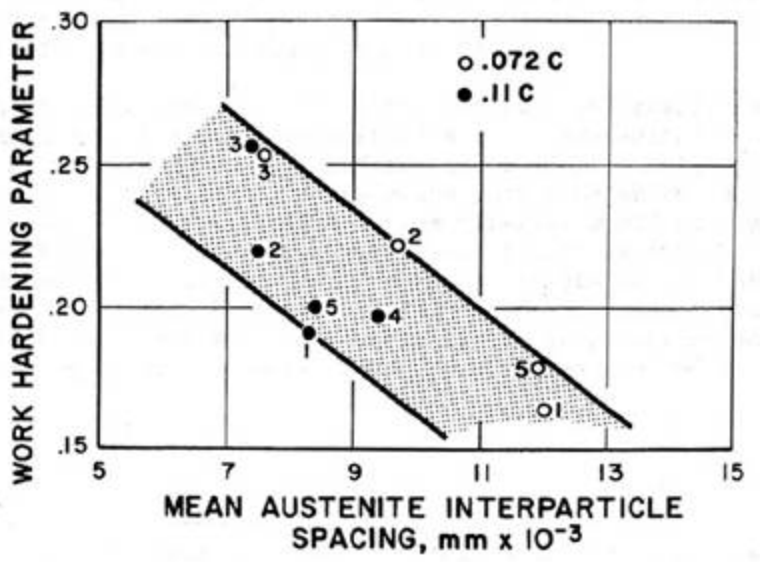

Figure 50 Effect of austenite dispersion on the work hardening parameter[46]

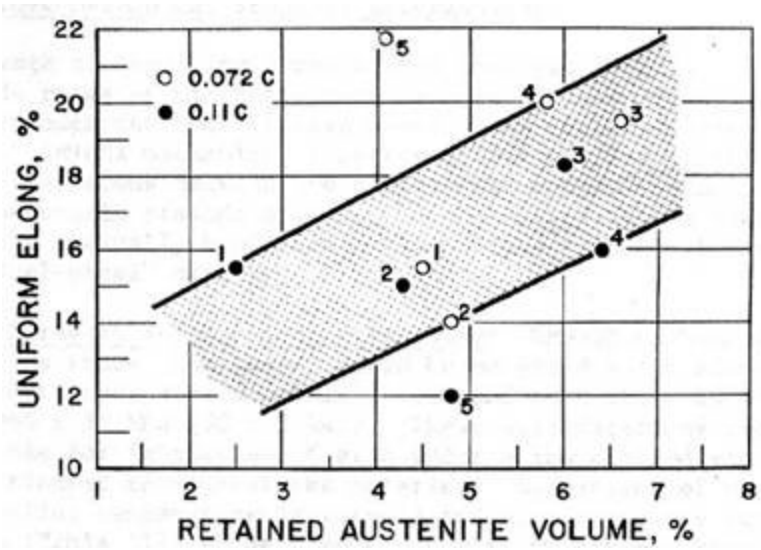

Figure 51 Effect of austenite content on uniform elongation[46]

Balliger and Gladman noted this result, but then observed (without reference or justification, however) that "…retained austenite is not a prerequisite for the achievement of 'dual-phase' properties[120]." Both Balliger and Gladman[120] and Lanzilotto and Pickering[121] found retained austenite in their 'dual' phase steels. Balliger and

Gladman further noted that all retained austenite in deformed samples had decomposed before the onset of necking, which is (see section 2.1.1) the modern interpretation of the TRIP effect.

Nakaoka et al.[123] found that cryogenic treatment of retained-austenite-containing dual-phase steels resulted in a loss of ductility, and that the loss was greatest in the steel containing the most retained austenite. This clearly indicates the beneficial effect of retained austenite on steels that were not originally designed to contain it. They also found that, if a ratio of yield strength to tensile strength of less than 0.6 was desired, retained austenite was very beneficial.

Although retained austenite might not be necessary to achieve dual-phase properties, it certainly will not be detrimental to a dual-phase steel.

2.7.4 Ashby's Dislocation Theory of Work Hardening

In a dislocation-theory tour de force, Ashby[122] demonstrated that the presence of non-deformable particles in a deformable matrix will result in extraordinarily increased work-hardening of a material, and the rate of work hardening will scale as $\sqrt{f/d}$, where, in the present case of dual-phase steels, f and d will be f_{M-A} and d_{M-A}. The premise of the Ashby theory is that as the matrix deforms around the non-deforming particle, large numbers of dislocations will be required to maintain compatibility across the matrix-particle interface. For example, a cubic particle will be in an initially cubic hole. As a shear stress is applied, the hole will tend to a sheared parallelogram shape. However,

the presence of the non-deforming particle prevents the shape change of the hole; dislocation loops accommodate this misfit, as shown Figure 52.

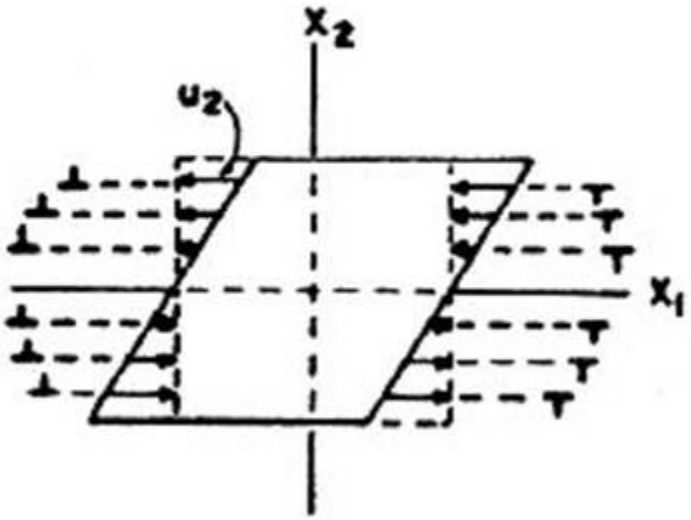

Figure 52 Dislocations accommodating the shear around a non-deformable particle[122]

The presence of particles thus results in geometrically necessary dislocations (GND's), of density ρ^G. For cube shaped particles of size d, volume fraction f, applied shear strain γ and dislocations of magnitude b, Ashby derived:

$$\rho^G = \frac{8f\gamma}{bd} \tag{2-5}$$

This, Ashby warns, is an approximate expression. These GND's are in addition to the classical dislocation density ρ^S of statistically stored dislocations (SSD's).

Because each particle thus has an envelope of increased dislocation density around it, increasing the volume fraction will increase ρ^G, resulting in the scaling $\rho^G \propto f$; more particles (at constant f) will also result in increased ρ^G, resulting in the scaling $\rho^G \propto 1/d$.

Ashby also defines a geometric slip distance, λ^G, which is characteristic of the microstructure and roughly scales as d/f, such that:

$$\rho^G = \frac{1}{\lambda^G}\frac{4\gamma}{b} \tag{2-6}$$

The competing densities of GND's and SSD's were plotted by Ashby for increasing strain at various values of λ^G; Figure 53.

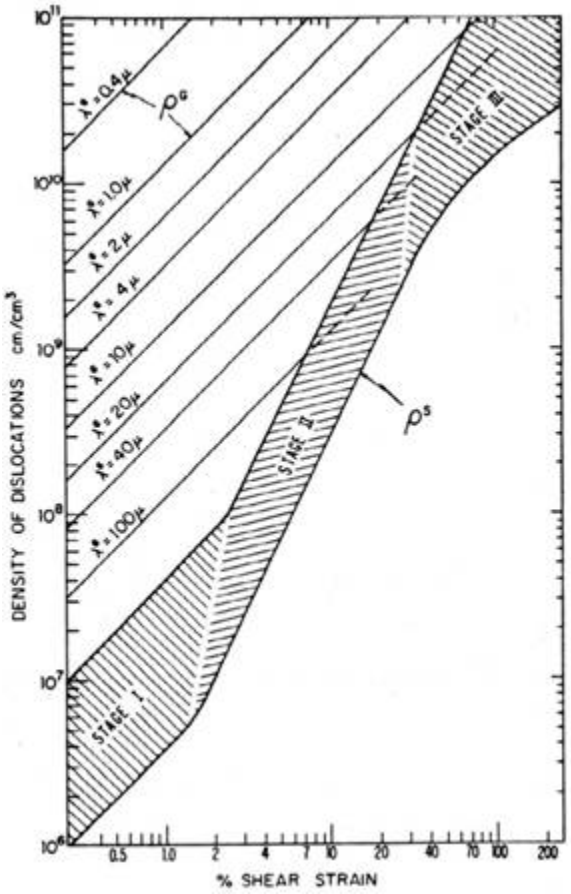

Figure 53 Dislocation densities vs shear strain % for different particle dispersions λ^G (122)

For finely spaced particles (λ^G small), GND's dominate at all strains. For large λ^G (widely spaced particles) SSD's dominate the dislocation density after only a small

amount of strain. This is because ρ^G scales as γ, but ρ^S scales roughly as γ^2 during stage-2 slip. Ashby defined $\lambda^G \leq 2$ micron as "small," and $\lambda^G \geq 100$ micron as large.

Interestingly, this theory can be applied to any plastically non-homogeneous material; Ashby derived a $d^{-1/2}$ law consistent with the Hall-Petch equation for single-phase polycrystals. Because extra dislocations at grain boundaries are necessary to maintain the compatibility between grains in a deformed polycrystal, the above arguments still hold.

The general result derived by Ashby began with the well-know equation for flow stress as a function of dislocation density:

$$\tau = \tau_0 + CGb\sqrt{\rho^{TOTAL}} \tag{2-7}$$

for flow stress τ, constants τ_0 and C, shear modulus G and total dislocation density ρ^{TOTAL}. If GND's dominate, $\rho^{TOTAL} \approx \rho^G$. Then, after accounting for constant factors:

$$\tau = \tau_0 + 2CG\sqrt{\frac{fb\gamma}{d}} \tag{2-8}$$

Or, after differentiation,

$$\frac{d\tau}{d\gamma} = C'\sqrt{\frac{b}{\gamma}}\sqrt{\frac{f}{d}} \tag{2-9}$$

where C′ is a combination of the other constants. This result was expounded upon[120,121] to explain the behavior of dual-phase steels of varying microstructures.

2.7.5 Applications of Ashby's Theory

Balliger and Gladman[120], from their microstructural and mechanical properties studies, derived the following equation from Ashby's work as applied to their steels:

$$\frac{d\sigma}{d\varepsilon} = 0.78kG\sqrt{\frac{b}{\varepsilon}}\sqrt{\frac{f_{M-A}}{d_{M-A}}} \tag{2-10}$$

where k~1 and ε is the true strain. From the stereological relations given[120], the same equation in terms of f_{M-A} and L_{M-A} can be derived:

$$\frac{d\sigma}{d\varepsilon} = 0.78kG\sqrt{\frac{b}{\varepsilon}}\sqrt{0.982\frac{0.885\sqrt{f_{M-A}} - f_{M-A}}{L_{M-A}}} \tag{2-11}$$

For f_{M-A} <0.784. (Beyond this value of f_{M-A}, the stereological relation for L_{M-A} becomes complex.) These relations are both consistent with the microstructure/mechanical property trends discussed above.

Similarly, Lanzillotto and Pickering[121] derived:

$$\frac{d\sigma}{d\varepsilon}(f_{M-A} = 0.20) = 40.1\sqrt{\frac{1}{\lambda_{M-A}}} \tag{2-12a}$$

$$\frac{d\sigma}{d\varepsilon}(f_{M-A} = 0.30) = 51.4\sqrt{\frac{1}{\lambda_{M-A}}} \tag{2-12b}$$

These equations are consistent with the experimental data summarized in 2.7.3 above and the theoretical calculations of Ashby in 2.7.4.

Jiang et al.[124] extended these analyses rigorously, and also included ferrite grain size in the relation. Their equations do not scale for f_{M-A} or d_{M-A} in the simple parabolic fashion

as the above analyses; rather, each variable is included several times, giving direct and inverse scaling. They do, however, obey the same general trends and predict flow stress with startling accuracy, and also obey the Hall-Petch law with respect to the ferrite grain size.

In short, the equations are interpretable as, "finer M-A particle dispersions and finer ferrite grain sizes, at constant volume fraction M-A, greatly improve the formability of dual-phase steels."

Other results have confirmed these predictions. Cribb and Rigsbee[119] note results for steel containing spherodized carbides as the hard second phase follow the same trends as they observed for dual-phase steels. Davies[125] found that the properties of dual-phase steels were independent of the hardness of the martensite; he found martensite volume fraction and ferrite grain size dominated the properties.

Any dislocation-based properties, not just work-hardening, appear to be susceptible to an Ashby-like influence. Ferrite-austenite duplex stainless steels were found to suffer a higher Baushinger effect than single phase austenite or ferrite steels; section 2.6. Erdogan and Priestner[126] found higher Baushinger mean back stresses in dual-phase steels of higher f_{M-A} or finer austenite dispersion. These both imply the higher dislocation densities of the multiphase structures

2.7.6 New Applications

TRIP steels, as stated above, are comprised of both a soft phase -- ferrite -- and various hard second phases: martensite, bainite and retained austenite. Thus, by dispersing the second phases more finely within the microstructure, the properties of TRIP steels should be vastly improved.

Thus, the intelligent microalloying of TRIP steels is a necessary avenue of their further improvement, and must be coupled with the proper thermomechanical treatment schemes to take advantage of this microalloying. A TRIP steel of a given volume fraction second phase is expected to have much improved properties when the second phase is dispersed by microalloying and thermomechanical treatment. As discussed in section 2.4.4, this finer retained austenite should have the bonus effect of being more stable. However, as also discussed in section 2.4.4, over-stabilization of the austenite will result in degraded properties.

Dual-phase steels usually have higher work hardening rates than TRIP-steels during the first 1-2% of strain[96]; Yi et al.[127] note that most retained austenite transforms in this regime. It seems likely that the volume expansion of the packets as they transform from austenite to martensite will lead to an increase in the ρ^G in the surrounding ferrite, resulting in Ashby-like work hardening.

Proper applications of the Ashby effect, while carefully considering Rigsbee's stability observations, should allow for the maximum improvements of TRIP steel properties.

2.8 Copper in Steels

Because it is speculated that copper additions may make an important contribution to future TRIP-steel alloying schemes, the metallurgy of copper in steels is reviewed below.

2.8.1 Fundamental Metallurgy

Historically, copper is most often added to steel in small amounts to improve corrosion resistance. At levels ~1%, copper is the most effective element at inhibiting corrosion in steels[128,129].

Copper also has the effect of lowering the transition temperatures (A_3, A_1, B_s, M_s) of steels[129]. This effect was found to be especially profound in boron-doped steels; transition temperatures' depressions in Cu+B steels were much greater than in the presence of either alloying element alone, indicating a combined effect. A steel containing 1.79%Cu-0.009%B had transition temperatures ~100°C lower than a 0.001%B steel.

Copper's effect on hardenability is small, much less than that of manganese, molyebdenum or chromium, and on the order of the effect of nickel. Despite that, in a

0.02%C, 6%Ni cryogenic steel, copper additions improved the distribution of retained austenite[130]

Although copper-added steel can suffer hot-cracking in welding, this is easily avoided by keeping the subsequent hot strain below some critical value (determined for each alloy), or by welding only descaled steel; if the nickel content is between 0.5 and 0.8 of the copper content, hot cracking is eliminated entirely[130] (but see below for more detail). Copper has little effect on cold-cracking as copper only slightly affects hardenability[130].

Copper greatly improves heat-affected-zone (HAZ) toughness[130]. Indeed, this was one of the driving forces toward the heavy plate research discussed in section 2.8.3 below. Copper-boron steels were found to have especially good HAZ toughness[130].

Thus, copper steels can be welded if proper precautions are taken. Copper-nickel steels are easily welded.

As copper as limited solid solubility in iron, copper can be used for precipitation hardening of ferrite. In general, copper additions of 0.3 to 0.5% are required to see precipitation hardening[128,130]. For many years, copper was believed to precipitate in the sequence[129,130]:

$$Fe_{\alpha}\text{ (supersaturated)} \rightarrow Fe_{\alpha} + Cu_{clusters}\text{ (BCC)} \rightarrow Fe_{\alpha} + Cu_{\varepsilon}\text{ (FCC)}$$

Recent HRTEM[131,132] evidence has shown two intermediate steps: between the BCC clustering stage (typically at ~2 nm particle size) and the FCC precipitate stage (typically at >30nm), the precipitates exist in a faulted 9R structure at sizes ~4-6nm. As these 9R particles grow, they transform to a 3R structure at sizes ~18nm. This 3R structure is heavily distorted from FCC, and aligned several degrees away from the ideal Kurdjumov-Sachs relation. As the particles continue to grow, the lattice around the 3R precipitates relaxes and, by about 30nm in size, the distorted 3R particles revert to FCC ε-Cu in the K-S relation. In summary:

$$\alpha_{Fe}\,(\text{supersaturated}) \rightarrow \alpha_{Fe} + \text{clusters}_{Cu} \rightarrow \alpha_{Fe} + 9R \rightarrow \alpha_{Fe} + 3R \rightarrow \alpha_{Fe} + \varepsilon_{Cu}$$

(zero size) (~2nm) (~4-6nm) (~18-30nm) (>30nm)

The smallest clusters have been found to contain significant fractions of Fe in Fe-Cu alloys or both Fe and Ni in Fe-Ni-Cu ternaries, but by 4-5nm in size, the particles are considered pure copper[132,133,134]. Manganese, nickel and silicon were found to have little effect on precipitation, while molybdenum was found to slow precipitation[130]. Buswell et al.[134] noted that peak hardness was obtained while some copper was still in solution. They also found that while the precipitates are $\geq$95% copper, nickel was segregated to the interface of the precipitates.

Although the precipitation hardening in a Cu-Ni-Nb steel was superior to that of a Cu-Ni steel[129,135], it was found copper precipitation hardening, in the simultaneous presence of microalloy-carbide precipitation hardening, could embrittle the steel[130]. Thus, it was

concluded that microalloying should be used primarily for grain refinement, rather than hardening. Despite the two precipitating species (Cu and NbC), they found a unimodal hardness-vs-time curve, indicating concurrent precipitation[135]. Also, no incubation period was observed, except at the lowest aging temperatures, and peak hardness was achieved in approximately 5-10 minutes at 700°C.

Cold work of the ferrite was found to speed and increase precipitation hardening. Isochronal studies, for instance, showed a decrease in temperature to precipitate ε-copper in thirty minutes from 525°C to 250°C after cold-drawing[129]. Krishnadev et al.[136] found that cold work between solutionizing and aging resulted in both faster and larger age-hardening responses; in a 0.05C-2.14Cu-1.45Ni steel cold-reduced 50%, peak hardness was achieved after 5-10minutes at 500°C. Krishnadev et al. note that areas of a formed part that suffered larger forming strains than other areas will thus reach the over-aged state faster. The author notes that, although paint-bake-hardening cycles occur at very low temperatures, a hypothetical steel optimized for maximal copper precipitation may suffer property changes during a paint baking cycle along these lines.

In a similar result, Banadkouki et al.[137] found that a bainitic or martensitic matrix lead to both faster and larger hardening increments in age hardening than a ferritic as-rolled matrix, which they attributed to a higher supersaturation and high dislocation density, which is a result similar to the cold-work studies above.

The effect of pre-deformation was also verified by Militzer and co-workers[138,139]

Complex precipitations can also occur. Morita et al.[140] noted complex, sandwich-like precipitates of Cu and Ti-C-S in Cu-added Ti-IF steels.

Copper precipitation after cold work was found to slow recrystallization and preserve the rolling texture while retarding the development of an annealing texture[129]. Copper was also found to improve the deep-drawabilty of a CRA rimming steel, while reducing its stretchabilty[130].

Additions of copper were found to reduce grain size in an ULC grade (0.003-0.004C) by Kimura and Takaki[141]. Kimura and Takaki also studied the different effects of copper additions on either slow-cooled or quenched microstructures. In 0.003C, 0.5-4.0Cu, 0.35Mn alloys, they found that air cooling always resulted in a ferritic structure, whereas water quenching led to lath martensite in steels of 2-4%Cu. In steels of a constant cooling rate, the higher-copper compositions always showed higher hardnesses, as expected. In general, the quenched steels had higher strength than air-cooled steels of the same composition, with the exception of the 4%Cu grade. In that case, the air-cooled material showed sufficient precipitation to have the highest hardness of any steel studied.

Kimura and Takaki stated that ε-Cu precipitation was complete in the air-cooled materials, leaving only coarsening as a further possible reaction. However, this assertion was made on the basis of lattice-parameter measurements via x-ray

diffraction. The author questions their assertion, as XRD lattice parameter measurements are not as accurate as other methods, and the lattice parameter value of ferrite will only be slightly affected by copper (Fe and Cu reside near each other on the periodic table). The author feels analytical electron microscopy, such as PEELS analysis, or time-of-flight atom-probe spectrometry should have been performed before making such as assertion.

Copper additions of 1.5% were found to slow austenite decomposition to ferrite by reducing the rates of both nucleation and growth of ferrite[142]. This result implies the possibility of profound copper influences on TRIP steels; slowing the ferrite transformation might allow easier production of austenite-enriching bainite, aiding the TRIP effect, or could potentially suppress all diffusional processes, poisoning the TRIP steel, rendering it a dual-phase ferrite-martensite steel by preventing enrichment of the austenite during the isothermal bainite transformation.

Copper steels have also been found to show excellent fatigue properties[129,130]. Copper was also found to favor the formation of the desirable δ_1 phase during hot-dip galvanizing[143]

2.8.2 Detrimental Effects of Copper

Copper has a lower tendency to oxidize at high temperatures than iron, and copper has a lower melting point than iron. These two factors contribute to "hot shortness," the

observation that hot-worked copper-steels will have poor surface quality characterized by cracks and slivers of scale worked into the substrate[144].

This is typically not observed in steels in which the copper content is <~0.5%[144].

At high temperatures, especially 1050°C to 1150°C, the iron oxidizes preferentially, leaving a film of almost pure copper between the iron-rich scale and the austenite substrate. At these temperatures, the copper-compound is liquid and penetrates the austenite grain boundaries, leading to cracking and "hot shortness."

By adding nickel to the steel, in the range of one-half of the copper content to equal to the copper content (by weight), hot-shortness is eliminated. This is because nickel is very soluble in copper and increases the melting point of the copper compound, reducing attack of the austenite grain boundaries.

Imai et al.[145,146] found that a 0.3Cu steel suffered little hot-cracking, and only at ~1100°C, whereas 0.3Cu-0.04Sn steel suffered severe cracking from 1000° to over 1100°C. However, zero-Cu-0.04Sn steel suffered no cracking, indicating that tin exacerbates the effect of copper, but tin does not cause cracking on its own. Nickel equal to one-half the copper was found to arrest hot-cracking in a 0.3Cu-zero Sn steel, but nickel had to be added to a level equal to the copper level in a 0.3Cu-0.04Sn steel. Thus, tin and similar residuals are an important design factor for copper-bearing

compositions. Imai et al. also noted that oxidation, rather than deformation, conditions dominated the hot-cracking behavior.

Seo et al.[147] found that adding single additions of either 0.4Si or 0.02P reduced hot-shortness, but increased oxidation. A dual addition of 0.4Si and 0.02P reduced both hot-shortness and oxidation. However, these results seem to be industrially uninteresting: silicon and phosphorus added steels lead to hot-dip coating problems. Seo et al. also noted reheating at 1200°C led to less surface hot-shortness in all steels than re-heating at 1100°C.

Although copper, as a tramp element, is increasing in remelted steels (see Ref. 148 for reviews and many articles), the work of Militzer et al.[138] indicates that tramp concentrations (<1%) should not seriously affect mill rolling loads or mechanical properties of the steel. The lack of effect on mill loads is based on hot-deformation simulations of 0.05 and 0.8% Cu steels, and the projected lack of effect on properties is attributed to the slow precipitation hardening response.

2.8.3 Copper in Heavy Plate Steel

In the 1980's and 1990's, the US Navy sponsored research into heavy plate steels with low carbon contents. Low carbon contents result in enhanced toughness, especially at low temperatures, and improved weldability.

The steel HSLA-100 was a primary focus of this research. With an approximate composition of 0.03C-1Mn-3.6Ni-0.6Cr-1.6Cu-0.59Mo-0.025Nb, this is a very low carbon, Nb-microalloyed steel that contains large amounts of hardenabilty improving additions. The most notable difference between this steel and steels for similar applications, such as ultra-low-carbon bainitic ULCB-100, is the presence of copper[149,150].

Research at the University of Pittsburgh's Basic Metals Processing Research Institute determined these major effects of copper in the aging and tempering of HSLA-100 steel[149] (most of which are consistent with section 2.8.1 above):

1) Solutionized copper will lower B_s and M_S.
2) Copper precipitates contribute to strength, especially when the material is tempered ~450°C.
3) Copper precipitates slow recovery and recrystallization of the as-quenched matrix.
4) As aging temperature increases, the amount of copper in solution in austenite increases, lowering the A_{c1}, causing new austenite to form at lower temperatures.
5) Formation of austenite at lower temperatures means the austenite forms in a matrix of a higher strength level.
6) Newly formed austenite in the aging regime 640-670°C is highly enriched in alloying elements and is retained upon cooling. This results in highly improved notch-toughness.

Most important to the discussion at hand are points (2) and (6).

From point (2): samples austenitized and quenched showed a peak in hardness when aged at ~450°C; see Figure 54[149].

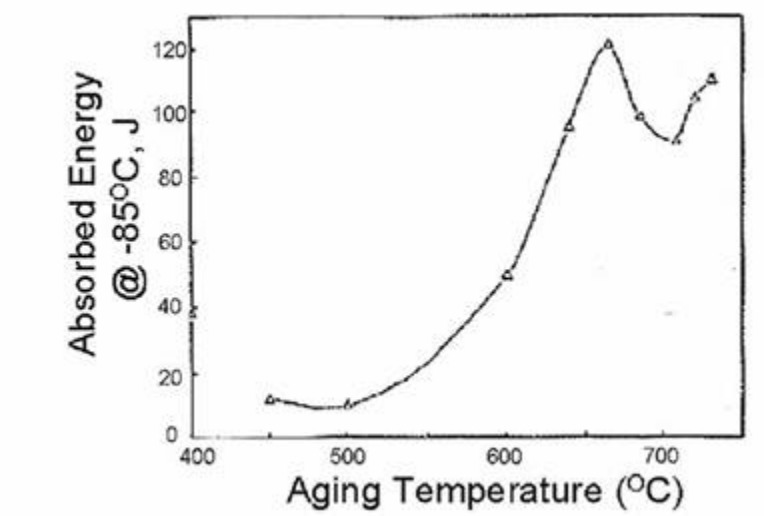

Figure 54 CVN energy vs aging temperature

Because the copper fully dissolves at the austenitization temperature, this strength peak is attributed to the precipitation of small coherent precipitates from supersaturated solid solution. TEM shows evidence for this theory[150].

From point (6): a substantial increase in toughness around 640-670°C is attributed to the presence of retained austenite. TEM studies showed that the retained austenite existed as small packets trapped in between martensite laths or present as small islands[150].

However, the toughness peak decreases quickly with aging above the peak temperature. This is due to a reduction in retained austenite volume fraction f_v^{γ}. As aging temperature increases, the volume fraction of intercritical austenite will increase, resulting in a concomitant loss in enrichment of this austenite. Thus, the austenite will transform to embrittling phases such as martensite or bainite, rather than the ductility-improving retained austenite.

Copper bearing plates produced by direct quenching were found to have superior toughness at a given value of yield strength[151], in comparison to reheated-and-quenched plates. In addition, they showed the direct-quenched plates had a higher strength at a given tempering temperature than reheated and quenched plates. However, this study did not report the presence or absence of retained austenite.

Banerjee et al.[152] studied a boron- and niobium-bearing copper steel of composition similar to HSLA-80. They varied the hot-rolling schedules to study the effects of TMP on the microstructure. They noted that copper precipitates very quickly, mostly during the TMP. However, it is well known[153,154] that, regardless of nucleation rates, the coarsening of copper precipitates is very slow.

Studies on HSLA-80/A710 type heavy-plate steels[155,156] also showed that copper precipitated quickly during cooling after being totally dissolved during austenitization. Interestingly, they showed fine NbC and Fe_XC precipitates in retained austenite

particles, and copper only in the areas around austenite, further confirming the easy solubility of copper in austenite, especially in comparison to other precipitate phases.

2.8.4 Prospects for Copper in TRIP Steel

Because TRIP steels depend on retained austenite packets for their improved ductility, any means to retain austenite to room temperature, or increase the stability of retained austenite (within limits -- see section 2.4.4) bears consideration for TRIP steel production.

Copper additions allow austenite to be retained at very low bulk carbon contents, which bodes well for the weldabilty of copper-based TRIP steels. Further, these copper-bearing plates were processed either by a quench-and-temper route[149,150,157] or a direct-quench[151] route, rather than the convoluted hot roll-cold roll-intercritical anneal-bainite austemper route required of conventional TRIP-assisted multiphase steels (see section 2.1.2).

Thus, it may be possible to produce steels of large retained austenite volume fractions using a dual-phase like processing route. Perhaps, although unlikely, properly alloyed Cu-Ni steels could be processed like a conventional HSLA steel -- though with finishing or coiling in the intercritical region -- and still contain appreciable retained austenite. In either case, it seems quite feasible to eliminate the "bainte hold" required for Si-Mn-Al TRIP steels (section 2.1.2).

However, the loss of the bainite constituent may result in Cu-Ni TRIP steels having low levels of strength. Copper precipitation could, perhaps, be used to obtain strengths equal to those of conventional TRIP steels.

A reheat-quench-and-temper cycle is not feasible for mass-production of strip or sheet for automotive applications. Thus, the improved properties of the direct-quenched HSLA plates discussed above[151] are heartening results. Perhaps by hot rolling a copper-bearing strip and rapidly cooling or coiling such as to produce copper precipitates will allow the nucleation of enriched austenite during either continuous or batch annealing, which could result in retention of austenite in the finished product.

The author speculates that the effects of cold work on copper precipitation discussed above (section 2.8.1) may transfer well to industrial production of TRIP steels.

A thought experiment: a Cu-Ni steel is hot rolled and cooled rapidly, leaving the copper in supersaturated solution in the finished strip. This strip is then cold-rolled. During the heating cycle in preparation for charging into the CAL furnace, copper should precipitate very rapidly, thanks to the cold work in the structure. These copper precipitates would then act to nucleate highly enriched austenite at low temperatures during annealing at 600-700°C. When the sheet is cooled from the annealing temperature, this enriched austenite may be retained, producing a TRIP steel from a normal cold-roll-and-anneal processing path.

Similarly, if a Cu-Ni steel is cooled from annealing to retain supersaturated solid solution, strain during forming might be used to precipitate copper particles during a paint-bake cycle.

2.9 Summary of Literature

The above literature review makes many points, but a few of the most important bear repetition.

- Retained austenite stability will depend strongly on C and Mn solute content.
- Retained austenite stability will also depend strongly upon the size and shape of the particles.
- Although many alloying elements are, at least by current theory, considered necessary to TRIP steels, some must be eliminated before TRIP steels can be feasibly commercialized. Most notably, Si.
- Simply measuring retained austenite volume fraction will not be sufficient characterization of it, especially for correlations to formability.
- Diffraction techniques will not be sufficient for characterization. Although they must be used, electron beam techniques will also be necessary.
- Fine dispersions of the second phases will improve mechanical properties.
- Copper is a promising alloying prospect. Ni, Cr, Mo and Nb also need more study. The development of high-strength (>~800MPa UTS) TRIP steel will be a

hopeless task without some combination of alloying additions and microstructural refinement.

3.0 STATEMENT OF OBJECTIVES

The objectives of this study were two-fold:

I. Develop, refine and validate the experimental techniques necessary for future work on TRIP-assisted multiphase steels.
   a. Microscopic techniques: SEM, TEM, optical.
   b. Retained austenite volume fraction techniques: X-ray diffraction, magnetometry.
   c. Tensile techniques: above and below room temperature.

II. Study the decomposition of austenite following intercritical annealing in TRIP-assisted multiphase steels.
   a. Study effects of cooling rate on microstructure and properties.
   b. Study effects of isothermal holding time on microstructure and properties.
   c. Construct a CCT-curve for this intercritically annealed material.

The purpose of objective I. is to allow for meaningful studies to be performed. Microscopic techniques must be refined because multiphase steels are difficult to microscopically characterize, and only through accurate micro-characterization can conclusions relating structure to properties be drawn.

The most important microstructural parameter for TRIP steels is that of retained austenite content; because several different techniques are in routine use in the literature, it was deemed important to explore these for possible use.

Finally, a coil of TRIP steel may experience a wide range of temperatures throughout its service life. Storage at a press shop during winter months, for example, might subject the coil to temperatures of perhaps -20°C; adiabatic heating during the press-forming step or a crash event could lead to temperatures well in excess of 100°C. Thus, room-temperature mechanical properties are not necessarily the most interesting, and a means of testing the material at a range of temperatures was desired.

For objective II., a disparity was noted between published results (such as Sakuma et al.[65]) which indicated a strong effect of intercritical parameters, and more recent results, as well as observations made in the early parts of this study, that intercritical parameters are second order. It was hypothesized that cooling-rate from the intercritical anneal to the isothermal hold would control whether the bulk of the austenite-decomposition reaction took place in the form of epitaxial ferrite or bainite.

Indeed, as the microscopic techniques were validated, the observation was made that these steels contained almost no bainite, despite the large discussion of the "isothermal bainitic hold" in the literature. This observation, in light of Sakuma et al.'s results, lead to the formation of objective II.

Given the results reviewed above in Section 2.4.4 (retained austenite morphology), it was realized that cooling rate could strongly affect final properties. If a high cooling rate were used, resulting in a bainitic reaction, the majority of the retained austenite would take the form of inter-bainitic-lath films, perhaps 100nm wide by several microns long, which would be very stable. At slower cooling rates, an epitaxial ferrite reaction might lead to massive inter-ferritic islands, roughly circular with dimensions ~0.5-5 micron. These islands would have lower stability. Thus, even at a constant volume fraction of retained austenite, two TRIP steels could have very different properties. This very result was observed in Mishra and Jha's[40] work: a Cr steel contained massive retained austenite, but a V steel contained film-type austenite; the V-steel showed better mechanical properties.

If the hardness of bainite is taken into account (much higher than that of epitaxial ferrite), the properties could be even more different.

Because the eventual, long-term goal of this research program is to perform a fundamental study retained austenite stability with respect to mechanical strain, it is important to learn how to control the morphology, size and composition -- and thus stability -- of retained austenite in TRIP steels.

Further, a reaction during cooling might replace or supercede the isothermal reaction, at least to a degree. It was thus deemed worthwhile to study isothermal hold parameters following the cooling stage.

From the data gathered, it was possible to construct a CCT curve; this is thus an important, original contribution to the literature.

4.0 EXPERIMENTAL PROCEDURE

4.1 Materials Used

Four materials were used; Table II. The Si-CAL and Si-CGL materials were industrially produced trial heats of Si-Mn based TRIP steel, intended to have 590-600 MPa tensile strength. Al-only and Si-Al were vacuum melted, laboratory hot and cold rolled produced sheet, intended again to be of 590-600MPa grade, but of improved coatability. The 1.2%Si materials had excellent mechanical properties at only 0.10%C, but poor coatability. The lower-Si grades needed increased C content -- 0.20wt% -- to achieve the 590-600MPa goal. This is because Al shows much less solid solution hardening than Si. The Si-Al and Al-only materials should thus be expected to have improved coatability, but deteriorated weldability.

Table II Compositions and designations of steels used, in weight percent.

Designation	Production	C	Si	Mn	Al	P
Si-CAL	Commercial CAL	0.10	1.2	1.6	0.0	<0.006
Si-CGL	Commercial CGL	0.10	1.2	1.6	0.0	<0.006
Al-only	Laboratory	0.20	0.0	1.7	1.5	<0.006
Si-Al	LAboratory	0.20	0.5	1.8	1.0	<0.006

CAL=continuous annealing line; CGL=continuous galvannealing line

4.2 Metallography

4.2.1 Introduction

The metallography of dual-phase and TRIP steels has been well developed by previous researchers. Metallographic techniques in x-ray diffraction, optical microscopy, scanning electron microscopy, transmission electron microscopy and magnetometry have all been published, and were used in this study.

4.2.2 X-Ray Metallography

Careful comparison of the integrated intensities of Bragg peaks for different phases can be used to determine the relative volume fractions. Under the assumption that only ferritic and austenitic phases are present, this relative volume fraction of ferrite to austenite, f_α/f_γ, can be converted to absolute volume fractions with the identity $f_\alpha+f_\gamma=1$. This is the so-called "direct comparison method[158]". As TRIP steels contain only negligible amounts of carbide (if any at all), this assumption should hold.

Ratios of volume fractions are calculated from the integrated intensities I^α and I^γ and constants R^α and R^γ:

$$\frac{I^{\gamma}}{I^{\alpha}} = \frac{R^{\gamma} f_{\gamma}}{R^{\alpha} f_{\alpha}} \tag{4-1}$$

The R-values are constants determined by the particular phase, the particular Bragg reflection and the wavelength of the incident X-rays:

$$R = \left(\frac{1}{v^2}\right)\left[FF^* p\left(\frac{1+\cos^2 2\theta}{\sin^2\theta\cos\theta}\right)\right]\exp[-2M] \tag{4-2}$$

where ν is the volume of the unit cell, F is the structure factor, F^* its complex conjugate, p the multiplicity of the reflection, θ the Bragg angle and exp[-2M] the Debye-Waller temperature factor.

For Cu-Kα radiation of wavelength 0.154 nm, De Meyer et al calculated these R-values[159].

Table III Ferrite R values

Peak	(110)	(200)	(211)	(220)
R_{hkl}	250	36	71	25

Table IV Austenite R values

Peak	(111)	(200)	(220)	(311)
R_{hkl}	184	83	47	58

These values are within 5% of values calculated by the author, using the techniques and tables of Cullity[158].

Samples for X-ray diffraction were prepared by standard grinding and polishing to 0.05μm alumina. Samples chemically polished in 95% H_2O_2 (30% grade) - 5% HF (46-48% grade) solution[160] gave identical results, indicating the mechanical polishing was sufficient to remove deformation imparted by the rough grinding. Diffraction experiments were performed using a Phillips X-ray diffractometer using Ni-monochromated Cu-Kα radiation. A detector monochromator reduced the effect of Cu-Kα fluorescence of the iron sample.

Comparisons were made by averaging values obtained from ferrite (110), (200), (211) and (220) peaks and austenite (111), (200), (220) and (311) peaks. To verify the technique, a sample of 304-grade austenitic stainless steel transfer bar, known to contain 4-5% retained delta ferrite, was examined. The sample was polished to 0.05μm alumina and electropolished using 95% acetic acid (glacial grade)-5% perchloric acid (66-70% grade) solution at approximately 40 volts for three seconds in a Buehler Electromet 4 electropolisher. (This steel did suffer mechanical polishing-induced transformation, thus requiring chemical polishing, unlike the TRIP steels.) Ignoring the small volume fraction of carbides identified by XRD, a value of 93% austenite was obtained using this X-ray technique, showing adequate agreement.

The mathematical technique used was to calculate the value, f_γ, associated with every combination of $(hkl)_\alpha$ and $(hkl)_\gamma$ listed above, and then obtain an average and standard

deviation. Thus, individual $f_\gamma^{i,j}$ values were calculated from a ferrite/austenite peak pair i,j as:

$$f_\gamma^{i,j} = \frac{\frac{I_{hkl}^{\gamma}}{R_{hkl}^{\gamma}}}{\frac{I_{hkl}^{\gamma}}{R_{hkl}^{\gamma}} + \frac{I_{hkl}^{\alpha}}{R_{hkl}^{\alpha}}} = \frac{\frac{I_{hkl}^{\gamma}}{I_{hkl}^{\alpha}}}{\frac{I_{hkl}^{\gamma}}{I_{hkl}^{\alpha}} + \frac{R_{hkl}^{\gamma}}{R_{hkl}^{\alpha}}} \tag{4-3}$$

Or, the average f_γ value by:

$$\langle f_\gamma \rangle = \left(\frac{1}{16}\right) \sum_i \sum_j f_\gamma^{i,j} \tag{4-4}$$

For I= (111), (200), (220) and (311) and j= (110), (200), (211) and (220). For the purposes of this work, $\langle f_\gamma \rangle$ values obtained by XRD will be abbreviated to f_γ because a single $f_\gamma^{I,j}$ value will likely not resemble the actual phase content and only these averages were used.

This equation provides similar results to the equations such as those published elsewhere[159],[161] but with the significant advantage that a standard deviation can also be obtained.

Unfortunately, a standard deviation is necessary because XRD is only suitable for materials of random or near-random crystallography[162] -- such as the stainless-steel transfer bar above. This technique has, in fact, been well-validated for near-random steels[163]. Experiments performed in the earliest proof-of-concept phase of this study

using as-cast material showed excellent results, whereas XRD experiments on cold rolled and annealed or cold rolled and galvannealed steels gave results with extraordinary experimental scatter, due to texture. EBSD and XRD texture studies[159,164,165] concluded that while ferrite or bainite is weakly textured in TRIP steels, retained austenite is heavily textured. This was confirmed in this study, as I^{γ}/R^{γ} ratios for $(111)_{\gamma}$, $(200)_{\gamma}$ and $(311)_{\gamma}$ were approximately one order of magnitude lower than I^{γ}/R^{γ} for $(220)_{\gamma}$, indicating profound texture in austenite. This is in nearly exact agreement with published results[159,164,165].

In the commercial Si-CRA steel and the commercial Si-CGL steel, retained austenite volume fractions were measured as approximately 5±6% using the Phillips XRD powder diffractometer and the averaging equation above. Thus, XRD was deemed an unsuitable technique for examining cold rolled or heavily hot-rolled material for retained austenite volume fractions, or for examining steels after mechanical testing such as tensile testing.

However, XRD is still the method of choice for qualitative phase identification, assuming the particles of interest are large enough to detect by XRD, typically ~100nm or larger[166], and present in sufficient volume fraction.

Average carbon content of retained austenite, C_{γ}, can be estimated using X-ray diffraction. From the XRD-determined lattice parameter of austenite, a_{γ}, carbon content can be estimated as[63]:

$$C_\gamma = \frac{a_\gamma - 3.5467}{0.0467} \tag{4-5}$$

where a_γ is in angstroms and C_γ is in weight percent.

4.2.3 Optical Metallography

Optical metallogaphy samples in this study were prepared using standard techniques by grinding and polishing to 0.05μm alumina. All samples were freshly polished on 0.05μm alumina immediately (i.e., within 15 seconds) before etching to eliminate passivation due to atmospheric exposure.

Various etching procedures have been developed to emphasize different phases in multiphase steels[46,167,168,169,170,171,172,173]. Many of these techniques are summarized in Vander Voort[174].

These techniques are summarized in Table V.

Table V Etchants used

Technique	Chemicals	Published Effects	Ref.
Rigsbee & VanderArend	2g $(NH_4)_2S_2O_8$ 2mL HF 50ml Acetic Acid 150ml water	Martensite dark, retained austenite light	46
10% $Na_2S_2O_5$	3% nital pre-etch, then 10% $Na_2S_2O_5$(aq)	Martensite dark, Ferrite off-white, Austenite white, Bainite Brown	167,168, 169,173
Bandoh	Solution A (23.5ml): 7g $Na_2S_2O_3$ 100ml water Solution B (23.5ml): 5g picric acid 100ml ethanol Solution C (3-10ml): 4ml nitric acid 96ml ethanol	Ferrite blue, Martensite and austenite yellow, Bainite brown	170
LePera	Picral pre-etch, then Solution A (50ml): 1% $Na_2S_2O_5$ in water Soluton B (50ml): 4% picric acid in methanol	Martensite white, Bainite black, Ferrite tan	171
Modified LePera	Picral pre-etch, then Solution A (50ml): 2% $Na_2S_2O_5$ in water Solution B (50ml): 4% picric acid in ethanol	Martensite white, Bainite black, Ferrite tan	172
Klemm's 1	Nital Pre-etch, 50ml water saturated with $Na_2S_2O_3$(aq) + 1g $K_2S_2O_5$	Ferrite light or dark blue, Martensite brown or black, Austenite white	174

All of these etching techniques were attempted. The LePera techniques and Bandoh's technique did not differentiate between martensite and austenite. Rigsbee and VanderArend's technique, although excellent in principle, gave poor contrast in practice.

Of these techniques, only three -- LePera's technique, 10% $Na_2S_2O_5$ and Klemm's 1 -- were found to give satisfactory results. Although Klemm's 1 gave excellent results on occasion, the quality was so inconsistent between different areas of the same sample and different attempts to etch the same sample that the technique could not be used with any reliability.

Attempts were made to improve the Klemm's I technique. Samples were etched with various degrees of oscillation, ranging from none to violent. This did not help. The chemistry was also modified by adding 1-2g $Na_2S_2O_5$. Although this addition sped etching, it did not improve the consistency. Sodium dodecylbenzene sulfonate was added in an attempt to improve surface wetting, but did not help. Etching using the standard tint-etching techniques of Bramfitt and Benscoter[175] did not help.

The 10% $Na_2S_2O_5$ technique gave moderate metallographic contrast almost every time, especially when combined with an 8-10 second 3% nital pre-etch. Further, the technique's simplicity resulted in highly consistent etching. LePera's technique was very consistent if care was taken to prevent air contact by storing the sample under alcohol immediately after polishing. LePera's technique gave the best austenite-ferrite contrast. However, LePera’s technique was found to give inconsistent etching response in high-bainite-fraction (i.e., >5%) materials. The 10% $Na_2S_2O_5$ technique, however, provided excellent bainite contrast, even if its ferrite-austenite contrast was less pronounced. The Modified LePera technique was found to be over-aggressive and thus

hard to control; as such, the original LePera technique was used, and not the Modified LePera technique.

In summary, LePera technique was the primary etching method used in this in materials with little bainite. However, the 10% $Na_2S_2O_5$ technique was used when bainite, or lack of bainite, was of interest. It was also found that, although LePera's original paper called for the use of ethanol as the picral solvent, methanol was found to give better results. The picral pre-etch was also not used.

These two techniques were not "etches" in the normal sense of the word, but rather tints, so the tint-etching precautions listed in Bramfitt and Benscoter[175] should be scrupulously followed, lest poor results be obtained. Most importantly: 1) the sample should not be moved or oscillated during the tint-procedure, and 2) the tinted sample should be rinsed gently in a beaker of distilled water, rather than under running water. Both of these precautions are due to the fragile nature of the deposited sulfite film.

The use of polarizing filters or Nomarski filters were not found to give helpful results. In fact, with small particles of retained austenite or martensite, Nomarski filtering gave misleading contrast effects.

De et al.[173] present a concise review of color tint-etching techniques, along with excellent color micrographs.

4.2.4 Scanning Electron Metallography

When examining a sample etched by any of the techniques above in the scanning electron microscope (SEM), austenite and martensite could not be distinguished. By tempering samples at 200°C for 2 hours, it becomes possible to differentiate the two phases by SEM[176] -- Girault et al.'s technique. During this tempering regime, ε-carbides precipitate in martensite; deep nital etching will reveal a substructure in martensite islands while leaving the austenite islands smooth.

A Phillips field emission gun SEM at the University of Pittsburgh and JEOL JSM-840A or JXA-6400V SEMs at US Steel Corporation's Technical Center were used to examine specimens.

4.2.5 Transmission Electron Metallography

TEM is the most powerful technique for the examination of retained austenite bearing steels. Sheet samples were thinned to 200-300 microns by mechanical grinding under running water. Samples were not thinned mechanically beyond this point for fear of transforming the retained austenite or introducing dislocations. These wafers were thinned to less than 75 microns in thickness using a solution of 50ml water, 50ml hydrogen peroxide (30% grade) and 7ml HF (46-48% grade)[160,177].

Care should be taken if repeating these experiments, as both 30% hydrogen peroxide and HF are spectacularly dangerous chemicals to work with. Hydrogen peroxide will

burn any tissue and HF passes through soft tissue to destroy bone[178,179]. Further, do not place large samples into the HF-H_2O_2 solution, as the heat evolved can result in boiling of the solution. HF should also never be stored in glass containers, only plastic. Starting samples should be no larger than 1cm x 1cm x 0.3mm. Bramfitt and Benscoter[160] suggested maintaining the solution at 20-25°C; it was found in this study that placing the reactant container in a larger container of ice water significantly slowed the reaction but improved safety by maintaining the temperature of the solution, thus preventing autocatalytic boiling of the solution by decomposition of H_2O_2. Sometimes a gold-colored oxide formed on the surface; this was removed by final electropolishing and thus could be ignored.

Attempts to chemically thin in 50-67% H_2O_2 (30% grade) - 33-50% H_3PO_4 (85% grade) were made; this resulted in a slimy coating on the steel, and an adherent gold oxide. Attempts were then made to clean and pickle these phosphoric acid-thinned, oxidized steels in HCl or HCl+H_2SO_4 solutions, which simply resulted in destruction of the thin wafers by etching. H_2O_2-HF, despite its drawbacks, was the only successful thinning technique.

Samples were thinned to at most 75 microns thickness. Less than 50 microns was considered ideal, but seldom achieved. Thinner samples seemed to yield larger electron-transparent areas, and the smaller magnetic mass associated with a thinner sample resulted in less aberration of the TEM optics by the samples' magnetic fields.

Disks of 3mm diameter were then punched from the wafers. These disks were thinned into TEM foils using 90% acetic acid (glacial grade)-7% percholoric acid (66-70% grade) solution in a Fischione twin-jet electropolisher operating at 70-90 milliamps.

Approximately 80-90 milliamps current was found to give consistently excellent results, if:

1) The foils were immediately cleaned in ethanol

2) The electrolyte was reasonably new

3) The samples were stored in a dessicator (if not used immediately)

Samples should never be cleaned in distilled water after electropolishing, no matter how briefly, as oxides may form on the foil, ruining it.

Oxidized samples could be identified by a mottled contrast in TEM imaging mode, or by unexpected diffraction rings in the TEM's back focal plane. Oxide was removed by mixing a solution of 50-100ml methanol with 2-3 drops of HCl[180,181]. Samples were dipped in the solution, oscillating, for approximately 3-5 seconds. The reaction was then quenched by immediately placing the samples in a large beaker of methanol. In principle, light ion milling could be used to clean these samples, but the amount of damage imparted by the HCl solution was so minor, and the cleaning so effective, the chemical technique was considered best. Samples cleaned in this way occasionally showed holes or pits in the thinnest regions near the central hole. Simply moving a few hundred nanometers from these damaged regions allowed microscopy of well-polished and clean material.

Multiphase structures often require special techniques to successfully electropolish[178,182]. For example, Murayama et al.[183] found that highly overaged copper precipitates in 17-4 PH stainless steel were dissolved by electropolishing, which meant that ion-milling was required for TEM sample preparation. However, in this study, standard ambient-temperature polishing provided excellent results (if points (1) to (3) above were observed), whereas low-temperature polishing provided poor results. Ion milling was not needed in this study, due to the small size of the precipitates. Rigsbee and Aaronson[57] reported that acetic-perchloric acids provided poor results in austenite-bearing dual-phase steels, and resorted to an acetic acid-chromic oxide-water solution. However, in this study, acetic-perchloric acid was found to give excellent foils. Thus, all TEM micrographs in this study are from samples polished at ambient temperatures as described above.

Foils were examined in a JEOL 200CX TEM operating at 200kV at the University of Pittsburgh or in a JEOL 200CX TEM operating at 200kV at US Steel Corporation's Technical Center.

4.2.6 Magnetometry

Ferrite, martensite, bainite and cementite are all ferromagnetic; austenite is paramagnetic. Thus, the volume fraction of austenite can be determined by comparing the magnetic properties of a TRIP steel to that of a non-austenite-bearing steel[184,185,186,187]. In general, for saturation magnetizations M^{SAT},

$$f_\gamma = \frac{M_{REF}^{SAT} - M_{TRIP}^{SAT}}{M_{REF}^{SAT}} \tag{4-6}$$

For two steels, REF and TRIP, of the same bulk composition, where TRIP contains a volume fraction f_γ of paramagnetic austenite and REF is fully ferromagnetic.

Magnetometry was performed in a vibrating specimen magnetometer (VSM) at the University of Pittsburgh. Three mm disks were prepared using the techniques described for TEM sample preparation above, but were not thinned to perforation -- that is, thin, as-punched disks were used. If the disks exhibited the gold oxide surface film, they were cleaned in dilute HCl using the same technique as described for cleaning thin foils above, or in a solution of 50% water - 30%HNO_3 (69-71% grade) - 10% HF (46-48% grade) and 15% HCl (46.5-48% grade)[188].

Reference samples were prepared by quenching the samples in liquid nitrogen or liquid helium, or by annealing at 500-600°C for three hours under inert atmosphere followed by slow cooling. X-ray diffraction measurements and TEM investigations indicated that some retained austenite remained in the cryogenically quenched materials, whereas the annealed samples were fully ferritic steels. In the annealed references, XRD indicated

carbide peaks either barely above noise level of the scans, or no discernable carbide peaks at all. TEM investigation of as-annealed references showed a ferritic structure with small volume fraction of fine carbides present. As such, the annealed references were used.

Some studies[66,186] used a reference-less technique. Saturation values were calculated as a linear function of the weight percent alloying additions, rather than measuring saturation on a reference. Although calculated values, in principle, may correct for carbide-induced errors in reference samples, they will not account for nonlinear magnetic interactions between the alloying additions. The author's judgment is that the reference technique will be superior to the reference-less technique, so references were used.

Unique references were prepared for each chemical composition studied.

Magnetometry was the preferred method for obtaining retained austenite volume fractions in this study, as it was considered to be the most accurate (especially for textured samples or samples containing austenite particles too small to detect using XRD or optical microscopy) and was the fastest technique. However, magnetometry is only as good as the reference, so the reference must be thoroughly characterized by XRD and TEM before trusting measured f_γ values.

4.3 Mechanical Testing Procedure

Two types of mechanical tests were performed: standard room temperature ASTM tensile tests and variable-temperature tensile tests.

All mechanical tests were performed on ATSM sub-size tensile samples of 25.4mm (1") nominal gauge length and 6.4mm (0.25") nominal width. All samples were machined parallel to the rolling direction.

Standard room temperature tests were performed at US Steel's Research and Technology center on an MTS tensile machine. These tests were performed at 2.54mm/min crosshead speed.

Variable temperature tensile testing was performed in a Gleeble 3500 unit at US Steel's Research and Technology center. This unit was chosen because it is capable of using resistive heating for above-room-temperature tests, and has gas-jet ports for below room temperature testing.

High temperature tests were performed at 100°C. By monitoring multiple thermocouples, temperatures were found to be ±5°C at 100°C.

A copper coil was immersed in liquid nitrogen. Nitrogen gas was passed through this coil and then directed onto the gauge length of the samples for low-temperature tests.

By monitoring thermocouples welded to the sample and controlling the flow rate of the nitrogen gas, temperature uniformity of $\pm$5°C at 0°C were typically achieved, and $\pm$10°C at -20°C.

These tensile tests were performed at 2.54 mm/min strain rate.

Samples from industrial (Si-CAL, Si-CGL) coils were tested by the standard room temperature procedure and in the Gleeble at room temperature, in order to verify the calibration of the Gleeble unit. Tensile stresses agreed to within 7 MPa (1 ksi) and elongations agreed to within 1%.

Samples galvanized in the laboratory had heavy zinc coats on their entire length. The samples' grip ends -- but not gauge lengths -- were dipped in HCl solution to remove the zinc prior to testing. This eliminated slippage.

In the Gleeble unit, a laser extensometer was used to measure strain. The laser reported an initially 0.000mm value, which decreased over the course of the test; this laser value was denoted ΔW. The initial width recorded from the laser unit was denoted W_0. Assuming a Poisson's ration of ν=0.5 for the plastic regime, it was possible to calculate the tensile-axis engineering strain e_X:

$$e_x = -2\frac{\Delta W}{W_0} \tag{4-7}$$

True strain ε and true stress σ can be calculated from the engineering strain and stress, e and S, respectively:

$$\varepsilon = LN(e+1)$$
$$\sigma = S(e+1) \tag{4-8}$$

From the true stress and true strain, the strain hardening rate, n can be calculated:

$$n = \frac{\varepsilon}{\sigma}\frac{d\sigma}{d\varepsilon} \tag{4-9}$$

The slope, $d\sigma/d\varepsilon$, was calculated by averaging the slope of the twenty data points on either side of the point of interest, thus minimizing experimental noise.

Microhardness tests were performed on a Leco Vicker's hardness tester with diamond pyramid indenter under 500g loads on bakelite-mounted optical metallography samples.

4.4 Annealing Studies Procedure

4.4.1 Mechanical Properties Samples

The study material used for annealing studies was cold-rolled Al-Si steel (0.20C-1.8Mn-0.5Si-1.0Al; Table II). Samples were annealed in the Gleeble 3500 unit. For annealing studies, specialized annealing grips exist that produce excellent temperature uniformity were used. These grips are made of stainless steel to allow excellent electrical but only

poor thermal conduction. Samples of cold-rolled sheet 25cm long and 5cm wide are used. The temperature has been found to vary by less than 10°C at typical annealing temperatures, in a region more than 5 centimeters long and across the sample's full 5 centimeter width. This region is located in the middle of sample length. This allows two ASTM sub-size tensile samples to be taken from each annealed sheet's uniform area, as well as samples for metallography. Mechanical tests also show variations of less than about 5 MPa UTS and less than 1% total elongation across the width of the sample, confirming the excellent uniformity.

Samples, also of 25x5 cm size, were heated under vacuum to 843°C and soaked for 2 minutes at 843°C. This soaking was followed by average cooling rates of 0.4°C/sec or 4°C/sec. The slowest cooling rate required no special cooling; radiation through the samples' length and conduction through the grips allowed excellent temperature control. The 4°C/sec cooling rate was achieved by a forced air quench applied by gas jets located under the sample.

For the 0.4°C/sec cooling rate, samples were held at 416°C for 2 minutes, then rapidly forced-air-cooled to room temperature. Following the 4°C/sec average cooling rate cycle, samples were held for times ranging from 0 to 5 minutes at 416°C. This hold was sometimes followed by a temperature spike and approximately 30-second hold that simulated industrial galvanneal processing. Figure 55 shows a schematic of the 4°C/sec runs, which are labeled S-RT through S-5.

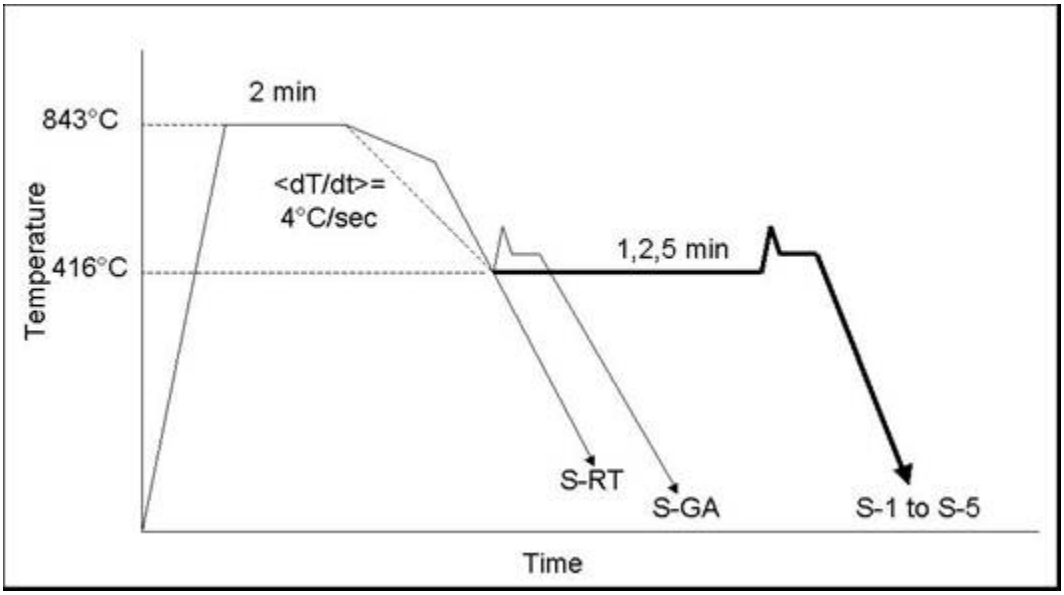

Figure 55 Schematic of the 4°C/sec runs, which are labeled S-RT through S-5

Figure 56 shows schematically the 0.4°C/sec condition, SLOW, with a 4°C/sec curve superimposed for comparison.

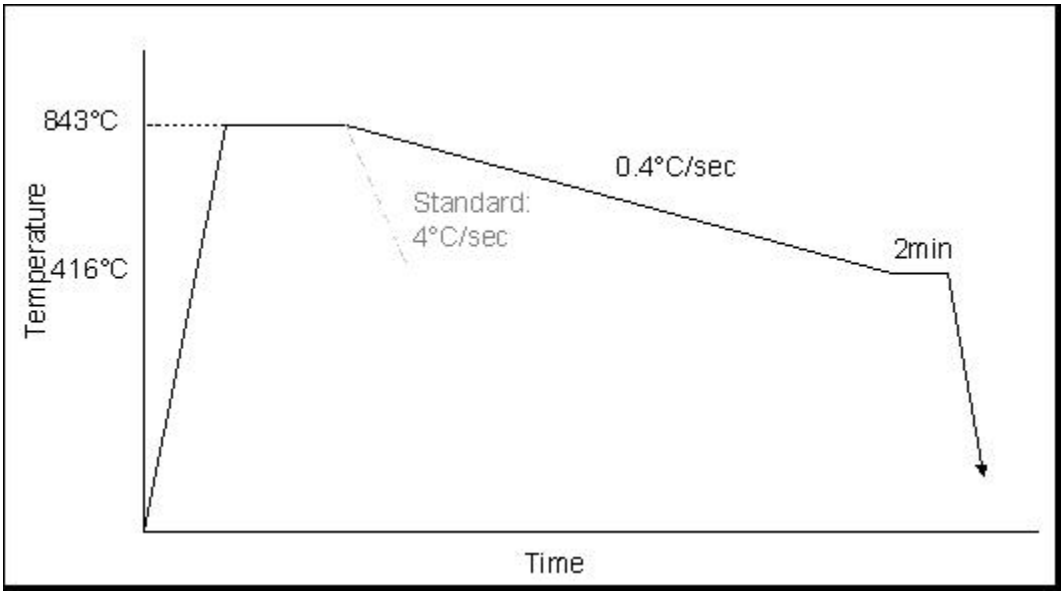

Figure 56 Sample condition SLOW, cooled at 0.4°C/sec

Following holding and/or galvannealing, samples were forced-air-quenched to room temperate.

Finally, samples were soaked in a salt pot at ~843°C for two minutes, transferred quickly to a ~416°C salt pot for two minutes, and then quenched. These samples are referred to as “Salt Pot.”

Tensile samples were cut from all these conditions and tested with standard room-temperature mechanical tests. Samples were also cut for standard metallographic examination (optical, SEM, TEM).

Samples for the study of GA (galvannealing) parameters were heat-treated in the fashion of S-2 above, but by varying the temperature of the GA step to either 437°C, 482°C, or by quenching after the end of the two-minute hold, completely foregoing the GA step. These conditions are referred to as 2-437, 2-482, and 2-NONE.

4.4.2 Dilatometry

The Gleeble unit was also used for dilatometric studies. This was performed by installing the "low-force" sample grips and configuring them in their free-floating, "no force" mode. This prevented externally applied strain during the samples' examination.

Samples were heated either under vacuum or helium gas. A laser extensometer was used to measure dilation across the sample width.

Samples were sheet cut to 12-13mm widths. Lengths varying from 50 to 100mm were used. Much of the samples' cooling was imparted from conduction through the water-cooled copper grips holding the samples. Thus, a smaller sample would allow for higher cooling rates, but would exhibit less lengthwise temperature uniformity. As such, care was taken to make sure the laser extensometer fell exactly on the point where the control thermocouple was welded; this made sure the recorded temperatures corresponded to the recorded dilations. See Figure 57.

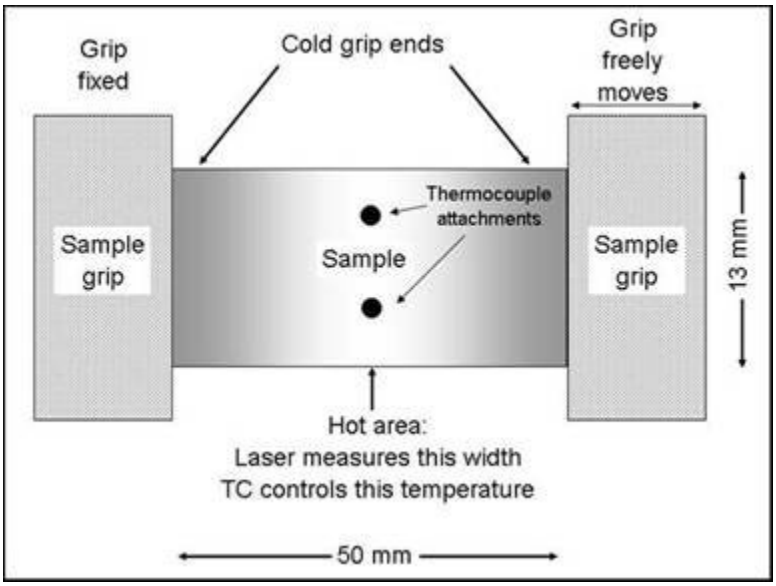

Figure 57 Schematic of dilatometer setup

Samples cooled at faster rates (40, 100 and 200°C/sec) were cooled by helium gas jets; samples cooled at 4 or 0.4°C/sec used natural cooling. All cooling cycles were computer controlled via the welded thermocouple.

Samples were heated to 843°C and soaked for 2 minutes, then cooled at rates varying from 0.4 to 200°C/sec to 416°C, where they were held 5 minutes. After the 416°C hold, samples were helium quenched to room temperature. Five minutes was the chosen time to ensure that the isothermal reactions, being measured by the dilatometer, were driven to completion; see Figure 58.

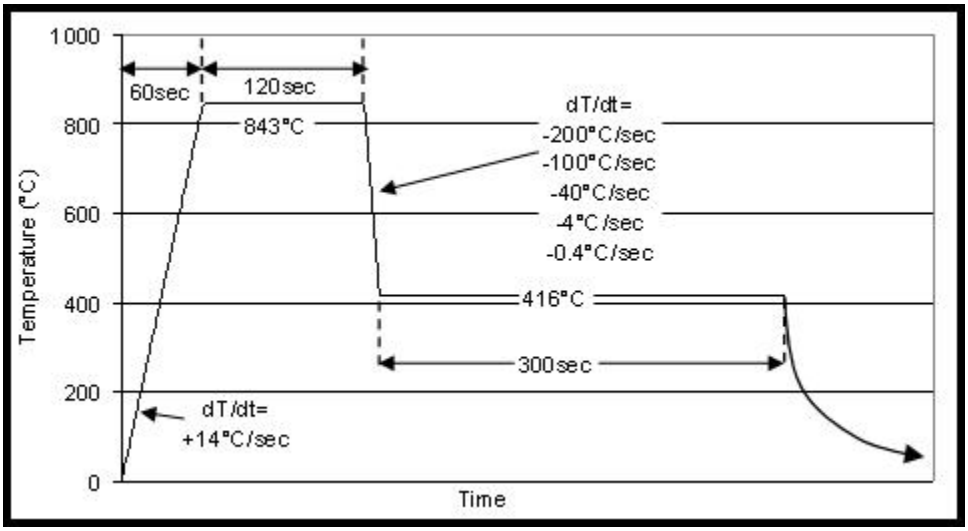

Figure 58 Dilatometry thermal profiles

Care was taken to ensure that metallographic preparation of the samples showed the areas nearest the control thermocouples, which corrected for potential temperature non-uniformity in the specimens' lengths. Specifically, samples were ground and polished such that the plane of polish contained the thermocouple attachment points, ensuring the examined surface experienced the thermal path recorded by the thermocouples.

Samples were also heat treated in the above fashion, but not studied dilatometrically, as follows. Samples were heated to 843°C and held for two minutes, using the same heating and soaking profile as for dilatometry, then helium-quenched to room

temperature (not 416°C) at cooling rates in excess of 200°C/sec, providing the intercritical structure as it was in other conditions before cooling to the IBT. (Cooling at >200°C/sec was expected to suppress epitaxial ferrite formation.) Similarly, samples were heated to 800°C/sec for two minutes and quenched. Samples were heated to 800°C/sec for 2 minutes and cooled at rates of either 4 or 200°C/sec to 416°C, transformed isothermally for 5 minutes, then helium-quenched to room temperature.

These conditions (called 843°C-quench, 800°C-quench, and 800°C-4°C/sec and 800°C-200°C/sec, respectively) were to provide comparisons to the above dilatometrically-studied conditions. These samples were prepared metallographically in the same fashion as were the dilatometer samples. The 843°C-quench and 800°C-quench samples gave the state of the material at the end of the intercritical hold.

Microhardnesses were tested in a Leco microhardness tester operated at a 500g load. The microhardness samples were epoxy- or bakelite-mounted metallographic specimens. For the Salt Pot and S-2 conditions, the samples were cut from the center of the annealed sheet; for dilatometry samples, the same samples used for optical microscopy were tested by microhardness.

5.0 RESULTS

5.1 Metallographic Technique Development Results

5.1.1 X-Ray Diffraction Results

The Si-CAL steel was studied by XRD; a typical XRD trace is given in Figure 59.

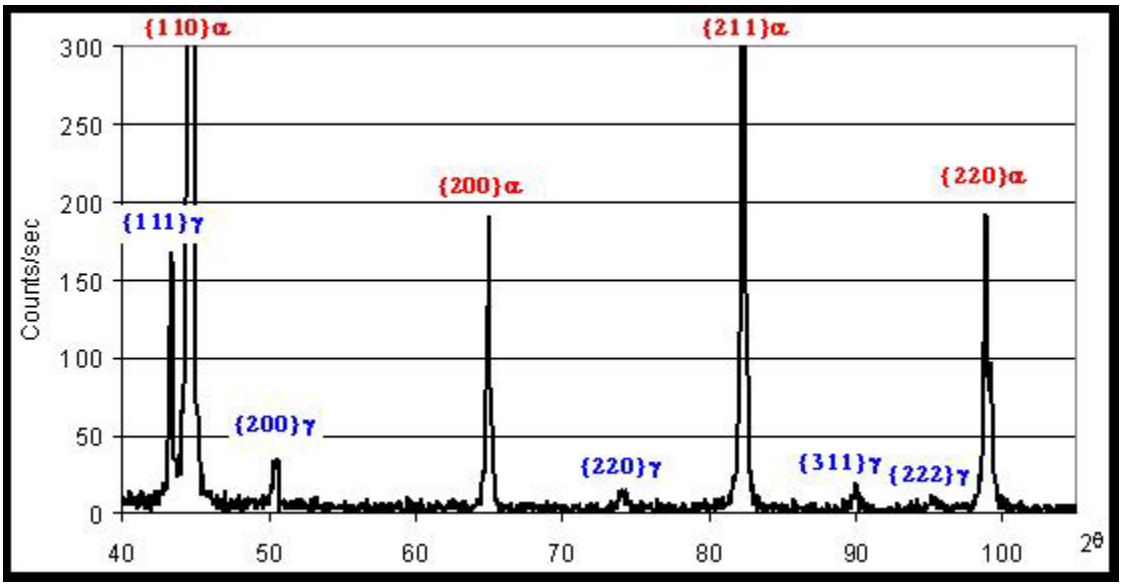

Figure 59 Example XRD trace (from TD sample) with peaks labeled; Si-CAL steel

Samples of Si-CAL, taken in the ND, and stacks of samples prepared to examine the RD and TD, were examined by XRD. Traces are given in Figure 60.

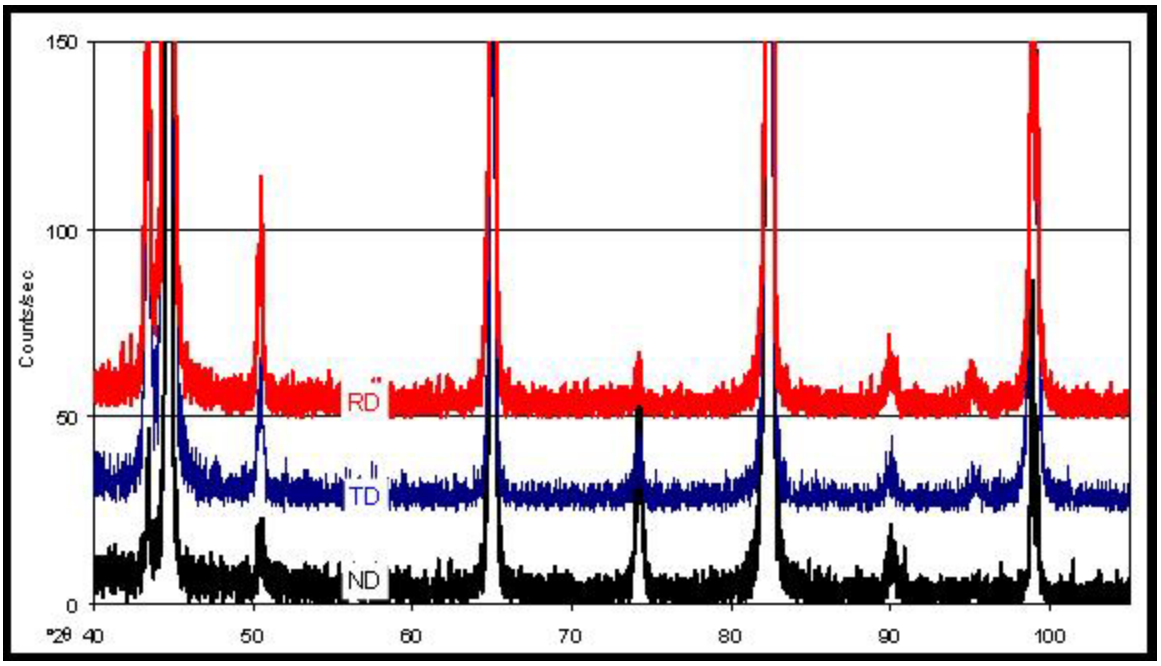

Figure 60 XRD traces for ND, TD and RD samples of Si-CAL steel

Details of Figure 60 are given in Figure 61.

a)

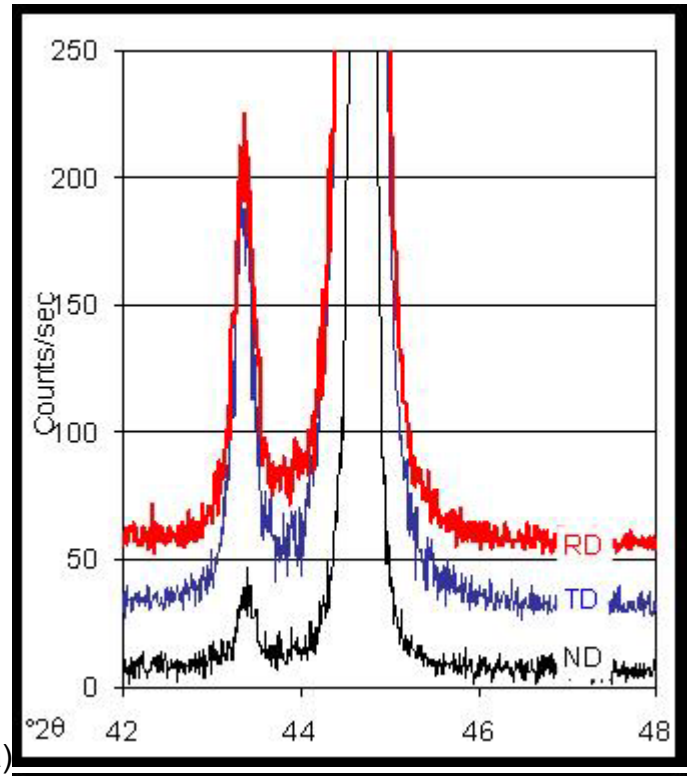

b)

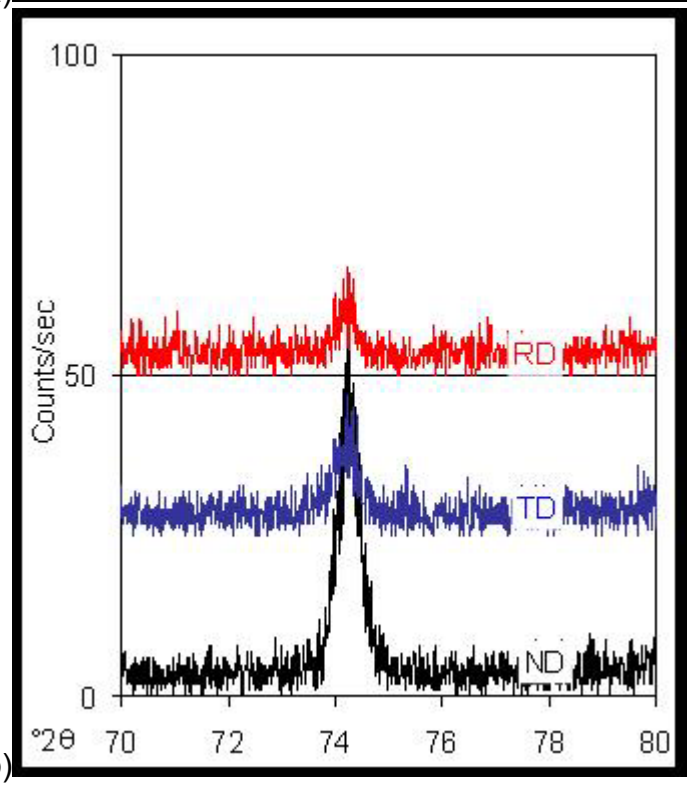

Figure 61 (a), (b) Details of Figure 60.

Note differences in magnitude of the peaks between the ND, TD and RD samples, indicating differences in texture between the samples.

Table VI I/R ratios for the peaks, measured from the traces in Figure 18.

Normalized I_{hkl}/R_{hkl}	Examined face: || ND	|| RD	|| TD
(111)γ	0.017	0.050	0.036
(200)γ	0.042	0.107	0.017
(220)γ	0.267	0.011	0.022
(311)γ	0.063	0.037	0.008
(110)α	1.000	1.000	1.000
(200)α	3.114	1.276	0.282
(211)α	3.132	0.981	0.337
(220)α	1.042	1.617	0.760

The ferrite peaks should -- in untextured material -- all equal 1.000. The austenite values should be less than 1, but should be equal to each other.

Table VII Matrix of 16 f_V values.

(a)

	(110)α	(200)α	(211)α	(220)α
(111)γ	1.7	0.5	0.5	1.6
(200)γ	4.0	1.3	1.3	3.8
(220)γ	21.1	7.9	7.9	20.4
(311)γ	5.9	2.0	2.0	5.7

(b)

	(110)α	(200)α	(211)α	(220)α
(111)γ	4.7	3.7	4.8	3.0
(200)γ	9.6	7.7	9.8	6.2
(220)γ	1.1	0.9	1.1	0.7
(311)γ	3.5	2.8	3.6	2.2

(c)

	(110)α	(200)α	(211)α	(220)α
(111)γ	3.5	11.3	9.6	4.5
(200)γ	1.7	5.7	4.8	2.2
(220)γ	2.1	7.1	6.0	2.8
(311)γ	0.8	2.8	2.3	1.1

Calculated using the technique developed in this study, from the (a) ND, (b) TD and (c) RD samples. Note radical variations.

Table VIII f_V values (in volume %)

	|| ND	|| RD	|| TD
This technique			
$\langle f_v \rangle \pm \sigma_{fv}$=	5.5±6.4	4.1±2.9	4.3±3.0
Alternate techniques			
Miller f_v=	8.0	9.3	5.1
ASTM f_v=	4.6	5.0	2.1
Deshayes f_v=	12.9	12.8	5.6
Mod. ASTM f_v=	3.4	4.5	4.0

"This technique" denotes values obtained from average and standard deviations from the 16 values from Table 3 (a)-(c). Other techniques are listed in section 4.2.2

5.1.2 SEM Technique Development Results

Typical SEM micrographs (nital etched) are shown in Figure 62.

a)

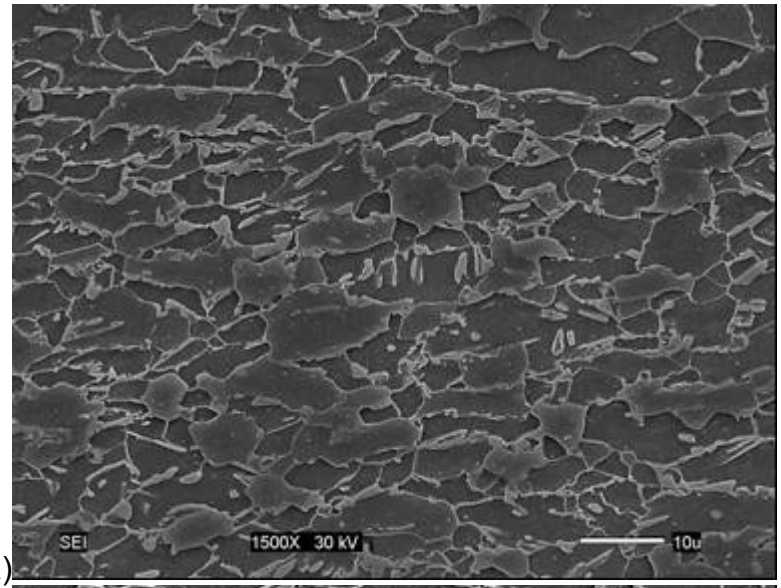

b)

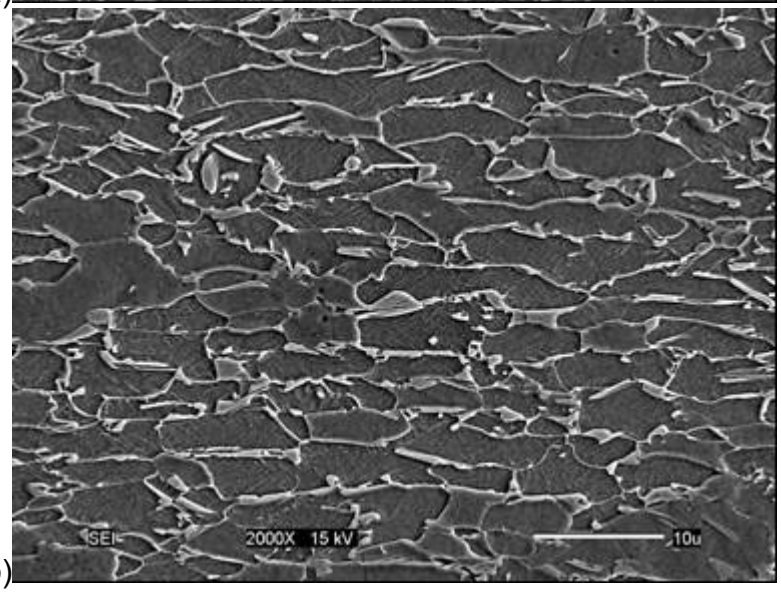

Figure 62 Low magnification SEM micrographs of (a) Si-CAL as-received (b) Si-CAL pulled to failure. Tempered 2hours@200°C + 2% Nital

The SEM imaging shows excellent contrast between the matrix and other phases, although differentiating the "other" phases from each other is somewhat difficult. Figure 63 shows the application of Girault et al.'s technique to differentiate martensite from austenite.

(a)

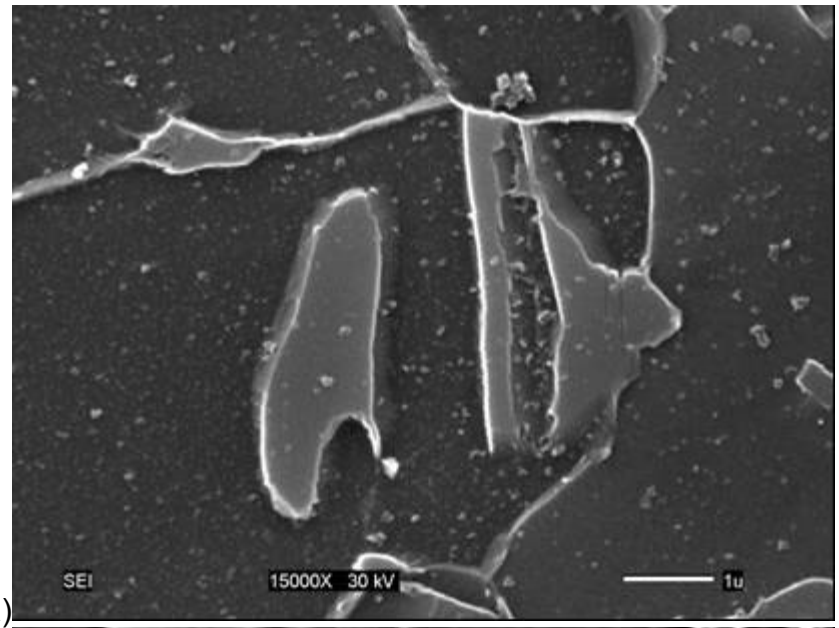

(b)

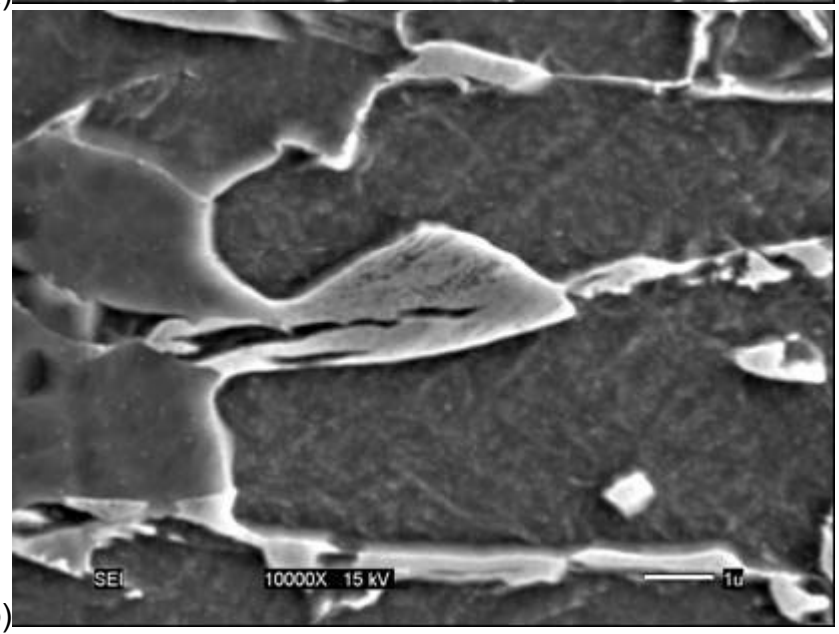

Figure 63 Comparison of unstrained and failed Si-CAL. (a) as-received, (b) pulled to failure. Both tempered 2 hours@200°C + 2% Nital

The martensite clearly shows substructure, whereas the austenite remains featureless.

5.1.3 TEM Technique Development Results

TEM is the only technique capable of examining the substructure of phases; for example, Figure 64, Figure 65, Figure 66, Figure 67 and Figure 68.

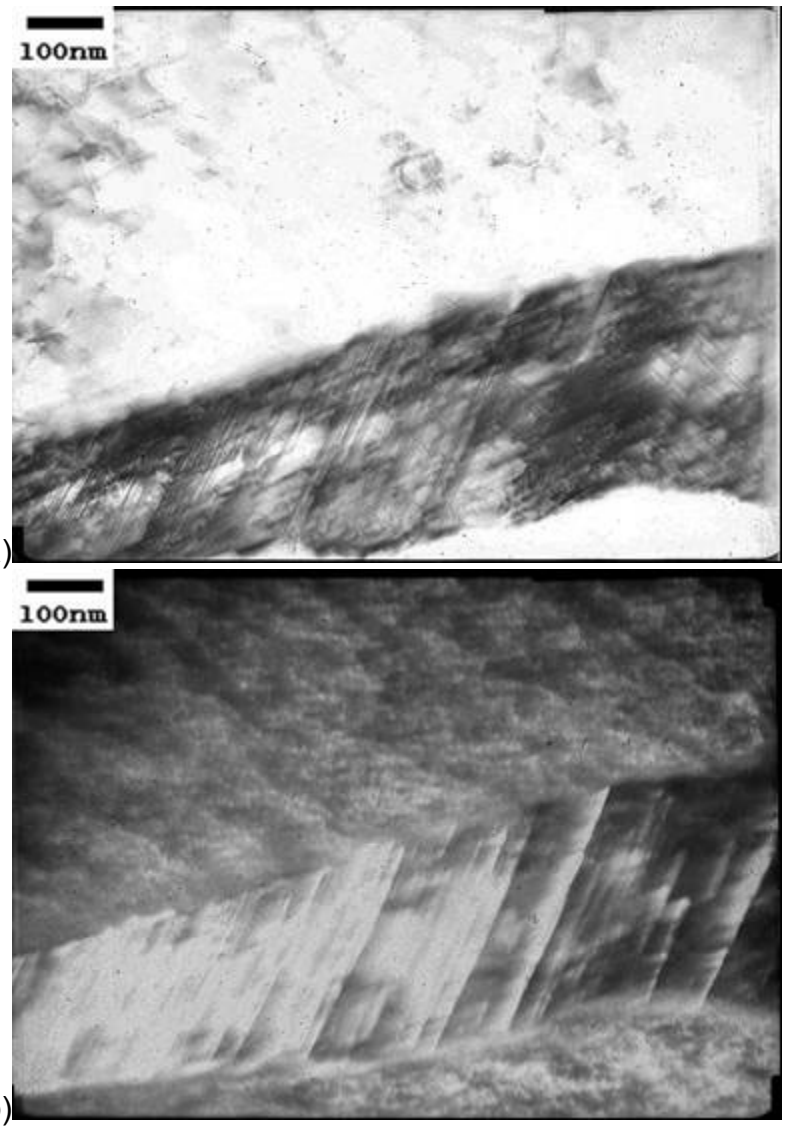

Figure 64 Twinned martensite in Si-CGL pulled 10% in tension. (a) BF, (b) DF

(a)

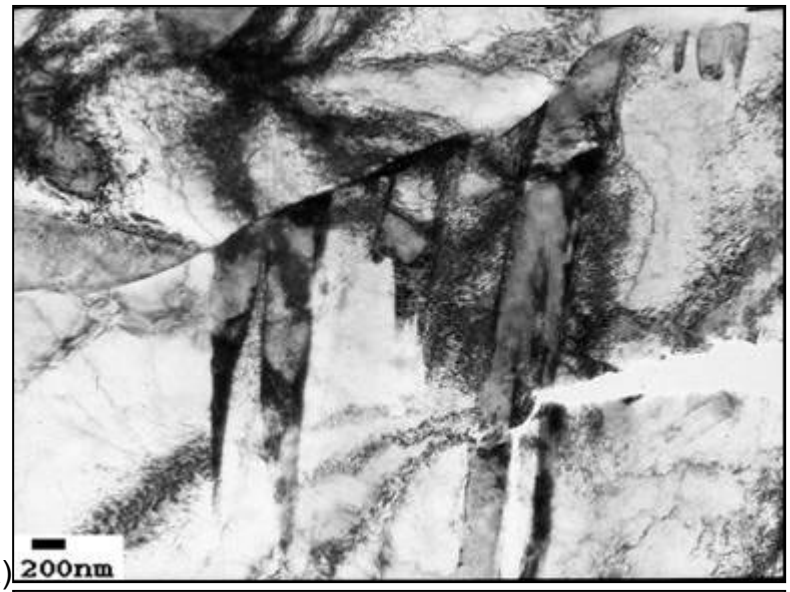

(b)

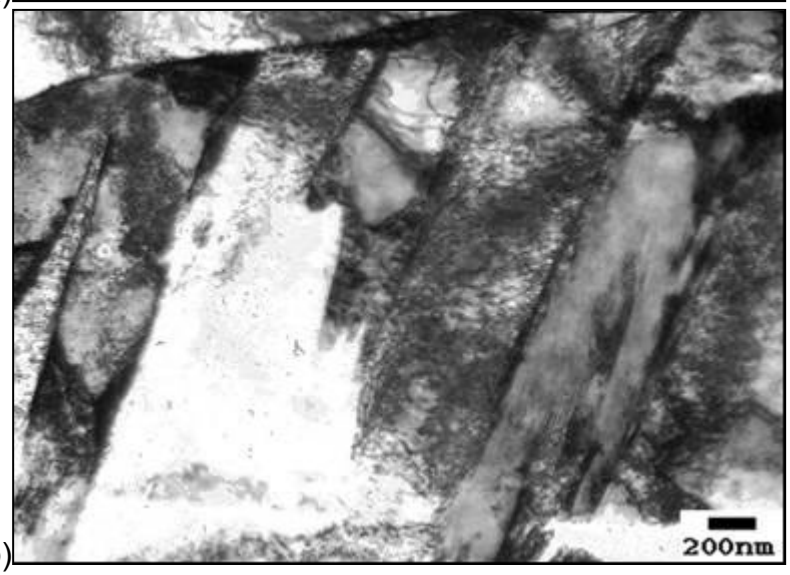

Figure 65 Grain-boundary sideplates, speculated to be bainitic ferrite, in as-received Si-CAL

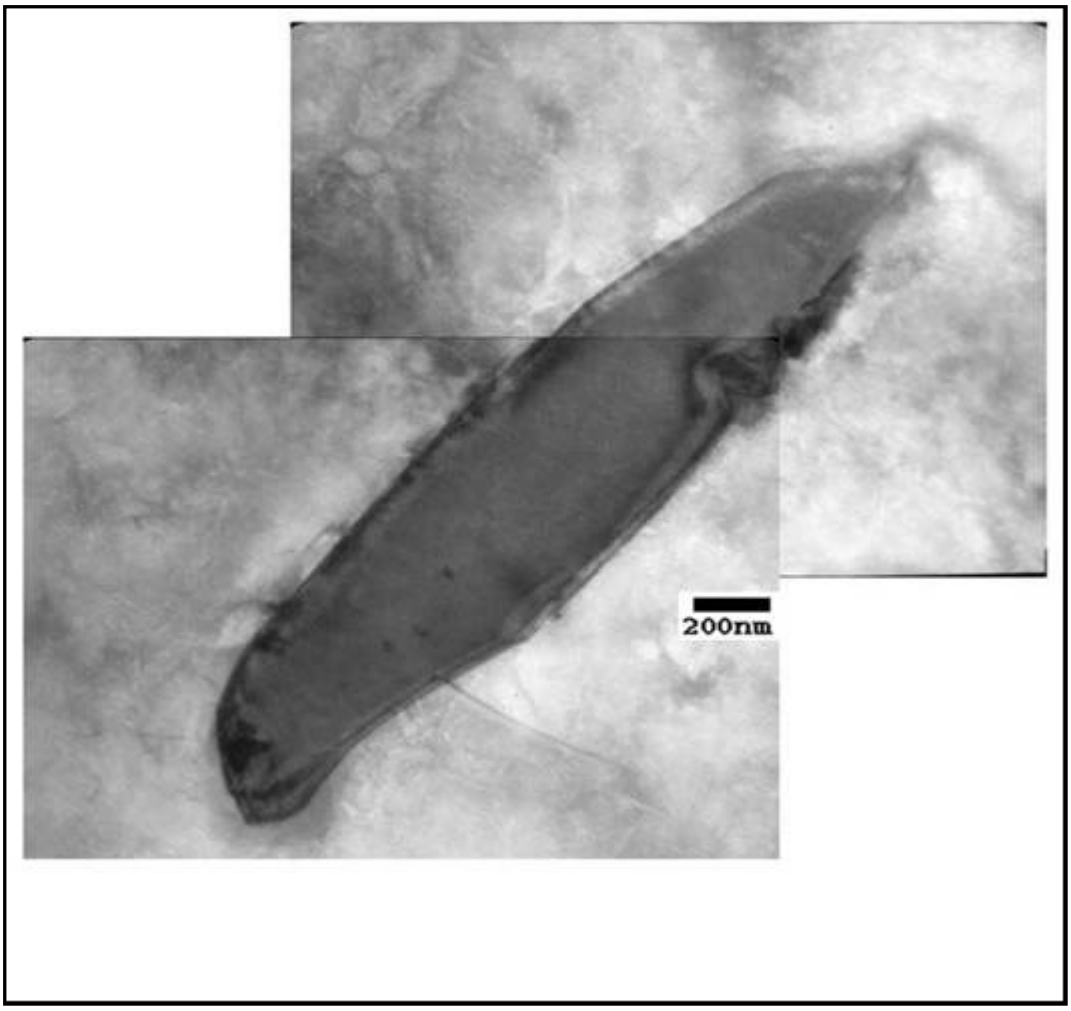

Figure 66 Retained austenite particle in Si-CAL, after liquid nitrogen quench

a)

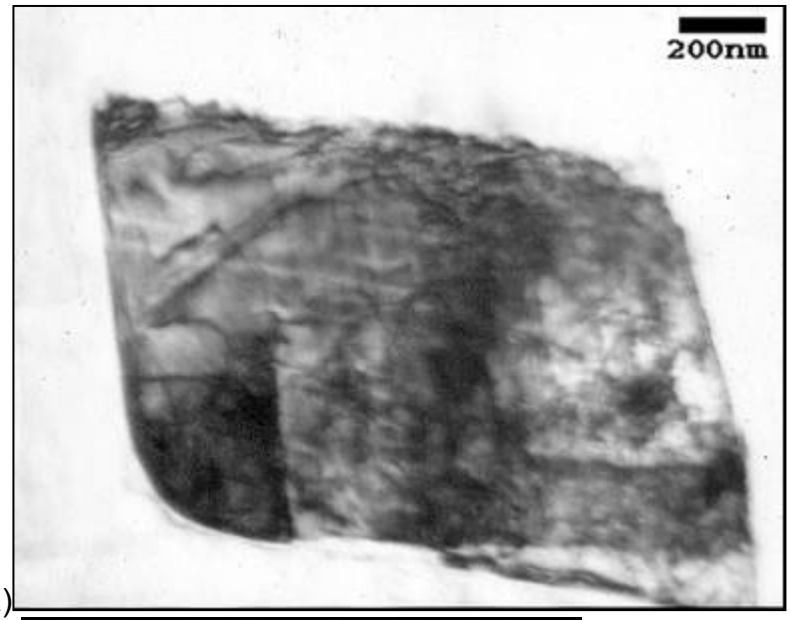

b)

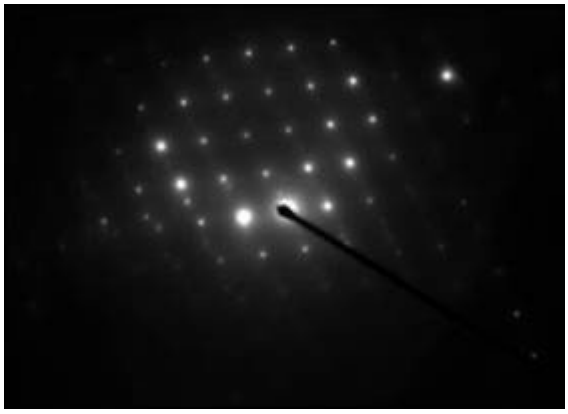

c)

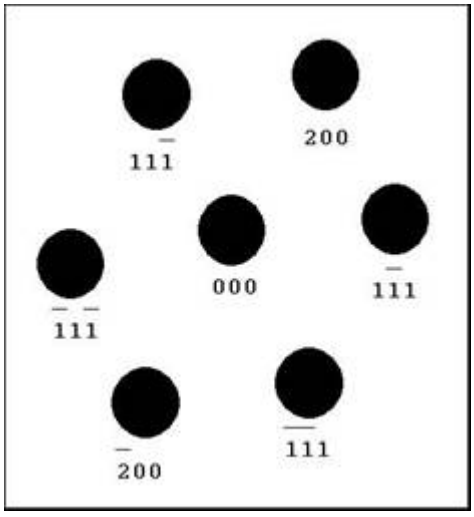

Figure 67 Retained austenite (a), as verified by (b) [0 -1 -1]γ_R diffraction pattern, in Si-CGL pulled 20% in tension.

Note that the particle has not transformed despite the large tensile strain, and the dense sub-structure within the particle

a)

b)

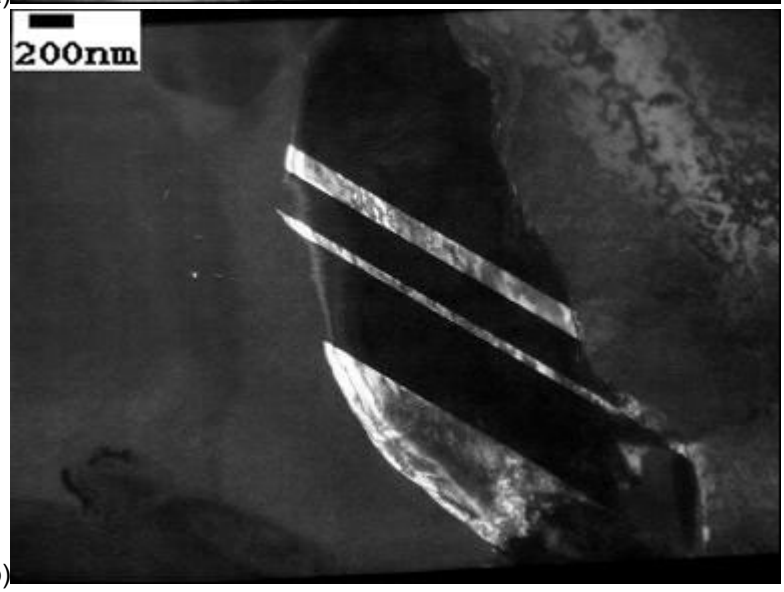

c)

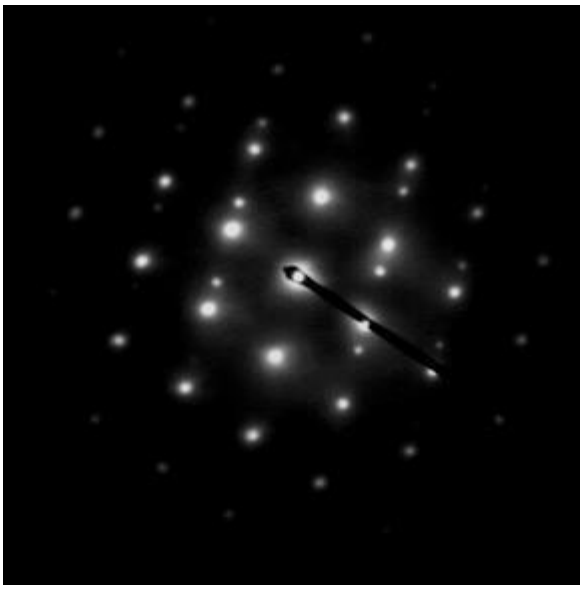

d)

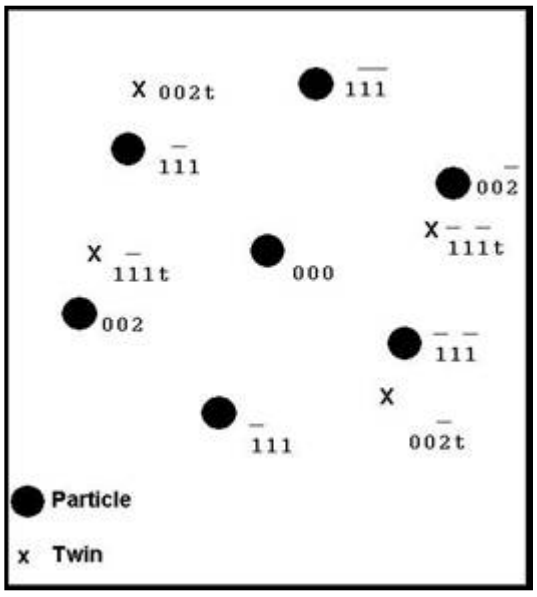

Figure 68 TEM micrographs from 200°C/sec dilatometer specimen.

(a) BF of retained austenite (b) DF, showing clear twinning (c) [-1 -1 0]γ_R SADP, also clearly showing twins (d) Indexed SADP.

5.1.4 Magnetometry Technique Development

Reference samples, annealed 600°C for 3 hours, were shown to be austenite-free by XRD and TEM examination; see Figure 69.

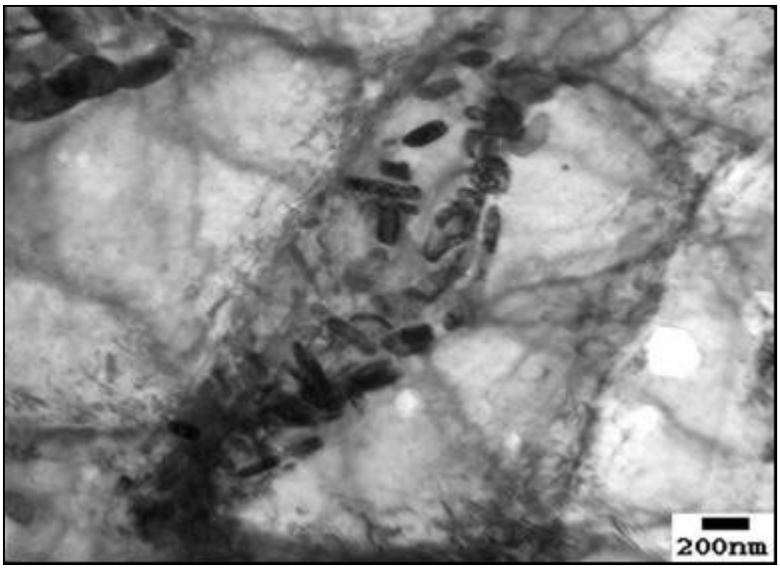

Figure 69 3hour@600°C annealed Si-CAL. Shown is a prior-retained-austenite particle delineated by precipitated carbides.

Example magnetometric data is given in Figure 70.

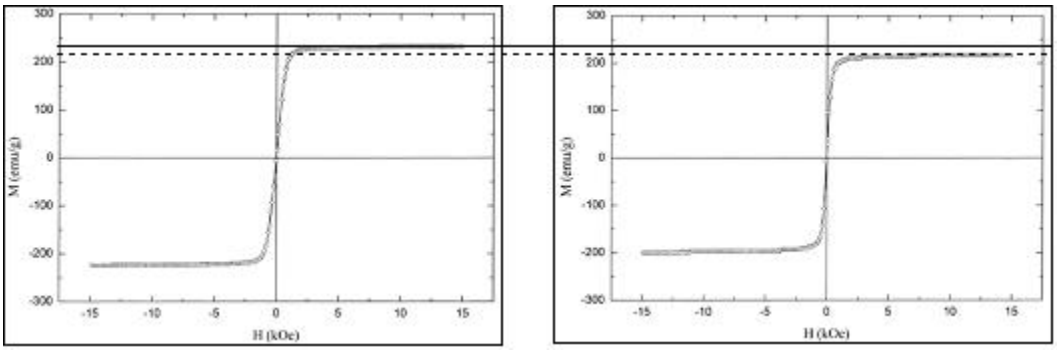

Figure 70 Magnetization curves for reference and TRIP specimens of Si-CAL; indicates 8.7% retained austenite.

Samples of fully-processed TRIP steel were subjected to tensile tests at -20 to 100°C. Example flow curves for the Si-Al material are presented in Figure 71.

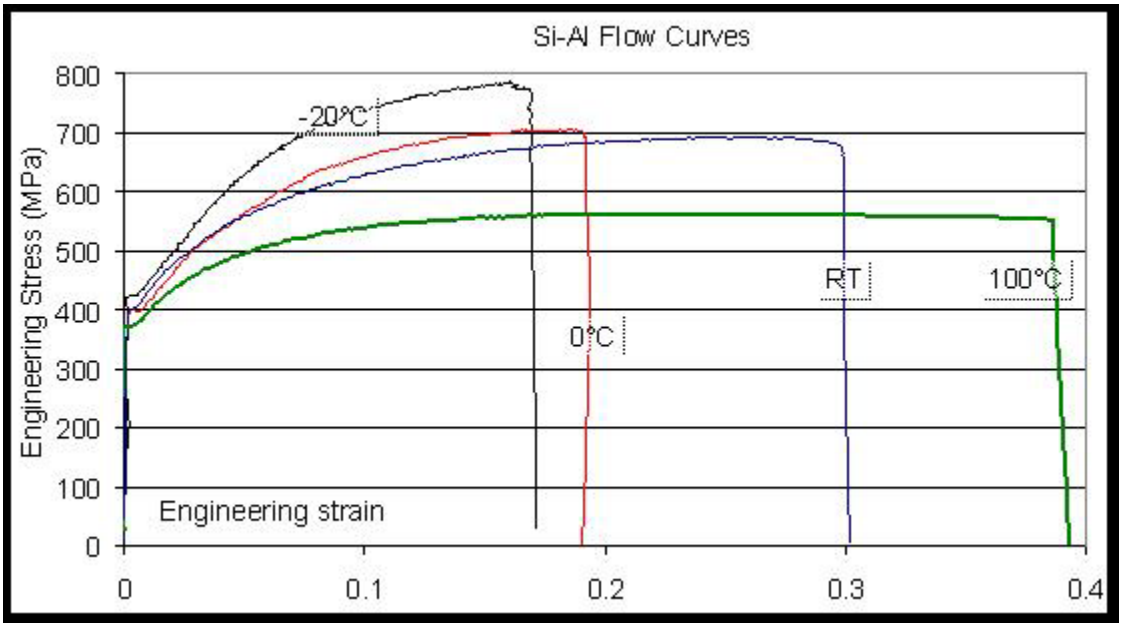

Figure 71 Typical variable-temperature flow curves; samples are Si-Al laboratory annealed steel

The flow hardening behavior for the Si-Al material, representative of all flow curves, is shown in Figure 72.

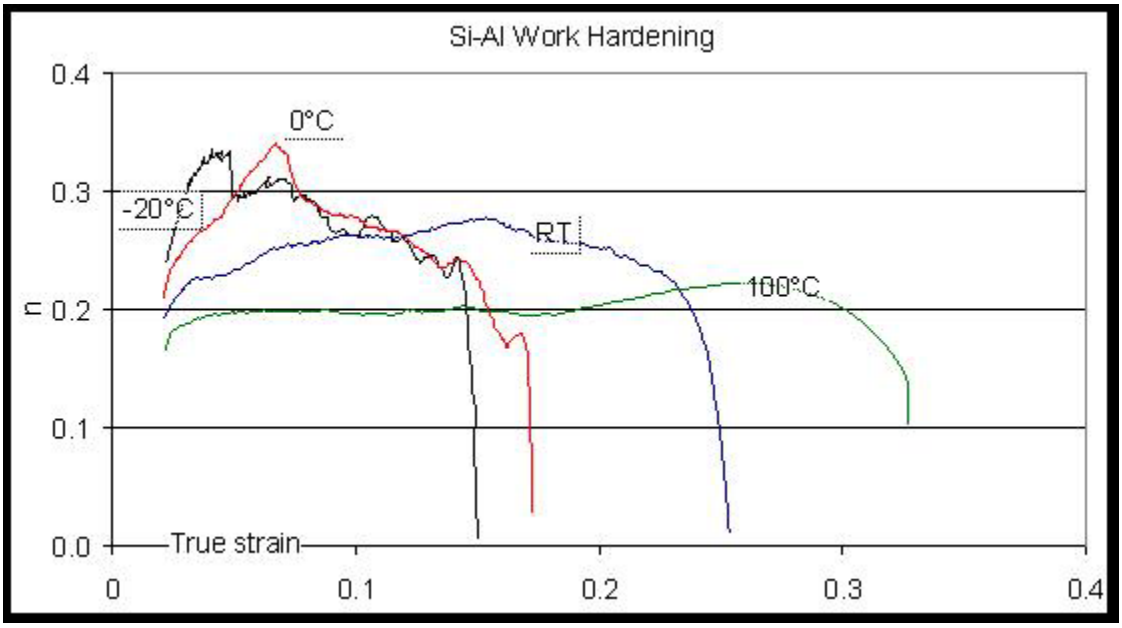

Figure 72 Work-hardening behavior of Si-Al steel

Reasonably, the lower temperature tensile tests showed the highest tensile strengths and lowest total elongations. The low-temperature tests showed high-n value early in the test, followed by a precipitous drop. The high-temperature test showed a uniform and low n value. The RT tests showed a uniform and high n value.

UTS data for all conditions are summarized in Figure 73.

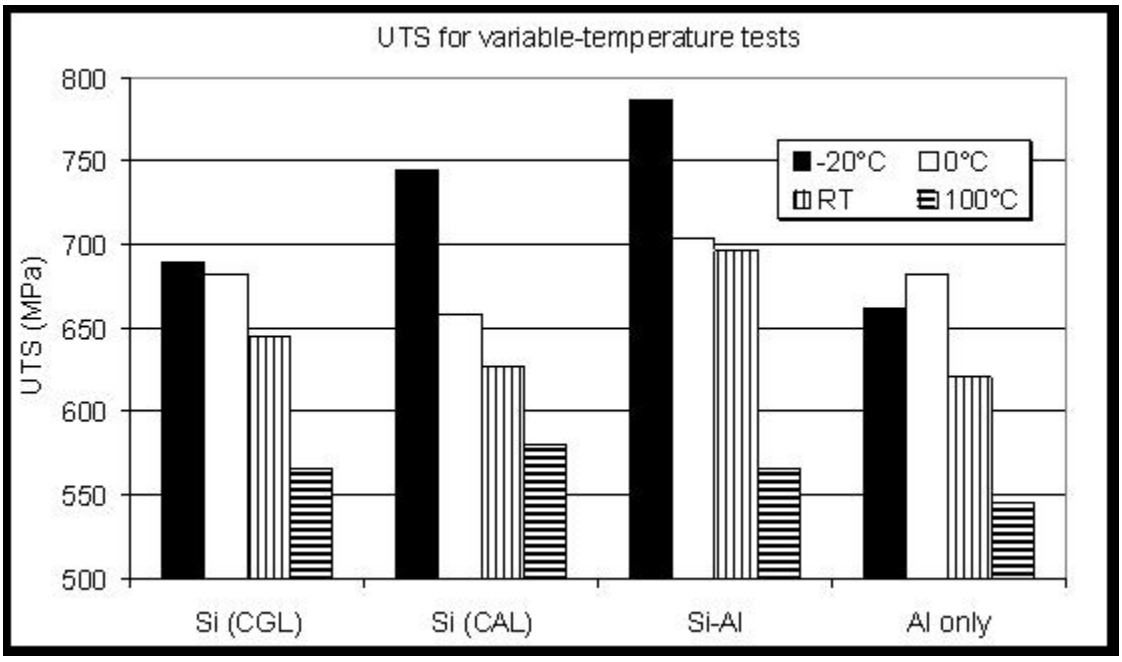

Figure 73 Summary of UTS values for all samples

Similarly, total elongations are summarized in Figure 74.

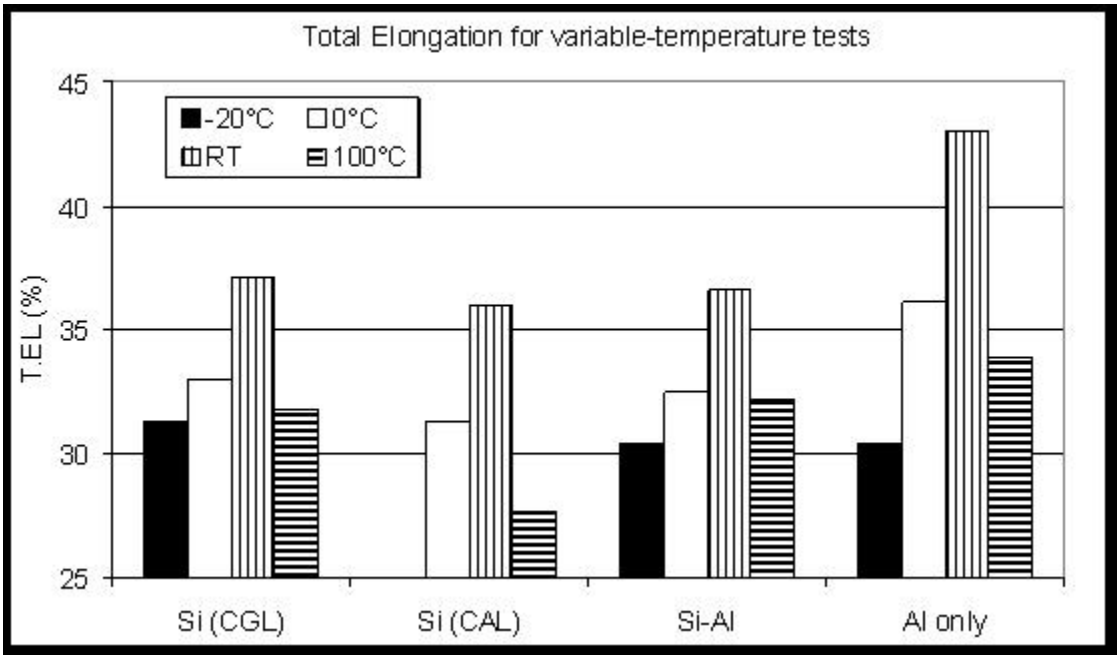

Figure 74 Summary of total elongation values for all conditions

In short, samples show their highest strength at low temperature, but their highest ductility at room temperature. Higher temperatures reduce strength; higher and lower temperatures reduce ductility.

5.3 Annealing Studies Results

The starting condition for all annealing and dilatometric studies was cold-rolled sheet of composition 0.20C-1.8Mn-0.5Si-1.0Al. Micrographs of the as-cold-rolled structure showed it was cold-rolled pearlite/ferrite, Figure 75.

a)

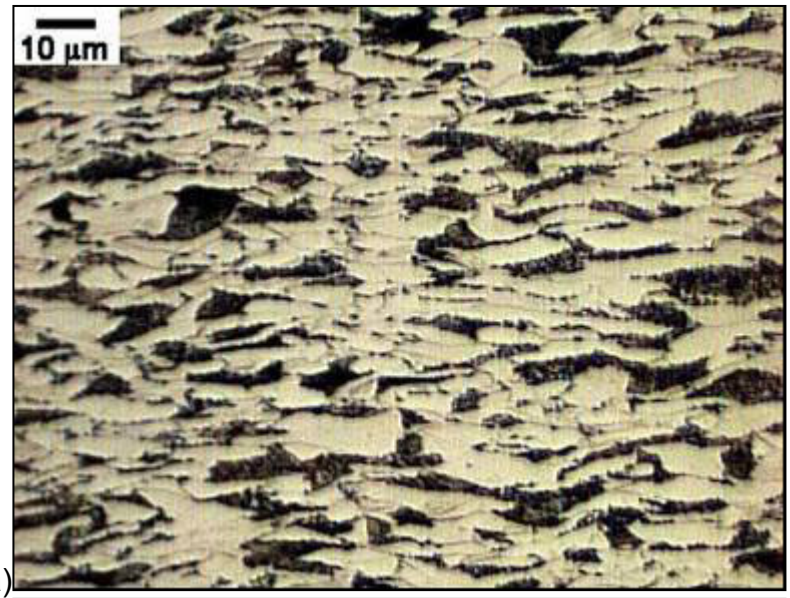

b)

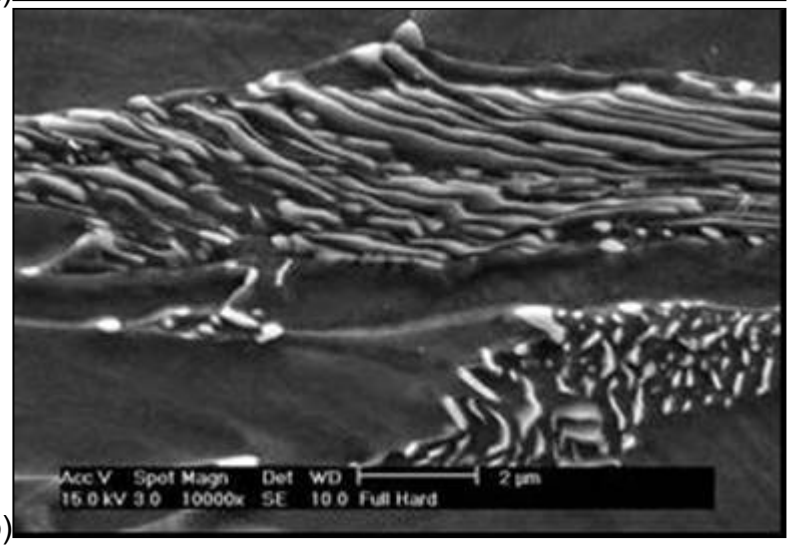

Figure 75 (a) 3% nital + 10% $Na_2S_2O_5$ etched optical micrograph. (b) 3% nital etched SEM micrograph.

The intercritical structure was examined by reheating samples of cold-rolled sheet (under the same thermal path as for dilatometry studies) to 800°C or 843°C for 2 minutes and helium-jet quenching. Quenching was in excess of 200-250°C/sec. Micrographs are presented in Figure 76; point-counts on optical micrographs indicates that the intercritical structure was ~52% austenite after 2 minutes at 800°C and ~62% austenite after 2 minutes at 843°C

a)

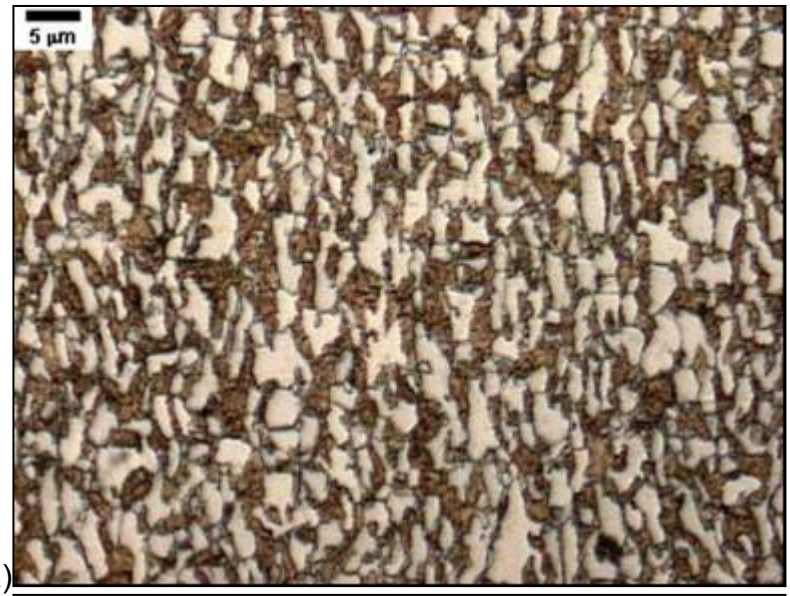

b)

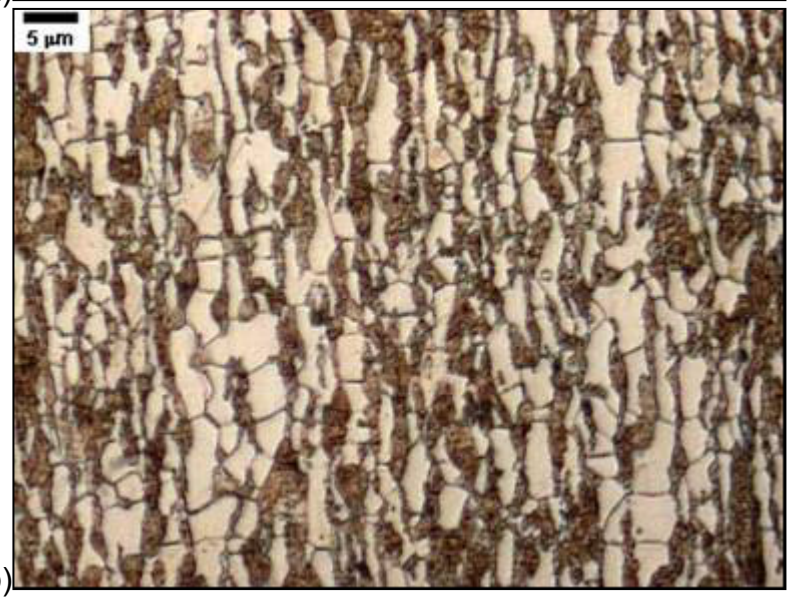

Figure 76 3% nital+10% $Na_2S_2O_5$ etched optical micrographs. Reheated and quenched samples.

Dark phase is martensite, light phase ferrite, indicating intercritical austenite + ferrite structure. (a) 843°C 2minutes + quench (62vol% α'); (b) 800°C 2minutes + quench (52vol% α').

5.3.1 IBT Parameters Study

Conditions SLOW, S-RT, S-GA, S-1, S-2 and S-5 (as defined in Section 4.4.1, Figure 55 and Figure 56) were subjected to standard mechanical tests; results from these tests are summarized in Table IX and Figure 77.

Table IX Summary of mechanical properties for IBT study conditions

Sample Designation	<dT/dt> (°C/sec)	t_{IBT} (min)	GA Step?	YS (MPa)	UTS (MPa)	T.EL (%)	UTSx T.EL (MPa%)	YPE (%)
S-5	4	5	Yes	432	668	45.2	30194	0.6
S-2	4	2	Yes	409	687	43.7	30022	0.4
S-1	4	1	Yes	390	698	42.5	29665	0.3
S-GA	4	0	Yes	377	764	37.4	28574	< 0.1
S-RT	4	0	No	308	804	30.0	24120	0.0
Slow	0.4	2	No	485	647	29.2	18892	1.3

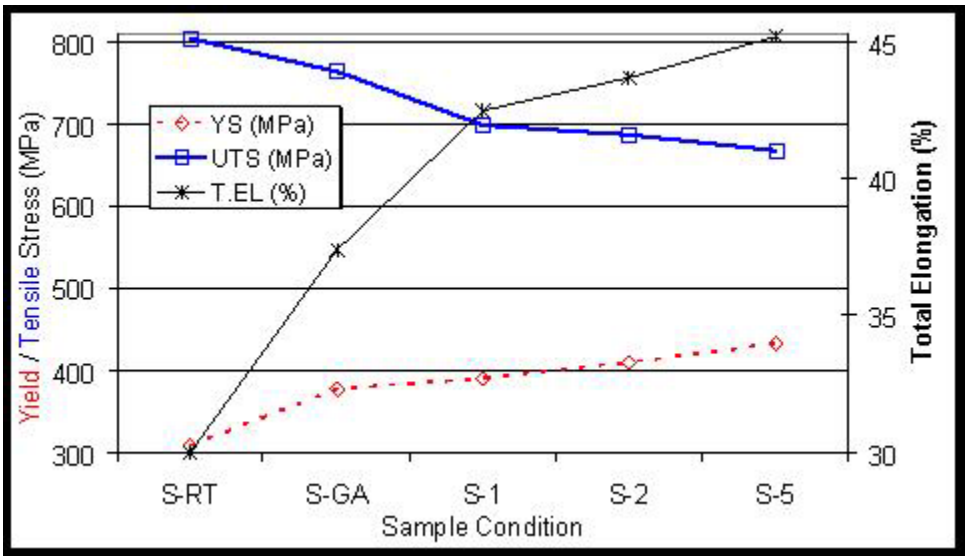

Figure 77 Mechanical properties of standard-cooling-rate samples.

Firstly, sample SLOW showed both the lowest tensile strength and lowest total elongation, and largest yield-point-elongation. It also showed the highest yield stress. Metallographic examination showed that sample SLOW consisted of pearlite and a small fraction retained austenite in a ferritic matrix. Figure 78 shows micrographs of this sample condition.

a)

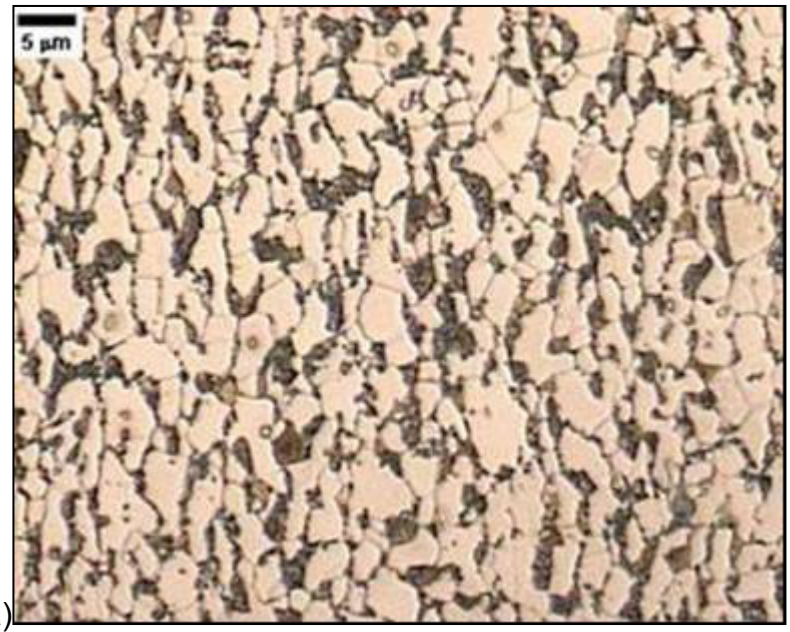

b)

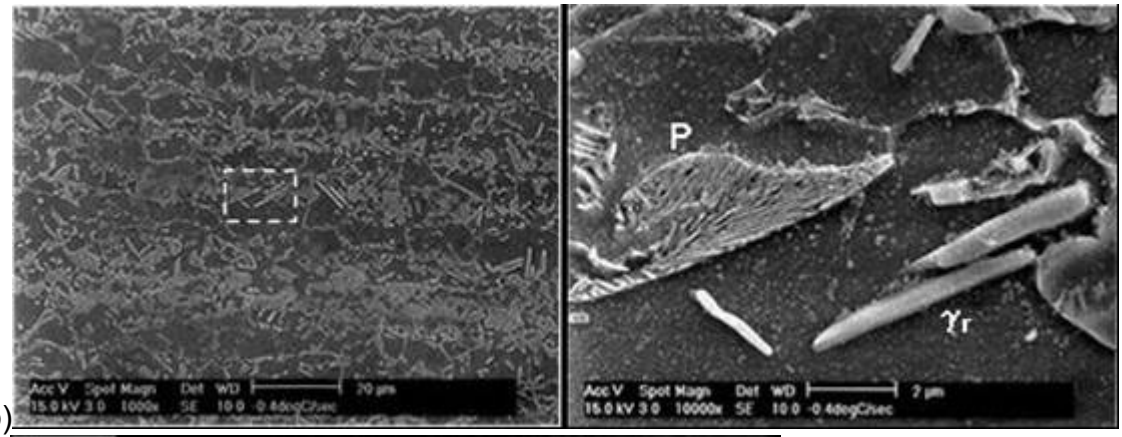

c)

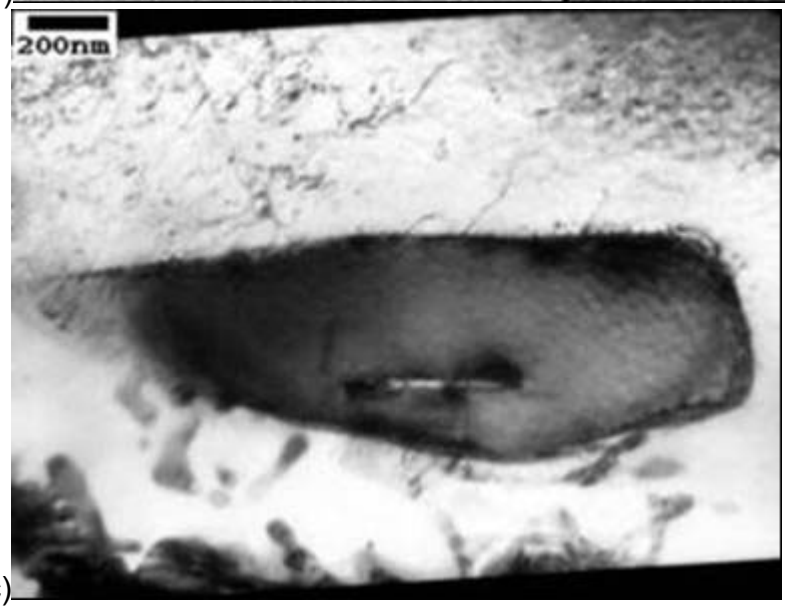

d)

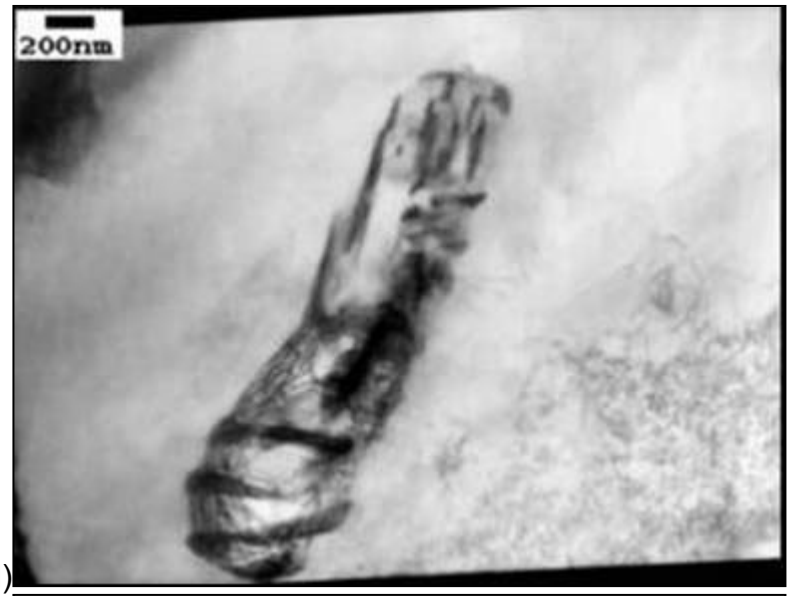

e)

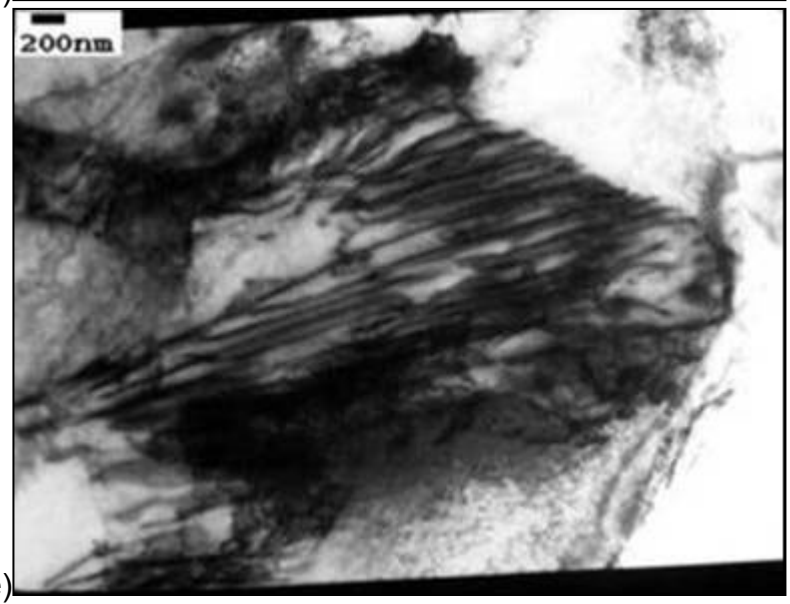

f) 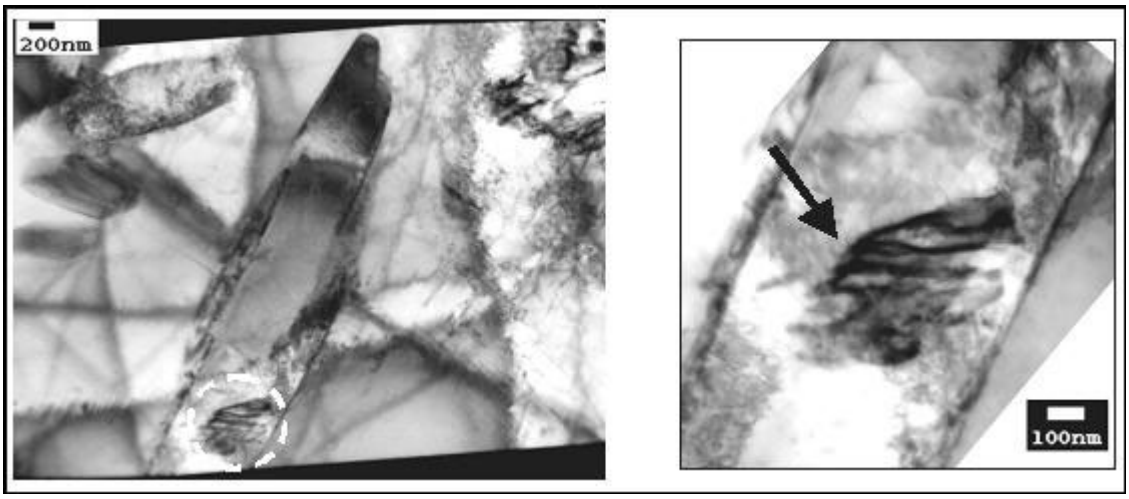

Figure 78 Micrographs of sample condition SLOW.

(a) 3% nital + 10% $Na_2S_2O_5$ etched optical micrograph; pearlite (large dark constituents) and retained austenite (small light constituents, present in only a small fraction) in ferrite matrix. (b) 2% nital etched SEM micrographs; boxed area in left micrograph indicates detailed area in right micrograph; pearlite P and retained austenite γ_R labeled. (c) BF-TEM micrograph of retained austenite particle. (d) BF-TEM micrograph of a former-retained-austenite particle that decomposed into ferrite+carbide. (e) BF-TEM of eutectoid pearlite. (f) Retained austenite particle undergoing incipient carbide precipitation; circled area in left micrograph indicates detailed area in right micrograph. Arrow points to area where carbide precipitation is just beginning.

As shown in Figure 78, the sample contains pearlite and retained austenite.

Sample conditions S-RT through S-5 show monotonically increasing (1) total elongation, (2) yield point elongation and (3) yield stress as IBT time increases; they also show monotonically decreasing tensile stress. Micrographs of condition S-RT are shown in Figure 79 and Figure 80; condition S-GA in Figure 81. S-1, S-2 and S-5 gave very similar microstructures, so micrographs from condition S-2 are representative of all three conditions, and are presented in Figure 82.

a)

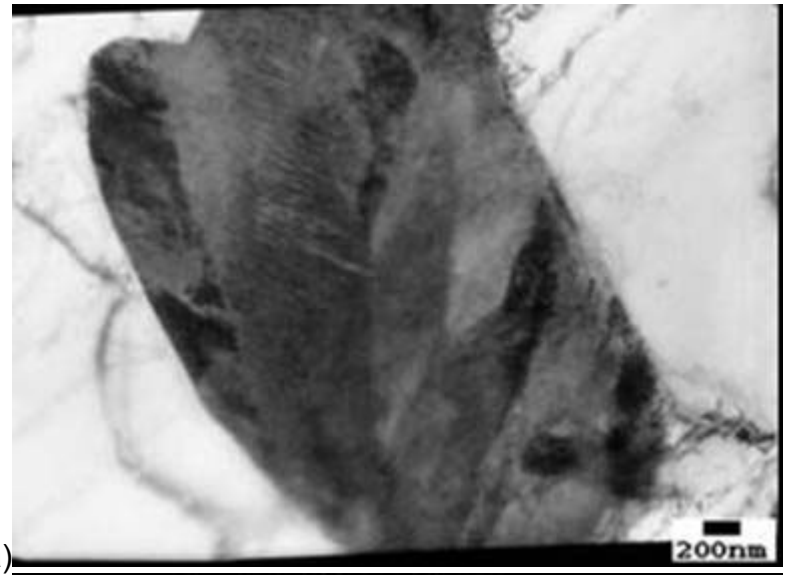

b)

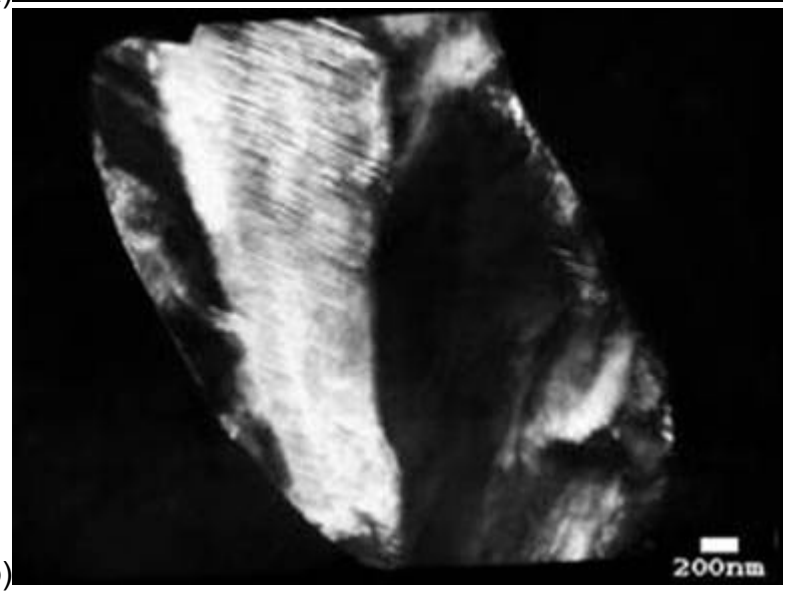

Figure 79 Sample condition S-RT; (a) BF-TEM and (b) DF-TEM of twinned martensite.

a)

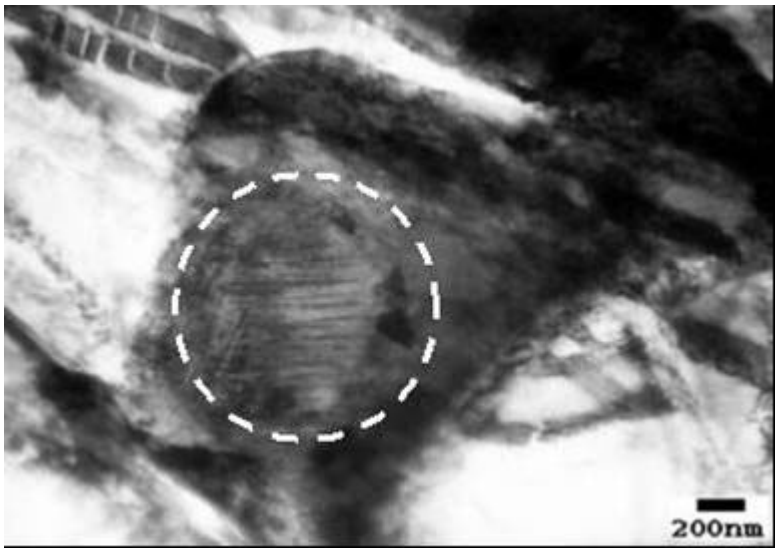

b)

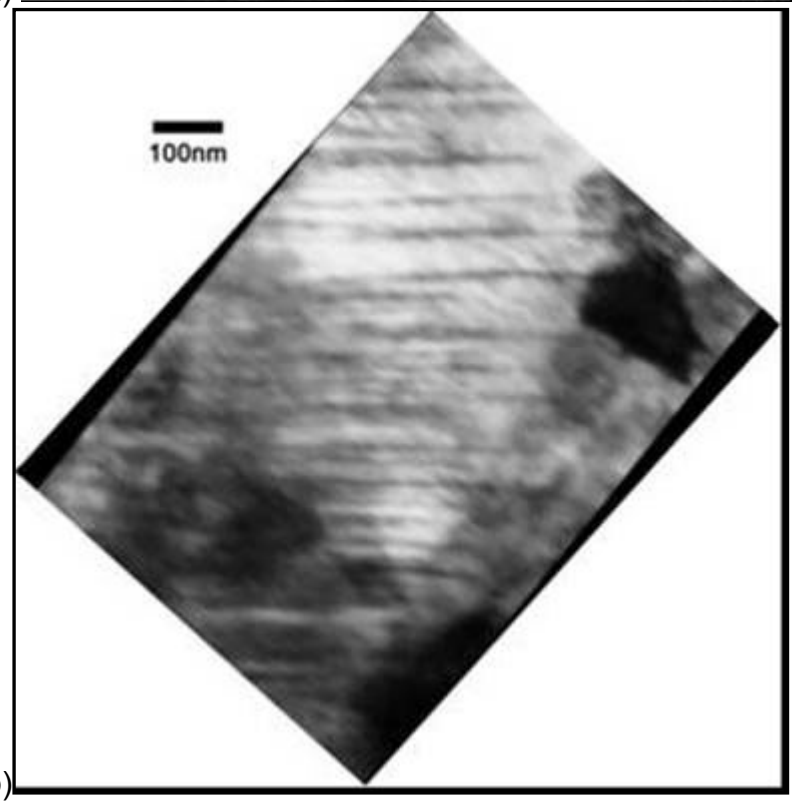

c)

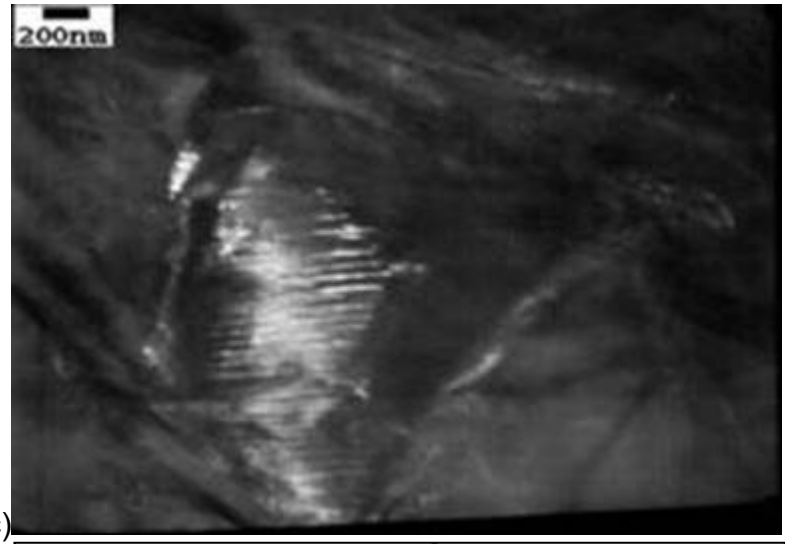

d)

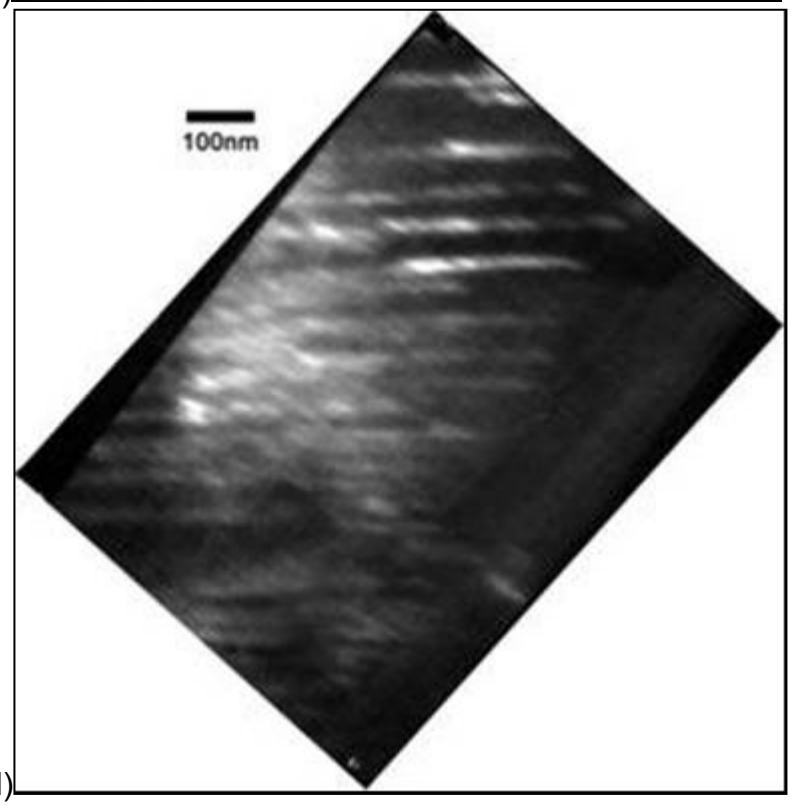

Figure 80 Sample condition S-RT. BF-TEM of particle containing twinned martensite: (a) full particle and (b) detail of area circled in (a). DF-TEM of same particle: (c) full particle and (d) detail of area circled in (a).

a)

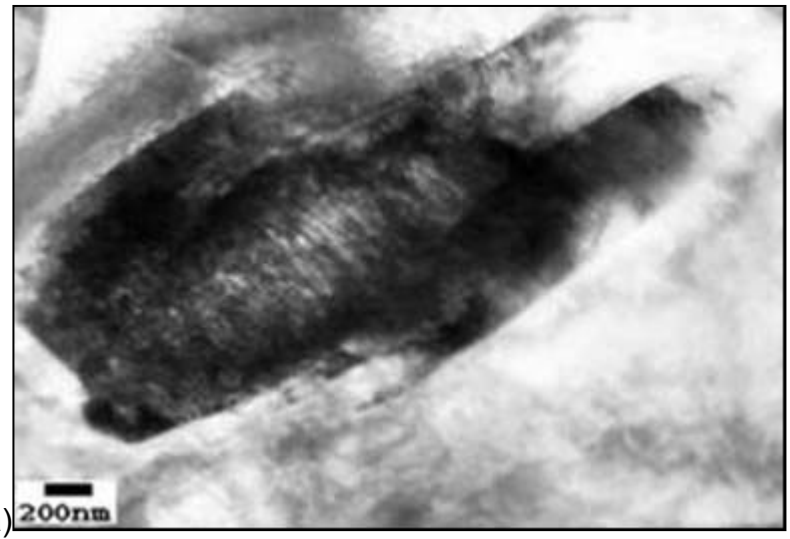

b)

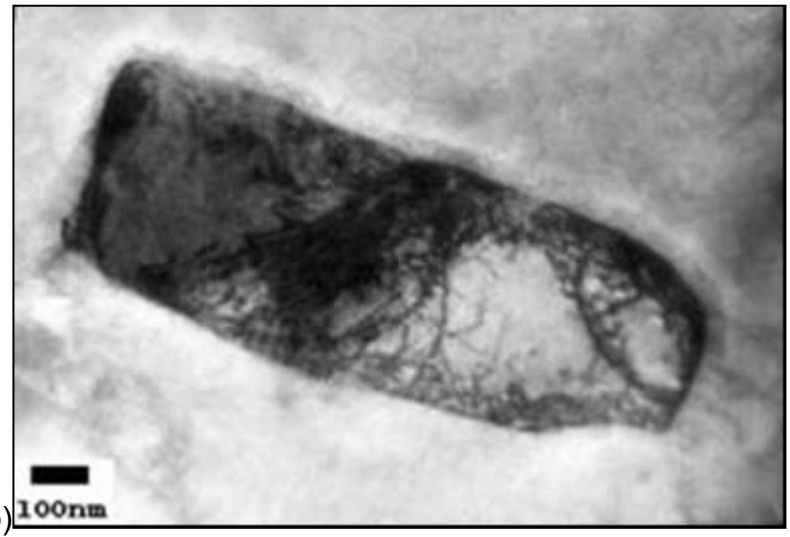

Figure 81 Sample condition S-GA. (a) BF-TEM of twinned martensite. (b) BF-TEM of retained austenite.

a)

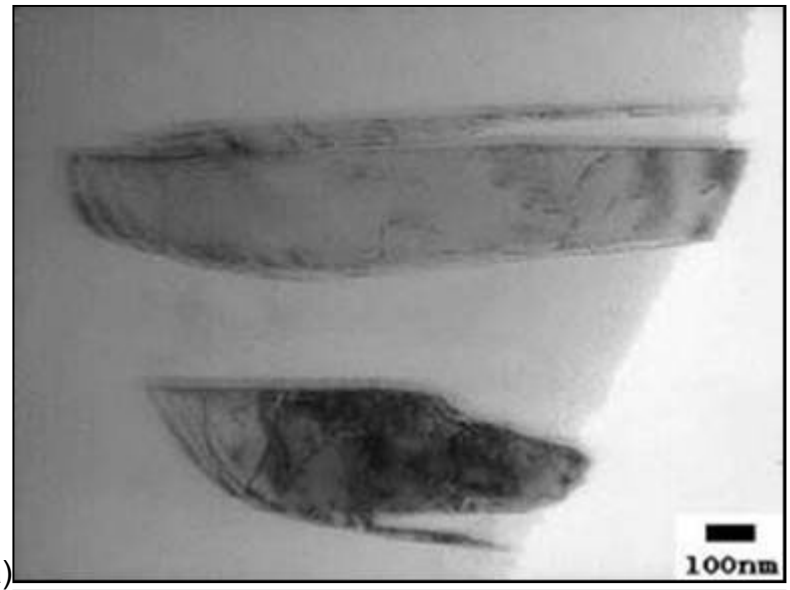

b)

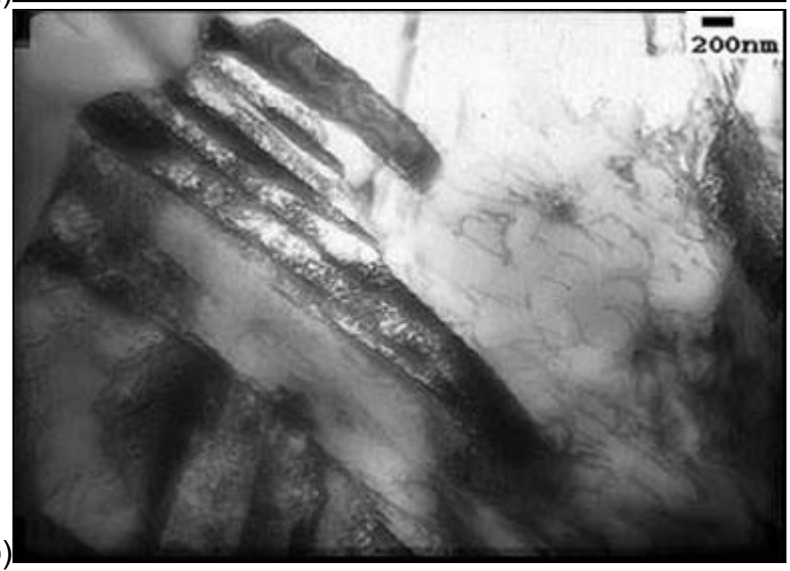

Figure 82 Sample condition S-2. (a) BF-TEM of massive retained austenite in ferrite matrix. (b) BF-TEM of bainitic ferrite containing interlath retained austenite films.

As shown in the above figures, the structures progress from a dual-phase-like martensite/ferrite mix containing a small fraction of retained austenite in condition S-RT to a mixture of ferrite and retained austenite, with a small fraction bainitic ferrite, in the S-1, S-2 and S-5 conditions.

It is important to note that extensive TEM investigation of the S-2 sample condition showed almost no bainite in the structure; most retained austenite was in the form of massive inter-ferritic islands, rather than bainitic inter-lath films; see Figure 82a above, and Figure 83.

a)

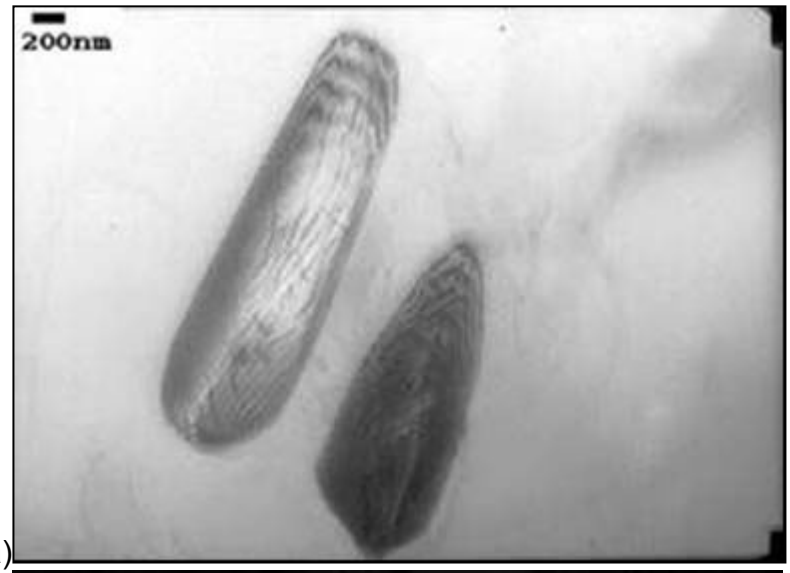

b)

Figure 83 Massive retained austenite surrounded by ferrite; (a) BF and (b) DF TEM micrographs.

These microstructural results are summarized in Table X.

Table X Microstructures (summarized)

Sample	Major constituents	Minor constituents
S-RT	Ferrite Martensite	Austenite
S-GA	Ferrite Martensite	Austenite
S-1,2,5	Ferrite Austenite	Bainite
SLOW	Ferrite Pearlite	Austenite

5.3.2 GA Parameters Study

Sample conditions 2-NONE, 2-437°C and 2-482°C had mechanical properties as shown in Figure 84 and microstructures as shown in Figure 85.

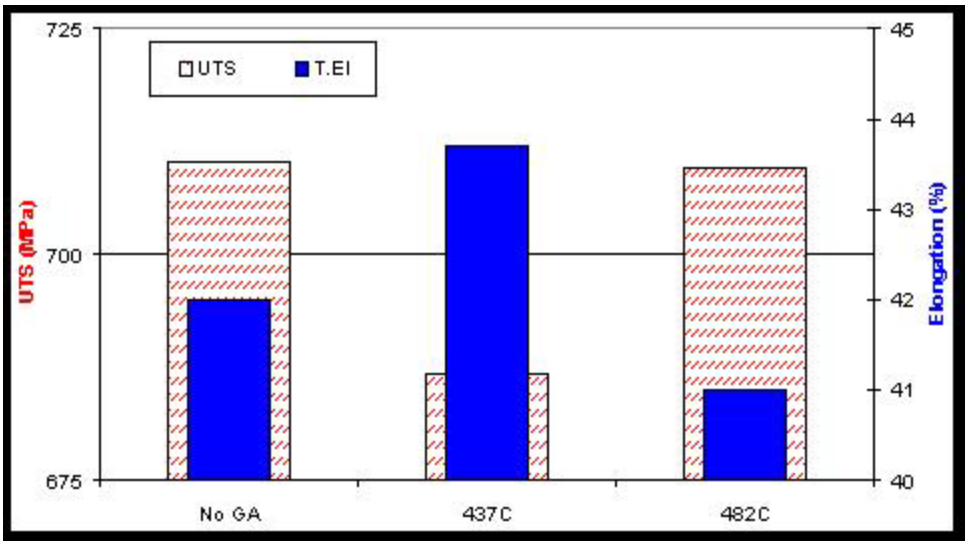

Figure 84 Mechanical properties of GA study conditions.

a)


gleeble annealing, 2mn IBT, no GA
0.010 mm

b)


gleeble anneal 2mn IBT, 437C GA
0.010 mm

c) 

Figure 85 LePera etched optical micrographs of sample conditions (a) 2-NONE; (b) 2-437°C; (c) 2-482°C.

The micrographs and mechanical properties show that the differences between the GA conditions are very minor.

5.3.3 Salt-Pot Annealing

Samples treated by annealing in salt-pots were compared to the 2-NONE condition. Mechanical properties are shown in Figure 86; micrographs of the two conditions are shown in Figure 87.

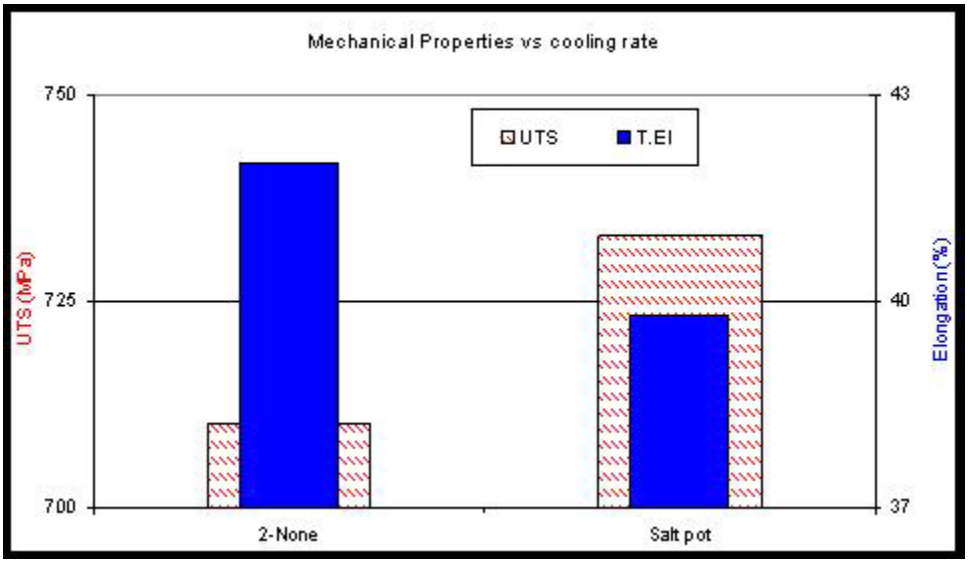

Figure 86 Mechanical properties of a sample treated at the standard cooling rate (2-NONE) vs a sample treated by salt pot.

a)

b)

Figure 87 3% nital + 10% $Na_2S_2O_5$ etched optical micrographs of (a) standard annealed and (b) salt-pot annealed samples.

Both samples consist of retained austenite in ferrite; little bainite is observed.

The mechanical properties are nearly identical; the salt-pot treated specimens have a slightly higher UTS and slightly lower elongation. Optical micrographs indicate little difference between the structures.

Like the samples treated at the standard cooling rate, the salt pot samples also showed, after extensive TEM investigation, mostly massive inter-ferritic retained austenite and only small quantities of bainitic interlath-film retained austenite; Figure 88.

a)

b)

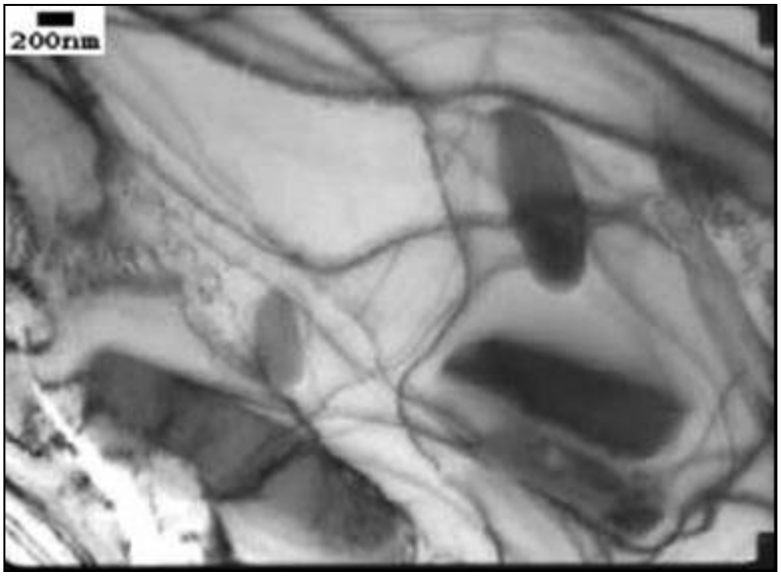

c)

d)

e)

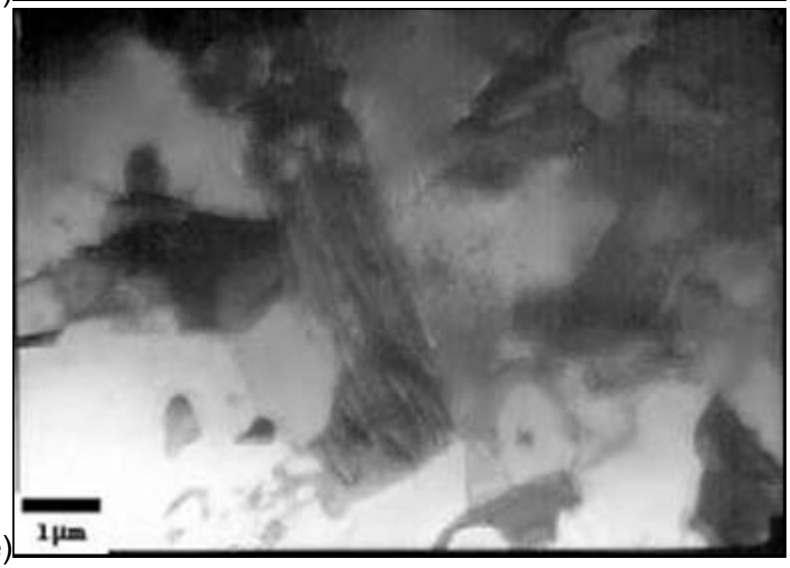

f) 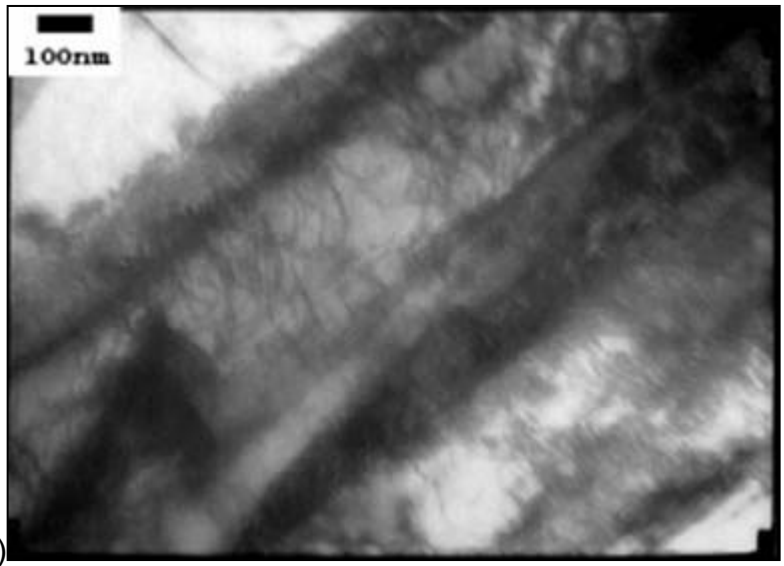

Figure 88 TEM micrographs of the salt-pot treated condition.

(a) and (b) BF-TEM of retained austenite islands in ferrite. (c) BF- and (d) and DF-TEM images of a retained austenite island in ferrite. (e) BF-TEM of a bainitic packet; (f) detail of dislocated ferrite laths in the bainitic packet.

5.3.4 Dilatometry Reactions

Samples for dilatometry were heat treated, as discussed in Section 4.4.2, by cooling from 843°C to 416°C at constant cooling rates <dT/dt> from 0.4°C/sec to 200°C/sec. Reaction temperatures, as determined by dilatometry and confirmed by metallographic examination, are presented in Table XI.

Table XI Reaction temperatures from dilatometry.

Dilatometry Summary			
<dT/dt> (°C/sec)	Pearlite Start (°C)	Epitaxial Ferrite Start (°C)	Bainite Start (°C)
200	-	-	-
100	-	-	480
40	-	690	510
4	-	740	-
0.4	610	810	-

The reactions taking place during the isothermal bainitic hold were also monitored dilatometrically; these IBT reactions are presented in Figure 89.

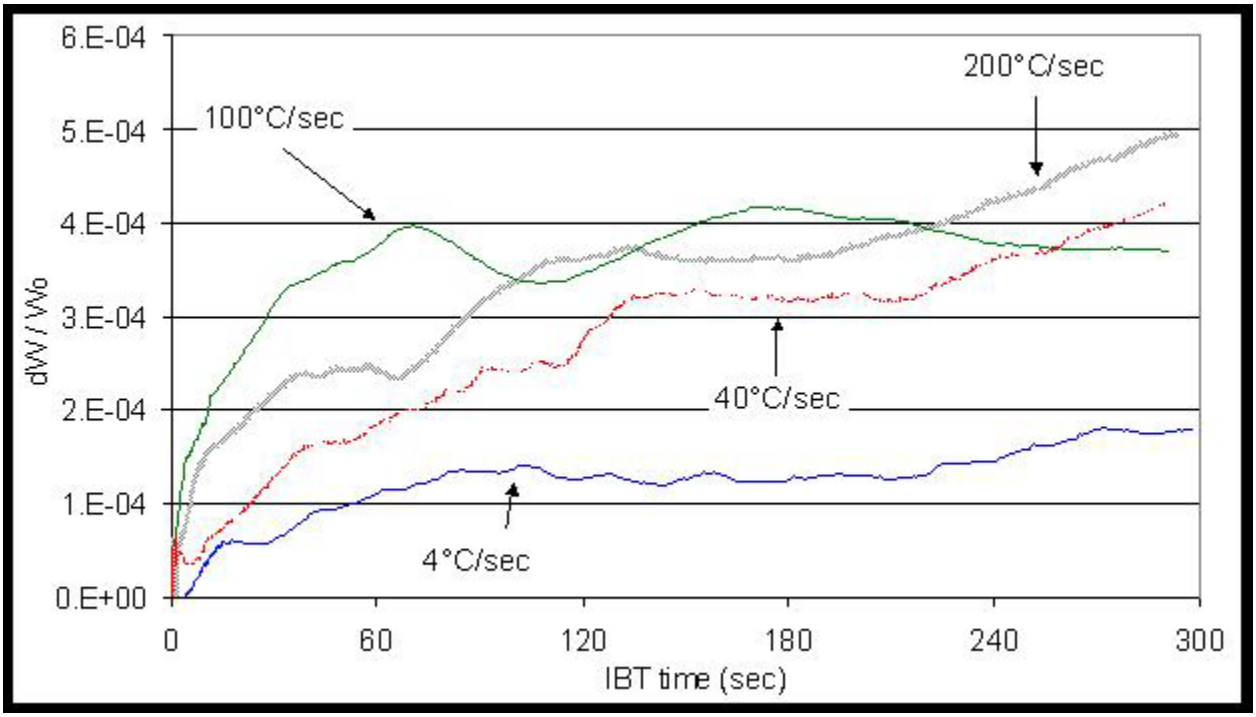

Figure 89 IBT dilatometry.

Note in Figure 89 that the reactions reach completion in ~60-90 seconds; that is, the curves become mostly steady after that time. Also note that the high-cooling-rate curves show IBT's of greater magnitude than the curves at lower cooling rates.

From the reactions listed in Table XI and the assumption that, after 200°C/sec cooling the bainitic reaction start immediately upon the beginning of the isothermal stage, a CCT curve for this intercritically annealed steel can be constructed, Figure 90.

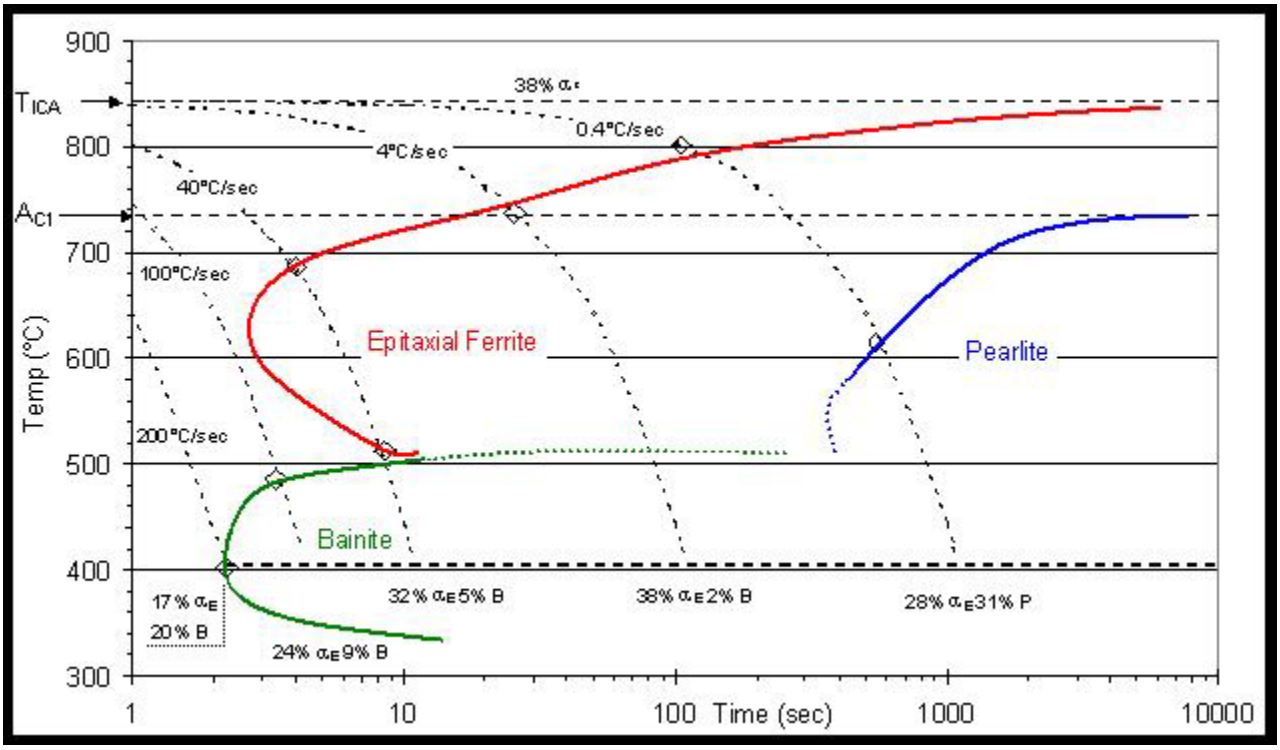

Figure 90 CCT curve constructed from dilatometry data. α_I denotes intercritical ferrite, α_E epitaxial ferrite, P pearlite, and B bainite.

Dilatometry at a heating rate of 10°C/sec to 1200°C gave reaction temperatures of A_{C1}=760°C and A_{C3}=870°C; this A_{C1} value is indicated in Figure 90. The T_{ICA}=843°C is also shown. It is assumed that the pearlite C-curve will asymptotically approach A_{C1} and the epitaxial ferrite curve T_{ICA}.

5.3.5 Dilatometry Microstructures

Extensive optical and TEM characterization of the dilatometer specimens showed approximately constant volume fractions of retained austenite in the 4°C/sec to 200°C/sec specimens, an increasing volume fraction of bainite, and a decreasing volume fraction of ferrite. Optical microstructures are shown in Figure 91; volume fractions were determined by point-counts on multiple fields for each condition.

a)

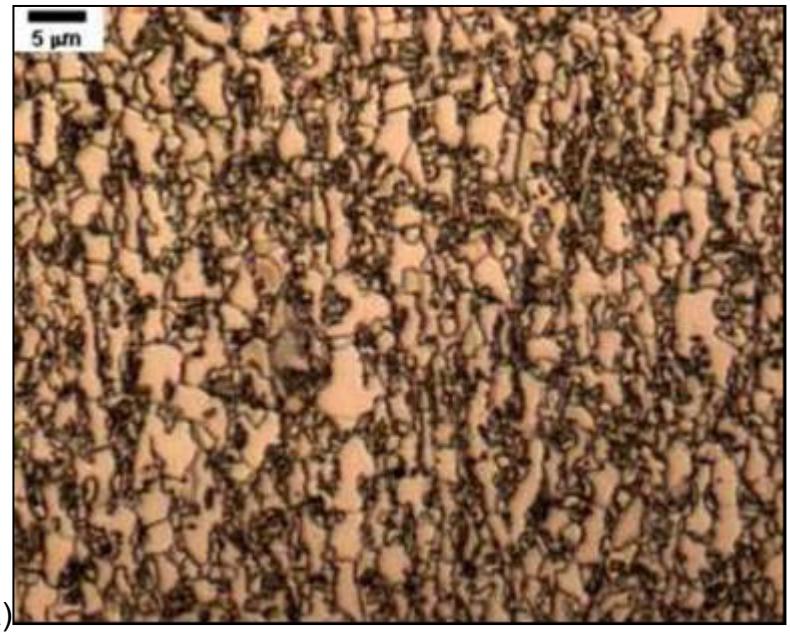

b)

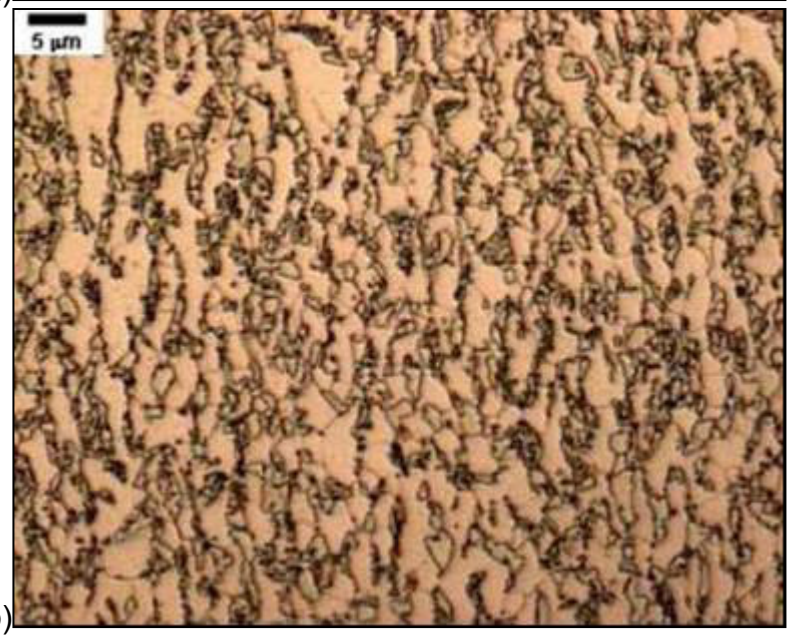

c)

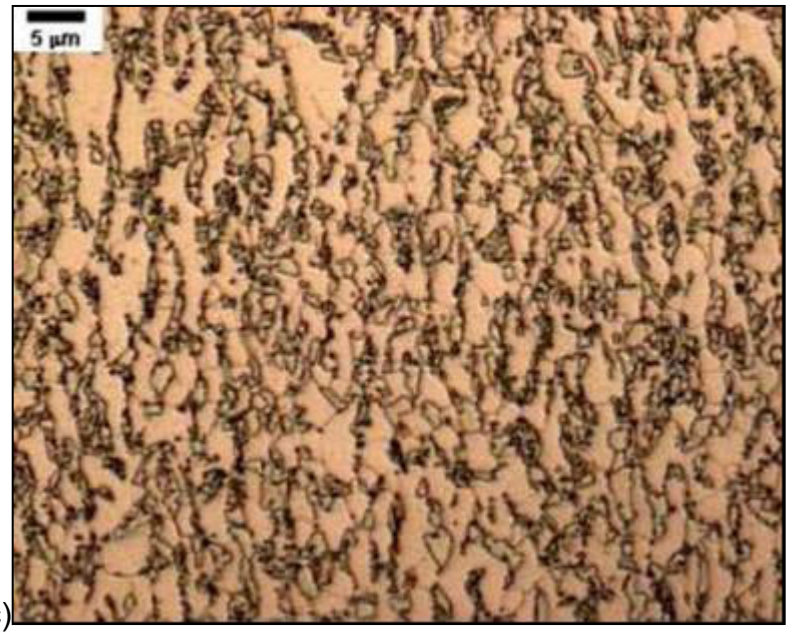

d)

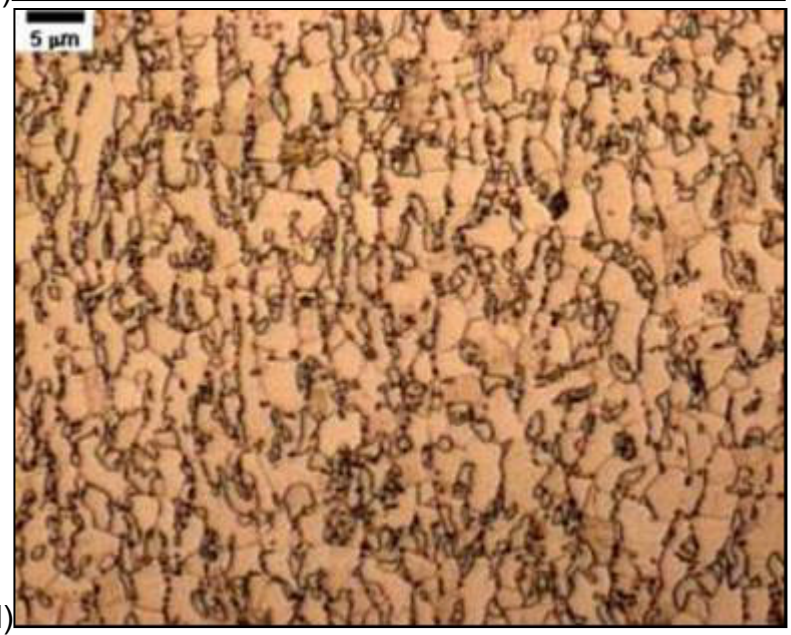

Figure 91 3% nital + 10% $Na_2S_2O_5$ etched dilatometer specimens.

All were intercritically annealed 2 minutes at 843°C and isothermally transformed 5 minutes at 416°C. (a) 200°C/sec; 20% bainite. (b) 100°C/sec; 9% bainite. (c) 40°C/sec; 5% bainite. (d) 4°C/sec; 2% bainite. Dark phase is bainite; white/off-white phase is retained austenite; matrix is ferrite.

It is important to note that the ferrite grains in intercritically annealed steel consist of both intercritical and epitaxial components. Because the epitaxial ferrite reaction simply results in the growth of existing ferrite, there are no boundaries between the ferrite

present during the anneal and the ferrite formed during the cool. Thus, a given ferrite grain will likely have been present in the same crystallographic orientation, but smaller, during the intercritical anneal. Thus, in a micrograph, there exists only a single "ferrite" population.

The results of the quantitative metallography are summarized in Figure 92a for samples of 4°C/sec to 200°C/sec after annealing at 843°C, and in Figure 92b for samples cooled at 4 or 200°C/sec after annealing at 800°C. The 843°C anneal 0.4°C/sec cooling condition exhibited approximately 66vol% ferrite, 31% pearlite and 3% retained austenite, and is not pictured.

a)

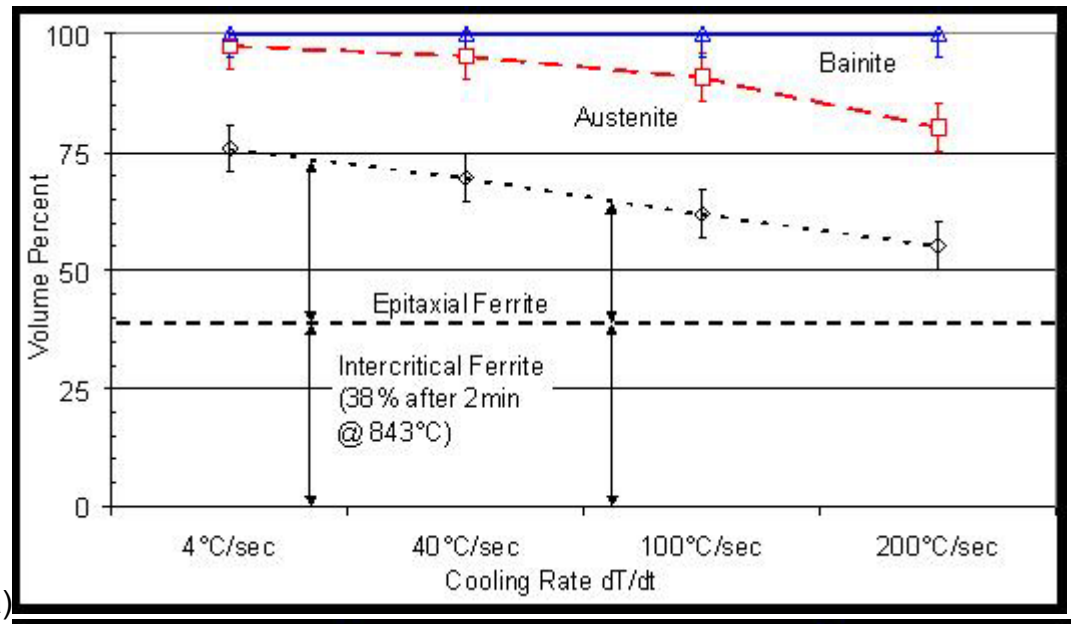

b)

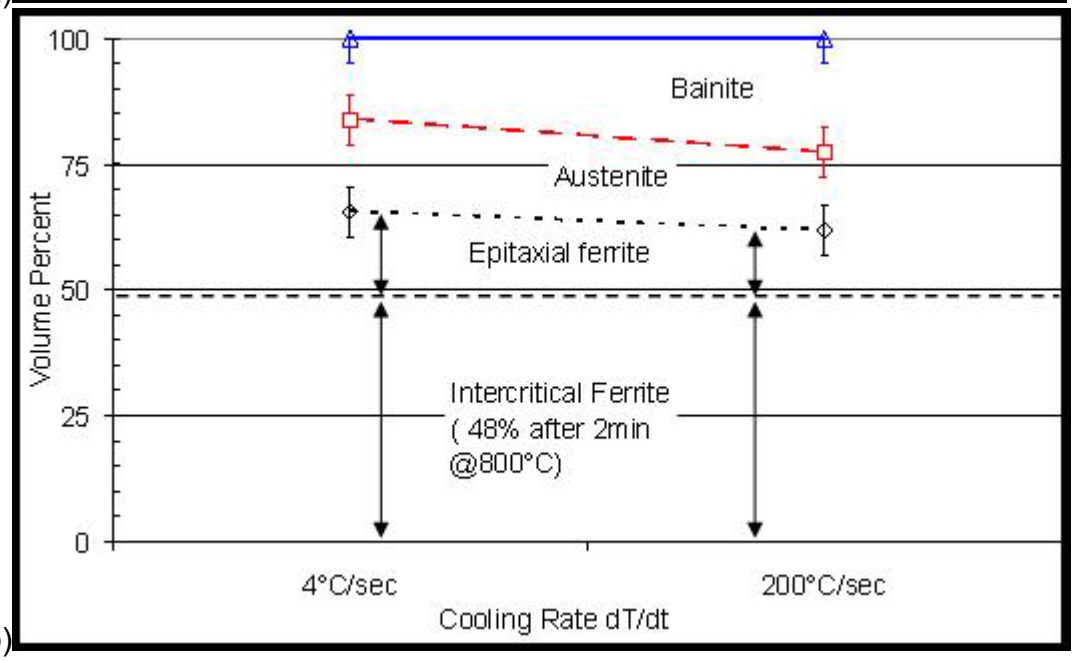

Figure 92 Variation of microstructure with cooling rate (a) after 2min@843°C and (b) after 2min@800°C.

TEM examination showed that all samples from 4°C/sec to 200°C/sec contained both massive and bainitic retained austenite; Figure 93.

a)

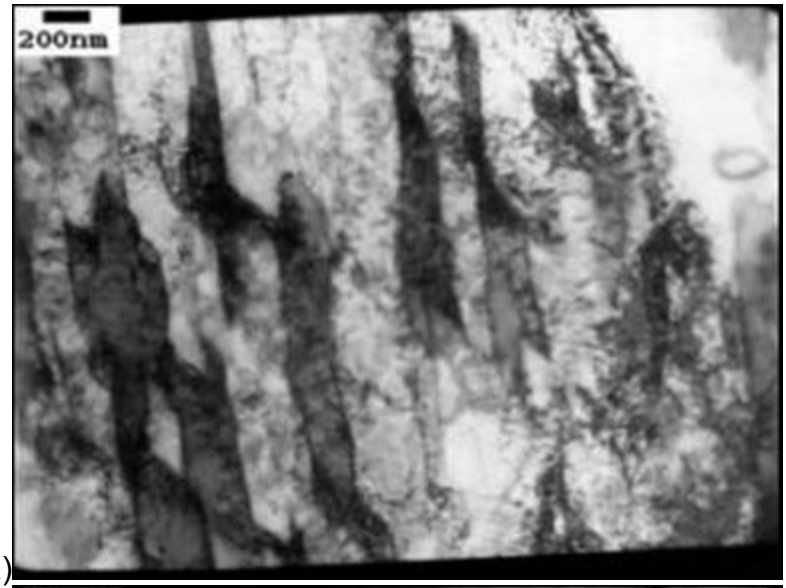

b)

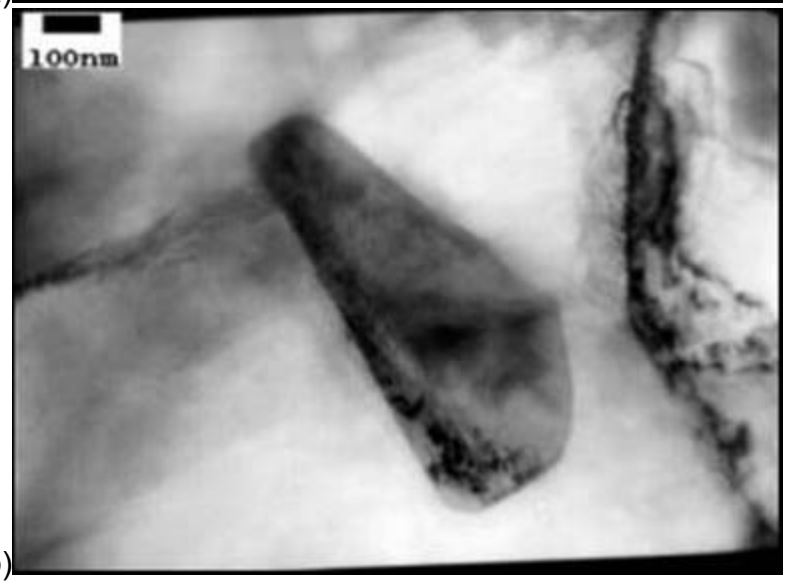

Figure 93 BF-TEM micrographs from dilatometer specimens.

(a) Interlath retained austenite (dark phase) surrounded by bainitic ferrite laths (light phase); 100°C/sec sample. (b) Massive retained austenite surrounded by ferrite; 40°C/sec sample.

In order to verify that th4e assumed etching-behavior of the optical micrographs was correct, SEM and TEM micrographs were compared to the optical microstructures in 200°C/sec samples, Figure 94.

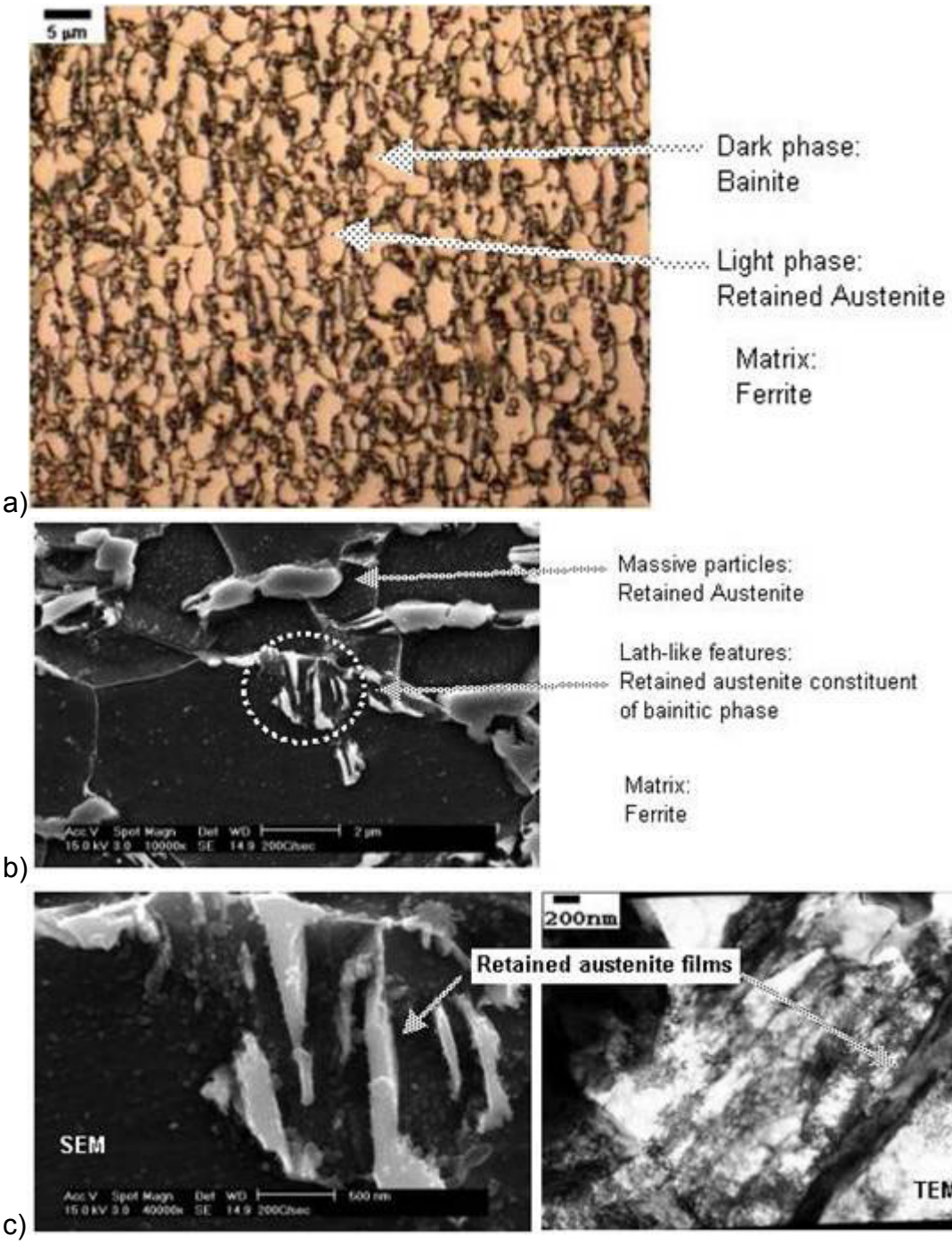

Figure 94 Verification of phase-contrast in the $Na_2S_2O_5$ etch.

(a) Optical micrograph, 3% nital + 10% $Na_2S_2O_5$ etch; phases labeled. (b) SEM micrograph, 3% nital etched; bainite and retained austenite marked. (c) SEM and BF-TEM micrographs, showing that the lathlike phase in the SEM image is retained austenite films of 150-200nm width, consistent with TEM observation.

Figure 94 shows that the contrast (bainite, ferrite, austenite) from the optical etch assumed for the quantitative metallographic counts is an accurate description of the phases present.

Ferrite grain sizes from dilatometer specimens are summarized in Table XII and Figure 95.

Table XII Average ferrite grain sizes <d>$\pm\sigma_d$, in microns, for dilatometer conditions <dT/dt>. Sample size for each condition = 100 grains.

<dT/dt>	<d>	σ
200°C/sec	3.95	1.14
100°C/sec	3.94	1.11
40°C/sec	3.93	1.06
4°C/sec	3.51	0.94

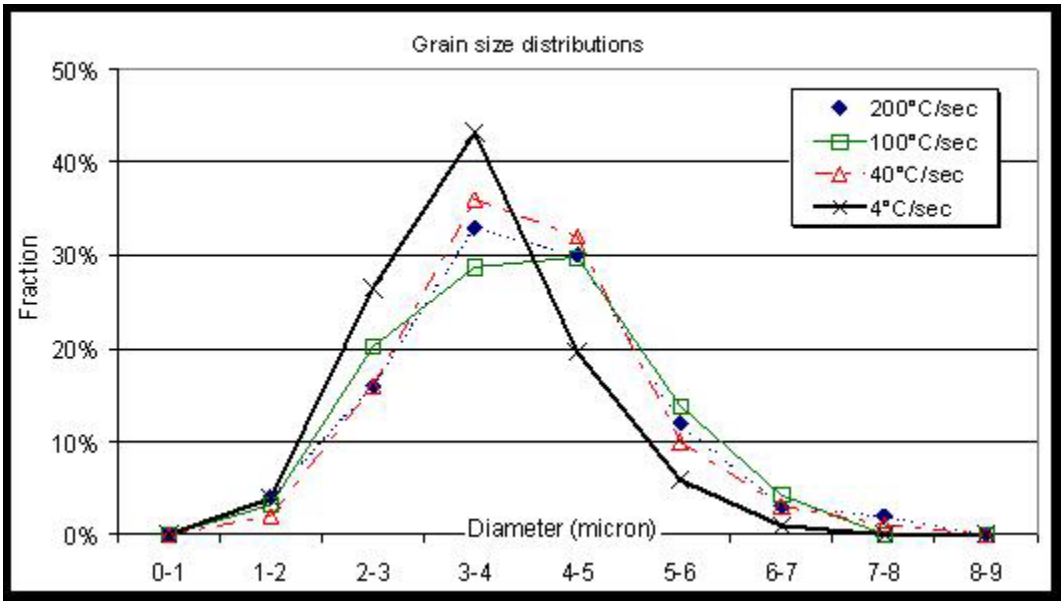

Figure 95 Ferrite grain size distributions.

5.3.6 Microhardness Data

Because of the small size of dilatometer samples -- 50x13mm, with a uniform-temperature area of only ~5x13mm -- standard tensile tests could not be performed. As such, microhardness values were obtained as a means of comparison of mechanical properties.

Firstly, in order to convert VHN values into tensile strength values, a VHN-to-UTS conversion table was found (Davis[189]). A second-order polynomial regression was fit to the data in the table, where UTS is in MPa:

$$UTS = 0.0189(VHN)^2 - 4.5466(VHN) + 805.72 \quad (5\text{-}1)$$

This regression had an R-value of 0.9975.

In order to test this conversion factor, samples from the Salt Pot and S-2 conditions (above) were subjected to microhardness tests. Microhardness values of 206±6.5 and 193±10.6 VHN, respectively, were measured; these translate, via equation 5-1, to 673±21 and 633±29 MPa. Actual tensile test data indicated tensile strengths of 733±4 and 687±4 MPa; see Figure 96.

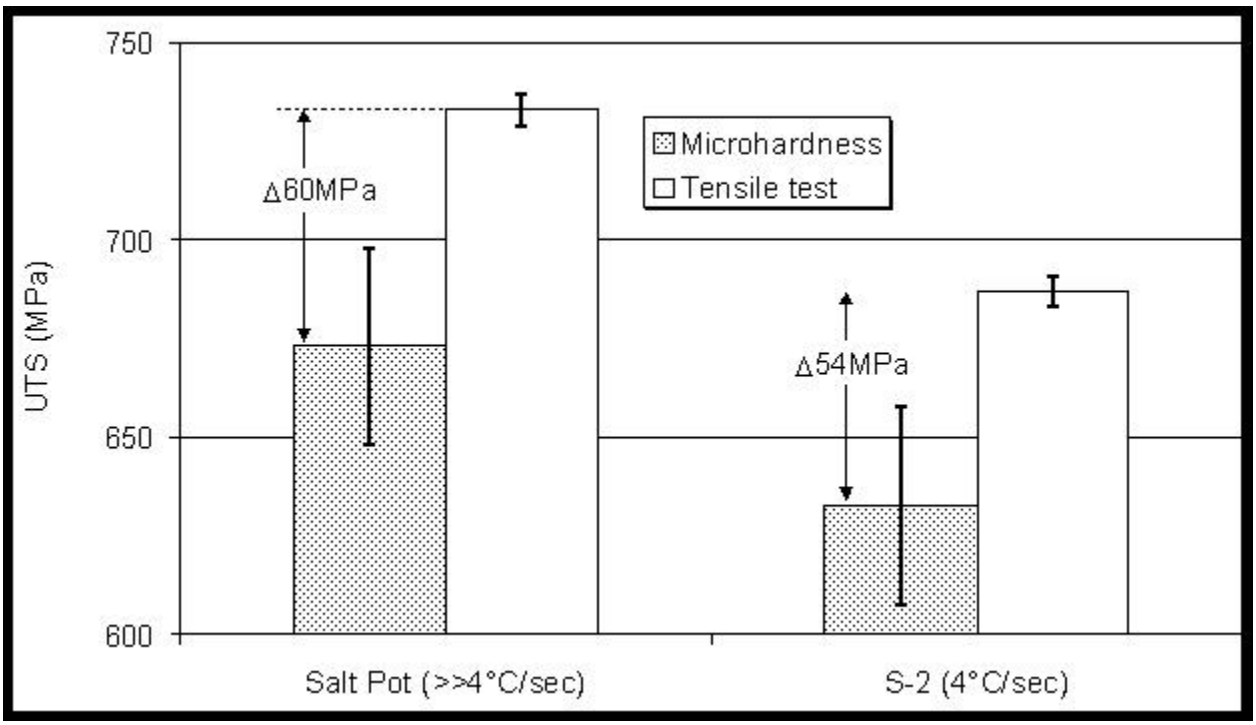

Figure 96 Comparison of tensile test derived and microhardness derived UTS values.

This figure indicates an average underestimate of Δ=-57MPa via microhardness measurements and conversion.

Samples of 4°C/sec to 200°C/sec dilatometry runs were subjected to microhardness measurements; results of estimated tensile strength (both with and without the +57MPa bias) are presented in Figure 97.

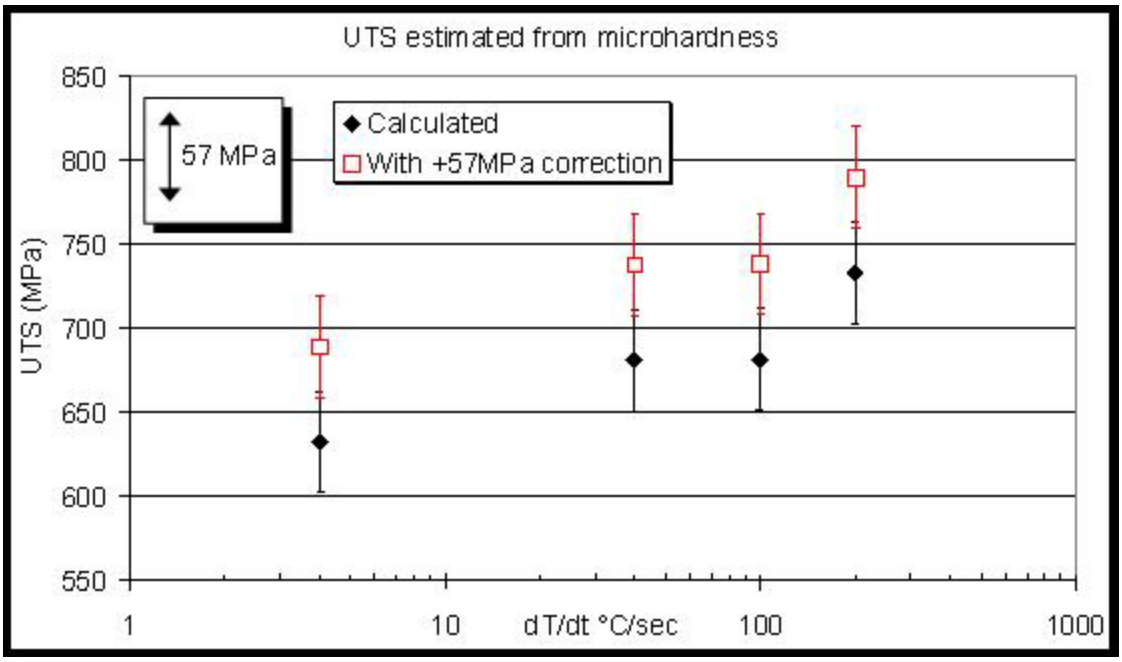

Figure 97 Tensile strengths derived from microhardness values for 843°C dilatometry specimens.

Values of estimated tensile strength (with the +57MPa bias) for samples annealed at both 800 and 843°C are given in Figure 98.

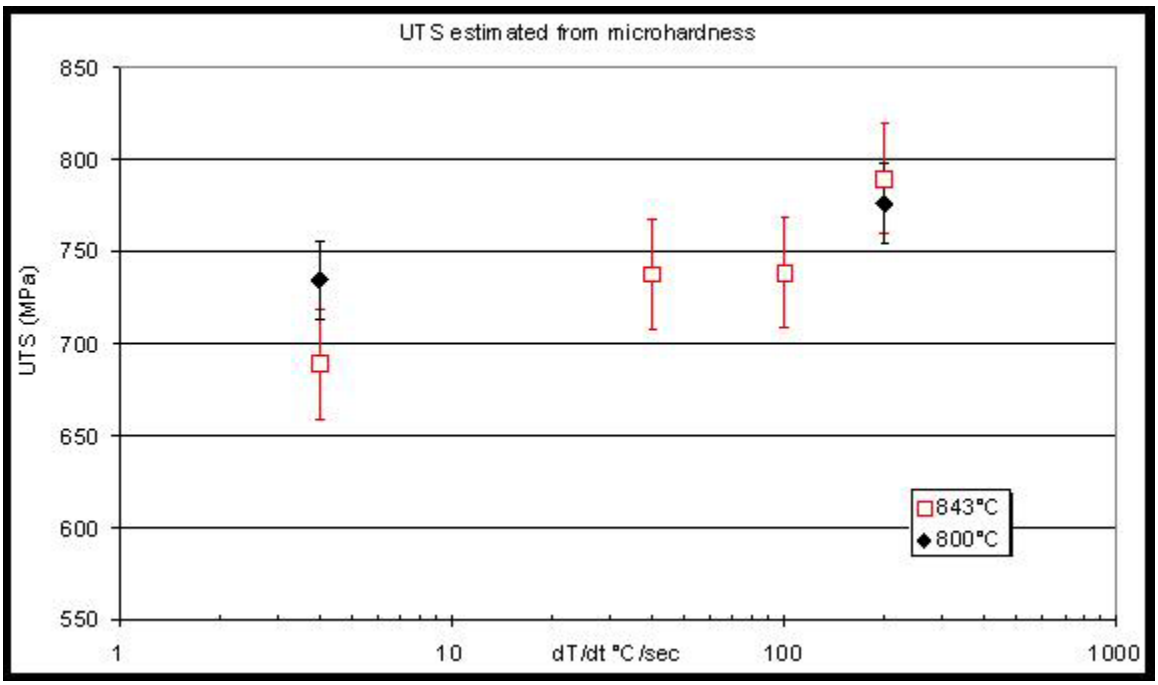

Figure 98 Estimated tensile strength values for both 800 and 843°C annealing conditions.

Typical microhardness indentations are given in Figure 99.

a)

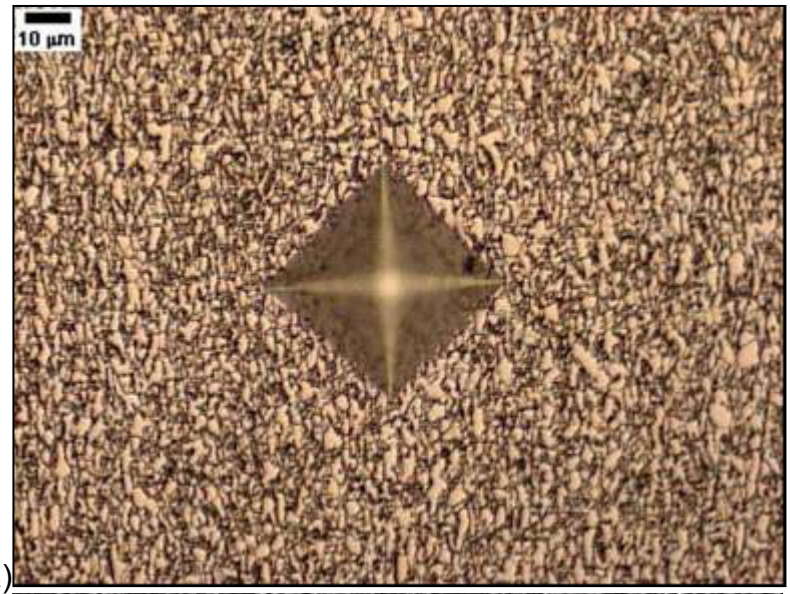

b)

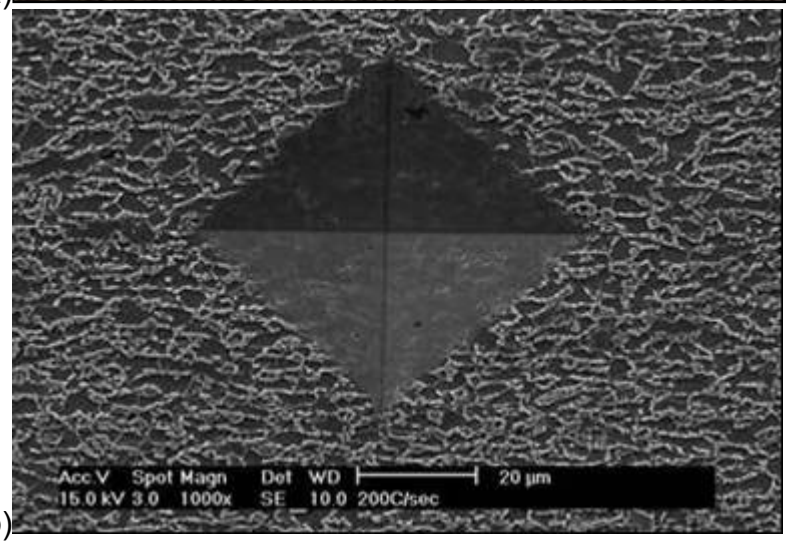

Figure 99 3% nital + 10% $Na_2S_2O_5$ etched (a) optical and (b) SEM micrographs from 200°C/sec dilatometer specimen.

Figure 99 clearly indicates that the 500-gram-load microhardness indentations average over many ferrite grains/austenite particles/bainite packets, and thus should be representative of the agglomerate mechanical properties.

6.0 DISCUSSION

6.1 Experimental Technique Development Discussion

6.1.1 XRD Discussion

Although the XRD techniques for retained austenite quantification have been validated for steels of random or near-random crystallographic texture[190], the results presented above (Table VI, Table VII, Table VIII) are clearly not correct. Standard deviations of the same order of the measured values -- for the ND sample, greater than the measured value -- indicate unacceptable experimental error.

For XRD measurements to be valid, the I/R ratios within a phase must be approximately equal. Here, ferrite peaks vary by as much as 5 times, and austenite values by as much as 16 times.

Interestingly, however, most published TRIP papers that studied the variations of volume fraction with processing, by means of XRD quantification, found reasonable trends in their data. Is it possible that, by coincidence, the measured values are actually accurate, despite the large standard deviations? If there were no variant selection in

the decomposition of retained austenite with strain, it would be expected that straining the TRIP steel would result in decreasing all the austenite I/R values at an equal rate, thus yielding the expected trend, even if the absolute number is not accurate.

The exact means by which XRD measurements relate to the true value of f_V is not known, but these results indicate that, at least in the heavily textured Si-CAL material, XRD is not the quantification technique of choice.

6.1.2 SEM Technique Discussion

Examination of the as-annealed materials indicates that they lack measurable martensite fractions in their structures -- no rough-surfaced islands are observed. The Si-CAL sample that had been pulled to failure did show large numbers of rough-surfaced islands, indicating that it contained an appreciable fraction of martensite. This shows that validity of the etching technique.

In the failed samples, it is also interesting to note that the larger M-A particles are more likely to be martensite, whereas the small particles seem to stay austenitic. This is consistent with the particle-size effects discussed in Section 2.4.4.

Tempering and nital etching is the only viable method (short of TEM) to differentiate austenite from martensite in TRIP steels.

6.1.3 TEM Technique Discussion

The micrographs presented in Section 5.1.3 indicate the power of the TEM for the complete characterization of TRIP-type steels.

Figure 64 shows a plate-martensite island in a Si-CGL TRIP steel pulled 20% in tension. This indicates that, indeed, martensite does form during the tensile test, and that the martensite formed is the high-carbon twinned type. This is expected because, despite the 0.1%C bulk content, the austenite in TRIP steels is highly enriched during the intercritical anneal and the IBT.

As noted in the microscopy sections (Section 5.1), almost no bainite is observed in the industrially annealed or industry-simulator annealed materials. Figure 66 & Figure 67 show retained austenite particles that are not associated with bainite.

Also, Figure 67 shows a medium sized (~1-2 micron) austenite particle that has not tripped despite 20% tensile strain. The dense dislocation structure within the particle indicates that, despite obvious microstrain, the particle is still stable. This indicates that a combination of the chemical enrichment and small particle effects (discussed in Section 2.4.4) allow the particle to remain very stable.

The use of TEM is necessary to examine the substructure of TRIP steels, and to differentiate clearly between the sub-types of martensite (lath or plate) and bainite

(upper or lower bainite, or the bainitic ferrite/retained austenite composite common in Si- or Al-bearing steels). It is also necessary to identify phases unequivocally: although etching procedures can give high-confidence results, only diffraction techniques allow the quantitative identification of a phase. Further, only TEM can show deformation structures such as dislocation cells, deformation twins, etc., that may be present in the different phases (especially retained austenite).

6.1.4 Magnetometry Discussion

For the Si-CAL steel, magnetometry showed a retained austenite content of 8.7%. XRD quoted values varying from 2 to 13 percent, the best estimate having been 5.5±6.4vol%. Magnetometry will not be affected by particle size or texture, and should thus show the most accurate value for retained austenite content.

6.2 Mechanical Properties Discussion

In the variable-temperature-tensile-testing study, ultimate tensile strength increased rapidly with decreasing temperature, and ductility fell dramatically to either side of room temperature. Room temperature runs showed an initially high n value that stayed steady, whereas low temperature n-curves spiked very high at low strain and dropped off rapidly, and high-temperature n-curves showed low and steady n values.

In short, formability is vastly superior at room temperature than at temperatures even slightly different from room temperature.

At temperatures near M_S (i.e., lower temperatures), the driving force for the transformation of the austenite to martensite will be high, and the austenite will likely trip at low strains, which will leave no austenite available at large strains, resulting in a loss of formability. At high temperatures, the driving force will be low, and much of the austenite will remain untransformed even beyond ultimate strain. As un-transformable austenite does not benefit ductility, this over-stabilization of the austenite at high temperatures results in a loss of formability. Thus, a compromise value of temperature will lead to the best formability. Recent crashworthiness studies found that adiabatic heating caused over-stabilization of austenite and a loss of ductility[191].

The huge increase of UTS with decreasing temperature is less readily explained. Although standard mechanical metallurgy predicts increasing strength with lower temperature, the loss of ~70MPa with only a 100°C change in temperature near room temperature is rather more than would be expected. This likely can be related to the n-curves: the high n-values at low strains in the low-temperature samples resemble the work hardening of dual phase steels. In dual-phase steels, the retained austenite typically transforms within a few percent strain, leading to a high initial n value. Likely, in these TRIP steels at low temperature, large amounts of austenite transform quickly, leading to the high initial n value. This quickly leads to the formation of large quantities

of martensite. The martensite is a very hard phase and will result in composite strengthening of the material, leading to the high UTS values.

The similar loss of UTS at high temperature probably results from the less complete austenite-to-martensite transformation and concomitant loss of martensite volume fraction.

Figure 100 shows schematically typical n curves for dual-phase, ferrite-pearlite, and TRIP steels. These can be seen to resemble the low, high, and room-temperature curves, respectively, found in this study.

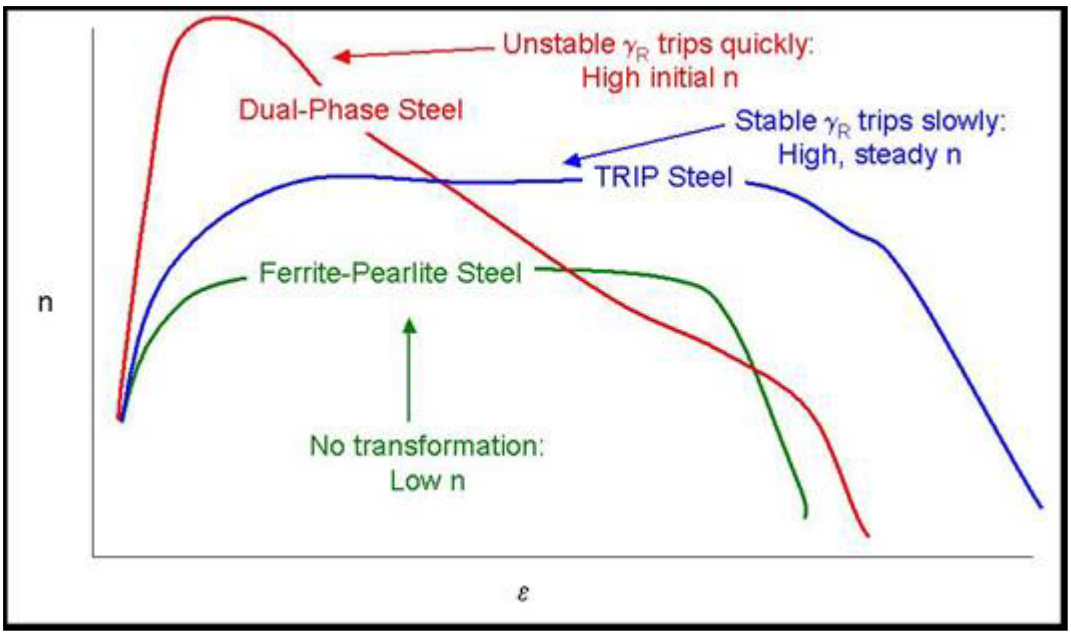

Figure 100 Schematic n-vs-ε curves for DP, TRIP and ferrite-pearlite steel

Although there is significant loss of formability at temperatures away from room temperature, even those "deteriorated" mechanical properties are superior to those of

other classes of steel, such as dual-phase. TRIP steels have formability ranging from "excellent" at room temperature to merely "very good" at varied temperatures.

6.3 Annealing Studies Discussion

6.3.1 IBT Parameters Study

As shown in Table IX and Figure 77, tensile strength decreases with increasing length of IBT time; total elongation, yield stress and yield-point elongation all increase.

This behavior can be justified in terms of dual-phase theory. Dual-phase steels (see Section 2.7) typically have very low yield strengths due to the large number of unpinned dislocations associated with the dislocations surrounding the martensite particles. However, dual-phase steels have very high tensile strengths because of composite-strengthening effects associated with the volume fraction of very hard martensite in their structure.

Only sample conditions S-RT and S-GA contained martensite; these conditions had the lowest yield strength and highest tensile strength, in comparison to the isothermally transformed conditions. This is consistent with S-RT and S-GA resembling dual-phase steels more than TRIP steels. As S-RT showed no yield point elongation, S-GA showed only incipient (<0.1%) yield-point elongation, and the S-1 through S-5 conditions

showed pronounced YPE (≥0.3%), and dual-phase steels typically show no YPE, it seems apparent that the S-GA condition is on the transition point between DP and TRIP behavior. S-GA's strength-ductility balance UTSxT.EL of 28,574 MPa-% places it nearly in the same class as the TRIP-like conditions (S-1 through S-5) at ~30,000 MPa-%.

Although the S-RT and S-GA conditions show less total elongation than the S-1, S-2 and S-5 conditions, they have excellent total elongations in comparison to commercial DP steels; this is likely due to enhanced stability of their small retained-austenite fraction, in comparison to the poor stability of retained austenite in other DP steels.

As is well-known, martensite of <~0.6%C will take a lath-like morphology. The TEM-examined martensite morphologies in the S-RT and S-GA conditions show a plate-type twinned martensite. This indicates that during the 4°C/sec cooling stage, the epitaxial ferrite (and, to a lesser extent, possibly bainite) reactions enrich the originally 0.25-0.35%C intercritical austenite (estimated from a mass-balance assuming 0.01%C in the 38vol% ferrite and the remaining carbon segregated to the 62vol% austenite) to at least 0.6-0.8%C (or more), resulting in the twinned martensite structure.

For the S-1 to S-5 samples, the mechanical properties are quite steady. This implies that the reactions are mostly complete by the first minute; this is consistent with the IBT dilatometry shown in Figure 89, which indicates the reactions level off after ~60-90 seconds. Thus, for this material and annealing conditions, TRIP properties are achieved rapidly and persist.

In S-2 condition, XRD measurements (Table XIII) indicated a carbon content of 1.50±0.13wt%, which is a massive increase compared to the initial intercritical carbon content ~0.3wt%.

Table XIII XRD measurements of austenite carbon content.

Peak $(hkl)_\gamma$	N $=h^2+k^2+l^2$	2θ °	a_γ nm	C_γ wt%
$(111)_\gamma$	3	43.362	0.3612	1.41
$(200)_\gamma$	4	50.296	0.3626	1.70
$(220)_\gamma$	8	74.227	0.3612	1.39
$(311)_\gamma$	11	90.004	0.3614	1.44
$(222)_\gamma$	12	94.997	0.3620	1.58
$<a_\gamma>=$	0.3617	±	0.00062	nm
$<C_\gamma>=$	1.50	±	0.13	wt%

The SLOW sample condition (pearlite-ferrite-retained austenite) shows poor mechanical properties in comparison to the other conditions. This is due, quite simply, to the presence of pearlite. Current TRIP steel theory requires locking as much carbon as possible into the retained austenite, stabilizing the austenite against strain. SLOW shows inferior mechanical properties to the other samples because most of the carbon is locked up in the form of pearlite, rather than in solid solution in austenite, and thus the carbon is not contributing to mechanical stability. However, 29.2% total elongation is rather good for a 0.20% carbon pearlitic steel; this is probably explained by the small volume fraction of retained austenite. Smith[192] quotes values of ~450MPa at 35-36% elongation for normalized 1020 steel; in other words, a strength-ductility balance of

~16,000 MPa-%. The SLOW condition of this study showed 18,892 MPa-%: a significant increase.

Metallographic analysis shows that the retained austenite in SLOW is thermodynamically unstable and transforming to ferrite+carbides. Figure 78d shows a former retained austenite particle that decomposed into a carbide colony. Figure 78f shows a retained austenite particle in the process of this transformation. (Strictly speaking, all retained austenite is thermodynamically unstable, but only in SLOW condition does Si and Al diffusion have the kinetic opportunity to allow the formation of carbides.)

Even with this decomposition, the majority of the carbide is in the form of massive (i.e., eutectoid) pearlite that was never in the form of small retained austenite particles, but rather transformed directly from intercritical austenite. This is consistent with the presence of a pearlite curve cut by the 0.4°C/sec cooling curve on the CCT diagram, Figure 90.

6.3.2 GA Parameters Study Discussion

As was noted above for the S-1, S-2 and S-5 samples, the TRIP properties are achieved rapidly, and persist. Thus, it should not come as a surprise that variations in GA parameters should have little effect on final mechanical properties, as the GA step followed the two-minute hold. Thus, the properties/microstructure should be locked-in by the time the two-minute hold is complete, so that the short GA step will have only

minimal effects on the stabilized structure. From this data, it is apparent that 37 seconds at 400-500°C is not long enough to decompose the retained austenite. Similarly, the non-GA condition (2-NONE) shows effectively the same mechanical properties as the GA conditions, simply because the structure is locked in by the time the 2-minute IBT is complete.

6.3.3 Salt-Pot Annealing Discussion

The salt-pot experiments were performed in order to test the effect of higher-than 4°C/sec cooling rates on the structure. As metallographic examination indicated little or no bainite in the 4°C/sec structures, it was hypothesized that the higher cooling rates associated with a "salt quench" type annealing might force a bainitic reaction. Schematic cooling curves for the slow-cooling-rate processing used in this study and the higher cooling rate processing paths associated with the original TRIP literature -- and the high bainite fractions reported therein -- are shown in Figure 101.

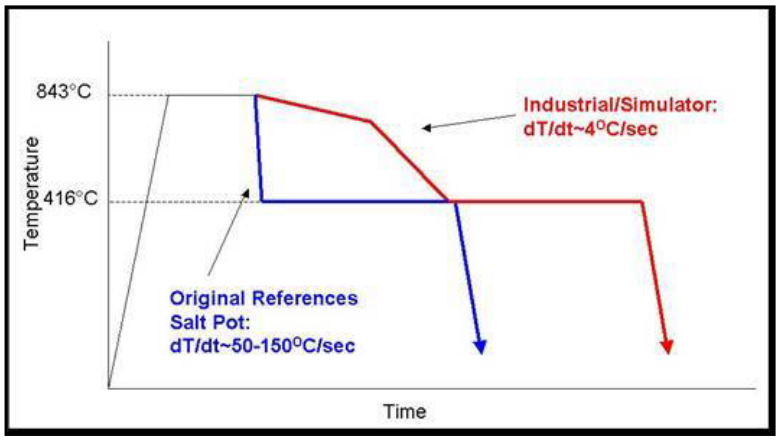

Figure 101 Schematic salt-pot vs simulator cooling curves.

It was hypothesized that the CCT diagram would be in the general form shown in Figure 102.

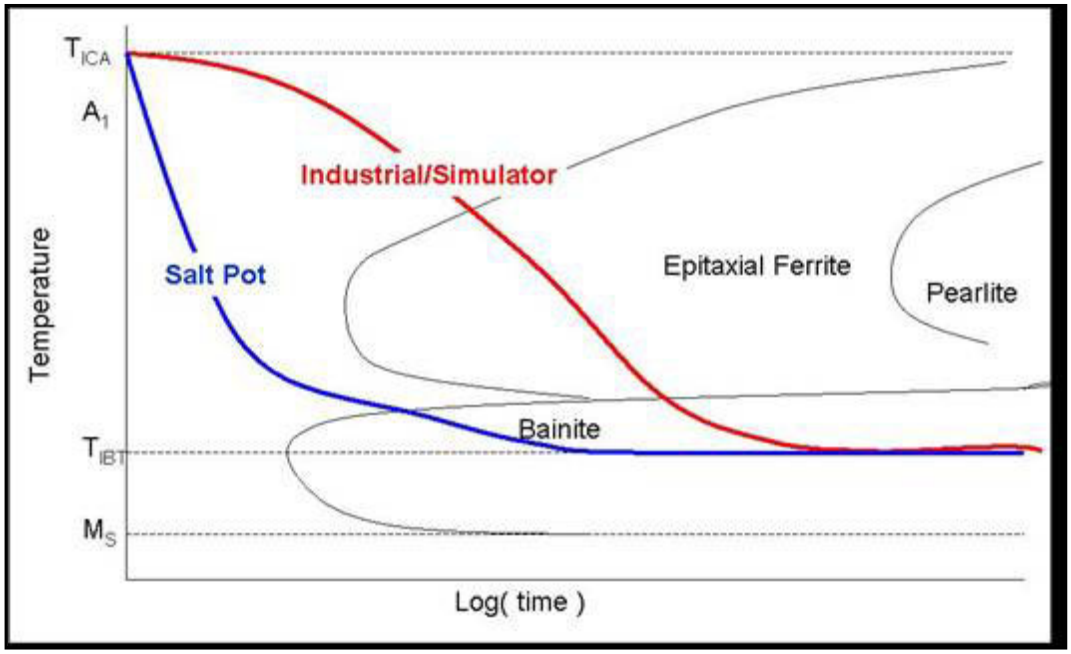

Figure 102 Hypothetical CCT curve for Salt pot vs simulator cooling.

However, as shown in Figure 87 & Figure 88, the salt pot condition did not exhibit a significant bainite fraction, either. Thus, the hypothetical CCT curve Figure 102 had to be modified to the form shown in Figure 103.

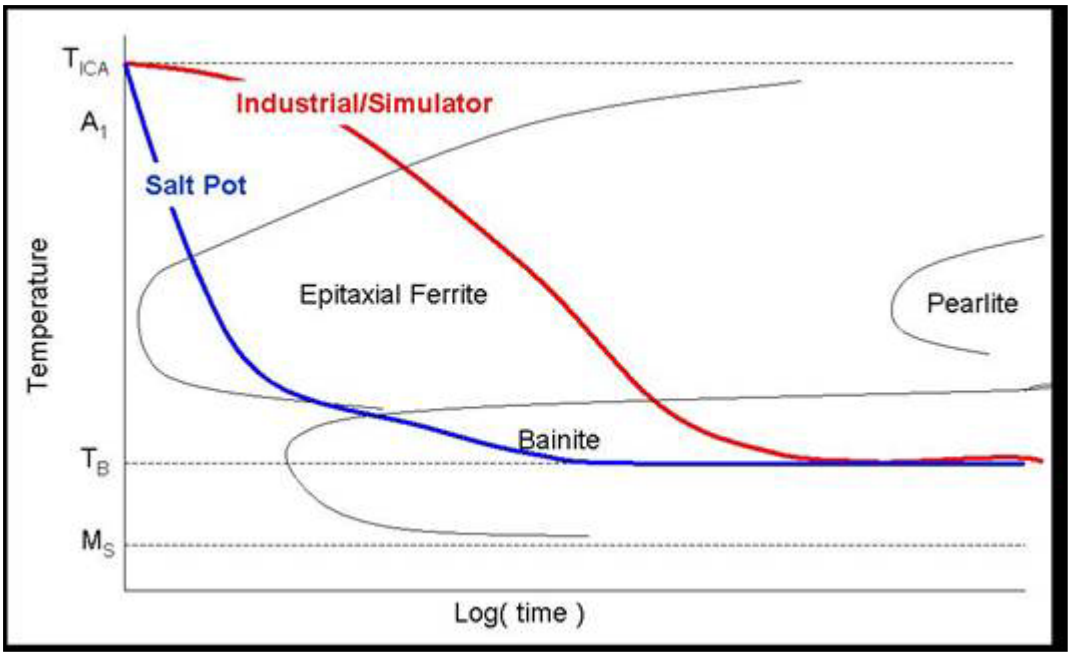

Figure 103 Revision of hypothetical CCT curve.

Likely, the thickness of the laboratory-cold-rolled sheet used -- 1.6mm -- contributed to a slower cooling rate. Various published results, such as Sakuma et al.[65], used 0.6mm sheet, which would result in much faster cooling.

Because the structure contains so little bainite, it is inferred that the transformable austenite decomposed into epitaxial ferrite rather than bainite. Although the salt-pot treated sample had a slightly higher tensile strength, implying a larger fraction of bainite, the difference was relatively minor (especially in comparison with the microhardness results to be discussed below.)

6.3.4 Dilatometry Discussion

The dilatometry study shows, most clearly, the nature of the epitaxial-vs-bainitic ferrite balance. As noted in Figure 90, the epitaxial ferrite C-curve is cut by any cooling curve up to ~100°C/sec. This is important, as the cooling rates achievable in a production facility will likely be far below this rate. CGL lines will likely be restricted to ~10-40°C/sec, and CAL lines only slightly more.

Through dilatometry, it is shown how the large additions of Si, Al or P to modern TRIP steels (see section 2.5.6) clearly are effective at suppressing the formation of pearlite/carbides. Only the 0.4°C/sec condition showed pearlite/carbides in its structure. For example, a 1320 steel has nearly the same chemical composition as this steel, with the exception of the Si-Al addition (i.e., 1320 contains 1.88 Mn and 0.2%C, compared to 0.2C-1.8Mn-1Al-0.5Si for this TRIP steel). A TTT curve for 1320 shows pearlite formation after approximately 2 seconds at 600°C[193], whereas in this study, dilatometry showed the pearlite formation after approximately 600 seconds (although under CCT rather than TTT conditions). This disparity indicates the effectiveness of the carbide-inhibitors[16,30].

The reaction temperatures (Table XI, derived from dilatometry data) are consistent with standard theory. That is, at higher cooling rates, the temperature for a given reaction (bainte or epitaxial ferrite, in these cases) is pushed to lower temperatures.

Significant quantities of epitaxial ferrite formed at all but the highest cooling rates. Brandt[194] showed that cooling rates ~120°C/sec were necessary to suppress epitaxial ferrite formation in a 1.2%Mn steel, and ~50°C/sec in a 2.4%Mn steel. Brandt's results are comparable to the present results, which show a critical cooling rate ~100°C/sec in 1.8%Mn steel.

The explanation of the manganese effect seems related to the observation that in TRIP and DP steels, at slow cooling rates, intercritical annealing temperature seems to have little effect on final phase fractions. Comparing the 800°C and 843°C annealed samples in this study, the 4°C/sec cooled samples showed only slightly more bainite and somewhat higher tensile strength in the 800°C condition as compared to the 843°C condition. This indicates a slight increase in hardenability resulting from the increased carbon content. As shown in Figure 92, all 4°C/sec samples suffer a large amount of epitaxial ferrite reaction.

Speich and Miller[195], in a similar result (Figure 104), showed that the final volume fraction of martensite in a dual-phase steel was relatively insensitive to intercritical temperature at cooling rates of 1.4 or 10°C/sec. Only at 115°C/sec did the fraction of martensite increase with increasing intercritical temperature.

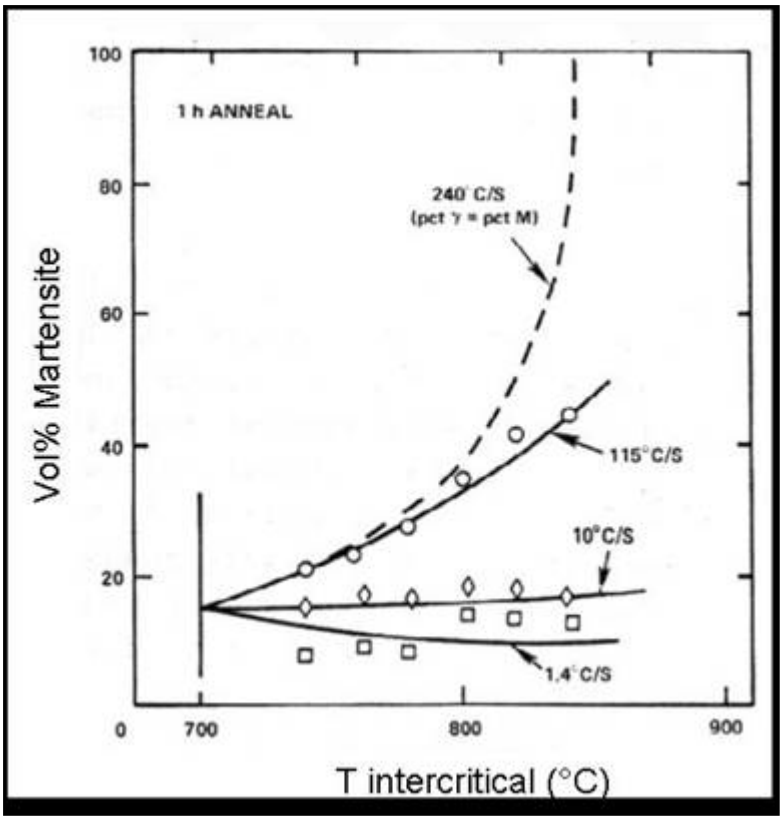

Figure 104 Effect of cooling rate on martensitic transformation efficiency[195]

Priestner et al.[196,197,198] studied austenite particle dispersion and chromium content on transformation efficiency. Firstly, Priestner[196] showed from geometrical calculations that a more finely dispersed austenite, at constant volume fraction, will suffer worse epitaxial ferrite formation; that is, a higher quenching power is necessary to obtain the same amount of martensite in the final structure. Sarwar and Priestner, though warm-rolling experiments, showed that this is indeed the case[197]. Thirdly[198], they showed that alloying, such as with chromium, can improve the yield of martensite at lower cooling rates, although it increases the critical cooling rate for zero epitaxial reaction. However, since the critical cooling rate for zero-epitaxial-reaction approaches 1000°C/sec, it is irrelevant to industrial practice. However, the partial suppression of the epitaxial

reaction at lower cooling rates by chromium is an important result: it shows alloying can make up for (at least partially) the slow cooling rates imposed by industrial processing constraints.

Higher manganese contents will inhibit epitaxial ferrite formation by the solute-drag-like effect[199,200]. Manganese decreases the activity of carbon in austenite; it also segregates to the austenite-ferrite interface. Because of this, the driving force for diffusion of carbon away from the interface (into the austenite) is reduced (i.e., manganese segregation attracts carbon to the interface, whereas the reaction requires the carbon diffuse away from the interface), slowing the kinetics of the transformation. Thus, a small amount of manganese substitutional (slow) diffusion is required to "unpin" the interface, leading to growth[199,200]. At higher cooling rates, or higher Mn contents, this unpinning cannot take place. At low cooling rates or Mn concentrations, the epitaxial ferrite grows easily. Quidort and Bréchet[201] note that substitutional alloying elements have little effect on the thermodynamics of the bainite transformation, but strongly affect its kinetics, indicating the importance of solute-drag in the bainitic reaction, as well.

As the temperature drops, the ferrite reaction will transform to a bainitic reaction; as shown in Table XI, the steel used in this study, when annealed at 843°C, shifted from ferrite to bainite at B_S~500°C. As the epitaxial ferrite or bainitic ferrite growth continues, the residual austenite will become enriched in carbon and (at least during epitaxial ferrite growth), to some minor extent in manganese. Once the carbon concentration

reaches the T'_O line, the reaction is arrested. As the T'_O line is approached, the reaction will slow; this is because the driving force for the reaction is reduced as the austenite increases in carbon content. Recall that T'_O is defined as the carbon content, at some given temperature, at which the ferrite and austenite have the same free energy (Figure 26). This reduction in driving force/kinetic rate likely explains the "leveling off" shape of the IBT dilatometry curves, Figure 89.

These dilatometry results are also consistent with results of Park and Eldis[202]. Park and Eldis studied austenite decomposition in intercritically annealed DP steels by means of dilatometry, and produced CCT curves qualitatively very similar to the ones produced by this study. Importantly, they showed an epitaxial ferrite reaction in all steels at all cooling rates. (Their maximum cooling rate was 40°C/sec).

Traint et al.[68,203], Girault et al.[204], Bleck et al.[205] and Ohlert et al.[206] also performed dilatometry of TRIP steel isothermal bainitic transformations. Their results were consistent with the results presented here. Firstly, Traint et al.[68,203] showed that the magnitude of the dilatometrically measured isothermal transformation increased as dT/dt increased from 10 to 70°C/sec. The results presented here confirm and continue these trends to 200°C/sec. Traint et al. showed that the magnitude of the IBT's of high cooling rate conditions were more closely spaced than those of slow cooling rate conditions; similarly, these new results show that, beyond about 100°C/sec for the steel studied, there is little variation in IBT magnitude. The current work shows that the IBT reaction nears completion after about 60 seconds for T_{IBT}=416°C; the previous

studies[68,203,204,205,206] show that IBT's at higher temperatures reach completion much more quickly than those at lower temperatures. A temperature of 416°C falls within the "high-temperature" IBT range, as shown by the other works. The silicon-bearing TRIP steel of Girault et al. [204] showed near-completion of the bainitic transformation after 80-100 seconds at 416°C, in near-perfect agreement with the present results in silicon-aluminum steel. However, none of these earlier works presented continuous-cooling dilatometric data. The results and CCT curve produced by this study are qualitatively similar to the early dual-phase CCT work performed by Park and Eldis[202], which implies validity of these results, although they are obviously different in detail from the dual-phase work.

From the CCT curve, and verified by the microstructural studies, it is apparent that a critical cooling rate $\langle dT/dt \rangle_{CRIT}$ exists between 40°C/sec and 100°C/sec for this steel; above this cooling rate, epitaxial ferrite is suppressed and bainite dominates the austenite decomposition. Below this cooling rate, the opposite is true. TRIP steels with other chemical compositions/intercritical parameters will likely have their own critical cooling rate, $\langle dT/dt \rangle_{CRIT}$. Above or below this cooling rate, microstructures and mechanical properties evolve in rather different fashions. Because the cooling rates available to a particular industrial concern are likely fixed by the design of the CAL/CGL line and economic considerations such as linespeed, it is important that alloying and process design account for which side of $\langle dT/dt \rangle_{CRIT}$ the particular TRIP steel in question will be processed on. Traint et al.[203] showed reactions during cooling at 70°C/sec; the reaction was less pronounced in an aluminum TRIP steel than in a silicon

TRIP steel. Similarly, they showed dilatometric data, which indicated an IBT of larger magnitude after cooling in the aluminum steel than in the silicon steel. This implies that aluminum steels suffer less austenite transformation (epitaxial ferrite formation) during cooling than silicon steels; proper aluminum alloying may be an excellent means to design future alloying schemes to accommodate multi-million-dollar CAL/CGL equipment fixed to a particular range of slow cooling rates. Unfortunately, aluminum steels tend to have lower strength than silicon steels, due to aluminum's rather weak solid-solution hardening, in comparison to silicon's solid-solution-hardening. If aluminum steels do favor bainite formation over silicon steels, the increased volume fraction of this harder phase may partially compensate for the loss of strength associated with low silicon contents.

Obviously, the composition, size and morphology of the austenite pools will dominate the decomposition reactions, but these factors will vary strongly with bulk composition and thermal processing parameters. Thus, for example, the differences in the reactions between aluminum or silicon steels (Traint et al.) noted above will actually result from changes in the austenite pools, but those changes are, in turn, effects of the change in chemical composition from Si to Al-based alloying schemes.

The microhardness results, especially Figure 97, clearly indicate that higher cooling rates result in higher hardness material. This is likely a simple composite-strengthening effect of the increased bainite fraction, Figure 105.

a)

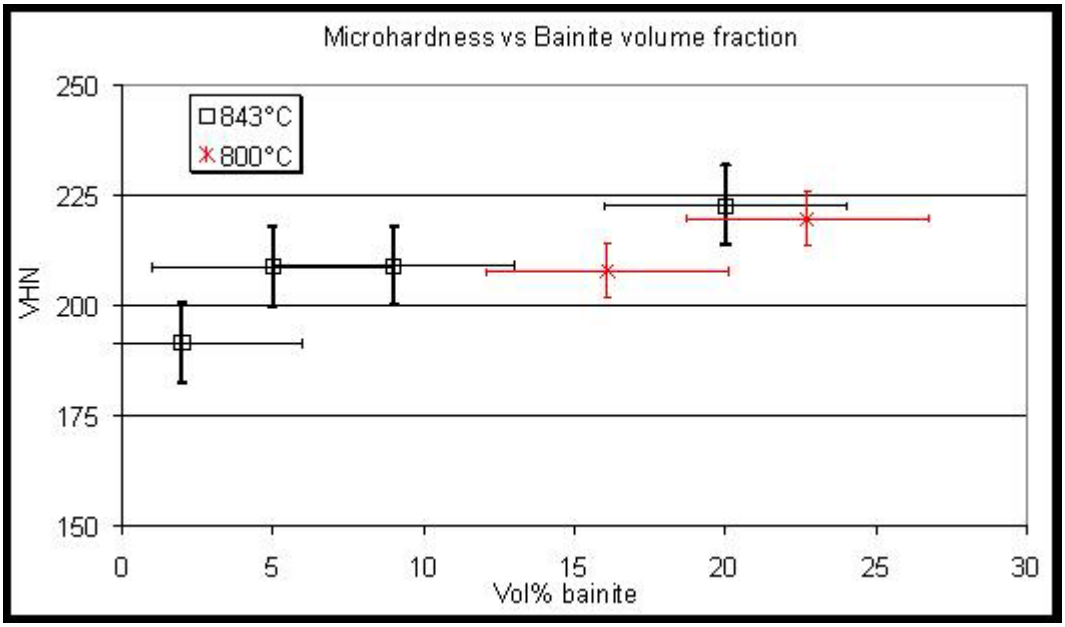

b)

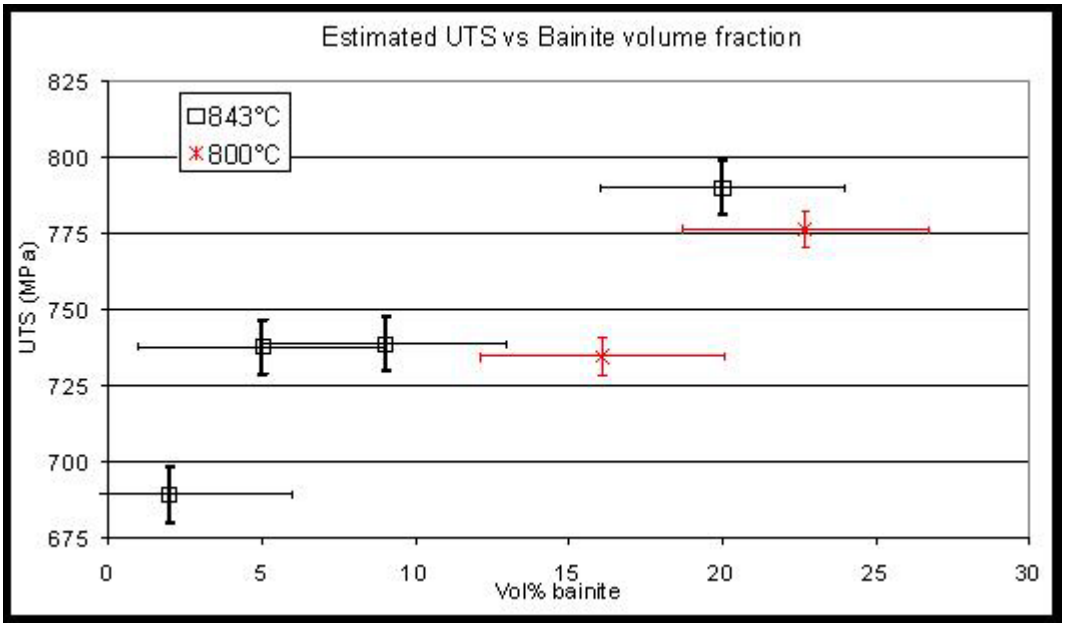

Figure 105 (a) Microhardness and (b) tensile strength estimated from microhardness as a function of bainite content.

Figure 105 is qualitatively similar to Figure 97 (tensile strength vs cooling rate). As shown by Figure 92, the bainite fraction increases monotonically with cooling rate from a given annealing temperature; the concomitant increase in hardness/strength with

cooling rate is obviously due to the increasing bainite fraction, as bainite is a harder phase than ferrite (which it replaces) and will lead to composite strengthening.

Figure 89 (IBT dilatometric data) is an important result for explaining the annealing behavior of TRIP steels. It shows a number of important points. First, the reactions begin very rapidly through their first few seconds, and then the reactions slow and level off, having been mostly completed after about 60 seconds. Secondly, the reactions for the higher-cooling-rate conditions (i.e., 100 and 200°C/sec) are significantly larger in magnitude than the reactions for the low-cooling-rate conditions (i.e., 4 and 40°C/sec).

As noted above in the mechanical properties section, the properties of the steels become steady after even just one minute of IBT time (S-1). This can be explained in terms of the leveling-of of the IBT dilatometry curves before the one minute mark is reached; that is, because the reaction is arrested by the time the S-1, S-2 and S-5 mechanical property specimens were taken, they should obviously have near-identical mechanical properties.

The large jump in mechanical properties between S-RT and S-GA (24,120MPa-% vs 28,574MPa-%; Table IX) can be explained in terms of the rapid reaction at short IBT times shown in Figure 89. The S-RT condition would experience only a small bainitic reaction as it was cooled through the narrow temperature range between the bainite-start and martensite-start. The S-GA specimen, however, spent approximately 30 seconds in the bainitic regime during the GA step, in addition to the cooling stages

before and after the GA step; dilatometry showed that the first few seconds of the reaction are the most profound, so it comes as no surprise that even a short treatment in the bainitic temperature regime, as S-GA received, would cause a larger evolution in mechanical properties than, for example, the difference experienced between S-5 and S-GA.

Given the relatively small magnitude of IBT transformation observed by dilatometry after 4°C/sec cooling, and the small (~2%) volume fraction, it is surprising that such a massive change in mechanical properties occurs (Table IX). It seems unlikely that the enrichment of austenite associated with a conversion of 2% bainitic ferrite could have such a profound effect, especially in comparison to the ~36% epitaxial ferrite conversion. What may be the case is, rather than enrichment, a homogenization of carbon is taking place. Using Brandes'[207] values of carbon diffusion in austenite, and extrapolating to 416°C, a diffusion constant $D_C=5x10^{-4}$ μm^2/sec is calculated. A diffusion distance $\sqrt{Dt}$ calculation[208,209,210] indicates diffusion distances of 170nm for C in austenite after 1 minute at 416°C, and 390nm after 5 minutes. Because the dimensions of retained austenite in these steels are on the order of 100-200nm (inter-lath films) or ~1000nm (massive inter-ferritic islands), this indicates that simple homogenization is a possible mechanism of the stabilization between zero IBT and 5 minutes IBT.

If, for example, an austenite island present at the start of the IBT had a steep carbon gradient, in which the boundaries were enriched, it might be possible that the boundary area would have an M_S well below room temperature, while the center of the particle still

had M_S > RT. Thus, upon cooling, the center of the particle would necessarily transform to martensite. If the martensitic transformation is burst-type, then the entire particle would transform as soon as martensite nucleated anywhere within it. However, after carbon homogenization, the areas of high-carbon-content would have been depleted in carbon while the lower carbon areas were enriched. If this pushed all regions of the particle below M_S, the particle would necessarily be retained upon cooling to room temperature. Figure 106 shows schematically this hypothetical situation, both before (a) and after (b) the homogenization during the hold. Thus, although there is little dilatometrically observable transformation, the IBT would still show a significant effect upon room-temperature properties.

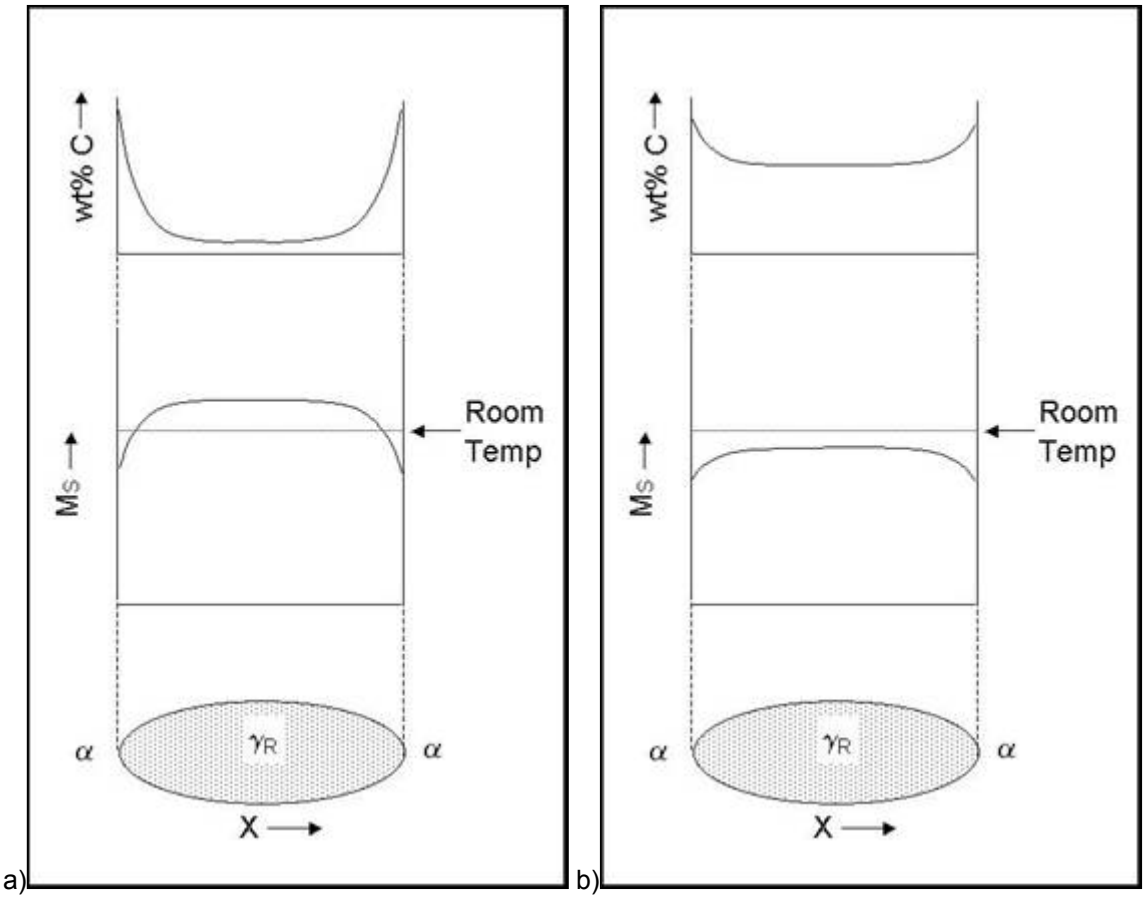

Figure 106 Hypothetical effect of IBT on carbon distribution within austenite islands.
(a) Before IBT homogenization. (b) After.

The greater magnitude of IBT reaction experienced by the higher cooling rate conditions is due to the suppression of the epitaxial ferrite reaction at higher cooling rates. For example, the 4°C/sec condition contains ~76vol% ferrite (epitaxial + intercritical), whereas the 200°C/sec condition contains ~55%, both at roughly the same retained austenite fraction. This difference is due to the lesser magnitude of the epitaxial ferrite reaction under high-cooling rate conditions. Because there is less austenite remaining upon reaching T_{IBT} in the slower-cooling-rate samples, the magnitude of the austenite decomposition measured by dilatometry during the IBT will be necessarily lower. Thus,

the increased IBT reaction at 100-200°C/sec is a result of the increased opportunity to transform isothermally to bainite rather than to ferrite during cooling.

Although compositions such as this, 0.20C-1.8Mn-1.0Al-0.5Si, or the other compositions used in the mechanical properties study, are suitable for producing 600MPa grade steel, they are unsuitable for 780-800MPa grade or higher material. Thus, some applications, such as automotive crash-members or wheel disks, are out of the reach of these alloys. It is possible to use alloying, such as Cr-Mo additions, to increase the austenite hardenability, thus forcing a higher bainite fraction and achieving a 780-800MPa material. Park and Eldis[202], in DP steels, showed that an increase in Mo content allowed the formation of bainite at significantly slower cooling rates. They did not, however, present quantities of epitaxial ferrite as a function of alloying content.

As shown by this work, neglecting any hardening from the alloying additions themselves (such as solid-solution hardening), but rather just considering the alloying additions effects on hardenability and concomitant increased bainite fraction, an increase of bainite fraction ~20vol% can achieve ~780MPa strengths (Figure 105b). As shown by the results of Kim et al.[39] in Cr-Ni-Cu TRIP steels, there may also be martensite present in the Cr-bearing alloys, which would increase strength even more than an equivalent amount of bainite. Quidort and Bréchet[201] note that Cr-additions can prevent the bainitic reaction from progressing to completion; Figure 107 shows their dilatometric data for a series of Cr-added 0.20C-1.5Mn steels reacted at 480°C. It is possible that this reaction-arresting-phenomenon results in less-complete IBT transformation, therefore in

less-complete carbon enrichment of the residual austenite, leaving it with a higher propensity for conversion to martensite.

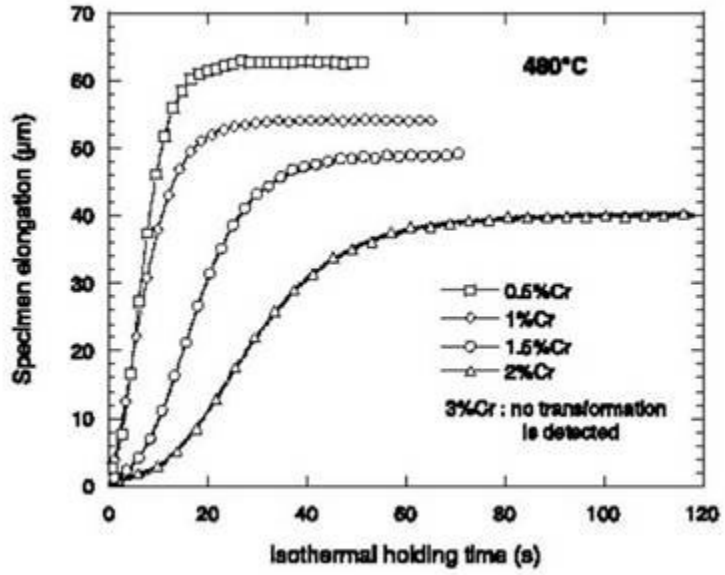

Figure 107 Effect of Cr on bainitic transformation[201]

Sverdlin and Ness[24] show the effects of different alloying elements on TTT behavior, Figure 108.

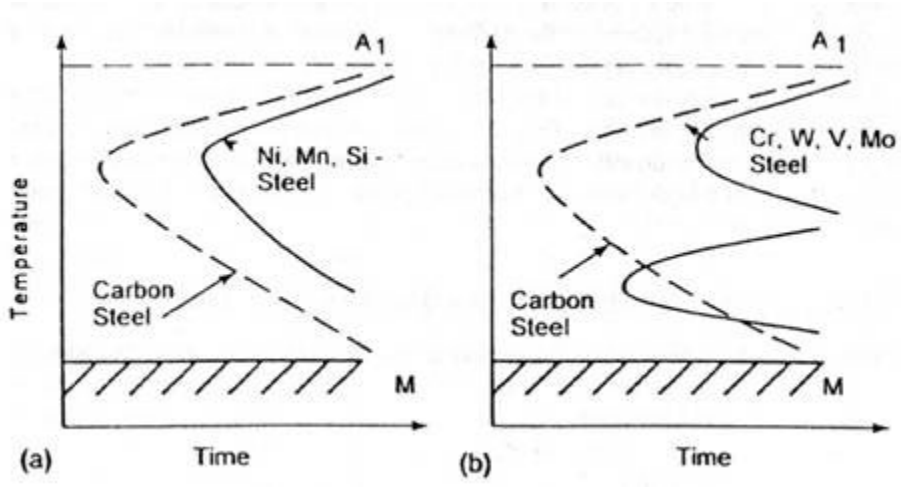

Figure 108 Effects of hardenability additions[24]; (a) Ni, Mn, Si (b) Cr, W, V, Mo.

Although the illustration is derived for a fully austenitic steel, the principle still holds: any of the additions (Ni, Mn, Si, Cr, W, V, Mo) will suppress the proeutectoid/epitaxial reaction, and the addition of Cr, W, V, or Mo will push the bainite bay to shorter times. Thus, adding these elements will be tantamount to an increase in cooling rate. Although the nose of the CCT curve will be shifted to much faster cooling rates in an intercritically annealed steel (in comparison to a fully austenitic steel), the alloying mentioned should still shift the C curves in the same direction, even if the magnitudes of the shift are different. In light of results such as those listed in Section 2.3.10, these additions may also favor martensite formation, leading to even more hardening. Of course, if the Ni, Mn, or Si additions push the epitaxial ferrite reaction to longer times (as shown by, for example, Brandt[194] for Mn), they should also leave more austenite available for consumption by the bainitic reaction. Quidort and Bréchet note that Ni additions strongly slow the bainitic transformation, as well, via solute-drag effects[201].

As noted in section 2.8.1, copper in austenite slows diffusional transformation processes significantly[142]; copper (or related) alloying, even neglecting its austenite-stabilizing effects, may very well improve TRIP steel properties by slowing the growth of epitaxial ferrite and thus favoring bainite.

Alloying, however, is a high-cost means of achieving increases in strength. Alloying beyond a certain level will also affect other properties, such as welding, coating, or galvannealing. Any other means of increasing bainite fraction would be preferable. The

two possible means of achieving this would be to either increase the cooling rate or increase the hardenability of the austenite by non-alloying means.

Firstly, an increase in cooling rate would be difficult to achieve in practice. Line speeds and configurations will likely restrict cooling rates to ~50°C/sec or, more likely, less.

The only way to increase austenite hardenability by non-alloying means is to reduce the intercritical annealing temperature. This will result in a smaller fraction of intercritical austenite, with higher carbon content. This higher carbon content will lead to a slower epitaxial ferrite reaction.

As the epitaxial ferrite reaction will be diffusion controlled, a higher carbon concentration will require more time to deplete the transformation-front diffusionally. Figure 109 is adapted from Porter and Easterling[211]. $C\alpha$ is the carbon content in ferrite, $C\gamma$ in the intercritical austenite, and $C\alpha\gamma$ at the interface. ΔC_0 is $C\alpha\gamma$ - $C\gamma$. Particle half-width is X, and growth rate v. Making the assumption that the diffusionally enriched zones have not yet begun to impinge on each other, austenite away from the interface will be of the carbon content $C\gamma$, inherited from the intercritical state, and will not yet have been enriched.

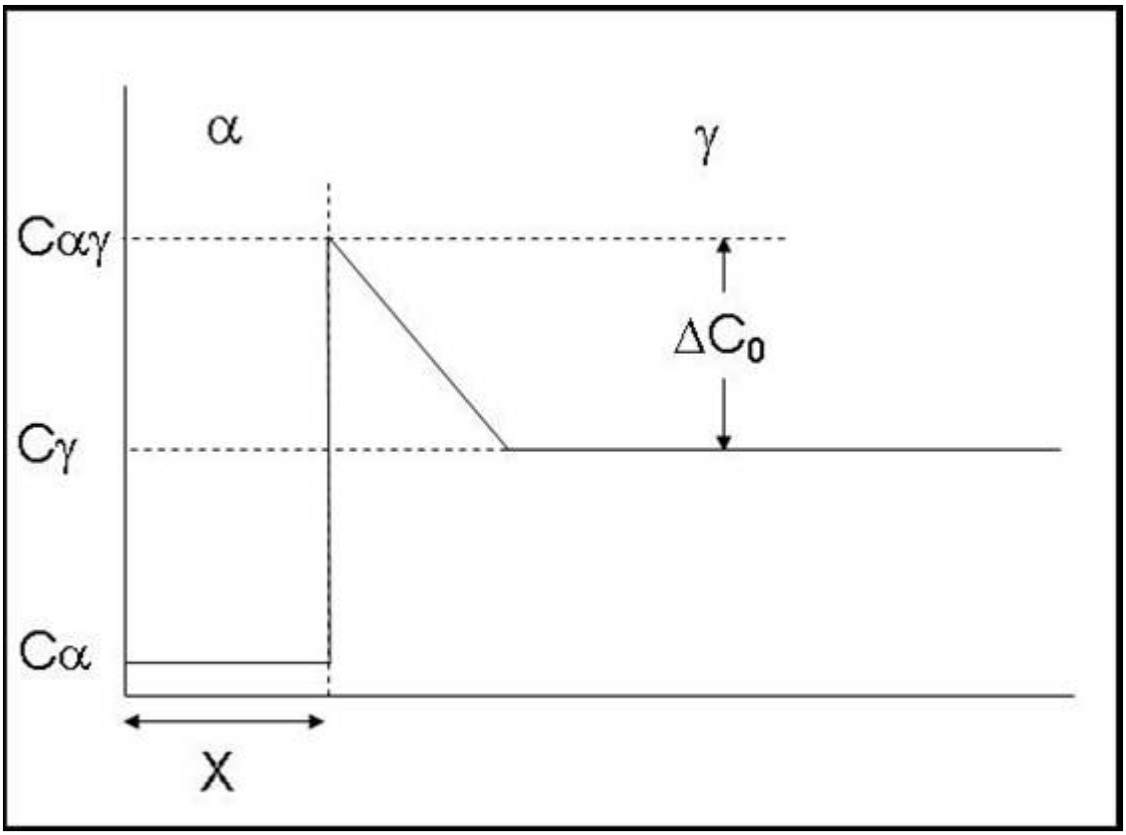

Figure 109 Diagram of ferrite growing into austenite. Adapted from Porter and Easterling[211].

Adapting Porter and Easterling's equation for diffusion-controlled growth rate of a planar incoherent interface, when translated into Cα, Cγ, Cαγ and ΔC_0 terminology:

$$v = \frac{D(\Delta C_0)^2}{2(C_\alpha - C_{\alpha\gamma})(C_\alpha - C_\gamma)X} \qquad (6\text{-}1)$$

If the intercritical temperature is lower, Cγ will increase, ΔC_0 will decrease (ΔC_0^2 will decrease strongly), Cα - Cγ will become more negative, and X will increase. All of these variations will lead to slower growth (v decreasing). Further, as Cγ increases, the driving force (difference between Cγ and the carbon content described by the T_0 line) for the reaction will be reduced.

Obviously, as the reaction progresses and the diffusion fields begin to impinge, the reaction will slow; this is a partial explanation for the leveling-off of the IBT dilatometry reactions, although a reduction in T_0-related-driving-force will likely be the dominant effect in the slowing of the reaction. Although equation 6-1 is derived for a planar growth front, it can be adapted to lathlike growth fronts by accounting for tip-curvature; the above variations with carbon content will still hold.

As the 800°C annealed conditions in this study showed, the increased hardenability brought about by lower intercritical annealing temperatures did slightly increase bainite fraction and hardness. However, at industrially achievable cooling rates (such as 4°C/sec) this effect was not enough to place the material into the 780-grade range (at least insofar as UTS was estimated from VHN). Further, material annealed at these lower temperatures tends to have inferior mechanical properties, especially ductility[212].

Recall Figure 18[(72)], repeated (in part) as Figure 110a, which showed the variation of phase fractions with intercritical annealing temperature; final bainite + austenite fraction was found to increase with intercritical temperature (i.e., increased with intercritical austenite fraction). That same result was observed here in the 200°C/sec samples, Figure 110b; this means that at these high cooling rates, epitaxial ferrite has no chance to form. Interestingly, the 4°C/sec samples (Figure 110c) showed the opposite effect, indicating that at lower cooling rates, the increased hardenability at 800°C (vs 843°C) suppresses the epitaxial transformation.

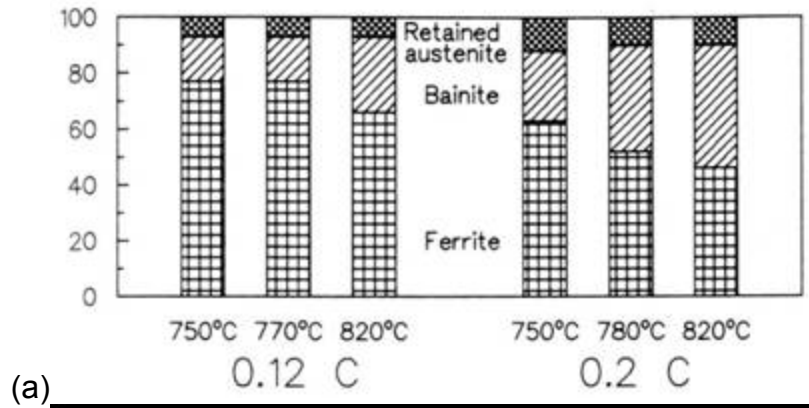

(a)

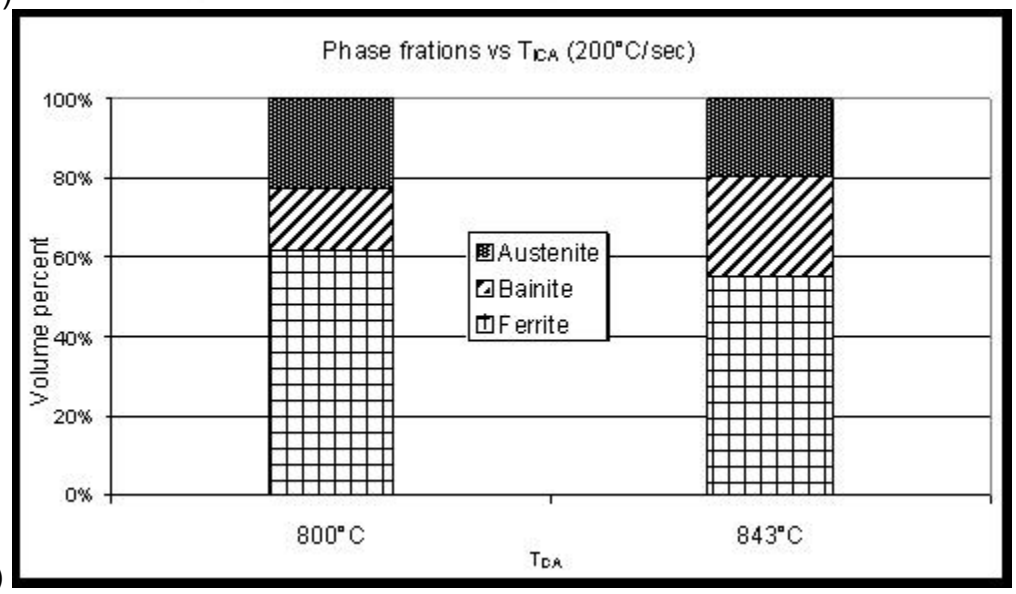

(b)

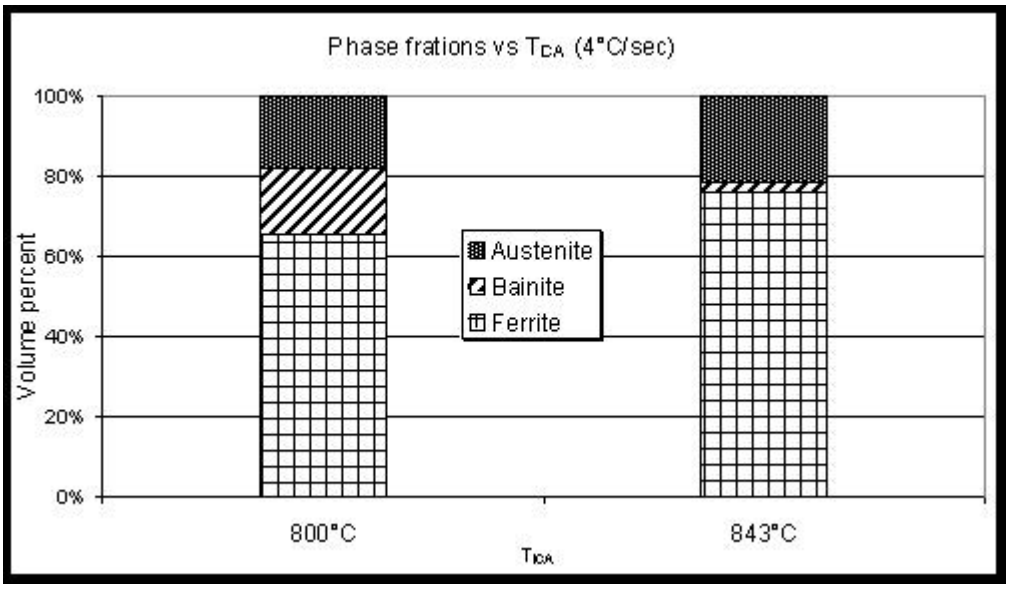

(c)

Figure 110 Phase fractions as a function of intercritical temperature. (a) From Sakuma et al.[72]; salt-pot cooling rates. (b) 200°C/sec. (c) 4°C/sec. Data in (b) and (c) is derived from Figure 92 (which shows error bars).

A combination of increased cooling rate and lower intercritical temperature will likely provide an increased yield of bainite (in terms of fraction final bainite per fraction intercritical austenite), but because of the reduced amount of intercritical austenite, this higher yield could conceivably result in a lower final fraction of bainite. The 200°C/sec cooled conditions annealed at both 800 and 843°C in this study showed almost the same quantities of bainite and hardness, indicating this trade-off results in little difference in final structure at high cooling rates. Microhardness values cannot speak to ductility, however.

Further, increased industrial cooling rates would require increasing linespeed for CAL- or CGL-produced material. This would necessarily result in a shorter IBT time, as well. A combination of less transformation during the cooling stage (i.e., higher cooling rates, lead to a shorter cooling-stage time) and a shorter IBT would likely lead to less overall austenite transformation. Thus, the austenite might not be sufficiently carbon-enriched to be retained upon cooling, and would thus transform to martensite, ruining the desired TRIP effect. One means of compensating for this would be to perform the IBT at a higher temperature (i.e., 425°C-475°C), see Section 2.5.5. This would result in completion of the reaction in a shorter time, as desired. Consider the results of Girault et al.[204], Figure 111: they showed significantly faster IBT reaction kinetics at higher temperature. However, the cost of a higher bainitic transformation temperature is bainite of a lower hardness[33]. Thus, it would require an even greater increase in bainite fraction to yield a desired increment in tensile strength.

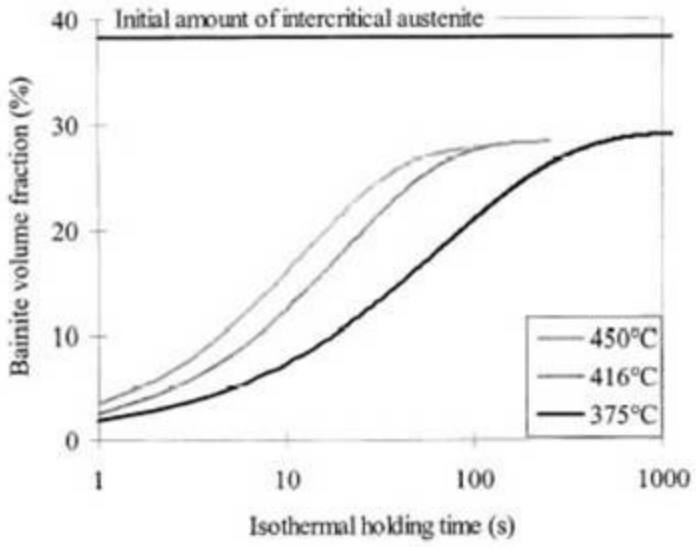

Figure 111 Comparison of IBT kinetics at various temperatures[204]

Using published microhardness values, it is possible to perform order-of-magnitude calculations to predict these materials' hardness, and compare to the actually measured values. Firstly, values of microhardness for individual constituents must be obtained from the literature. (Because of the micron- to sub-micron-size of the micro-constituents in these materials, it was not possible to obtain these values directly.)

From Sverdlin and Ness[24], the microhardness of ferrite is estimated at 160 VHN. This is based on a value of ~1.8wt% Mn in ferrite; Sverdlin and Ness show Mn as hardening much more than Si or Al, and Si and Al are present in much smaller amounts in this material (1.8%Mn compared to 1.0% Al and 0.5% Si; Table II), it was assumed that the Mn content would be dominant.

Bainite formed in these conditions will not form at the 0.20% bulk carbon content, but rather from highly enriched austenite. If ~75% of the steel is in the form of ferrite (epitaxial or intercritical) at the beginning of the bainite transformation, then the remaining austenite -- from whence the bainite forms -- would be ~0.6-0.8wt% carbon. Bhadesia[33] quotes a value 350 VHN for 0.69%C bainite ausformed at ~416°C, so Bhadesia's value is used.

Retained austenite microhardness values are not published. However, Furnémont et al.[213] published nanohardness values for the phases in TRIP steel. From their data, retained austenite has a nanohardness of ~1.25 times that of bainite. So, from the bainite value of 350 VHN above, retained austenite hardness was estimated at ~438 VHN. In summary, Table XIV.

Table XIV Microhardness values used for modeling

Phase	Ferrite	Bainite	Retained Austenite
Hardness (VHN)	160	350	438
Reference	24	33	33, 213

Using these microhardness values and the volume fractions determined above (Figure 92), microhardness values for these conditions can be estimated. The estimated contributions of each phase, and the measured microhardnesses, are presented in Figure 112.

a)

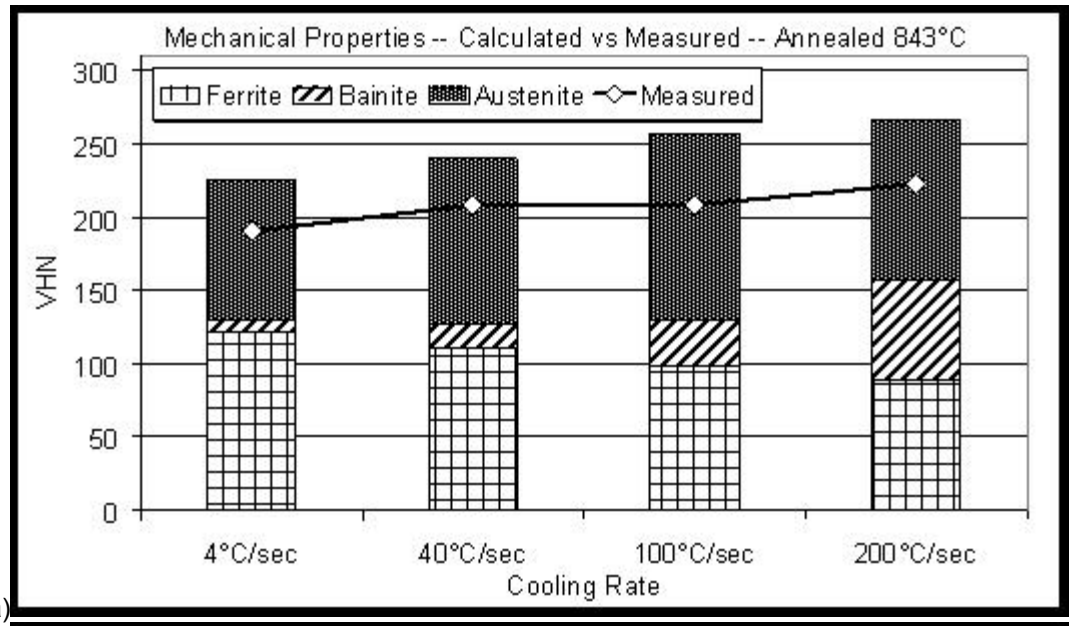

b)

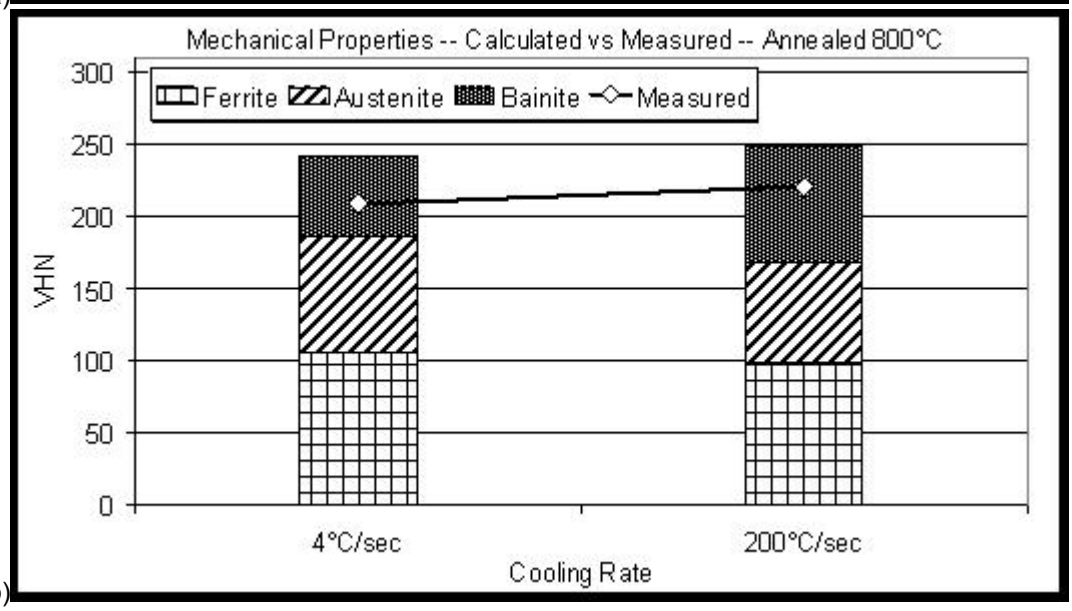

Figure 112 Estimated and measured microhardnesses.
(a) Conditions annealed at 843°C. (b) Conditions annealed at 800°C

Although the estimated values consistently fall above the measured values, they show quite reasonable agreement, ±20-40 VHN.

6.3.5 Annealing Summary

IBT time (or lack of IBT) has a profound effect on the mechanical properties and microstructures of TRIP steels, due to the stabilization of the residual austenite during the IBT.

GA parameters (within reasonable limits; i.e., <~500°C) have almost no effect on TRIP properties following a proper IBT.

Cooling rate, however, has profound effects on the transformation kinetics and microstructures of isothermally transformed TRIP steels. Suppression or encouragement of the epitaxial ferrite reaction -- whether through cooling rate, alloying, or a combination of the two -- will be a very profound means of controlling properties and microstructures of TRIP steels.

7.0 FUTURE WORK

The author recommends that the following research fields be pursued:

1. Study of carbon and other solute content and distribution in retained austenite. Using STEM and APFIM, it should be possible to study the effects of IBT time on the re-distribution of solutes. For example, the hypothetical model of Figure 106 could be confirmed or refuted. (See section 2.6)
2. Study effects of other alloying elements on the austenite decomposition reactions. Repeating these experiments, especially dilatometry, on TRIP steels bearing other alloying additions such as Cr, Mo, W, etc., would allow the study of the epitaxial-vs-bainitic balance and subsequent phase balance. Nb, V and Ti microalloying also should be studied, especially with respect to reactions during cooling and grain refinement. Although these elements (with the exception of W) have been studied in TRIP steels in the literature, an austenite-decomposition study of the depth presented here has not been reported. Certainly, no dilatometry studies have been performed on TRIP steels alloyed in any scheme other than with the "plain-carbon" Mn-Si-Al or microalloyed Mn-Si-Al-Nb schemes.
3. The hardenability agents mentioned above, such as Cr, Mo and W, are ferrite stabilizers; the study of alloying with austenite-stabilizing hardenability agents such as Cu-Ni would also be an important field of parallel research, as the additional

stabilizing effect of Cu-Ni would be similar to that of Mn. This might allow the bulk carbon content of TRIP-steel to be reduced. As TRIP steels contain large carbon additions, 0.1-0.2wt%, their potential for industrial weldability is poor. Un-weldable steels will be of no commercial relevance. Any alloying that might allow reduction of carbon contents, and thus increases in weldability, must be pursued vigorously.

4. Boron alloying of TRIP steels has been completely ignored in the literature. Boron alloying, in conjunction with the other alloying schemes, especially Cu, would be an interesting field of study because of the strong effects boron has on phase transformations, especially in conjunction with other elements. As boron is a relatively inexpensive alloying element, and tends to have strong effects even in trace concentrations, it has the potential to improve the economics of TRIP steel production.
5. The size, shape and distribution of phases during intercritical annealing, even at given volume fractions, will strongly affect the behavior of the steel during cooling/IBT. Thus, these effects should be both modeled and studied.

8.0 CONCLUSIONS

Conclusions can be drawn regarding the two primary objectives of this study:

I. Develop and refine experimental techniques for TRIP steels
    a. Optical etching techniques, especially the LePera and $Na_2S_2O_5$ techniques, provide adequate contrast for most TRIP-steel metallography. SEM also provides reasonable contrast.
    b. SEM and TEM are also necessary characterization steps, in addition to optical microscopy.
    c. X-ray diffraction is suitable for qualitative phase analysis and lattice parameter measurements, but not for quantification of volume fractions.
    d. Magnetometry is a suitable quantification technique, providing a much more accurate volume fraction measurement than XRD.

II. Study cooling rate and IBT time effects
    a. Increasing IBT time leads to rapid changes in mechanical properties during the first 30-60 seconds, but then slows dramatically. Samples improved from UTSxTEL=24,120 MPa-% with no IBT to 30,194 MPa-% after five minutes.
    b. Cooling rate has a dominant effect upon the austenite decomposition reaction; the epitaxial-vs-bainitic ferrite balance must be accounted for in

any future TRIP steel development programs. Cooling at 4°C/sec lead to 2vol% bainite, whereas 200°C/sec resulted in 20vol% bainite.

c. Increasing the fraction of bainite, regardless of the means used to achieve this, should lead to a strong increase in tensile strength. This is due to the composite-strengthening effects of the hard bainite phase.

d. A CCT curve for intercritically annealed Si-Al TRIP steel has been constructed, and is a new and important contribution to the TRIP literature.

BIBLIOGRAPHY

1. WA Smith, *Structure and Properties of Engineering Alloys*, 2nd ed., McGraw-Hill, 1993, P114-118

2. AJ DeArdo, CI Garcia and EJ Palmiere, "Thermomechanical Processing of Steels," *ASM Handbook, Vol 4: Heat Treating*, ASM Intl., Materials Park, 1991, P237-255

3. EJ Palmiere, CI Garcia, AJ DeArdo, "The Influence of Niobium Supersaturation in Austenite on the Static Recrystallization Behavior of Low Carbon Microalloyed Steels," *Met. Trans. A*, V27A, 1996, P951-960

4. AJ DeArdo, ed., *IF Steels 2000 Conference Proceedings*, ISS, Warrendale, 2000

5. B Engl, U Heidmann, and W Müschenborn, "Cold Formability and Light Weight Construction – Driving forces for recent steel development," in *Modern LC and ULC Sheet Steels for Cold Forming: Processing and Properties*, ed. W Bleck, Verlag Mainz, Aachen, 1998, P39-50

6. MF Ashby, *Materials Selection in Mechanical Design,* Butterworth-Heinemann, 1999, P421

7. RM Jones, *Mechanics of Composite Materials,* 2nd ed., Taylor & Francis, 1999, P18-25

8. G Savage, "Formula 1 Materials Engineering," *Material Science: Its Nucleation and Growth,* ed. M McLean, Inst. Mat., London, 2001, P155-183

9. WA Smith, *Structure and Properties of Engineering Alloys*, 2nd ed., McGraw-Hill, 1993, P119-123

10. VF Zackay, ER Parker, D Fahr and R Busch, "The Enhancement of Ductility in High-Strength Steel," *Transactions of the ASM*, V60, 1967, P252-259

11. WC Leslie, *The Physical Metallurgy of Steels*, Techbooks, 1981, P295-296

12. O Matsumura, Y Sakuma and H Takechi, "Enhancement of Elongation by Retained Austenite in Intercritical Annealed 0.4C-1.5Si-0.8Mn Steel," *Trans ISIJ,* V27, 1987, P570-579

13. A Zarei-Hanzaki, PD Hodgson and S Yue, "The Influence of Bainite on Retained Austenite Characteristics in Si-Mn TRIP Steels," *ISIJ Int*, V35, 1995, P79-85

14. A Zarei-Hanzaki, PD Hodgson and S Yue, "Retained Austenite Characteristics in Thermomechanically Processed Si-Mn Transformation-Induced Plasticity Steels," *Met Trans A*, V28A, 1997, P2405-2414

15. I Tsukatani, S Hashimoto and T Inoue, "Effect of silicon and manganese Addition on Mechanical Properties of High-Strength Hot-Rolled Sheet Steel Containing Retained Austenite," *ISIJ Int,* V31, 1991, P992-1000

16. HC Chen, H Era and M Shimizu, "Effect of Phosphorus on the Formation of Retained Austenite and Mechanical Properties in Si-Containing Low-Carbon Steel Sheet," *Met Trans A*, V20A, 1989, P437-445

17. P Jacques, X Cornet, Ph Harlett, J Ladrière and F Delannay, "Enhancement of the Mechanical Properties of a Low-Caron, Low-silicon Steel by the Formation of a Multiphased Microstructure Containing Retained Austenite," *Met Trans A*, V29A, 1998, P2383-2393

18. S Traint, A Pichler, R Tikal, P Stiaszny and EA Werner, "Influence of Manganese, Silicon and Aluminum on the Transformation Behavior of Low-Alloyed TRIP-Steel," 42nd MWSP Conference, 2000, P549-562

19. M Brandt, "Bainitic Stabilization of Austenite in Low Alloy Sheet Steels," Ph.D. Dissertation, Northwestern University, 1997

20. B Mintz, "Hot Dip Galvanizing of Transformation Induced Plasticity and Other Intercritically Annealed Steels," *International Materials Reviews*, V46, 2001, P169-197

21. J Mahieu, J Maki, S Claessens and BD De Cooman, "Hot-Dip Galvanizing of Al Alloyed TRIP Steels," *43rd MWSP Conf Proc*, ISS, 2001, P397-407

22. J Mahieu, BC De Cooman, J Maki and S Claessens, " Hot-Dip Galvanizing of Al Alloyed TRIP Steels," *Iron & Steelmaker*, V29, June 2002, P29-34

23. G Krauss *Steels: Heat Treatment and Processing Principles,* ASM, 1989, P52-53

24. AV Sverdlin and AR Ness, "The Effects of Alloying Elements on the Heat Treatment of Steel," in *Steel Heat Treatment Handbook*, ed. GE Totten and MA Howes, Marcel-Dekker, New York, 1997, P45-91

25. NC Goel, JP Chakravarty, K Tangri, "The Influence of Starting Microstructure on the Retention and Mechanical Stability of Austenite in an Intercritically Annealed-Low Alloy Dual Phase Steel," *Met Trans A*, V18A, 1987, P5-9

26. WA Smith, *Structure and Properties of Engineering Alloys*, 2nd ed., McGraw-Hill, 1993, P141-143

27. AF Crawley, MT Shehata, N Pussegoda, CM Mitchell and WR Tyson, "Processing, Properties and Modeling of Experimental Batch-Annealed Dual-Phase Steel," in *Fundamentals of Dual-Phase Steels*, RA Kot and JW Morris, eds., TM-AIME, 1979, P181-197

28. W Bleck, "Using the TRIP Effect -- The Dawn of a Promising New Group of Cold Formable Sheets," *Int. Conf. on TRIP-Aided High Strength Ferrous Alloys*, ed BC De Cooman, GRIPS, Ghent, 2002, P13-23

29. WA Smith, *Structure and Properties of Engineering Alloys*, 2nd ed., McGraw-Hill, 1993, P130

30. WC Leslie and GC Rauch, "Precipitation of Carbides in Low-Carbon Fe-Al-C Alloys," *Met Trans A*, V9A, 1978, P343-349

31. SK Ray, S Mishra and ON Mohanty, "TEM Study of Carbide Precipitation in a Phosphorus-Bearing Low-Carbon Steel," *Scripta Met*, V16, 1982, P43-47

32. SK Ray, S Mishra and ON Mohanty, "Magnetic Aging Characteristics of a Phosphorus-Bearing Low-Carbon Steel," *Scripta Met,* V15, 1981, P971-973

33. HKDH Bhadeshia, *Bainite in Steels*, The Institute of Materials, 1992

34. M De Meyer, D Vanderschueren and BC De Cooman, "The Influence of the Substitution of Si by Al on the Properties of Cold-Rolled C-Mn-Si TRIP Steels," *ISIJ Int*, V39, 1999, P813-822

35. A Zarei-Hanzaki, PD Hodgson and S Yue, "Hot Deformation Characteristics of Si-Mn TRIP Steels with and Without Nb Microalloy Additions," *ISIJ Int*, V35, P324-331

36. S Jiao, F Hassani, RL Donaberger, E Essadiqi and S Yue, "The Effect of Prior Heat Treated Structure on a Cold Rolled and Annealed Mo-Nb Microalloyed TRIP Steel," *43rd MWSP Conf. Proc*, ISS, 2001, P385-395

37. A Lucas, J-C Herman and A Schmitz, "Cu-Containing TRIP steels," *Int. Conf. on TRIP-Aided High Strength Ferrous Alloys*, ed BC De Cooman, GRIPS, Ghent, 2002, P231-236

38. S Traint, A Pichler, K Hauzenberger, P Stianszy and E Werner, "Influence of Silicon, Phosphorus, and Copper on the Phase Transformations of Low Alloyed TRIP-steels," *Int. Conf. on TRIP-Aided High Strength Ferrous Alloys*, ed BC De Cooman, GRIPS, Ghent, 2002, P121-128

39. S-J Kim, C-G Lee, W-C Jeong and I Park, "Microstructure and Mechanical Properties of the 0.15%C TRIP-Aided Cold-Rolled Steels Containing Cu, Ni and Cr," *Int. Conf. on TRIP-Aided High Strength Ferrous Alloys*, ed BC De Cooman, GRIPS, Ghent, 2002, P165-169

40. S Mishra and BK Jha, "A Low-Carbon TRIP-Aided Formable Hot Rolled Steel," in *Modern LC and ULC Sheet Steels for Cold Forming: Processing and Properties*, ed. W Bleck, Verlag Mainz, Aachen, 1998, P109-120

41. BK Jha and S Jha, "Retention and deformation Characteristics of Austneite in a TRIP Aided Hot-Rolled Steel," *44th MWSP Conf. Proc,* ISS, 2002, P179-185

42. Z. Nishiyama, *Martensitic Transformations*, Academic Press, 1978, Ch. 5

43. GN Haidemenopoulos and AN Vasilakos, "Modelling of Austenite Stability in Low-Alloy Triple-Phase Steels," *Steel Research*, V67, 1996, P513-519

44. AN Vasilakos, K Papamantellos, GN Haidemenopoulos and W Bleck, "Experiemntal Determination of the Stability of Retained Austenite in Low Alloy TRIP Steels," *Steel Research*, V70, 1999, P466-471

45. I Tamura and CM Wayman, "Martensitic Transformations and Mechanical Effects," in *Martensite*, GB Olson and WS Owen, eds., ASM International, 1992, Ch. 12

46. JM Rigsbee and PJ VanderArend, "Laboratory Studies of Microstructures and Structure-Property Relationships in 'Dual-Phase' HSLA Steels," in *Formable HSLA Steels*, AT Davenport, ed., TMS-AIME, 1979, P56-86

47. JM Rigsbee, "Inhibition of the Martensitic Transformation of Small Austenite Particles in Low-Alloy Steels," *ICOMAT 1979*, ed. WS Owen, Cambridge, MA, 1979, P381-387

48. RE Cech and D Turnbull, "Heterogeneous Nucleation of the Martensite Transformation," *Trans AIME*, V206, 1956, P124-132

49. CL Magee, "The Kinetics of Martensite Formation in Small Particles," *Met Trans*., V2, 1971, P2419-2430

50. K Sugimoto, M Misu, M Kobayashi and H Shirasawa, "Effect of Second Phase Morphology on Retained Austenite Morphology and Tensile Properties in a TRIP-aided Dual-Phase Steel Sheet," *ISIJ Int*., V33, 1993, P775-782

51. T Sakaki, K Sugimoto and T Fukazato, "Role of Internal Stress of Continuous Yielding of Dual-Phase Steels," *Acta Met*., V31, 1983, P1737-1746

52. JM Moyer and GS Ansell, "The Volume Expansion Accompanying the Martensite Transformation in Iron-Carbon Alloys," *Met Trans A*, V6A, 1975, P1785-1791

53. CM Wayman, *Introduction to the Crystallography of the Martensitic Transformation*, MacMillin, 1964

54. SV Radcliffe and M Schatz, "The Effect of High Pressure on the Martensitic Reaction in Iron-Carbon Alloys," *Acta Met*., V10, 1962, P201-207

55. HJ Koh, SK Lee, SH Park, SJ Choi, SJ Kwon and NJ Kim, "Effect of Hot Rolling Conditions on the Microstructure and Mechanical Properties of Fe-C-Mn-Si Multiphase Steels," *Scripta Met*, V38, 1998, P763-768

56. JM Rigsbee and HI Aaronson, "A Computer Modeling Study of Partially Coherent FCC:BCC Boundaries", *Acta Met,* V27, 1979, P351-363

57. JM Rigsbee and HI Aaronson, "The Interfacial Structure of the Broad Faces of Ferrite Plates", *Acta Met,* V27, 1979, P365-376

58. K Sugimoto, M Kobayashi and S Hashimoto, "Ductility and Strain-Induced Transformation in a High-Strength Transformation-Induced Plasticity-Aided Dual-Phase Steel," *Met Trans A*, V23A, 1992, P3085-3091

59. S Godet, Ph. Harlet, F Delannay and PJ Jacques, "Effect of Hot-Rolling Conditions on the Tensile Properties of Multiphase Steels Exhibiting a TRIP Effect," *Int. Conf. on TRIP-Aided High Strength Ferrous Alloys*, ed BC De Cooman, GRIPS, Ghent, 2002, P135-140

60. A Basuki and E Aernoudt, "Effect of Deformation in the Intercritical Area on the Grain Refinement of Retained Austneite of 0.4C TRIP Steel," *Scripta Mat*, V40, 1999, P1003-1008

61. S Papaefthymiou, W Bleck, S Kruijver, L Zhao, J Seitsma and S van der Zwaag, "Microstructure Development and Mechanical Behavior of Al-Containg TRIP-Steels," *Int. Conf. on TRIP-Aided High Strength Ferrous Alloys*, ed BC De Cooman, GRIPS, Ghent, 2002, P341-345

62. NJ Kim and G Thomas, "Structure and Properties of As-Hot-Rolled Fe-0.06C-1.5Mn Steel: Potential for Line-Pipe Applications," *Mat Sci Tech*, V1, 1985, P32-37

63. KI Sugimoto, N Usui, M Kobayashi and SI Hashimoto, "Effects of Volume Fraction and Stability of Retained Austenite on the Ductility of TRIP-aided Dual-Phase Steels," *ISIJ International*, V32, 1992, P1311-1318

64. H Matsuda, F Kitano, K Hasegawa, T Urabe and Y Hosoya, "Metallurgy of Continuously Annealed High Strength TRIP Steel Sheet," *Int. Conf. on TRIP-Aided High Strength Ferrous Alloys*, ed BC De Cooman, GRIPS, Ghent, 2002, P113-119

65. Y Sakuma, O Matsumura and O Akisue, "Influence of C Content and Annealing Temperature on Microstructure and Mechanical Properties of 400°C Transformed Steel Containing Retained Austneite," *ISIJ Int*, V31, 1991, P1348-1353

66. A Pichler, S Traint, H PAuli, H Mildner, J Szinyur, M Blaimschein, P Stiaszny and E Werner, "Processing and Properties of Cold-Rolled TRIP Steels," *43rd MWSP Conf. Proc.*, ISS, 2001, P411-434

67. A Pichler and P Stiaszny, "TRIP Steel with Reduced silicon Content," *Steel Research*, V70, 1999, P459-465

68. S Traint, A Pichler, P Stiaszny, K Spiradek-Hahn and EA Werner, "Mechanical Properties and Phase Transformations of an Aluminum Alloyed TRIP Steel," *43rd MWSP Conf. Proc*, ISS, 2001, P449-467

69. CI Garcia and AJ DeArdo, "Formation of Austenite in 1.5 Pct Mn Steels," *Met Trans A*, V12A, 1981, P521-530

70. E Navara, B Bengtsson and KE Easterling, "Austenite Formation in Manganese-Partitioning Dual-Phase Steel," *Mat Sci Tech*, V2, 1986, P1196-1201

71. T Minote, S Torizuka, A Ogawa and M Niikura, "Modeling of Transformation Behavior and Compositional Partitioning in TRIP Steel," *ISIJ Int*, V36, 1996, P201-207

72. Y Sakuma, O Matsumura and H Takechi, "Mechanical Properties and Retained Austenite in Intercritically Heat-Treated Bainite-Transformed Steel and Their Variation with Si and Mn Additions," *Met Trans A*, V22A, 1991, P489-498

73. JG Speer and DK Matlock, "Recent Developments in Low-Carbon Sheet Steels," *JOM,* V54, 2002, P19-24

74. O Matsumura, Y Sakuma and H Takechi, "Retained Austenite in 0.4C-Si-1.2Mn Steel Sheet Intercritically Heated and Austempered," *ISIJ Int*, V32, 1992, P1014-1020

75. M De Meyer, BC De Cooman and D Vanderschueren, "The Influence of Al on the Properties of Cold Rolled C-Mn-Si TRIP Steels," *Iron & Steelmaker*, V27, 2000, P55-63

76. PJ Jacques, Ph Harlet and F Delannay, "Critical Assessment of the Phase Transformations Occurring During the Heat-Treatment of TRIP-Assisted Multiphase Steels," *Int. Conf. on TRIP-Aided High Strength Ferrous Alloys*, ed BC De Cooman, GRIPS, Ghent, 2002, P129-134

77. A Itami, M Takahashi and K Ushioda, "Plastic Stability of Retained Austenite in the Cold-Rolled 0.14%C-1.9%Si-1.7%Mn Sheet Steel," *ISIJ Int*, 1995, P1121-1127

78. A Bodin, J Flemming and EFM Jansen, "Development of As-Hot-Rolled Low-silicon and Micro-Alloyed Dual-Phase Steels," 42nd MWSP Conf. Proc., 20000, P563-571

79. S-J Kim, CG Lee, T-H Lee and S Lee, "Effects of Coiling Temperature on Microstructure and Mechanical Properties of High-Strength Hot-Rolled Steel Plates Containing Cu, Cr and Ni," *ISIJ Int*, V40, 2000, P692-698

80. B Mintz, "The Influence of Composition on the Hot Ductility of Steels and to the Problem of Transverse Cracking (Review)," *ISIJ Int,* V39,1999, P833-855

81. K Eberle, P Cantinieaux and Ph. Harlet, "New Thermomechanical Strategy for Production of High Strength Low Alloyed Multiphase Steel Showing Transformation Induced Plasticity Effect," *Ironmaking and Steelmaking*, V26, 1999, P176-181

82. S Yue, A DiChiro and A Zarei-Hanzaki, "Thermomechanical Processing Effects in C-Mn-Si TRIP Steels," *JOM*, September 1997, P59-61

83. K Sugimoto, K Nakano, S Song and T Kashima, "Retained Austenite Characteristics and Stretch-Flangeability of High-Strength Low-Alloy TRIP Type Bainitic Sheet Steels," *ISIJ Int.*, V42, 2002, P450-455

84. H Shirasawa, "Recent Developments of Cold Fromable High Strength Hot Rolled Steels in Japan," *High Strength Sheet Steels for the Automotive Industry,* ed. R Pradhan, ISS, 1994, P3-10

85. K Sugimoto, A Nagasaka, M Kobayashi and S Hashimoto, "Effets of Retained Austenite Parameters on Warm Stretch-Flangeability of TRIP-aided Dual-Phase Sheet Steel," *ISIJ Int.,* V39, 1999, P56-63

86. K Sugimoto, T Iida, J Sakaguchi and T Kashima, "Retained Austenite Characteristics and Tensile Properties in a TRIP-Type Bainitic Sheet Steel," *ISIJ Int.*, V40, P902-908

87. K Sugimoto, J Sakaguchi, T Iida and T Kashima, "Stretch-Flangeability of a High-Strength TRIP Type Bainitic Sheet Steel," *ISIJ Int,* V40, 2000, P920-926

88. K Sugimoto, M Kobayashi and S Hashimoto, "Ductility and Strain-Induced Transformation in a High-Strength Transformation-Induced Plasticity-Aided Dual-Phase Steel," *Met. Trans. A,* V32A, 1992, P3085-3091

89. K Sugimoto, M Kobayashi, A Nagasaka and S Hashimoto, "Warm Stretch-Formability of TRIP-Aided Dual-Phase Sheet Steels," *ISIJ Int.*, V35, 1995, P1407-1414

90. K Sugimoto and M Kobayashi, " Warm Stretch-Formability of TRIP-Aided Dual-Phase Sheet Steels," *High Strength Sheet Steels for the Automotive Industry,* ed. R Pradhan, ISS, 1994, P255-265

91. A Itami, M Takahashi and K Ushioda, "Cold-Rolled High-Strength TRIP Sheet Steels and Plastic Stability of Their Retained Austenite," *High Strength Sheet Steels for the Automotive Industry,* ed. R Pradhan, ISS, 1994, P245-254

92. O Matsumura, Y Sakuma, Y Ishii and J Zhao, "Effect of Retained Austenite on Formability og High Strength Sheet Steels," *ISIJ Int.,* V32, 1992, P1110-1116

93. A Itami, M Takahasi and K Ushioda, "Plastic Stability of Retained Austenite in the Cold-rolled 0.14%C-1.9%Si-1.7%Mn Sheet Steel," *ISIJ Int.,* V35. 1995, P1121-1127

94. M Takahashi, A Uenshi and Y Kuriyama, "Properties of High Strength TRIP Steel Sheets," *IBEC '97*, Stuttgart, 1997, P26-31

95. AM Streicher, JG Speer and DK Matlock, "Forming Response of Retained Austenite in a C-Si-Mn High Strength TRIP Sheet Steel," *Int. Conf. on TRIP-Aided High Strength Ferrous Alloys*, ed BC De Cooman, GRIPS, Ghent, 2002, 359-365

96. W Bleck, J Ohlert and K Papamantellos, "Sheet Metal Forming Behavior and Mechanical Properties of TRIP Steels," *Steel Research*, V70, 1999, P472-479

97. I Aoki, T Horita and T Herai, "Formability and Application of New Hot-Rolled High-Strength Sheet Steels," *Formability of Metallic Materials -- 2000 AD, ASTM STP 753*, ed. JR Newby and BA Niemeier, ASTM, 1982, P229-240

98. N Mizui, K Fukui, N Kojima, M Yamamoto, Y Kawaguchi, A Okamoto and Y Nakazawa, "Fundamental Study on Improvement in Frontal Crashworthiness by Application of High-Strength Sheet Steels," *SAE Paper #970156,* 1997, P205-210

99. WJ Kang, SS Cho, H Huh and DT Chung, "Identification of Dynamic Behavior of Sheet Metals for an Auto-Body with Tension Split Hopkinson Bar," *SAE Paper #981010,* 1998, P908-913

100. W Bleck and I Schael, "Determination of Crash-Relevant Material Parameters by Dynamic Tensile Tests," *Steel Res,* V71, 2000, P173-178

101. E Nakanishi, H Tateno, Y Hishida and K Shibata, "New Materials Technology for Acheviing Both Crashworthiness and Weight Reduction Using Energy-Absorbing Steel with Higher Strain-Rate Sensitivity," *SAE Paper #980953*, 1998, P680-686

102. IY Pychmintsev, RA Savrai, BC De Cooman and O Moriau, "High Strain Rate Behavior of TRIP-Aided Automotive Steels," *Int. Conf. on TRIP-Aided High Strength Ferrous Alloys*, ed BC De Cooman, GRIPS, Ghent, 2002, P299-302

103. RY Fu, XC Wei, W Shi, L Li, BC De Cooman, P Wollants, XD Zhu and L Wang, "Dynamic Tensile Characteristic of High Strength Low Alloy TRIP Steel and its Modelling," *Int. Conf. on TRIP-Aided High Strength Ferrous Alloys*, ed BC De Cooman, GRIPS, Ghent, 2002, 287-291

104. DM Haezebrouck, US Steel Corporation, Private Communication, 2002

105. TM Link, US Steel Corporation, Private Communication, 20002

106. Prof. PE Russell, North Carolina State University, Private Correspondence, 2002

107. M Onink, CM Brakman, FD Tichelaar, EJ Mittemeijer and S van der Zwaag, "The Lattice Parameters of Austenite and Ferrite in Fe-C Alloys as Functions of Carbon Concentration and Temperature," *Scripta Met*., V29, 1993, P1011-1016

108. C Scott and J Drillet, "Quantitative Analysis of Local Carbon Concentration in TRIP Steels," *Int. Conf. on TRIP-Aided High Strength Ferrous Alloys*, ed BC De Cooman, GRIPS, Ghent, 2002, P97-102

109. JW Steeds, "Convergent Beam Electron Diffraction," *Introduction to Analytical Electron Microscopy,*ed. JJ Hren, JI Goldstein and DC Joy, Plenum, 1979, P387-422

110. DB Williams & CB Carter, *Transmission Electron Microscopy*, Plenum, 1996, Chapters 37-39

111. DB Williams, *Practical Analytical Electron Microscopy in Materials Science*, Phillips Electronic Instruments, 1984, Chapter 5

112. RJ Keyse, AJ Garratt-Reed, PJ Goodhew and GW Lorimer, *Introduction to Scanning Transmission Electron Microscopy,* Bios Scientific Publishers, 1998, Chapter 6

113. RD Leapman, JA Hunt, RA Buchanan and SB Andrews, "Measurement of Low Calcium Concentrations in Cryosectioned Cells by Parallel-EELS Mapping," *Ultramicorscopy*, V49, 1993, P225-234

114. H Shuman and P Kruit, "Quantitative Data Processing of Parallel Recorded Electron Energy-Loss Spectra with Low Signal to Background," *Rev Sci Instrum,* V56, 1985, P231-239

115. S Harjo, Y Tomota, D Neov, P Lukas, M Vrana and P Mikula, "Baushinger Effect in α-γ Dual Phase Alloys Studied by *in situ* Neutron Diffraction," *ISIJ Int.*, V42, 2002, P551-557

116. CI Garcia, M Hua, AJ DeArdo and HR Piehler, "Forming Strain Path and Cold Work Embrittlement in Sheet Steels," *New Steel Sheet and Steel Bar Products and Processing¸SAE Spec. Pub. 1685*, SAE, 2002, P57-62

117. PL Carpentier and HR Piehler, "Properties of Formed Parts: Flow and Fracture Behavior after Cold Forming in HSLA steel Sheets," *Mems Sci Revs Met,* V77, 1980, P281-292

118. JM Rigsbee, JK Abraham, AT Davenport, JE Franklin and JW Pickens, "Structure-Processing and Structure-Property Relationships in Commercially Processed Dual-Phase Steels," *Structure and Properties of Dual-Phase Steels*, ed. RA Kot and JW Morris, TMS-AIME, 1979, P304-329

119. WR Cribb and JM Rigsbee, "Work-Hardening Behavior and its Relationship to the Microstructure and Mechanical Properties of Dual-Phase Steels," *Structure and Properties of Dual-Phase Steels*, ed. RA Kot and JW Morris, TMS-AIME, 1979, P91-117

120. NK Balliger and T Gladman, "Work Hardening of Dual-Phase Steels," *Met Sci*, V15, 1981, P95-108

121. CAN Lanzillotto and FB Pickering, "Structure-Property Relationships in Dual-Phase Steels," *Met Sci*, V16, 1982, P371-382

122. MF Ashby, "The Deformation of Plastically Non-Homogeneous Materials," *Phil Mag*, Ser.8, V21, 1970, P399-424

123. K Nakaoka, Y Hosoya, M Ohmura and A Nishimoto, "Reassessment of the Water-Quench Process as a Means of Producing Dual-Phase Formable Steel Sheets," *Structure and Properties of Dual-Phase Steels*, ed. RA Kot and JW Morris, TMS-AIME, 1979, P330-345

124. Z Jiang, J Liu and J Lian, "A New Relationship Between the Flow Stress and the Microstructural Parameters for Dual-Phase Steel," *Acta Met*, V40, 1992, P1587-1597

125. RG Davies, "Influence of Martensite Composition and Content on the Properties of Dual Phase Steels," *Met Trans A*, V9A, 1978, P671-679

126. M Erdogan and R Priestner, "Effect of Martensite Content, its Dispersion, and Epitaxial Ferrite Content on Baushinger Behavior of Dual Phase Steel," *Mat Sci Tech*., V18, 2002, P369-376

127. JJ Yi, KJ Yu, IS Kim and SJ Kim, "Role of Retained Austenite on the Deformation of an Fe-0.07C-1.8Mn-1.4Si Dual-Phase Steel," *Met Trans A,* V14A, 1983, P1497-1504

128. WT Lankford, NL Samways, RF Craven and HE McGannon, eds., *The Making, Shaping and Treating of Steel*, 10th ed., United States Steel, 1985

129. I LeMay and MR Krishnadev, "Fundamental Metallurgical Considerations," in *Copper in Iron and Steel*, ed. I LeMay and LM Schetky, Wiley-Interscience, 1982, P5-43

130. H Okada, S Sekino, Y Hosoi and T Murata, "Copper-Containing Structural Steels," in *Copper in Iron and Steel*, ed. I LeMay and LM Schetky, Wiley-Interscience, 1982, P83-133

131. PJ Othen, ML Jenkins, GDW Smith and WJ Phythian, *Phil Mag Lett,* V64, 1991, P383-391

132. PJ Othen, ML Jenkins and GDW Smith, "High-Resolution Electron Microscopy Studies of the Structure of Cu Precipitates in α-Fe," *Phil Mag A*, V70, 1994, P1-24

133. S Pizzini, KJ Roberts, WJ Phythian, CA English and GN Greaves, "A Fluorescence EXAFS Study of the Structure of Copper-Rich Precipitates in Fe-Cu and Fe-Cu-Ni Alloys," *Phil Mag Lett*, V61, 1990, P223-229

134. JT Buswell, CA English, MG Hetherington, WJ Pythian, GDW Smith and GM Worrall, "An Analysis of Small Clusters Formed in Thermally Aged and Irradiated FeCu and FeCuNi Model Alloys," *Effects of Radiation on Materials: 14th International Symposium (Volume II), ASTM STP 1046,* ed. NH Packan, RE Stoller and AS Kumar, ASTM, 1990, P127-153

135. MR Krishnadev and A Galibois, "Some Aspects of Precipitation of Copper and Columbium (Nb) Carbide in an Experimental High Strength Steel", *Met Trans A*, V6A, 1975, P222-224

136. MR Krishnadev, TN Goh and I Le May, "Effects of Prior Cold Work on the Aging and Mechanical Properties of a Copper-Bearing Steel," *Trans ISIJ*, V11, 1971, P40-41

137. SSG Banadkouki, D Yu and DP Dunne, "Age Hardening of Cu-Bearing High Strength Low Alloy Steel," *ISIJ Int.*, V36, 1996, P61-67

138. M Militzer, A Deschamps, S Dilney and D Meade, "Effect of Cu on Microstructure in Low-Carbon Steels," *41st MWSP Conf. Proc.*, ISS, 1999, P735-742

139. J Frimer, D Meade, M Millitzer and W Poole, "Precipitation Hardening of Copper-Containing IF Steels," *42nd MWSP Conf. Proc.,* ISS, 2000, P469-476

140. M Morita, K Sato and Y Hosoya, "Factors Affecting Texture Formation of Cu-Precipitation Hardening Cold-Rolled Steel Sheet," *ISIJ Int.*, V34, 1994, P92-98

141. Y Kimura and S Takaki, "Phase Transformation Mechanism of Fe-Cu Alloys," *ISIJ Int.*, V37, 1997, P290-295

142. H Ohtsuka, G Ghosh and K Nagai, "Effects of Cu on Diffusional Transformation Behavior and Microstructure in Fe-Mn-Si-C Steels," *ISIJ Int.*, V37, 1997, P296-301

143. A Komatsu, A Ando and T Kittaka, "Influences of Cu on the Formation of Alloy Layer [sic] in Hot-Dip Galvanizing," *ISIJ Int.,* V37, 1997, P283-289

144. L Habraken and J Lecomte-Beckers, "Hot Shortness and Scaling of Copper-Containing Steels," in *Copper in Iron and Steel*, ed. I LeMay and LM Schetky, Wiley-Interscience, 1982, P45-81

145. N Imai, N Komatsubara and K Kunishigee, "Effect of Cu, Sn and Ni on Hot Workability of Hot-Rolled Mild Steel," *ISIJ Int.*, V37, 1997, P217-223

146. N Imai, N Komatsubara and K Kunishigee, "Effect of Cu and Ni on Hot Workability of Hot-Rolled Mild Steel," *ISIJ Int.*, V37, 1997, P224-231

147. S-J Seo, K Asakura and K Shibata, "Effects of 0.4%Si and 0.02%P Additions on Surface Hot Shortness in 0.1%C-0.5%Mn Steels Containing 0.5%Cu," *ISIJ Int.*, V37, 1997, P240-249

148. "Special Issue on Effects of Cu and Other Tramp Elements on Steel Properties," *ISIJ Int. Special Issue*, V37, No. 3, 1997

149. AK Lis, M Mujahid, CI Garcia and AJ DeArdo, "The Role of Copper in the Aging Behavior of HSLA-100 Plate Steel," *Speich Symp. Proc.*, 1992, P129-138

150. M Mujahid, MS Thesis, University of Pittsburgh, 1990

151. JY Yoo, WY Choo, TW Park and YW Kim, "Microstructures and Age-Hardening Characteristics of Direct Quenched Cu Bearing HSLA Steel," *ISIJ Int.*, V35, 1995, P1034-1040

152. MK Banerjee, PS Banerjee and S Datta, "Effect of Thermomechanical Processing on the Microstructure and Properties of a Low-Carbon Copper Bearing Steel," *ISIJ Int.,* V41, 2001, P257-261

153. SR Goodman, SS Brenner and JR Low, "An FIM-Atom Probe Study of the Precipitation of Copper from Iron-1.4 At. Pct. Copper Part I: Field-Ion Microscopy," *Met Trans.*, V4, 1973, P2363-2369

154. SR Goodman, SS Brenner and JR Low, "An FIM-Atom Probe Study of the Precipitation of Copper from Iron-1.4 At. Pct. Copper Part II: Atom Probe Analyses," *Met Trans.*, V4, 1973, P2371-2378

155. SW Thompson, DJ Colvin and G Krauss, "Austenite Decomposition During Continuous Cooling of an HSLA-80 Plate Steel," *Met Trans A*, V27A, 1996, P1557-1571

156. SW Thompson and G Krauss, "Copper Precipitation During Continuous Cooling and Isothermal Aging of A710-Type Steels," *Met Trans A*, V27A, 1996, P1573-1588

157. RP Foley and ME Fine, "Microstructure and Property Investigation of Quenched and Tempered HSLA-100 Steel," *Low Carbon Steels for the 90's*, P.315-330

158. BD Cullity, *Elements of X-Ray Diffraction*, 2nd. ed., Addison-Wesley, 1978, P411-417

159. M De Meyer, D Vanderschueren, K De Blauwe and BC De Cooman, "The Characterization of Retained Austenite in TRIP Steels by X-Ray Diffraction," *41st MWSP Conf. Proc*, ISS, 1999, P483-491

160. BL Bramfitt and AO Benscoter, *Metallographer's Guide: Practices and Procedures for Irons and Steels,* ASM Intl., 2002, P300

161. L Zhao, J Moreno, S Kruijver, J Sietsma and S van der Zwaag, "Influence of Intercritical Annealing Temperature on Phase Transformations in a High Aluminum TRIP Steel," *Int. Conf. on TRIP-Aided High-Strength Ferrous Alloys,* Ghent, 2002, P141-145

162. ASTM Standard E975, *Annual Book of ASTM Standards*, V03.01, ATSM, 2000, P716-721

163. RW Hinton, "Interlaboratory Evaluation of ASTM Practice for X-Ray Determination of Retained Austenite in Steel with Near-Random Crystallographic Orientation (E 975)," *J Testing and Evaluation*, V15, 1987, P95-100

164. B Verlinden, Ph Bocher, E Girault and E Aernoudt, "Austenite Texture and Bainite/Austenite Orientation Relationships in TRIP Steel," *Scripta Mat*, V45, 2001, P909-916

165. M De Meyer, L Kestens, L Tosal-Martinez and BC De Cooman, "Texture Development in Intercritically Annealed TRIP Steels," *43rd MWSP Conf. Proc.*, ISS, 2001, P333-347

166. A Gunier, *X-Ray Diffraction in Crystals, Imperfect Crystals, and Amorphous Bodies*, trans. P Lorrain and D S-M Lorrain, Dover, 1994, Chapter 5

167. AR Marder and AO Benscoter, "Quantitative Analysis of Dual-Phase Steels," *Metallography,* V15, 1982, P73-85

168. AR Marder, "Factor Affecting the Ductility of Dual-Phase Alloys," *Formable HSLA and Dual-Phase Steels,* ed. AT Davenport, TMS/AIME, 1979, P87-98

169. AR Marder and BL Bramfitt, "Processing of Molybdenum-Bearing Dual-Phase Steel," *Structure and Properties of Dual-Phase Steels,* ed RA Kot and JW Morris, TMS/AIME, 1979, P242

170. S Bandoh, O Matsumura and Y Sakuma, "An Improved Tint Etching Method for High Strength Steel Sheets with Mixed Microstructures," *Trans ISIJ*, V28, 1988, P569-574

171. FS LePera, "Improved Etching Technique to Emphasize Martensite and Bainite in High-Strength Dual-Phase Steel," *JOM*, V32, March 1980, P38-39

172. D Colleluori, "Improved Etching Methods for Quantitative Analysis of HSLA Multi-Phase Steels," *Praktische Metallographie/Practical Metallography*, V20, 1983, P546-55

173. AK De, JG Speer and DK Matlock, “Color Tint-Etching for Multiphase Steels,” *Advanced Materials and Processes*, V161, February 2003, P27-30

174. GF Vander Voort, *Metallography: Principles and Practice*, McGraw-Hill, 1984, P216, P637-638

175. BL Bramfitt and AO Benscoter, *Metallographer's Guide: Practices and Procedures for Irons and Steels,* ASM Intl., 2002, P233-236

176. E Girault, P Jacques, Ph. Harlet, K Mols, J Van Humbeeck, E Aernoudt and F Delannay, "Metallographic Methods for Revealing the Multiphase Microstructure of TRIP-Assisted Steels," *Mater. Char.*, V40, 1998, P111-118

177. MR Plichta, HI Aaronson and WF Lange, "Chemical Polishing for Optical Microscopy," *Metallography,* V9, 1976, P455-457

178. PJ Goodhew, *Specimen Preparation for the Transmission Electron Microscopy of Materials,* Oxford University Press, 1984, Chapter 2

179. DB Williams & CB Carter, *Transmission Electron Microscopy*, Plenum, 1996, Chapter 10

180. PB Hirsch, A Howie, RB Nicholson, DW Pashley & MJ Whelan, *Electron Microscopy of Thin Crystals*, Plenum, 1965, Appendix 1

181. H Hu & S Szirmae, "Recrystalization of a Silicon-Iron Crystal as Observed by Transmission Electron Microscopy," *Trans AIME*, V221, P839-844

182. PJ Goodhew, "Specimen Preparation for Transmission Electron Microscopy of Metals," *MRS Symp. Proc. 115*, MRS, 1988, P51-62

183. M Murayama, Y Katayama and K Hono, "Microstructural Evolution in a 17-4 PH Stainless Steel after Aging at 400°C," *Met Trans A*, V30A, 1999, P345-353

184. L Zhao, NH van Dijk, E Brück, J Sietsma and S van der Zwaag, "Magnetic and X-ray Diffraction Measurements for the Determination of Retained Austenite in TRIP Steels," *Mat Sci Eng A*, VA313, 2001, 145-152

185. IY Pyshmintsev, M De Meyer, BC De Cooman, RA Savray, VP Shveykin and M Vermeulen, "The Influence of Stress State on the Plasticity of Transformation Induced Plasticity-Aided Steel," *Met Trans A*, V33A, 2002, P1659-1667

186. E Wirthl, A Pichler, R Angerer, P Stiaszny, K Hauzenberger, YF Titovets and M Hackl, "Determination of the Volume Fraction of Retained Austenite in Small Specimens by Magnetic Measurements," *Int. Conf. on TRIP-Aided High Strength Ferrous Alloys*, ed BC De Cooman, GRIPS, Ghent, 2002, P 61-64

187. L Zhai, O Tegus, E Bruck, NH van Dijk, SO Kruijver, J Sietsma and S van der Zwaag, "Magnetic Determination of the Thermal Stability of Retained Austenite in TRIP Steel," *Int. Conf. on TRIP-Aided High Strength Ferrous Alloys*, ed BC De Cooman, GRIPS, Ghent, 2002, P 71-74

188. SR Keown & FB Pickering, "A Chemical Thinning Technique for the Preparation of Thin Metal Foils for Transmission Electron Microscopy," *JISI*, V200, 1962, P757-758

189. *Metals Handbook: Desk Edition*, ed. JR Davis, ASM International, Materials Park, OH, P72-73

190. RW Hinton, "Interlaboratory Evaluation of ASTM Practice for X-Ray Determination of Retained Austenite in Steel with Near-Random Crystallographic Orientation (E 975)," *J Testing and Evaluation*, V15, 1987, P95-100

191. IY Pychmintsev, RA Savrai, BC De Cooman and O Moriau, "High Strain Rate Behavior of TRIP-Aided Automotive Steels," *Int. Conf. on TRIP-Aided High Strength Ferrous Alloys*, ed BC De Cooman, GRIPS, Ghent, 2002, P299-302

192. Smith, P110

193. *Atlas of Time-Temperature Diagrams for Irons and Steels*, ed. GF Vander Voort, ASM-International, Materials Park, OH, 1991, P16

194. ML Brandt, Ph.D. Thesis, Northwestern University, 1997

195. GR Speich and RL Miller, "Hardenability of Austenite After Intercritical Annealing," *Proc Int Conf on Solid → Solid Phase Transformations*, ed. HI Aaronson, DE Laughlin, RF Selerka and CM Wayman, TMS-AIME, 1981, P843-848

196. R Priestner, "Effect of Austenite Dispersion and Plastic Deformation on Phase Transformations in Dual-Phase Steel," *Phase Transformations 87*, ed. GW Lorimer, Inst. Met., 1987, P411-413

197. M Sarwar and R Priestner, "Hardenability of Austenite in a Dual-Phase Steel," *J Mat Eng Performance*, V8, 1999, P 380-384

198. M Sarwar, E Ahmad and R Priestner, "Effect of Termomechanical Processing in the Intercritical Region on Hardenability of Austenite in a Dual-Phase Steel," *J Mat Eng Performance*, V10, 2001, P662-669-384

199. M Militzer, R Pandi and EB Hawbolt, "Austenite to Ferrite Transformation Kinetics During Continuous Cooling", *Proc Int Conf on Solid → Solid Phase Transformations*, ed. WC Johnson, JM Howe, DE Laughlin and WA Soffa, TMS, 1994, P177-182

200. JR Bradley, GJ Shiflet and HI Aaronson, "A Current View of Alloying Element Effects on Growth Kinetics of Proeuctectiod Ferrite in Fe-C-X Alloys," *Proc Int Conf on Solid → Solid Phase Transformations*, eds. HI Aaronson, DE Laughlin, RF Selerka and CM Wayman, TMS-AIME, 1981, P824-848

201. D Quidort and Y Bréchet, "The Role of Carbon on the Kinetics of Bainite Transformation in Steels," *Scripta Met*, V47, 2002, P151-156

202. YJ Park and GT Eldis, "A Dilatometric Study of the Transformation Behavior of Intercritically Annealed Molybdenum- and Vanadium-Containing Dual Phase Steels," *Metallurgy of Continuous Annealed Sheet Steel*, ed. BL Bramfitt and PL Mangonon, Jr., TMS-AIME, 1982, P321-331

203. S Traint, A Pichler, P Stiaszny and EA Werner, “Silicon and Aluminum in Low Alloyed TRIP Steels,” *44th MWSP Conf. Proc.* ISS, 2002, P139-152

204. E Girault, P Jacques, P Ratchev, J Van Humbeeck, B Verlinden and E Aernoudt, “Study of the Temperature Dependence of the Bainitic Transformation Rate in a Multiphase TRIP-Assisted Steel,” *Mat Sci Eng A*, V273-275A, 1999, P471-474

205. W Bleck, K Hulka and K Papamentellos, "Effect of Niobium on the Mechanical Properties of TRIP Steel," *Mat Sci Forum*, V284-286, 1998, P327-334

206. J Ohlert, W Bleck and K Hulka, "Control of Microstructure in TRIP Steels by Niobium," *Int. Conf. on TRIP-Aided High Strength Ferrous Alloys*, ed. BC De Cooman, GRIPS, Ghent, 2002, P199-206

207. EA Brandes, *Smithells' Metals References Book*, 6th ed., Butterworths, London, 1983, Ch. 13

208. DA Porter and KE Easterling, *Phase Transformations in Metals and Alloys,* 2nd ed., Chapman and Hall, London, Ch. 2

209. P Shewmon, *Diffusion in Solids*¸2nd ed., TMS, Warrendale, PA, 1989, Ch.1

210. PG Shewmon, *Transformations in Metals*, McGraw-Hill, New York, 1969, Ch.2

211. Porter and Easterling, Ch. 5

212. DM Haezebrouck, US Steel Corporation, Personal Communication, 2003

213. Q Furnémont, M Kempf, PJ Jacques, M Göken and F Delannay, "On the Measurement of the Nanohardness of the Constitutive Phases of TRIP-Assisted Multiphase Steels," *Mat Sci Eng A*, V A328, 2002, P26-32